AD-A186 359 MAXIMUM ENTROPY/OPTIMAL PROJECTION DESIGN SYNTHESIS FOR 1/3
DECENTRALIZED CON (U) HARRIS CORP MELBOURNE FL
GOVERNMENT AEROSPACE SYSTEMS DIV D C HYLAND ET AL
UNCLASSIFIED MAY 87 AFOSR-TR-87-1196 F49620-86-C-0038 F/G 22/1 NL

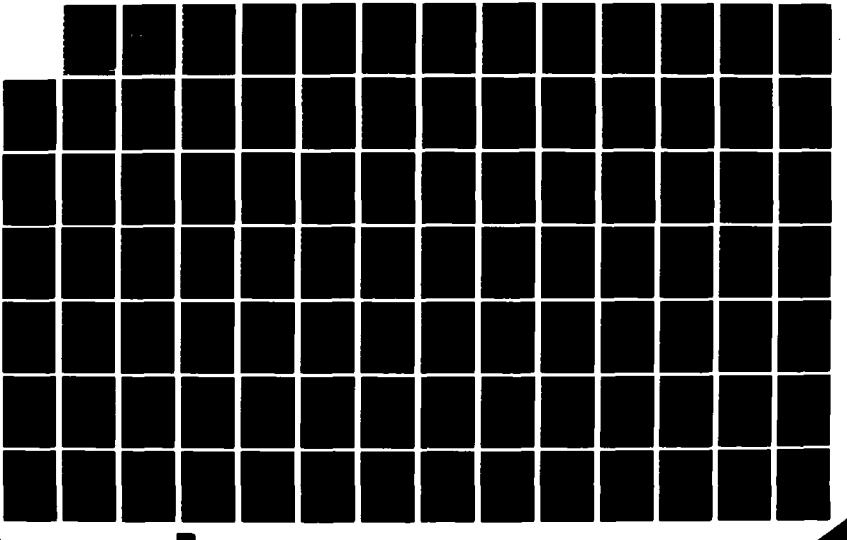

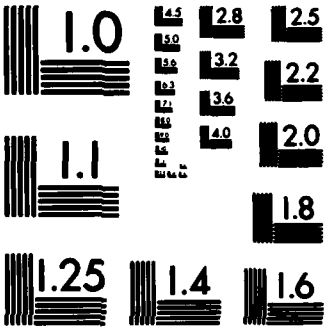

AFOSR-TR- 87-1196

Maximum Entropy/Optimal Projection Design Synthesis for Decentralized Control of Large Space Structures

D. C. Hyland
D. S. Bernstein

Harris Corporation
Government Aerospace Systems Division
Melbourne, Florida 32907

Interim Report
Contract No. F49620-86-C-0038

HARRIS

HARRIS CORPORATION GOVERNMENT AEROSPACE SYSTEMS DIVISION
P.O. BOX 94000, MELBOURNE, FLORIDA 32902, (305) 727-5115

UNCLASSIFIED

ADA186359

REPORT DOCUMENTATION PAGE

1a. REPORT SECURITY CLASSIFICATION Unclassified	1b. RESTRICTIVE MARKINGS
2a. SECURITY CLASSIFICATION AUTHORITY	3. DISTRIBUTION/AVAILABILITY OF REPORT Approved for public release; distribution unlimited.
2b. DECLASSIFICATION/DOWNGRADING SCHEDULE	
4. PERFORMING ORGANIZATION REPORT NUMBER(S)	5. MONITORING ORGANIZATION REPORT NUMBER(S) AFOSR-TR- 87-1196
6a. NAME OF PERFORMING ORGANIZATION Harris Corporation Government Aerospace Division	6b. OFFICE SYMBOL (If applicable)
6c. ADDRESS (City, State and ZIP Code) MS 22/4848 Melbourne,FL 32901	7b. ADDRESS (City, State and ZIP Code) Bldg 410 Bolling AFB DC 20332-6448
8a. NAME OF FUNDING/SPONSORING ORGANIZATION Air Force Office of Scientific Rsch	8b. OFFICE SYMBOL (If applicable) NA
8c. ADDRESS (City, State and ZIP Code) Building 410 Bolling AFB Washinton, DC 20322	9. PROCUREMENT INSTRUMENT IDENTIFICATION NUMBER F49620-86-C-0038
	10. SOURCE OF FUNDING NOS PROGRAM ELEMENT NO: 61102F; PROJECT NO: 2302; TASK NO: B1; WORK UNIT NO:

11. TITLE (Include Security Classification) MAXIMUM ENTROPY/ OPTIMAL PROJECTION DESIGN SYNTHESIS FOR DECENTRALIZED CONTROL OF LARGE SPACE STRUCTURES

12. PERSONAL AUTHOR(S)
Hyland, David, Charles Bernstein, Dennis, S.

13a. TYPE OF REPORT	13b. TIME COVERED	14. DATE OF REPORT (Yr. Mo. Day)	15. PAGE COUNT
Annual	FROM 10/86 TO 4/87	1987, May	

16. SUPPLEMENTARY NOTATION

17. COSATI CODES		
FIELD	GROUP	SUB GR
22	02	
12	01	

18. SUBJECT TERMS (Continue on reverse if necessary and identify by block number)
Robust control design, Derentralized controller, majorant robustness analysis.

19. ABSTRACT (Continue on reverse if necessary and identify by block number)

The Maximum Entropy/Optimal Projection (MEOP) methodology is a novel approach to designing implementable vibration-suppression controllers for large space systems. Two issues, in particular, have been addressed, namely, controller order (i.e. complexity) and system robustness (i.e., insensitivity to plant variations). Extensions developed herein include generalizations to decentralized controller architectures and a new robustness analysis technique known as Majorant Robustness Analysis.

20. DISTRIBUTION/AVAILABILITY OF ABSTRACT UNCLASSIFIED/UNLIMITED [X] SAME AS RPT [ ] DTIC USERS [ ]	21. ABSTRACT SECURITY CLASSIFICATION UNCLASSIFIED
22a. NAME OF RESPONSIBLE INDIVIDUAL ANTHONY K AMOS	22b. TELEPHONE NUMBER (Include Area Code) (202) 767-4935
	22c. OFFICE SYMBOL AFOSR/NA

DD FORM 1473, 83 APR EDITION OF 1 JAN 73 IS OBSOLETE

SECURITY CLASSIFICATION OF THIS PAGE

Maximum Entropy/Optimal Projection Design Synthesis for Decentralized Control of Large Space Structures

D. C. Hyland
D. S. Bernstein

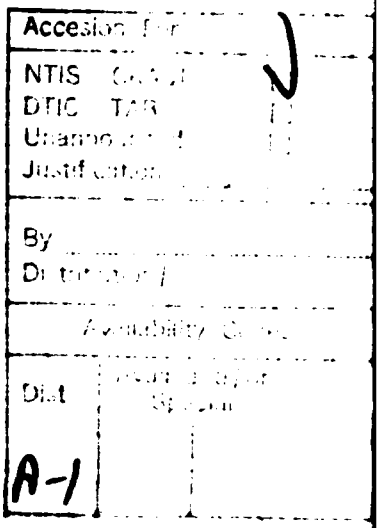

Harris Corporation
Government Aerospace Systems Division
Melbourne, Florida 32907

Interim Report
Contract No. F49620-86-C-0038

TABLE OF CONTENTS

LIST OF ILLUSTRATIONS

LIST OF ILLUSTRATIONS (Continued)

LIST OF APPENDICES

SECTION 1.0

INTRODUCTION AND STUDY OVERVIEW

1.0 INTRODUCTION AND STUDY OVERVIEW

As its name suggests, the Maximum Entropy/Optimal Projection (MEOP) theory of control design for large space systems represents the synthesis of two distinct and novel ideas: (1) minimum information stochastic modelling of parameter uncertainties (to characterize the inevitable tradeoff between robustness and performance) and (2) optimal reduced-order compensator design for a given high-order plant (to optimally quantify the tradeoff between controller complexity and performance). A previous AFOSR-funded study (contract no. F49620-84-C-0015) consolidated MEOP theory developments and successfully demonstrated the theory on a variety of flexible space structure models.

It is now possible to extend the basic MEOP theory and design capability to handle an even larger class of structural concepts. In particular, the sheer size, or dimensionality, of proposed flight structures (such as Space Station) necessitates what may be called <u>decentralized analysis and design.</u> In brief, this terminology refers to procedures that treat portions of the system individually and then combine the results. Often the need for such analysis arises from such basic constraints as computer capacity, i.e., the model may simply be too large to "fit" into the computer at one time.

Our thinking concerning decentralized analysis and design is closely related to the current literature on large scale systems. We propose to go beyond previous work by using the MEOP theory to quantify uncertain interactions among subsystems, thus providing an "informational" or statistical system partitioning. A major goal in this regard is to utilize our theory to extend the applicability of the concept of <u>connective stability</u> to complex, multibody spacecraft.

In practice, a direct consequence of the physical size and physical complexity of proposed spacecraft imposes severe constraints on the communication links between sensors, processors and actuators. Relevant issues include cabling mass and RF shielding problems along with reliability concerns. This leads to consideration of multiple sensor/processor/actuator subcontrollers or substations on the spacecraft without real-time intercommunication. Although the processors do not directly exchange data, preflight design of their software must, of course, account for complex operational interactions among subcontrollers via the structural response.

The design of such a decentralized architecture or implementation is clearly a nontrivial task and can be thought of as involving two interrelated steps:

1. Determination of the architecture of the control system including the number of substations and the assignment of sensors and actuators to particular substations; and

2. For a given architecture, design of the processor software for each subcontroller.

The aims of the present study are to extend MEOP to address both of the above items. Indeed, because maximum entropy modelling quantifies uncertainty (i.e., lack of knowledge) it is possible to directly include informational aspects in the system model. The statistical effects that result from this model can be used to evaluate the performance of proposed decentralized architectures. Thus, one goal is to quantify the degree of suboptimality resulting from the variance between subsystem partitionings due to interaction uncertainties and alternative controller architectures. Once a particular architecture is selected, the design of each subcontroller often requires iterative solution of high-dimensional design synthesis equations. A second major goal is to evolve efficient approaches to the solution of the MEOP design equations for optimal, decentralized control.

1.1 Objectives

The specific tasks required to accomplish the goals of this contract are discussed in detail within the original technical proposal and are summarized as follows:

Task 1: Undertake rigorous extensions of the MEOP design equations to the case of distributed controller architecture in a variety of settings. These developments include:

1.1 Extension of the continuous-time MEOP equations to the decentralized case for both static and dynamic controllers.

1.2 Derivation of the MEOP design equations for decentralized discrete-time control of discrete-time systems.

1.3 Extension of the MEOP design equations to a hierarchical controller architecture.

Task 2: Analyze the design equations derived in Task 1 to provide understanding of the role of uncertainty in decomposing the design procedure. In particular:

2.1 Analyze the effects of the maximum entropy uncertainty terms in decomposing the open-loop system for decentralized design procedures and decentralized implementation.

2.2 Derive methods for bounding the degree of suboptimality resulting from decentralized design and decentralized implementation.

2.3 Evolve effective methods for deriving uncertainty bounds which imply connective stability for the overall system.

Task 3: In order to verify the analysis carried out in Task 2, develop solution techniques for the decentralized form of the MEOP design equations. The *following* sequence of developments is planned:

3.1 Develop iterative procedures for solving the decentralized optimal projection equations assuming accurate plant models. Such algorithms would be limited to fixed-structure designs for which the order of the closed-loop system (plant plus subcontrollers) is less than 50.

3.2 Expand subtask 3.1 to develop iterative methods for solving the MEOP decentralized design equations which also account for high-frequency modal uncertainty effects.

3.3 Apply the techniques of subtask 3.2 to the problem of uncertain subsystem interaction. By designing for each subsystem separately and accounting for modal uncertainties, considerably larger systems can be treated. The results from subtask 2.3 can be used to assure robust stability of the resulting design.

Task 4: Apply the various decentralized extensions of MEOP to a realistic design problem. Two possible spacecraft control problems are the COFS I Program space flight test article and the space station. For either of these alternatives, the following subtasks encompass the desired goals:

4.1 Generate detailed state-space model, define uncertainty operators for mass, damping and stiffness, define sensor/actuator number, type and placement, and assign disturbance spectrum. Use system model to perform centralized control-tradeoff studies. Such designs may utilize decentralized design techniques.

4.2 Using the centralized tradeoff studies as baseline, determine decentralized/hierarchical implementation architectures based upon uncertainty patterns, physical constraints and processing requirements. For each design assess the degree of suboptimality resulting from the loss of centralization.

1.2 Progress to Date

In this section, we briefly summarize the results obtained under the tasks listed above. Further details are described in Sections 2.0 through 5.0 and the Appendices.

With regard to Task 1, subtask 1.1, the extension of the basic MEOP design equations to the decentralized case has been accomplished. In the light of previous derivations, subtask 1.2 is an entirely straightforward exercise and the results are to appear in future publications. On the other hand, subtask 1.3 involves significant additional complexities and will be addressed during the second year of this study. Further details on the MEOP design theory extensions carried out as part of Task 1 are given in Section 2.0.

In connection with Task 2, it should be noted that a good qualitative understanding of how the Maximum Entropy modelling approach combined with optimization tends to enforce decentralized control architectures has already been achieved in previous studies and has been documented in numerous publications. Further quantitative characterization of this phenomenon (as proposed in subtask

2.1) demands the prior completion of subtasks 2.2 and 2.3. Thus 2.2 and 2.3 have been given priority during the first year of this study.

The essential problem to be addressed in subtasks 2.2 and 2.3 is the determination of nonconservative bounds on system performance degradation due to uncertainties and/or subsystem interactions. Note that once performance (e.g., line-of-sight error, surface shape errors) degradation is characterized, so is robust stability. Thus both 2.2 and 2.3 are handled by development of a suitable performance robustness analysis. This has been accomplished by the development of a new robustness analysis tool, namely, Majorant Robustness Analysis (MRA). Based upon the work of Ostrowski and Dahlquist on matrix majorants, MRA determines bounds on the degradation of system performance due to unstructured or parametrically structured uncertainties and bounded subsystem dynamics. Since the basic development is carried out in a general operator setting, MRA can be applied within both a frequency-domain/input-output and a time-domain/state-space description. In the frequency domain/input-output setting MRA generalizes previous robustness results (e.g., singular-value analysis), while in the state-space setting, it is fully compatible with MEOP design synthesis. MRA thus provides a design analysis tool which nicely complements our design synthesis theory. Moreover, MRA reveals a direct link between the MEOP stochastic modelling and design formulation and a deterministic bound for robust performance, thereby immensely strengthening the foundations of the Maximum Entropy modelling approach. Section 3.0 sets forth the philosophy of MRA and sketches its theoretical development to date.

Under Task 3, subtask 3.3 requires amalgamating the results of 2.2 and 2.3 with 3.1 and 3.2. Thus, in the past year, subtasks 3.1 and 3.2 were given priority. To accomplish 3.2, the plan is to incorporate the "highly uncertain subsystems" asymptotic solution approach developed in the previous study [40] with the decentralized solution techniques derived within subtask 3.1. Thus, subtask 3.1, the development of efficient procedures for solving the MEOP decentralized design equations, is the crucial step. To complete this task, we have developed an iterative solution approach which reduces the overall problem to the sequential solution of standard MEOP design equations pertaining to each subcontroller. Since, however, each subcontroller problem may be of high dimension and the number of subsystems may often be considerable, it was recognized that an order of magnitude improvement was needed for the efficiency of the MEOP solution algorithm. To provide such improvement, S. Richter has developed and successfully

tested a homotopic continuation algorithm for solving the basic MEOP design equations. In place of solving four nxn (n = dimension of the plant) nonlinear matrix equations (as in the previously developed algorithms), Richter's method reduces the problem to solving four $n_c$xn (n_c = dimension of compensator) linear equations for a modest number of continuation steps. The algorithm converges to machine accuracy and, for n_c small, actually entails less computation than is required for the standard Riccati solutions involved in the full-order compensator. Moreover, using the continuation approach together with topological degree theory, Richter has succeeded in resolving many heretofore intractable issues connected with multiplicity of solutions and convergence to the global minimum. These results essentially complete the theoretical foundation of the optimal projection theory of fixed-order dynamic compensator design. Further details on the iterative approach to decentralized design and on Richter's algorithm are given in Section 4.0.

Finally, both dynamic modelling and determination of baseline centralized control designs have been completed for two realistic example problems thus completing subtask 4.1. The two candidate examples comprise (1) vibration control of the beam subsystem of NASA's COFS I program Flight Test Article and (2) overall space station attitude control combined with pointing control of the solar dynamic concentrator power generation subsystem. Details on the dynamic models and initial control design results for both examples are given in Section 5.0. The second year of this study will follow up this work with (subtask 4.2) detailed decentralized control designs for these examples.

SECTION 2.0

MEOP DESIGN SYNTHESIS EXTENSIONS TO DECENTRALIZED CONTROL

2.0 MEOP DESIGN SYNTHESIS EXTENSIONS TO DECENTRALIZED CONTROL

2.1 Review of Centralized Theory

Optimal projection control-design theory has undergone considerable development over the past several years. As shown in Figure 2.1, optimal projection theory now encompasses problems in reduced order, robust modelling, estimation and control in both continuous-time and discrete-time settings. A comprehensive reference list appears in Section 6.0.

For control-design purposes optimal projection theory provides new machinery for synthesizing multivariable feedback controllers. This machinery consists of a system of algebraic design equations which characterize optimal feedback controllers while accounting for both controller order and parameter uncertainties. The design equations consist of a system of two algebraic Riccati equations and two algebraic Lyapunov equations coupled by both an oblique projection and uncertainty terms. The Riccati equations are directly related to the pair of separated Riccati equations arising in LQG theory. Indeed, when the controller order is set equal to the order of the plant and all uncertainties are absent, then the design equations specialize immediately to the standard LQG equations. Numerical algorithms for solving these equations are described in Section 4.0. Further discussion of centralized MEOP theory can be found in [69] (see Appendix A).

2.2 Extensions to Decentralized Controllers

In keeping with the optimal projection philosophy, our approach to decentralized control design is based upon fixed-structure optimization. That is, we assume that the structure of the controller is determined by implementation constraints and/or subsystem analysis. Once the controller architecture is fixed, the feedback gains can be chosen to optimize the performance functional for the closed-loop system. Of course, this approach can be used to determine preferable controller architectures by varying the decentralized information structure and optimizing the performance of each configuration.

The fixed structure approach is distinct from methods which are based upon subsystem decomposition with centralized design procedures applied to the

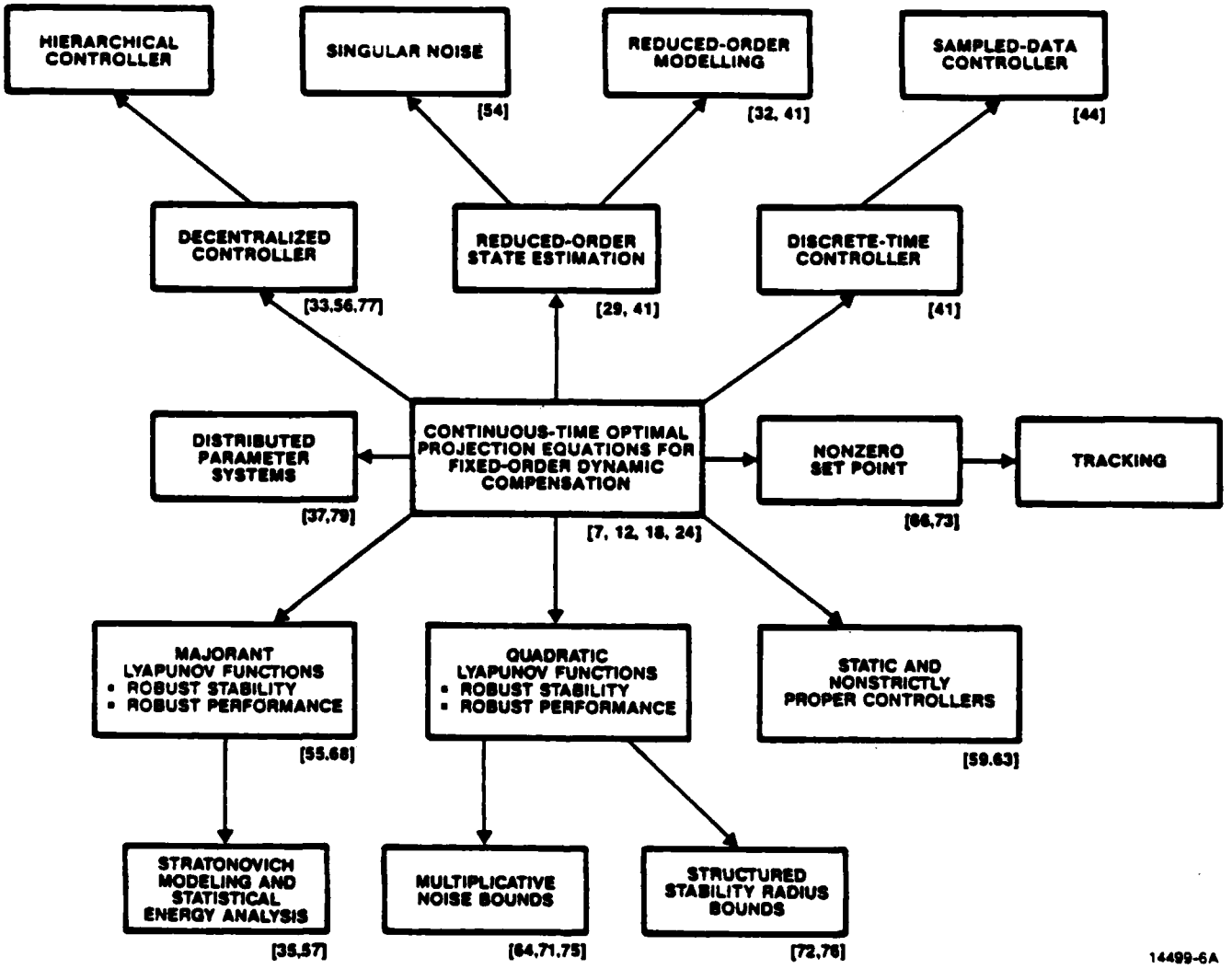

Figure 2.1. Scope of MEOP

individual subsystems. For such methods there remains the problem of determining conditions under which the reassembled closed-loop system has acceptable behavior. An additional drawback of decomposition methods is that the decentralized controller architecture specified by implementation constraints may be completely unrelated to desirable architectures arising from physical considerations. For example, physical implementation constraints may impose a particular decentralized architecture which does not correspond to any discernible dynamical decomposition. Furthermore, subsystem decomposition as a design tool may constrain the class of attainable designs at the expense of achievable performance.

Of course, in many cases, such as in the presence of high dimensionality, subsystem decomposition is absolutely essential for making progress in designing decentralized controllers. However, only by developing methods which avoid unnecessary constraints on the design space can the efficiency of decomposition methods be assessed. Furthermore, methods which retain the full system dynamics may provide a useful context for applying existing decomposition techniques as well as an advantageous starting point for developing new methods.

Our overall approach is thus to regard the fixed-structure approach as complementary to subsystem decomposition techniques. To this end, majorant robustness analysis has been developed (see Section 3.0) to account for subsystem interactions arising, for example, from system uncertainties. In addition, majorant robustness analysis is closely related to MEOP synthesis particularly with regard to nondestabilizing uncertainties.

2.2.1 Decentralized Controller Design for Static Controllers

We first consider the problem in which each subcontroller is assumed to be static, i.e., a fixed gain multiplying the measurements. For realism, of course, only the physical measurements are assumed to be available for feedback. Earlier versions of this problem were considered in [2.1, 2.2]. The most general treatment of this problem obtained thus far can be found in [77] (see Appendix B). The development in [77] includes, in particular, noisy and nonnoisy measurements, weighted and unweighted controls, and parameter uncertainties in the A, B and C matrices. The optimality conditions for this problem are given in the form of a pair of modified Riccati equations coupled by a pair of oblique projections corresponding, respectively, to singular measurement noise and

singular control weighting. By utilizing a Lyapunov function to guarantee robust stability, these optimality conditions serve as sufficient conditions for robust stability and performance over a specified range of parametric uncertainty.

2.2.2 Decentralized Controller Design for Dynamic Controllers

A more complex situation arises when the decentralized subcontrollers are allowed to be fixed-order dynamic compensators. In this case it does not appear possible to characterize optimal gains for each subcontroller explicitly in terms of the plant dynamics alone. This situation arises from the fact that each subcontroller must be a projection of the dynamics of the controlled system which, in this case, is not just the original plant but rather the original plant augmented by the remaining subcontrollers' dynamics. It would be desirable, of course, if each subcontroller could be characterized by an nxn projection. This expectation is unrealistic, however, since each dynamic subcontroller increases the dimension of the closed-loop system. Hence each projection for the individual subcontrollers must account for the dimension augmentation.

Thus we have discovered that optimal decentralized dynamic compensator design must be viewed as a collection of subcontroller designs obtained for an augmented system. Essentially, each subcontroller is viewed as a reduced-order controller for the plant augmented by all other subcontrollers. This problem is thus a direct application of centralized optimal projection theory. To apply centralized theory each dynamic subcontroller can be determined sequentially, accounting fully for previously specified subcontrollers. After initial gains have been specified for each subcontroller, the overall design can be refined sequentially by replacing current subcontroller gains with improved gains. Finally, subsystem decomposition techniques are relevant to the approach suggested here by providing a near-optimal starting point for subsequent refinement.

In sequentially applying reduced-order design methods to decentralized control, a number of issues immediately arise, including the subcontroller refinement sequence, feasibility of the reduced-order design method at each step, and convergence of the overall process. Note that after initial gain determination the existence of a stabilizing design at each step is not at issue here since at least one stabilizing controller exists, namely, the present gain values supplied by the previous step. One of the chief concerns, however, is that the reduced-order design method be sufficiently reliable to permit flexibility in

choosing the refinement sequence. Many reduced-order design methods do not, however, consistently yield stabilizing controllers of a given order even when stabilizing controllers are clearly known to exist. For example, in [74] (see Appendix E), the LQG reduction methods reviewed in [2.3] were compared to the optimal projection approach to fixed-order dynamic compensation. For an 8th-order example over a range of control authorities, only the optimal projection approach consistently provided stable designs for each case considered. Thus, the optimal projection approach appears to be suitable for reliable sequential subcontroller refinement.

In addition to reliably producing stable designs at each step, the optimal projection approach is based upon a quadratic performance criterion which readily permits assessment of convergence of the refinement procedure. Specifically, at each subcontroller refinement step, a given subcontroller is replaced by an improved subcontroller. Here "improved" refers to the situation in which all subcontrollers except one are "frozen," while the performance functional is optimized with espect to the remaining free gains. If this procedure is feasible at each step and if the global minimum for each subcontroller design problem is attainable, then the closed-loop performance must improve at each step. Since the performance is also bounded below by zero, then it must converge. Although such observations are immediate, they depend upon optimality considerations and hence are not valid for most reduced-order control-design procedures.

As discussed previously, stabilizability is not the issue here; after subcontroller initialization at least one stabilizing controller at each refinement step exists, namely, the gains provided by the previous step. Hence the principal remaining issues concern the existence of and ability to compute the global optimum. Using topological degree theory and homotopic continuation methods, these issues have been addressed in [58] (see Appendix F). These results show that the local extremals can be enumerated from the basic problem data and the global optimum can be efficiently computed. Furthermore, one of the principal results of [58] states that when the compensator order is greater than either the number of inputs or outputs minus the dimension of the unstable subspace, then the equations possess no more than one solution corresponding to the global minimum.

An immediate insight from this approach is the realization that design methods which fail to account for this intrinsic coupling are necessarily

suboptimal. In certain cases, such as in the presence of high dimensionality, it may not be possible to precisely account for the coupling. In such cases the optimal projection approach provides a rigorous context for determining suboptimal solutions.

A numerical example demonstrating the optimal projection approach for decentralized dynamic controllers is given in [56] (see Appendix C). The example involves a pair of simply supported Euler-Bernoulli beams interconnected by a spring. The objective of the problem is to design a two-channel decentralized controller with one subcontroller assigned to each beam. After selecting starting values for a pair of decentralized fourth-order subcontrollers, the optimal projection equations were used to iteratively refine the subcontroller gains. Closed-loop performance was improved at each iteration and convergence was attained.

2.3 References

[2.1] J. Medanic, "On Stabilization and Optimization by Output Feedback," Proc. Twelfth Asilomar Conf. Circ., Sys. Comp., pp. 412-416, 1978.

[2.2] S. Renjen and D.P. Looze, "Synthesis of Decentralized Output State Regulators," Proc. Amer. Contr. Conf., Arlington, VA, pp. 758-762, 1982.

[2.3] Y. Liu and B.D.O. Anderson, "Controller Reduction Via Stable Factorization and Balancing," Int. J. Contr., Vol. 44, pp. 507-531, 1986.

SECTION 3.0

PERFORMANCE DEGRADATION DUE TO UNCERTAINTIES AND SUBSYSTEM INTERACTIONS VIA MAJORANT ANALYSIS

3.0 PERFORMANCE DEGRADATION DUE TO UNCERTAINTIES AND SUBSYSTEM INTERACTIONS VIA MAJORANT ANALYSIS

The problem addressed here is the determination of bounds on the degradation of system performance due to uncertainties and/or unforeseen and imperfectly modelled subsystem interactions. Such bounding techniques represent a fundamental systems analysis tool that is indispensable for further elucidation of decentralized controller architectures and robust design.

Extensive work has been carried out within the controls community in the area of frequency-domain analysis of robust stability giving rise to the H-infinity theory of robustness characterization and robust design [3.1-3.5]. However, on several occasions we have remarked that although the H-infinity world-view is a beautiful and compelling theory within its proper province, its fundamental assumptions render it inapplicable to structural vibration control which involves parametric and often nondestabilizing open-loop uncertainties. A principal difficulty is the conservatism of H-infinity robustness characterizations. A stability robustness analysis technique is called conservative if the predicted set of nondestabilizing perturbations is a proper subset of the actual set of nondestabilizing perturbations. Note that conservatism jointly depends upon both the definition of admissible perturbation classes and the robustness analysis technique.

The well-known conservatism of H-infinity theory does not arise because it operates in the frequency domain, per se, or because the infinity norm is employed, but rather because of the crudeness of H-infinity bounds. What is the fundamental source of this crudeness? Possibly this arises because the fundamental intent of H-infinity development was the extension of classical control design concepts to the multivariable case whether or not classical concepts are truly suited to the problem at hand.

For example, in keeping with classical ideas, there has been widespread insistence upon couching all questions of performance and uncertainty in terms of simplistic (albeit traditional) unity gain feedback diagrams. Thus, singular value developments have lumped uncertainty in a single block thereby obscuring the often complex structure of modelling error. Moreover, this feedback paradigm is maintained even for structured uncertainty approaches [3.6].

Here, we contend that to achieve a less confining point of view, the first step is to represent uncertain systems by means of a large-scale system input-output formulation as depicted in Figure 3.0-1.

Referring to Figure 3.0-1, the overall system is represented by interconnected subsystems undergoing interactions. The subsystems, characterized by the operators G_k (k=1,...,r), represent the known dynamics of the system while the subsystem interactions, given by the operators H_{kj}, correspond to uncertainties. Note that the partitioned off-block-diagonal operator H is stipulated to belong to some compact arcwise connected set $\underline{H}$. The set $\underline{H}$ specifies both the character and extent of dynamical uncertainties.

The motivation for the above input-output formulation within the context of large-scale systems is obvious. But in addition, thanks to the Dynamic Inclusion Principle and related ideas elaborated by Siljak and his co-workers [3.7, 3.8] the representation of Figure 3.0-1 is also suitable for parametric perturbations in monolithic systems, i.e., systems without explicit interconnections.

The problem now addressed is how to bound the degradation of the system output vector y or the prediction accuracy $y-y_0$ due to the uncertainties.

To give this problem mathematical form, we must use the block-matrix results of Ostrowski [3.9] and define the <u>block-Lp norm matrix</u> of a partitioned operator $\widetilde{M}$ and the block-norm matrix of a partitioned matrix M as in the top half of Figure 3.0-2. With these definitions, the principal problem is to bound the block-norm vector of the system output y over all variations of the uncertain perturbations, i.e., bound $|y|_L$ as H varies over the whole set $\underline{H}$. Incidentally, bounding off-nominal prediction errors is handled similarly and so will not be given separate treatment here.

Referring again to Figure 3.0-2, it is evident that a suitable bound for $|y|_L$ takes the form of a <u>nonnegative matrix</u> (all elements nonnegative) (the "gain matrix" $\underline{\hat{L}}$) multiplied by the block-norm vector of the nominal output. Note that the double inequality sign relating two matrices indicates element-by-element inequality. The matrix $\underline{\hat{L}}$ is just a nonnegative bound on the <u>worst-case</u> value of the block-Lp norm matrix of the <u>output gain operator</u> $\underline{L}$. Note that, in essence, $\underline{\hat{L}}$ maps the nominal output into the actual output as corrupted by uncertain

LARGE-SCALE SYSTEM-INPUT-OUTPUT FORMULATION

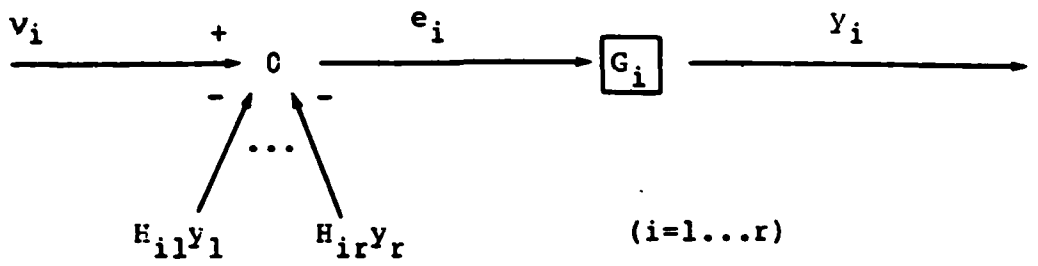

$$(I + GH)y = y_C$$

$$y_0 \triangleq Gv$$

$$G = \underset{k=1\ldots r}{\text{block-diag}}\ \{G_k\}; \qquad G_k \text{ known}$$

$$H = \begin{bmatrix} 0 & H_{12} & H_{13} & \cdots \\ H_{21} & C & H_{23} & \\ H_{31} & H_{32} & 0 & \\ \vdots & & & \end{bmatrix} \quad \epsilon\, \mathcal{H}$$

$\mathcal{H}$, some compact, arcwise connected set with off-diagonal block structure

uncertain subsystem interactions or parametric uncertainties

$\mathcal{H}$ specifies uncertainty about H

Problem: Bound output y or deviation from nominal, $y-y_0$, for all $H \epsilon \mathcal{H}$

Figure 3.0-1. Large-Scale System Input-Output Formulation

(A.M. Ostrowski, J. Math. Anal. Appl., Vol. 2, pp. 161-209, 1961.)

Block-L_p norm matrix of $\tilde{M}$:

$$|\tilde{M}|_{L_p} = \begin{bmatrix} \|\tilde{M}_{11}\|_{L_p} & \|\tilde{M}_{12}\|_{L_p} \cdots \\ \|\tilde{M}_{21}\|_{L_p} & \|\tilde{M}_{22}\|_{L_p} \cdots \\ \vdots & \vdots \end{bmatrix} \in R_+^{r \times r}$$

Block-norm matrix of M:

$$|M|_p = \begin{bmatrix} \|M_{11}\|_p & \|M_{12}\|_p \cdots \\ \|M_{21}\|_p & \|M_{22}\|_p \cdots \\ \vdots & \vdots \end{bmatrix} \in R_+^{r \times r}$$

Output bound:

$$|y|_L \leq \hat{y} = \hat{\mathcal{L}}\hat{y}_0$$

where $\hat{\mathcal{L}} \in R_+^{r \times r}$ and

$$\hat{\mathcal{L}}(\mathcal{H}) \geq \sup_{H \in \mathcal{H}} |\mathcal{L}|_L = \mathcal{L}^*(\mathcal{H})$$

where:

$$(I + GH)\mathcal{L} = \mathcal{I} \; ; \; |\mathcal{I}|_L = I$$

Conservative bound: $\hat{\mathcal{L}} \geq \mathcal{L}^* \; ; \; \hat{\mathcal{L}} \neq \mathcal{L}^*$

Nonconservative bound: $\hat{\mathcal{L}} = \mathcal{L}^*$

Finite $\hat{\mathcal{L}}(\mathcal{H})$ exists ===> Input-Output L_p stability

Figure 3.0-2. Block-Norm Matrices

interactions. In the following, we focus on bounding the gain operator. Note (from the bottom of Figure 3.0-2) that this formulation gives rise to a clear definition of conservatism. Note also that the existence of a finite bound $\hat{\underline{L}}(\underline{H})$ implies input-output stability (see [3.10]). Thus robust stability and performance degradation can be handled by one and the same theoretical apparatus.

Now, the above articulation of uncertainties into numerous interactions permits more finely articulated methods of computing bounds beyond singular value analysis, namely, methods associated with the majorant analysis of Dahlquist [3.11].

Following Dahlquist, we define the majorant and minorant matrices of a partitioned matrix or operator as in the top portion of Figure 3.0-3. The inequalities shown in the center of the figure follow directly from the definitions and indicate that the majorant and minorant are matrix generalizations of the maximum and minimum singular values, respectively. Moreover, these inequalities can be very efficently used to bound the block-Lp norm matrix of the output gain operator. In fact, what we seek is merely some majorant of the gain operator.

Figure 3.0-4 shows a simple example of how the inequalities of Figure 3.0-3 can be used to derive such a majorant for the gain operator, starting from the defining relation

$$(I + GH)\underline{L} = \underline{I}$$

for $\underline{L}$ given in Figure 3.0-2. The result obtained in Figure 3.0-4, namely:

$$|\underline{L}|_L \leq \leq \hat{\underline{L}}$$

$$(I-GH)\underline{L} = I_r$$

is, in fact, the crudest possible majorant bound and is equivalent to the small gain theorem for Lp input-output stability of a large scale-system [3.10]. When there is only one system block, this further reduces to the singular-value bound as a very particular special case.

(G. Dahlquist, Lin. Alg. Appl., Vol. 52/53, pp. 199-216, 1983)

Majorant: $\hat{A} \in R_+^{rxr}$; $\hat{A} \geq\geq |A|_L$

Minorant: $\check{A} \in Z^{rxr}$; $\check{A}_{kk} \leq \|A_{kk}^{-1}\|_L^{-1}$

$\check{A}_{kj} \leq - \|A_{kj}\|_L$; $k \neq j$

Inequalities:

$$|AB|_L \leq\leq \hat{A}\hat{B}$$

$$|A + B|_L \leq\leq \hat{A} + \hat{B}$$

$$|A^{-1}|_L \leq\leq (\check{A})^{-1}$$

$$\check{A} - \hat{B} = \text{minorant of } A + B$$

* $\hat{A}$ and $\check{A}$ are generalizations of maximum and minimum singular values

* Majorant/Minorant inequalities can be used to develop bounds on $|\mathcal{L}|_L$

Figure 3.0-3. Matrix Majorants and Minorants

$$|\mathcal{L}|_L = |(I + GH)^{-1}\mathcal{L}|_L$$

$$\leq\!\!\leq \overbrace{[(I+GH)^{-1}\mathcal{L}]}^{\mathcal{H}}$$

$$\leq\!\!\leq \overbrace{[(I+GH)^{-1}]}^{\mathcal{H}}\hat{\mathcal{L}}$$

$$\leq\!\!\leq \overbrace{[(I+GH)]}^{\mathcal{H}}{}^{-1} \qquad (|\mathcal{L}|_L = I)$$

$$\leq\!\!\leq [(I-\widehat{GH})^{*}]^{-1}$$

$$\leq\!\!\leq [(I-\hat{G}\hat{H})]^{-1}$$

$$\Downarrow\Downarrow$$

$$|\mathcal{L}|_L \leq\!\!\leq \hat{\mathcal{L}}$$

$$(I-\hat{G}\hat{H})\hat{\mathcal{L}} = I_r$$

* Bounding $|\mathcal{L}|_L$ means: Find a majorant of $\mathcal{L}\ \forall\ H \in \mathcal{H}$

* This is the crudest possible bound,
  $r = 1$ ==> singular value inequality

* There are much more refined bounds
  - obtained by iteration of operators...

Figure 3.0-4. Example of Bound Derivation

But the uncertain subsystem interaction format (introduced in Figure 3.0-1) in conjunction with majorant analysis gives an almost unlimited potential for formulating sharper bounds. Using a process of operator iteration, one can obtain the results displayed in the top half of Figure 3.0-5. Here we have a hierarchy of output bounds, where each successive member of the hierarchy requires more and more information but is less and less conservative (with respect to the set H). For the results shown in Figure 3.0-5, the sequence of bounds approaches the least upper bound under a norm-bounded uncertainty set, i.e., for this set H the hierarchy is nonconservative in the limit! Note also that, because we work in an operator setting, distinctions between the time and frequency domains are blurred. It is parochial to assert that only frequency-domain or time-domain methods must be used. What's needed is easy and fluent translation between the frequency and time-domain as provided here. Furthermore, the computational advantage of this kind of hierarchy is that each bound requires only the inversion of an M-matrix. This is quite straightforward and nicely tractable, even for many subsystems, since it involves computing a monotonically increasing sequence where each iteration involves an addition and a multiplication of low-order matrices. Figure 3.0-6 summarizes the relevant facts on the solution of majorant equations. One has only to contrast the simplicity of these results with the difficulties of the μ-function computation [3.12] to appreciate the power of the "uncertain subsystem" representation of Figure 3.0-1 and its allied bounding technique, majorant analysis.

The above discussion has set forth the general development of majorant robustness analysis within an operator setting which employs Lp norms to describe the "size" of subsystem outputs. For systems with stochastic inputs and time independent parameter uncertainties, the main lines of development are analogous. However, in this case one needs to work with the Lyapunov equation for the steady-state second-moment matrix of response and then derive majorant bounds for the block-norm matrix of the second moment. The general setup for undertaking majorant analysis for parametrically uncertain stochastic systems is shown in Figure 3.0-7. Here, the block-diagonal matrix A represents the known subsystem or nominal system dynamics while the off-block-diagonal matrix G represents uncertain subsystem interactions or parametric uncertainties. Generally, G is stipulated to be some element of a compact, arcwise connected set G which describes the geometry and severity of uncertainties. The simplest prescription, for example, is that G contains all off-diagonal block matrices such that the norm of each off-diagonal block is bounded by a stipulated number.

nth (m = 0, 1,...) member:

$$|\mathcal{L}|_L \leq\leq L^{(m)} \quad \forall \; H \in \mathcal{H}$$

$$(I-\mathcal{G}^{(m)})L^{(m)} = \mathcal{M}^{(m)}$$

$$G^{(m)} \triangleq \sup_{H\in\mathcal{H}} |(GH)^{2^m}|_L \in R_+^{rxr}$$

$$\mathcal{M}^{(m)} \triangleq \sup_{H\in\mathcal{H}} \left| \prod_{r=0}^{m-1} (I+(-GH)^{2^r}) \right|_L \in R_+^{rxr}$$

* Each member of the hierarchy requires more information and is sharper and sharper:

$$L^{(0)} \geq\geq L^{(1)} \geq\geq L^{(2)} \geq\geq \ldots$$

* Lowest member: $L^{(0)} = (I-\widehat{GH}^*)^{-1}$

* If $\mathcal{H} \triangleq \{H: |H|_L \leq\leq \bar{H} \in R_+^{rxr};\ \bar{H}_{kk} = 0\}$, then:

$$\lim_{m\to\infty} L^{(m)} = \mathcal{L}^*(\mathcal{H})$$

  - i.e. $L^{(m)}$ is <u>nonconservative</u> in the limit

* Input data can be given in time-domain or frequency domain - <u>as appropriate</u>

* Each member of the hierarchy requires only inversion of an rxr M-matrix

Figure 3.0-5. Hierarchy of Lp Output Bounds

All majorant bounds involve equations of the form:

$$(I_r - B)L = C$$

$$C,\ B \in R_+^{r \times r}$$

* $L \in R_+^{r \times r}$ exists iff $(I-B)$ is a nonsingular M-matrix

* $L \in R_+^{r \times r}$ exists iff the sequence:

$$L_0 = 0$$

$$(I-\{B\})L_{n+1} = \langle B \rangle L_n + C$$

($\{B\} \triangleq$ diagonal part of B
$\langle B \rangle \triangleq B - \{B\}$)

converges. If so, $L = \lim_{n \to \infty} L_n$

* $L \in R_+^{r \times r}$ exists iff the sequence:

$$\Lambda_0 = (I-\{B\})^{-1}\langle B \rangle,\ S_0 = I + \Lambda_0$$

$$K \geq 0:\ \Lambda_{k+1} = \Lambda_k^2\ ;\ S_{k+1} = S_k(I+\Lambda_{k+1})$$

converges. If so:

$$L = \lim_{k \to \infty} S_k (I-\{B\})^{-1} C$$

(nth iterate = 2^n simple iterations)

Figure 3.0-6. Solution of M-Matrix Equations

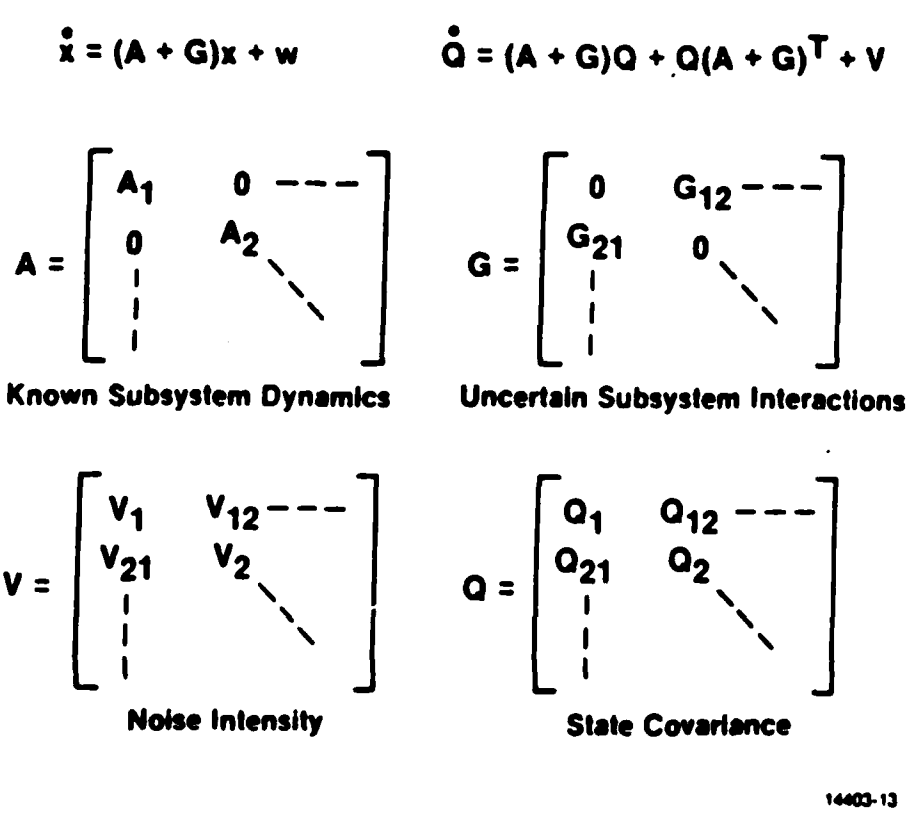

Figure 3.0-7. Subsystem Interaction Model

Note that the disturbance intensity V and the second-moment matrix Q are partitioned conformably with A and G. We bound performance degradation due to uncertain interactions G ranging over the admissible set $\underline{G}$ by bounding the block-norm matrix of Q. To do this, however, requires additional algebraic tools, such as the matrix calculus which centers on the VEC operator and the Kronecker product and Kronecker sum. These operations, which are defined by the relations shown in Figure 3.0-8, are critical to the development. The reader is encouraged to consult the review paper by Brewer [3.13] for a thorough discussion of the matrix calculus. Because of the algebraic complexity of deriving majorants for the second-moment matrix, the matrix calculus is far more than a mere notational convenience.

For our development, the standard matrix calculus is a completely adequate tool only when each subsystem (with dynamics A_k, k=1,...,r) is one-dimensional. However, we are concerned with systems composed of many high-dimensional subsystems. To handle the algebraic work, one needs a generalization of the matrix calculus, namely, the block-matrix calculus. The underlying operations of the VECb operator are the block Kronecker product and sum which are displayed in Figure 3.0-9. Note that while the VEC operator stacks the

~ Definitions ~

(J. W. Brewer, IEEE Trans. Circ. Sys., Vol. CAS-25, pp. 772-781, 1978.)

$(M, A, B \in R^{nxn})$

VEC operator, vec(M):

$$\text{vec}(M) \triangleq \begin{pmatrix} M_{11} \\ M_{21} \\ \vdots \\ M_{n1} \\ --- \\ M_{12} \\ M_{22} \\ \vdots \\ M_{n2} \\ --- \\ \vdots \end{pmatrix}$$

Kronecker Product, $\otimes$

$$A \otimes B \triangleq \begin{bmatrix} a_{11}B & a_{12}B & \cdots & a_{1n}B \\ a_{12}B & a_{22}B & \cdots & a_{2n}B \\ \vdots & \vdots & & \vdots \\ a_{n1}B & a_{n2}B & \cdots & a_{nn}B \end{bmatrix}$$

Kronecker Sum, $\oplus$

$$A \oplus B \triangleq A \otimes I_n + I_n \oplus B$$

Figure 3.0-8. Matrix Calculus

~ Definitions ~

1. Block vec operator, vecb(M).

$$\text{If } M = \begin{bmatrix} M_{11} & M_{12} & \cdots \\ M_{21} & M_{22} & \\ \vdots & & \end{bmatrix}, \text{ then:}$$

$$\text{vecb } M \triangleq \begin{pmatrix} \text{vec } M_{11} \\ \text{vec } M_{21} \\ \vdots \\ \text{vec } M_{r1} \\ \hline \text{vec } M_{12} \\ \vdots \\ \text{vec } M_{r2} \\ \hline \vdots \end{pmatrix}$$

2. Block Kronecker Product, $\bar{\otimes}$

$$A \mathbin{\bar{\otimes}} B \triangleq \begin{bmatrix} A_{11} \circledast B & A_{12} \circledast B & \cdots & A_{1r} \circledast B \\ A_{21} \circledast B & A_{22} \circledast B & \cdots & A_{2r} \circledast B \\ \vdots & & & \\ A_{r1} \circledast B & A_{r2} \circledast B & \cdots & A_{rr} \circledast B \end{bmatrix}$$

where:

$$M \circledast A \triangleq \begin{bmatrix} M \otimes A_{11} & M \otimes A_{12} & \cdots & M \otimes A_{1r} \\ M \otimes A_{21} & M \otimes A_{22} & \cdots & M \otimes A_{2r} \\ \vdots & & & \\ M \otimes A_{r1} & M \otimes A_{r2} & \cdots & M \otimes A_{rr} \end{bmatrix}$$

3. Block Kronecker Sum, $\bar{\oplus}$

$$A \mathbin{\bar{\oplus}} B \triangleq A \mathbin{\bar{\otimes}} I + I \mathbin{\bar{\otimes}} B$$

4. $\{\cdot\}$, $\langle\cdot\rangle$ and vecbd:

$$\{M\} \triangleq \text{bl-diag } \{M_{kk}\}, \quad \langle M \rangle \triangleq M - \{M\}$$

$$\text{vecbd } M \triangleq \begin{pmatrix} \text{vec } M_{11} \\ \text{vec } M_{22} \\ \text{vec } M_{rr} \end{pmatrix}$$

Figure 3.0-9. Block Matrix Calculus

columns of a matrix into a vector, the VECb operator stacks the VEC's of the columns of subblocks in a partitioned matrix. When, referring to Figure 3.0-9, the subblocks of the partitioned matrix M are all one-dimensional, the block matrix calculus definitions revert to those given in Figure 3.0-8. Moreover, the block matrix calculus is endowed with the same battery of identities as is standard in the matrix calculus. These identities, shown in Figure 3.0-10, are invaluable in effecting the required algebraic manipulations to obtain the results discussed below.

In particular, using the block matrix calculus, one can first reduce the second-moment Lyapunov equation into a rather compact equation determining the diagonal subblocks (the individual subsystem second-moment matrix) alone. This equation is the second from the top in Figure 3.0-11. With this as the starting point, one then applies majorant analysis to obtain a hierarchy of majorant bounds as shown in the bottom half of Figure 3.0-11. As in the Lp bound analysis, each successive member of the hierarchy offers less and less conservative bounds.

Note that having obtained the expressions shown in Figure 3.0-11, we do not calculate the block-Kronecker sums and products explicitly. Rather, in each case, we reverse the VECb operator to reduce each member of the hierarchy of bounds to a low-order modified Lyapunov equation for the matrix majorant of the second-moment matrix.

We now consider in more detail the first two members of the majorant hierarchy in order to illustrate the specific forms of the modified Lyapunov equations that are obtained.

For example, Figure 3.0-12 shows the first member of the second-moment majorant hierarchy. This gives the majorant Q as the solution of a simple nonnegative matrix equation, where * denotes the Hadamard (element by element) product and the row and column dimension of the equation in the number of subsystems. For the norm-bounded uncertainty set shown in Figure 3.0-12, the existence of a nonnegative solution implies a bound for the block-norm matrix of the second moment and robust stability, i.e., (A+G) is stable for all perturbations G in the norm-bounded set.

Identities

I.1 $(A+B) \bar{\otimes} C = A \bar{\otimes} C + B \bar{\otimes} C$

I.2 $A \bar{\otimes} (B+C) = A \bar{\otimes} B + A \bar{\otimes} C$

I.3 $(A \bar{\otimes} B)^T = A^T \bar{\otimes} B^T$

I.4 $(A \bar{\otimes} B)(C \bar{\otimes} D) = (AC) \bar{\otimes} (BD)$

I.5 $(A \bar{\otimes} B)^{-1} = A^{-1} \bar{\otimes} B^{-1}$

I.6 $\text{vecb}(AYB) = (B^T \bar{\otimes} A)\text{vecb } Y$

I.7 $\text{vecb}(AX + XB) = (B^T \bar{\oplus} A)\text{vecb}X$

I.8 $\text{vecb}(\{M\}) = \mathcal{E}\,\text{vecb}(M)$

$$\mathcal{E} \triangleq \sum_{k=1}^{r} \hat{e}^{(k,k)} \bar{\otimes} E^{(k,k)}$$

$$\hat{e}^{(k,k)} \triangleq \underset{m=1..r}{\text{diag}} \{\delta_{km}\}$$

$$E^{(k,k)} \triangleq \underset{m}{\text{bl-diag}} \{I_{n_k}\ \delta_{km}\}$$

I.9 $\text{vecb}(\langle M \rangle) = \mathcal{E}_1\,\text{vecb}(M); \quad \mathcal{E}_1 \triangleq I_{n^2} - \mathcal{E}$

I.10 $\text{vecb}(\{M\}) = \hat{\mathcal{E}}\,\text{vecbd}(M)$

$$\hat{\mathcal{E}} \triangleq \sum_{k=1}^{r} e^{(k,k)} \bar{\otimes} E^{(k,k)}; \quad e_n^{(k,k)} = \delta_{nk}$$

I.11 $\hat{\mathcal{E}}^T\hat{\mathcal{E}} = I_n$

I.12 $\hat{\mathcal{E}}^T\hat{\mathcal{E}} = \hat{\mathcal{E}}^T$

Figure 3.0-10. Identities for the Block Matrix Calculus

$$0 = (A+G)Q + Q(A+G)^T + V$$

$$\Updownarrow$$

$$[v + p] \begin{pmatrix} \text{vec } Q_{11} \\ \text{vec } Q_{22} \\ \vdots \\ \text{vec } Q_{rr} \end{pmatrix} = \begin{pmatrix} \text{vec } V_{11} \\ \text{vec } V_{22} \\ \vdots \\ \text{vec } V_{rr} \end{pmatrix}$$

$$v \triangleq - \underset{k=1\ldots r}{\text{block-diag}} (A_k \oplus A_k)$$

$$p \triangleq \hat{\mathcal{E}}^T(G \bar{\oplus} G)\mathcal{E}_1[A \bar{\oplus} A + G \bar{\oplus} G]^{-1}\mathcal{E}_1(G \bar{\oplus} G)\hat{\mathcal{E}}$$

Letting $\mathcal{Q} \triangleq (\hat{Q}_{11}, \hat{Q}_{22}, \ldots \hat{Q}_{rr})$; $\gamma \triangleq (\hat{V}_{11}, \hat{V}_{22}, \ldots \hat{V}_{rr})$ apply majorant analysis to get a <u>hierarchy</u> of bounds for the majorant of vecbd Q:

<u>1st member</u>:

$$[\hat{v} - \hat{\mathcal{E}}^T(\hat{G} \bar{\otimes} \hat{G})\mathcal{E}_1[A \bar{\oplus} A - \hat{G} \bar{\oplus} \hat{G}]^{-1}\mathcal{E}_1(\hat{G} \bar{\oplus} \hat{G})\hat{\mathcal{E}}]\mathcal{Q} = \gamma$$

<u>2nd member</u>:

$$[\hat{v}_2 - \hat{p}_2]\mathcal{Q} = \gamma$$

$$v_2 \triangleq v + \hat{\mathcal{E}}^T(G \bar{\oplus} C)(A \bar{\oplus} A)^{-1}(G \bar{\oplus} G)\hat{\mathcal{E}}$$

$$p_2 \triangleq \hat{\mathcal{E}}^T(G \bar{\oplus} G)(A \bar{\oplus} A)^{-1}\mathcal{E}_1 G \bar{\oplus} G[A \bar{\oplus} A + G \bar{\oplus} G]^{-1}\mathcal{E}_1(G \bar{\oplus} C)\hat{\mathcal{E}}$$

$\vdots$

etc.

Figure 3.0-11. A Hierarchy of Majorant Bounds for the Second-Moment Matrix

$$\mathcal{A} * \hat{Q} = \mathcal{G}\hat{Q} + \hat{Q}\mathcal{G}^T + \mathcal{V}$$

$$\bar{\sigma}(G_{ij}) \leq \mathcal{G}_{ij}$$

$$\Downarrow$$

$$Q \leq\leq \hat{Q}$$

$$\Downarrow$$

- **Robust Stability**
- **Robust Performance**

14403-16

Figure 3.0-12. Majorant Lyapunov Equation

One particular advantage of the first member of the hierarchy is that it correctly shows the effect of wide frequency separation of subsystems on performance degradation and robust stability. This effect is illustrated in Figure 3.0-13. Here we have two subsystems whose poles are indicated by the crosses in the complex plane, with γ denoting the minimum damping of the subsystems and $\omega_1 - \omega_2$ the minimum separation in frequencies. The majorant equation in Figure 3.0-12 gives the expression shown in Figure 3.0-13 for the square of the tolerable interaction strength under which stability is preserved. Thus, if the frequency separation $(\omega_1 - \omega_2)$ is large, then even very large uncertain interactions can be tolerated. In contrast, the vector Lyapunov function theory of [3.7, 3.8] would give γ^2 which is a much more conservative result for lightly damped systems. Thus, the majorant equation will correctly predict that as frequency separation becomes sufficiently large, subsystems become effectively decoupled. Such predictions cannot be made by the small gain theorem for large-scale systems or by vector Lyapunov theory. Thus, even the first member of the majorant hierarchy offers greatly reduced conservatism compared to previous results.

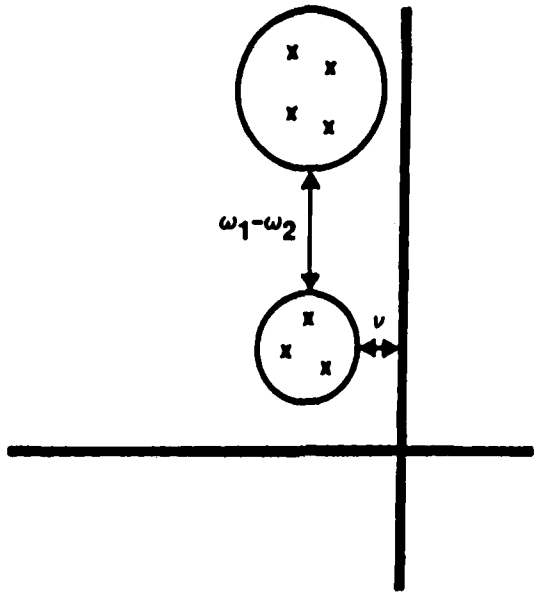

Majorant Lyapunov Equation Bound $\sim \nu \sqrt{(2\nu)^2 + (\omega_1-\omega_2)^2}$

14403-22

Figure 3.0-13. Robustness Due to Weak Subsystem Interaction

Moreover, note that thanks to the properties of M-matrices, the first (and all higher) members of the hierarchy of majorant bounds require only a simple iterative sequence for their computation. The relevant facts are summarized in Figure 3.0-14. The sequence is monotonically nondecreasing, and each iterate requires only two matrix additions, two multiplications and a Hadamard product for its computation. Convergence of the sequence implies robust stability while the degradation of a quadratic performance index J from its nominal (zero interaction) value J_0 is given in terms of $\underline{Q}$ by the simple expression at the bottom of Figure 3.0-14.

Furthermore, the second member of the second-moment majorant hierarchy, shown in Figure 3.0-15, gives even tighter bounds and can even predict the stabilizing effect of certain kinds of perturbations. The form of the majorant equation (top of Figure 3.0-15) is similar to the first member of the hierarchy except that the operator $\underline{H}[\underline{Q}]$ appears. This operator is precisely what would arise in the equation for the second-moment matrix for a system with Stratonovich noise parameters! So far, we have discussed a design analysis tool for predicting performance degradation due to uncertainty. This crucial observation brings us to

MLE has a unique solution iff $\{\hat{Q}_K, K=0, 1, \ldots, \infty\}$ where:

$$\hat{Q}_0 = 0$$

$$\hat{Q}_{K+1} = \mathcal{M}\{\cdot\} + (\mathcal{G}\hat{Q}_K + \hat{Q}_K\mathcal{G}^T + \mathcal{V})$$

$$(\mathcal{M}\{\cdot\}_{mn} \triangleq \mathcal{M}^{-1}_{mn})$$

converges. If so, then:

$$\hat{Q} = \lim_{K\to\infty} \hat{Q}_K$$

$$J - J_0 \leq 2\sum_{K=1}^{r} (\mathrm{tr}\,\hat{P}_K)(\mathcal{G}\hat{Q})_{KK}$$

$$(0 = A_K^T\hat{P}_K + \hat{P}_K A_K + R_K)$$

Figure 3.0-14. Numerical Solution of the Majorant Lyapunov Equation

Second member of the hierarchy:

$$\mathcal{M}\{\cdot\}\hat{Q} + \mathcal{M}[\hat{Q}] = \mathcal{G}\langle\hat{Q}\rangle + \langle\hat{Q}\rangle\mathcal{G}^T + \mathcal{V}$$

$$J - \mathrm{tr}[\hat{Q}R] \leq 2\sum_{K=1}^{r} (\mathrm{tr}\,\hat{P}_K)(\mathcal{G}\langle\hat{Q}\rangle)_{KK}$$

$$0 = A\hat{Q} + \hat{Q}A^T + \mathcal{M}[\hat{Q}] + V$$
$$0 = A^T\hat{P} + \hat{P}A + \mathcal{M}^\dagger[\hat{P}] + R$$

where:

$\langle\hat{Q}\rangle \triangleq$ off-diagonal part of $\hat{Q}$

$\mathcal{M}[\cdot]$ = Stratonovich model operator

- Tighter bound—incorporates more information on A and G
- Predicts stability when $(A + A^T)$ stable, $G = -G^T$
- "Nominal" performance, $\mathrm{tr}\,[\hat{Q}R]$, given by Stratonovich model

Figure 3.0-15. Second Member of the Majorant Hierarchy

consideration of the link between majorant robustness analysis and MEOP design synthesis theory.

Figure 3.0-16 illustrates this link and the accompanying sequence of logical developments. Overall, one may regard the MEOP design synthesis theory as arising from a particular robustness analysis tool. Although any member of the second-moment majorant hierarchy might be chosen as the basis of a design synthesis theory, we choose the second member of the hierarchy (see lower right block in Figure 3.0-16) to serve as the point of departure because it is the simplest bound that also handles nondestabilizing uncertainties. Referring to the lower left block of Figure 3.0-16, it is seen that the second-moment equation of a multiplicative Stratonovich noise model essentially gives an approximation to the majorant equation and a smooth optimization problem. The Stratonovich second moment equation then leads to an auxiliary optimization problem (upper left block in Figure 3-16), namely, choose dynamic compensator gains to minimize the quadratic performance of a system having multiplicative stochastic parameters. Because of the Stratonovich modifications to the standard form of the Lyapunov equation that appear in the equation for $\bar{Q}$, the robust stability condition implied by the majorant equation is still enforced since the optimization problem imposes a robust performance constraint.

This optimization of an apparently stochastic system actually approximates the majorant bound which was derived purely deterministically and leads to the rather elegant MEOP optimality conditions given in the upper right block in Figure 3.0-16.

Of course, the use of Stratonovich stochastic models was earlier indicated by maximum entropy principles and stochastic approximation theory, and this line of development still stands. But the import of the more recent majorant analysis developments is that there is a direct link between maximum entropy stochastic modelling and deterministic performance bounds. This link immeasurably strengthens the foundations of MEOP synthesis theory and, most importantly, tends to blur the distinctions between stochastic and deterministic points of view. This is just as well: The task confronting the controls and systems theory community is not to resolve the stochastic versus deterministic debate one way or the other, but rather to rise above it. As the work described here suggests, there is a plane upon which the points of view are numerically indistinguishable.

Auxilliary Optimization Problem

$$0 = A\bar{Q} + \bar{Q}A^T + \mathcal{H}[\bar{Q}] + V$$

$$\bar{J} = \mathrm{tr}[\bar{Q}R]$$

$$A = \begin{bmatrix} A & -EK \\ FC & A_c \end{bmatrix}$$

Find K, F, A_c to minimize $\bar{J}$

OPME Design Equations

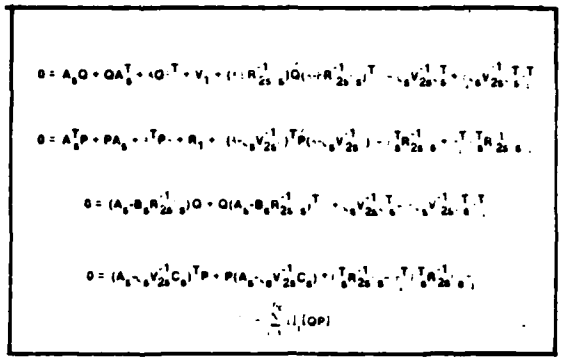

Stochastic Design Model

Stratonovich 2nd Moment Equation

$$0 = A\bar{Q} + \bar{Q}A^T + \mathcal{H}[\bar{Q}] + V$$

$$\{\bar{Q}\} \leq\leq |\{\bar{Q}\}|$$

$$J(\bar{Q}) - J_0 \leq J(\hat{Q}) - J_0$$

Majorant Hierarchy

$$\text{0th:} \quad (\hat{\nu} - \mathcal{A})\hat{Q} + \hat{Q}(\hat{\nu} - \mathcal{A})^T + \mathcal{V} = 0$$

$$\text{1st:} \quad \mathcal{A}^*\hat{Q} = \mathcal{A}\hat{Q} + \hat{Q}\mathcal{A}^T + \mathcal{V}$$

$$\text{2nd:} \quad \mathcal{A}^*\hat{Q} + \hat{\mathcal{H}}_2[\hat{Q}] = \mathcal{A}\langle\hat{Q}\rangle + \langle\hat{Q}\rangle\mathcal{A}^T + \mathcal{V}$$

$$\text{3rd:} \quad \mathcal{A}^*\hat{Q} + \hat{\mathcal{H}}_3[\hat{Q}] = \ldots$$

Figure 3.0-16. Majorant Hierachy and Stratonovich Models -- the Link Between Analysis and Synthesis

3.1 References

[3.1] J.C. Doyle and G. Stein, "Multivariable Feedback Design: Concepts for a Classical/Modern Synthesis," IEEE Trans. Autom. Contr., Vol. AC-26, pp. 4-16, 1981.

[3.2] G. Zames, "Feedback and Optimal Sensitivity: Model Reference Transformations, Multiplicative Seminorms, and Approximate Inverses," IEEE Trans. Autom. Contr., Vol. AC-26, pp. 301-320, 1981.

[3.3] G. Zames and B.A. Francis, "Feedback, Minimax Sensitivity, and Optimal Robustness," IEEE Trans. Autom. Contr., Vol. AC-28, pp. 585-601, 1983.

[3.4] G. Stein and M. Athans, "The LQG/LTR Procedure for Multivariable Feedback Control Design," IEEE Trans. Autom. Contr., Vol. AC-32, pp. 105-114, 1987.

[3.5] B.A. Francis, A Course in H-Infinity Control Theory, Springer-Verlag, New York, NY, 1987.

[3.6] J.C. Doyle, "Analysis of Feedback Systems with Structured Uncertainties," IEE Proc., Vol. 129, pp. 242-250, 1982.

[3.7] D.D. Siljak, Large-Scale Dynamic Systems, Elsevier/ North-Holland, 1978.

[3.8] M. Ikeda and D.D. Siljak, "Generalized Decomposition of Dynamic Systems and Vector Lyapunov Functions," IEEE Trans. Autom. Contr., Vol. AC-26, pp. 1118-1125, 1981.

[3.9] A.M. Ostrowski, "On Some Metrical Properties of Operator Matrices and Matrices Partitioned Into Blocks," J. Math. Anal. Appl., Vol. 2, pp. 161-209, 1961.

[3.10] M. Vidyasagar, "New Directions of Research in Nonlinear System Theory," Proc. IEEE, Vol. 74, pp. 1060-1091, 1986.

[3.11] G. Dahlquist, "On Matrix Majorants and Minorants, With Applications to Differential Equations," Lin. Alg. Appl., Vol. 52/53, pp. 199-216, 1983.

[3.12] M.K.H. Fan and A.L. Tits, "Characterization and Efficient Computation of the Structured Singular Value," IEEE Trans. Autom. Contr., Vol. AC-31, pp. 734-743, 1986.

[3.13] J.W. Brewer, "Kronecker Products and Matrix Calculus in System Theory," IEEE Trans. Circ. Sys., Vol. CAS-25, pp. 772-781, 1978.

4.0 COMPUTATIONAL ALGORITHMS FOR DECENTRALIZED MEOP DESIGNS

Two distinct computational algorithms have been developed for solving the MEOP design equations. An iterative algorithm has been utilized for several years and considerable experience using it has been obtained. More recently, a sophisticated algorithm utilizing a homotopy method has been developed by S. Richter. Here we shall review both methods and point out several advantages offered by the homotopy algorithm.

4.1 Iterative Algorithm

The original contribution of optimal projection theory was the discovery of the highly structured form of the necessary conditions for fixed-structure control design. An immediate benefit of this structure is the ability to apply novel computational algorithms which are distinct from gradient search methods. This goal has been realized by developing an iterative algorithm which operates through successive refinement of the optimal projection itself. A detailed description of this algorithm appears in [74] (see Appendix E) which also presents a thorough design study for a challenging 8th-order example considered in [4.1]. In [4.1] the authors present a detailed comparison of several controller-reduction methods over a range of control authorities. The following conclusion is immediately clear: None of the methods considered in [4.1] reliably yields stabilizing reduced-order controllers even when such controllers are known to exist.

The design study in [74] involved subjecting the iterative algorithm to each design case considered in [4.1]. In contrast to the results reported in [4.1], the optimal projection equations provided stable designs in 100 percent of the cases. Actually, this is not surprising since solutions of the optimal projection equations can be shown to be generically stabilizing. The clear-cut nature of these results can leave little doubt as to the effectiveness of optimal projection theory.

4.2 Homotopy Algorithm

To meet the increased demands of decentralized design, a more sophisticated algorithm has been developed (see [58] in Appendix F). In this regard the study contract was particularly fortunate to have S. Richter as a

contributor. Mr. Richter pioneered the application of homotopy algorithms to control problems including decentralized control (see [4.2-4.5]).

The concept behind homotopy methods is quite simple, namely, replace the desired, but difficult, problem with an easily solved problem, and then transform the solution of the easy problem into the desired solution. The mathematics required to render the procedure rigorous is far from trivial, however, and must be applied with some care. An important benefit of the homotopy approach is the tools it provides for analyzing the design equations. The principal result obtained thus far states that the design equation possess no more than a prescribed number of nonnegative-definite solutions each of which is stabilizing and each of which can be computed via a homotopic path. In particular, if the plan is stabilizable by means of a controller of given order and if the design problem possesses a solution, then the optimal gains can be computed via the homotopy.

An additional benefit of the homotopy path is the ability to exploit the structure of the design equations to an even greater extent than the iterative algorithm. Specificallyy, Richter has shown that the computational burden using the homotopy method involves solving four equations of order $n_c$xn. Hence, the computational requirements decrease as n_c decreases. This is, of course, quite pleasing since low-order controllers ought to be easier to design than high-order controllers. For decentralized control design this property is particularly advantageous since it will generally be true that $n_c \ll \tilde{n}$, where $\tilde{n}$ is the plant dimension augmented by all other subcontrollers. See Section 2.0 for details.

Since the computational burden of the iterative algorithm tends to increase as n_c decreases, the advantages of the homotopy algorithm over the iterative algorithm are obvious. Computational savings have been at least an order of magnitude, and final convergence has been greatly improved. Moreover, the example considered in [4.1] and [74] was reconsidered using the homotopy algorithm in [58] (see Appendix F). The main result was the ability to produce controllers as low as second order at control authorities which were three orders of magnitude beyond the cases considered in [4.1] and [74]. In each case the performance of the reduced-order controller was within 20 percent of the full-order design.

4.3 References

[4.1] Y. Liu and B.D.O. Anderson, "Controller Reduction Via Stable Factorization and Balancing," Int. J. Contr., Vol. 44, No. 2, 507-531, 1986.

[4.2] S. Richter and R. DeCarlo, "Continuation Methods: Theory and Applications," IEEE Trans. Autom. Contr., Vol. 28, pp. 660-665, 1983.

[4.3] S. Richter and R. DeCarlo, "A Homotopy Method for Eigenvalue Assignment Using Decentralized State Feedback," IEEE Trans. Autom. Contr., Vol. AC-29, pp. 148-155, 1984.

[4.4] S. Lefebvre, S. Richter and R. DeCarlo, "A Continuation Algorithm for Eigenvalue Assignment by Decentralized Constant-Output Feedback," Int. J. Contr., Vol. 41, pp. 1273-1292, 1985.

[4.5] D.R. Sebok, S. Richter and R. DeCarlo, "Feedback Gain Optimization in Decentralized Eigenvalue Assignment," Automatica, Vol. 22, pp. 433-447, 1986.

5.0 DECENTRALIZED MEOP DESIGN SYNTHESIS AND MAJORANT ANALYSIS FOR A REPRESENTATIVE LARGE SPACE SYSTEM

Task 4 of the study contract involves applying decentralized MEOP synthesis and majorant analysis to a representative large space system. Candidate systems to be considered include the 60-meter COFS I truss structure and the solar concentrator power generation subsystem for the space station. Here we report the status of the effort for each system.

5.1 COFS I Truss Structure

For the COFS I truss structure the present study has benefitted from extensive analyses carried out for the COFS project. Such analyses include detailed finite element modelling, sensor and actuator modelling, and baseline active damping control design. The baseline design is a decentralized output-feedback controller for damping augmentation. For the present study a centralized LQG design has been carried out for the truss structure and has been compared to the baseline (see [61] in Appendix G). A dynamic decentralized design study utilizing MEOP theory is planned for the next study phase.

5.2 Solar Concentrator Power Generation Subsystem

Power generation for the space station is planned to utilize solar energy as a thermal source. Solar energy will be concentrated via reflectors for maximum efficiency. An important control problem is the dynamic reflector fine pointing subsystem. This problem represents a natural application of decentralized feedback since it is desirable to control each solar reflector autonomously while minimizing transient effects to the ambient space station structure.

Under related programs initial analysis of this system has been completed. This analysis includes dynamic modelling of the space station with emphasis on attitude control and interaction with pointing control for the power generation subsystem. Figure 5.2 illustrates the mechanical design of the concentrator assembly.

Centralized MEOP control-design has been carried out for a design model which accounts for attitude errors and gimbal torques. The line of sight error

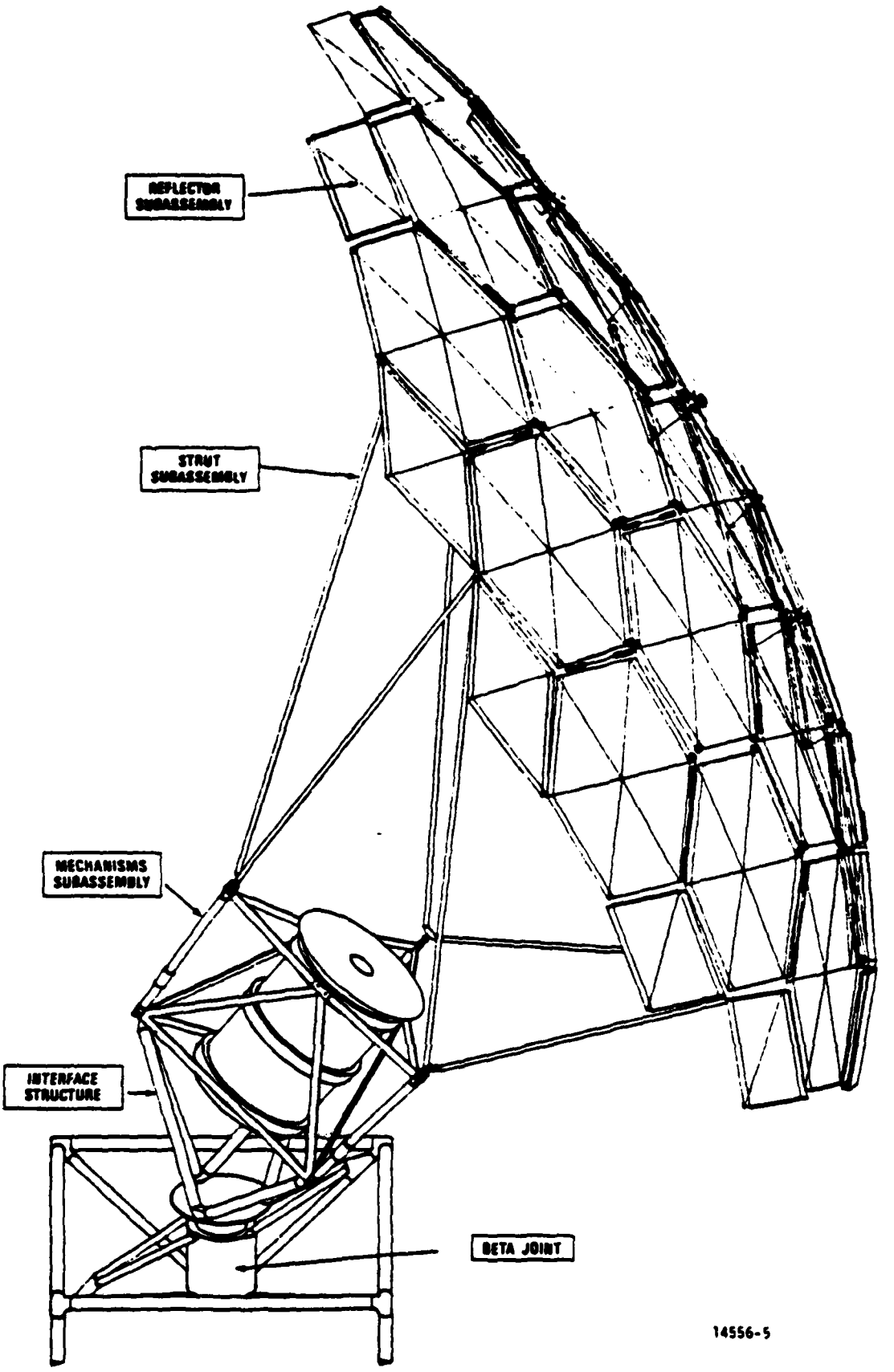

Figure 5.2. Solar Concentrator Assembly

for the closed-loop system was below the 0.1 degrees requirement, while the peak reboost transient was below the specification of 0.05 degrees. Future studies will focus on decentralized design as a tool for simplifying the control-system implementation.

SECTION 6.0

COMPREHENSIVE MEOP REFERENCE LIST

1. D. C. Hyland, "The Modal Coordinate/Radiative Transfer Formulation of Structural Dynamics--Implications for Vibration Suppression in Large Space Platforms," MIT Lincoln Laboratory, TR-27, 14 March 1979.

2. D. C. Hyland, "Optimal Regulation of Structural Systems With Uncertain Parameters," MIT Lincoln Laboratory, TR-551, 2 February 1981, DDC# AD-A099111/7.

3. D. C. Hyland, "Active Control of Large Flexible Spacecraft: A New Design Approach Based on Minimum Information Modelling of Parameter Uncertainties," Proc. Third VPI&SU/AIAA Symposium, pp. 631-646, Blacksburg, VA, June 1981.

4. D. C. Hyland, "Optimal Regulator Design Using Minimum Information Modelling of Parameter Uncertainties: Ramifications of the New Design Approach," Proc. Third VPI&SU/AIAA Symposium, pp. 701-716, Blacksburg, VA, June 1981.

5. D. C. Hyland and A. N. Madiwale, "Minimum Information Approach to Regulator Design: Numerical Methods and Illustrative Results," Proc. Third VPI&SU/AIAA Symposium, pp. 101-118, Blacksburg, VA, June 1981.

6. D. C. Hyland and A. N. Madiwale, "A Stochastic Design Approach for Full-Order Compensation of Structural Systems with Uncertain Parameters," Proc. AIAA Guid. Contr. Conf., pp. 324-332, Albuquerque, NM, August 1981.

7. D. C. Hyland, "Optimality Conditions for Fixed-Order Dynamic Compensation of Flexible Spacecraft with Uncertain Parameters," AIAA 20th Aerospace Sciences Meeting, paper 82-0312, Orlando, FL, January 1982.

8. D. C. Hyland, "Structural Modeling and Control Design Under Incomplete Parameter Information: The Maximum Entropy Approach," AFOSR/NASA Workshop on Modeling, Analysis and Optimization Issues for Large Space Structures, Williamsburg, VA, May 1982.

9. D. C. Hyland, "Minimum Information Stochastic Modelling of Linear Systems with a Class of Parameter Uncertainties," Proc. Amer. Contr. Conf., pp. 620-627, Arlington, VA, June 1982.

10. D. C. Hyland, "Maximum Entropy Stochastic Approach to Control Design for Uncertain Structural Systems," Proc. Amer. Contr. Conf., pp. 680-688, Arlington, VA, June 1982.

11. D. C. Hyland, "Minimum Information Modeling of Structural Systems with Uncertain Parameters," Proceedings of the Workshop on Applications of Distributed System Theory to the Control of Large Space Structures, G. Rodriguez, ed., pp. 71-88, JPL, Pasadena, CA, July 1982.

12. D. C. Hyland and A. N. Madiwale, "Fixed-Order Dynamic Compensation Through Optimal Projection," Proceedings of the Workshop on Applications of Distributed System Theory to the Control of Large Space Structures, G. Rodriguez, ed., pp. 409-427, JPL, Pasadena, CA, July 1982.

13. D. C. Hyland, "Mean-Square Optimal Fixed-Order Compensation--Beyond Spillover Suppression," paper 1403, AIAA Astrodynamics Conference, San Diego, CA, August 1982.

14. D. C. Hyland, "Robust Spacecraft Control Design in the Presence of Sensor/Actuator Placement Errors," AIAA Astrodynamics Conference, San Diego, CA, August 1982.

15. D. C. Hyland, "The Optimal Projection Approach to Fixed-Order Compensation: Numerical Methods and Illustrative Results," AIAA 21st Aerospace Sciences Meeting, paper 83-0303, Reno, NV, January 1983.

16. D. C. Hyland, "Mean-Square Optimal, Full-Order Compensation of Structural Systems with Uncertain Parameters," MIT Lincoln Laboratory, TR-626, 1 June 1983.

17. D. S. Bernstein and D. C. Hyland, "Explicit Optimality Conditions for Finite-Dimensional Fixed-Order Dynamic Compensation of Infinite-Dimensional Systems," presented at SIAM Fall Meeting, Norfolk, VA, November 1983.

18. D. C. Hyland and D. S. Bernstein, "Explicit Optimality Conditions for Fixed-Order Dynamic Compensation," Proc. 22nd IEEE Conf. Dec. Contr., pp. 161-165, San Antonio, TX, December 1983.

19. F. M. Ham, J. W. Shipley and D. C. Hyland, "Design of a Large Space Structure Vibration Control Experiment," Proc. 2nd Int. Modal Anal. Conf., pp. 550-558, Orlando, FL, February 1984.

20. D. C. Hyland, "Comparison of Various Controller-Reduction Methods: Suboptimal Versus Optimal Projection," Proc. AIAA Dynamics Specialists Conf., pp. 381-389, Palm Springs, CA, May 1984.

21. D. S. Bernstein and D. C. Hyland, "The Optimal Projection Equations for Fixed-Order Dynamic Compensation of Distributed Parameter Systems," Proc. AIAA Dynamics Specialists Conf., pp. 396-400, Palm Springs, CA, May 1984.

22. F. M. Ham and D. C. Hyland, "Vibration Control Experiment Design for the 15-M Hoop/Column Antenna," Proceedings of the Workshop on the Identification and Control of Flexible Space Structures, pp. 229-252, San Diego, CA, June 1984.

23. D. S. Bernstein and D. C. Hyland, "Numerical Solution of the Optimal Model Reduction Equations," Proc. AIAA Guid. Contr. Conf., pp. 560-562, Seattle, WA, August 1984.

24. D. C. Hyland and D. S. Bernstein, "The Optimal Projection Equations for Fixed-Order Dynamic Compensation," IEEE Trans. Autom. Contr., Vol. AC-29, pp. 1034-1037, 1984.

25. D. C. Hyland, "Application of the Maximum Entropy/Optimal Projection Control Design Approach for Large Space Structures," Proc. Large Space Antenna Systems Technology Conference, pp. 617-654, NASA Langley, December 1984.

26. D. C. Hyland and D. S. Bernstein, "The Optimal Projection Approach to Model Reduction and the Relationship Between the Methods of Wilson and Moore," Proc. 23rd IEEE Conf. Dec. Contr., pp. 120-126, Las Vegas, NV, December 1984.

27. D. S. Bernstein and D. C. Hyland, "The Optimal Projection Approach to Designing Optimal Finite-Dimensional Controllers for Distributed Parameter Systems," Proc. 23rd IEEE Conf. Dec. Contr., pp. 556-560, Las Vegas, NV, December 1984.

28. L. D. Davis, D. C. Hyland and D. S. Bernstein, "Application of the Maximum Entropy Design Approach to the Spacecraft Control Laboratory Experiment (SCOLE)," Final Report, NASA Langley, January 1985.

29. D. S. Bernstein and D. C. Hyland, "The Optimal Projection Equations for Reduced-Order State Estimation," IEEE Trans. Autom. Contr., Vol. AC-30, pp. 583-585, 1985.

30. D. S. Bernstein and D. C. Hyland, "The Optimal Projection Equations for Reduced-Order State Estimation," Proc. Amer. Contr. Conf., pp. 164-167, Boston, MA, June 1985.

31. D. S. Bernstein and D. C. Hyland, "Optimal Projection/Maximum Entropy Stochastic Modelling and Reduced-Order Design Synthesis," Proc. IFAC Workshop on Model Error Concepts and Compensation, Boston, MA, June 1985, pp. 47-54, R. E. Skelton and D. H. Owens, eds., Pergamon Press, Oxford, 1986.

32. D. C. Hyland and D. S. Bernstein, "The Optimal Projection Equations for Model Reduction and the Relationships Among the Methods of Wilson, Skelton and Moore," IEEE Trans. Autom. Contr., Vol. AC-30, pp. 1201-1211, 1985.

33. D. S. Bernstein, "The Optimal Projection Equations for Fixed-Structure Decentralized Dynamic Compensation," Proc. 24th IEEE Conf. Dec. Contr., pp. 104-107, Fort Lauderdale, FL, December 1985.

34. D. S. Bernstein, L. D. Davis, S. W. Greeley and D. C. Hyland, "The Optimal Projection Equations for Reduced-Order, Discrete-Time Modelling, Estimation and Control," Proc. 24th IEEE Conf. Dec. Contr., pp. 573-578, Fort Lauderdale, FL, December 1985.

35. D. S. Bernstein and D. C. Hyland, "The Optimal Projection/Maximum Entropy Approach to Designing Low-Order, Robust Controllers for Flexible Structures," Proc. 24th IEEE Conf. Dec. Contr., pp. 745-752, Fort Lauderdale, FL, December 1985.

36. D. S. Bernstein, L. D. Davis, S. W. Greeley and D. C. Hyland, "Numerical Solution of the Optimal Projection/Maximum Entropy Design Equations for Low-Order, Robust Controller Design," Proc. 24th IEEE Conf. Dec. Contr., pp. 1795-1798, Fort Lauderdale, FL, December 1985.

37. D. S. Bernstein and D. C. Hyland, "The Optimal Projection Equations for Finite-Dimensional Fixed-Order Dynamic Compensation of Infinite-Dimensional Systems," SIAM J. Contr. Optim., Vol. 24, pp. 122-151, 1986.

38. J. W. Shipley and D. C. Hyland, "The Mast Flight System Dynamic Characteristics and Actuator/Sensor Selection and Location," Proc. 9th Annual/AAS Guid. Contr. Conf., Keystone, CO, February 1986, pp. 31-49, R. D. Culp and J. C. Durrett, eds., American Astronautical Society, San Diego, CA, 1986.

39. D. S. Bernstein and S. W. Greeley, "Robust Controller Synthesis Using the Maximum Entropy Design Equations," IEEE Trans. Autom. Contr., Vol. AC-31, pp. 362-364, 1986.

40. D. C. Hyland, D. S. Bernstein, L. D. Davis, S. W. Greeley and S. Richter, "MEOP: Maximum Entropy/Optimal Projection Stochastic Modelling and Reduced-Order Design Synthesis," Final Report, Air Force Office of Scientific Research, Bolling AFB, Washington, DC, April 1986.

41. D. S. Bernstein, L. D. Davis and D. C. Hyland, "The Optimal Projection Equations for Reduced-Order, Discrete-Time Modelling, Estimation and Control," J. Guid. Contr. Dyn., Vol. 9, pp. 288-293, 1986.

42. D. S. Bernstein and S. W. Greeley, "Robust Output-Feedback Stabilization: Deterministic and Stochastic Perspectives," Proc. Amer. Contr. Conf., pp. 1818-1826, Seattle, WA, June 1986.

43. D. S. Bernstein, L. D. Davis and S. W. Greeley, "The Optimal Projection Equations for Fixed-Order, Sampled-Data Dynamic Compensation with Computation Delay," Proc. Amer. Contr. Conf., pp. 1590-1597, Seattle, WA, June 1986.

44. D. S. Bernstein, L. D. Davis and S. W. Greeley, "The Optimal Projection Equations for Fixed-Order, Sampled-Data Dynamic Compensation with Computation Delay," IEEE Trans. Autom. Contr., Vol. AC-31, pp. 859-862, 1986.

45. D. S. Bernstein, "Optimal Projection/Guaranteed Cost Control Design Synthesis: Robust Performance via Fixed-Order Dynamic Compensation," presented at SIAM Conference on Linear Algebra in Signals, Systems and Control, Boston, MA, August 1986.

46. D. C. Hyland, "Control Design Under Stratonovich Models: Robust Stability Guarantees via Lyapunov Matrix Functions," presented at SIAM Conference on Linear Algebra in Signals, Systems and Control, Boston, MA, August 1986.

47. D. S. Bernstein, "OPUS: Optimal Projection for Uncertain Systems," Annual Report, Air Force Office of Scientific Research, Bolling AFB, Washington, DC, October 1986.

48. B. J. Boan and D. C. Hyland, "The Role of Metal Matrix Composites for Vibration Suppression in Large Space Structures," Proc. MMC Spacecraft Survivability Tech. Conf., MMCIAC Kaman Tempo Publ., Stanford Research Institute, Palo Alto, CA, October 1986.

49. D. C. Hyland, "An Experimental Testbed for Validation of Control Methodologies in Large Space Optical Structures," SPIE Optoelectronics and Laser Applications Conference, Los Angeles, CA, January 1987.

50. J. W. Shipley, L. D. Davis, W. T. Burton and F. M. Ham, "Development of the Mast Flight System Linear DC Motor Inertial Actuator," 10th Annual AAS Guid. Contr. Conf., Keystone, CO, February 1987.

51. W. M. Haddad and D. S. Bernstein, "The Optimal Projection Equations for Discrete-Time Reduced-Order State Estimation for Linear Systems with Multiplicative White Noise," Sys. Contr. Lett., 1987, to appear.

52. D. S. Bernstein and W. M. Haddad, "The Optimal Projection Equations for Discrete-Time Fixed-Order Dynamic Compensation of Linear Systems with Multiplicative White Noise," Int. J. Contr., 1987, to appear.

53. D. C. Hyland and D. S. Bernstein, "Uncertainty Characterization Schemes: Relationships to Robustness Analysis and Design," Amer. Contr. Conf., Minneapolis, MN, June 1987.

54. W. M. Haddad and D. S. Bernstein, "The Optimal Projection Equations for Reduced-Order State Estimation: The Singular Measurement Noise Case," Amer. Contr. Conf., Minneapolis, MN, June 1987.

55. D. C. Hyland and D. S. Bernstein, "The Majorant Lyapunov Equation: A Nonnegative Matrix Equation for Guaranteed Robust Stability and Performance of Large Scale Systems," Amer. Contr. Conf., Minneapolis, MN, June 1987.

56. D. S. Bernstein, "Sequential Design of Decentralized Dynamic Compensators Using the Optimal Projection Equations: An Illustrative Example Involving Interconnected Flexible Beams," Amer. Contr. Conf., Minneapolis, MN, June 1987.

57. D. C. Hyland, "Majorant Bounds, Stratonovich Models, and Statistical Energy Analysis," Amer. Contr. Conf., Minneapolis, MN, June 1987.

58. S. Richter, "A Homotopy Algorithm for Solving the Optimal Projection Equations for Fixed-Order Dynamic Compensation: Existence, Convergence and Global Optimality," Amer. Contr. Conf., Minneapolis, MN, June 1987.

59. D. S. Bernstein, "The Optimal Projection Equations For Nonstrictly Proper Fixed-Order Dynamic Compensation," Amer. Contr. Conf., Minneapolis, MN, June 1987.

60. D. S. Bernstein and W. M. Haddad, "Optimal Output Feedback for Nonzero Set Point Regulation," Amer. Contr. Conf., Minneapolis, MN, June 1987.

61. F. M. Ham, B. L. Henniges, and S. W. Greeley, "Active Damping Control Design for the COFS Mast Flight System," Amer. Contr. Conf., Minneapolis, MN, June 1987.

62. W. M. Haddad and D. S. Bernstein, "The Optimal Projection Equations for Reduced-Order State Estimation: The Singular Measurement Noise Case," IEEE Trans. Autom. Contr., 1987, to appear.

63. D. S. Bernstein, "The Optimal Projection Equations for Static and Dynamic Output Feedback: The Singular Case," IEEE Trans. Autom. Contr., 1987, to appear.

64. D. S. Bernstein and D. C. Hyland, "The Optimal Projection Equations for Reduced-Order Modelling, Estimation and Control of Linear Systems with Multiplicative White Noise," J. Optim. Thy. Appl., 1987, to appear.

65. D. S. Bernstein, "Sequential Design of Decentralized Dynamic Compensators Using the Optimal Projection Equations," Int. J. Contr., 1987, to appear.

66. D. S. Bernstein and W. M. Haddad, "Optimal Output Feedback for Nonzero Set Point Regulation," IEEE Trans. Autom. Contr., 1987, to appear.

67. D. S. Bernstein, "Robust Static and Dynamic Output-Feedback Stabilization: Deterministic and Stochastic Perspectives," IEEE Trans. Autom. Contr., 1987, to appear.

68. D. C. Hyland and D. S. Bernstein, "The Majorant Lyapunov Equation: A Nonnegative Matrix Equation for Guaranteed Robust Stability and Performance of Large Scale Systems," IEEE Trans. Autom. Contr., 1987, to appear.

69. D. S. Bernstein and D. C. Hyland, "Optimal Projection for Uncertain Systems (OPUS): A Unified Theory of Reduced-Order, Robust Control Design," in Large Space Structures: Dynamics and Control, S. N. Atluri and A. K. Amos, eds., Springer-Verlag, New York, 1987.

70. W. M. Haddad, Robust Optimal Projection Control-System Synthesis, Ph.D. Dissertation, Department of Mechanical Engineering, Florida Institute of Technology, Melbourne, FL, March 1987.

71. D. S. Bernstein, "Robust Stability and Performance via the Extended Optimal Projection Equations for Fixed-Order Dynamic Compensation," submitted.

72. D. S. Bernstein and W. M. Haddad, "The Optimal Projection Equations with Petersen-Hollot Bounds: Robust Controller Synthesis with Guaranteed Structured Stability Radius," submitted.

73. W. M. Haddad and D. S. Bernstein, "Optimal Output Feedback for Nonzero Set Point Regulation: The Discrete-Time Case," submitted.

74. S. W. Greeley and D. C. Hyland, "Reduced-Order Compensation: LQG Reduction Versus Optimal Projection," submitted.

75. W. M. Haddad and D. S. Bernstein, "The Unified Optimal Projection Equations for Simultaneous Reduced-Order, Robust Modeling, Estimation and Control," submitted.

76. W. M. Haddad and D. S. Bernstein, "Robust, Reduced-Order, Nonstrictly Proper State Estimation Via the Optimal Projection Equations with Petersen-Hollot Bounds," submitted.

77. D. S. Bernstein and W. M. Haddad, "Robust Decentralized Optimal Output Feedback: The Static Controller Case," submitted.

78. D. S. Bernstein and W. M. Haddad, "The Optimal Projection Equations for Robust, Reduced-Order Dynamic Compensation," in preparation.

79. D. S. Bernstein and I. G. Rosen, "A Numerical Study of Approximations for Finite-Dimensional, Fixed-Order Compensation of Infinite-Dimensional Systems," in preparation.

APPENDIX A

REFERENCE 69

OPTIMAL PROJECTION FOR UNCERTAIN SYSTEMS (OPUS): A UNIFIED THEORY OF REDUCED-ORDER, ROBUST CONTROL DESIGN

Dennis S. Bernstein and David C. Hyland
Harris Corporation
Government Aerospace Systems Division
Melbourne, Florida 32902

This research was supported in part by the Air Force Office of Scientific Research under contracts F49620-86-C-0002 and F49620-86-C-0038.

Abstract

OPUS (Optimal Projection for Uncertain Systems) provides new machinery for designing active controllers for suppressing vibration in flexible structures. The purpose of this paper is to review this machinery and demonstrate its practical value in addressing the structural control problem.

1. Introduction

For many years it has been widely recognized that the desire to orbit large, lightweight space structures possessing high-performance capabilities would require active feedback control techniques. More generally, the need for such techniques may arise due to the combinations of either 1) moderate performance requirements for highly flexible structures with low-frequency modes or 2) stringent performance requirements for semi-rigid structures with relatively high-frequency modes (Figure 1). Applications include pointing, slewing, and aperture shape control for optical and RF systems.

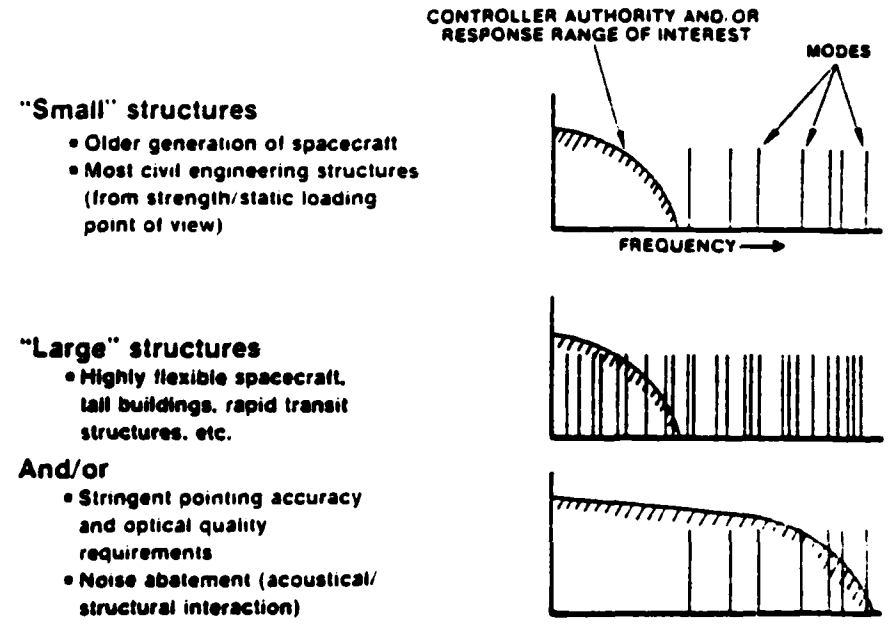

Figure 1. The Need for Active Structural Control Arises From Stringent Performance Requirements or Low-Frequency Modes

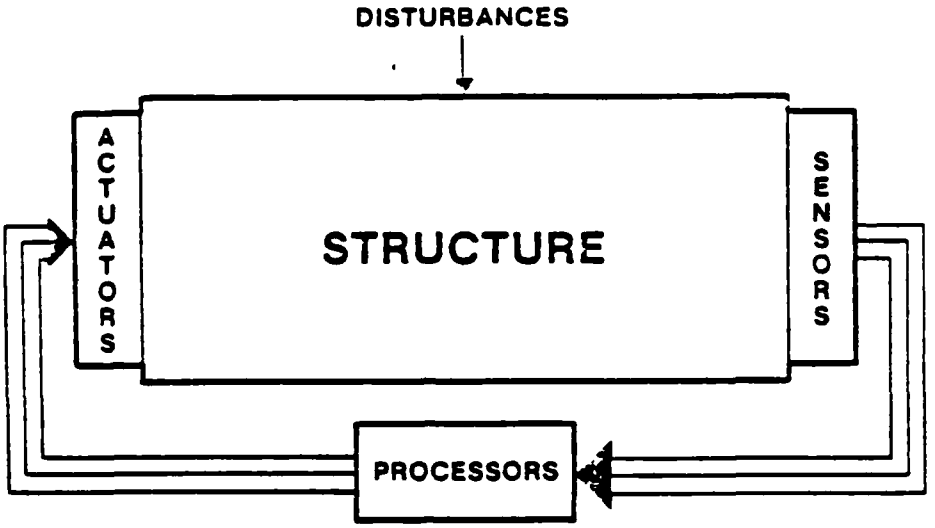

Figure 2. Vibration Control Systems Utilize Sensors, Processors and Actuators to Suppress Disturbances

The problem of active vibration suppression (Figure 2) entails the following considerations:

1. Multiple, highly coupled feedback loops. The potentially large number of sensors and actuators leads to a fully coupled multi-input, multi-output feedback control system.

2. Limited actuator power. The control authority available from on-board actuators is limited by weight, size, cost and power considerations.

3. High-dimensional models. Large structures subjected to broadband disturbances are typically represented by high-order finite element models.

4. Limited processor capacity. Reliability and cost considerations limit the processor capacity available for on-board real-time implementation of the control system.

5. Highly uncertain models with structured uncertainty. Finite element models often exhibit significant error particularly as modal frequency increases. Although modal testing and related identification methods may be used to improve modeling accuracy, residual uncertainty always remains and unpredictable on-orbit changes due to aging, thermal effects, etc., must be tolerated.

6. Stringent performance requirements. Since active space structure control is most relevant in precision applications, it can readily be expected that performance specifications will be particularly stringent.

7. Design efficiency. Because of implementation complexity due to the presence of multiple loops, high dimension, and high levels of uncertainty, the control design approach should efficiently utilize both synthesis and analysis techniques (Figure 3).

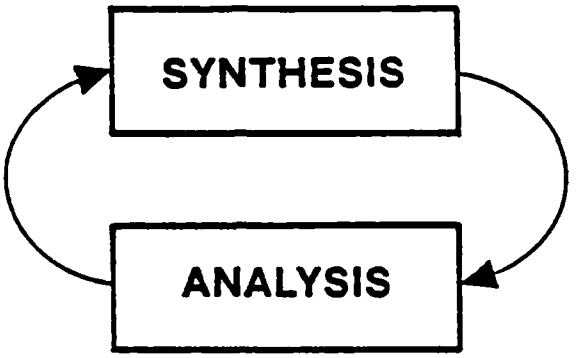

Figure 3. Control-System Design Must Efficiently Utilize Both Synthesis and Analysis Techniques

These considerations pose a considerable challenge to the state-of-the-art in control-design methodologies. For example, the presence of multiple, coupled feedback paths essentially precludes the effectiveness of single-loop design techniques. The sheer number of loops, their interaction, and the need to address a host of other issues render such methods inefficient and unwieldy.

In addition to the presence of multiple loops, the high dimensionality of dynamic models places a severe burden on control-design methodologies. For example, although LQG (linear-quadratic-Gaussian) design is applicable to multi-loop problems, such controllers are of the same order as the structural model (Figures 4 and 5). Thus LQG and similar high-order controllers can be expected to place an unacceptable computational burden on the real-time processing capability. Hence it is not surprising that a variety of techniques have been proposed to reduce the order of LQG controllers. A comparison of several such methods is given in [1].

All of the above difficulties are severely exacerbated by the fact that the dynamic (i.e., finite element) model upon which the control design is predicated may be highly inaccurate in spite of extensive modal identification. Hence, applicable control-design methodologies must account for modeling uncertainties by providing robust (i.e., insensitive) controllers. Furthermore, because of stringent

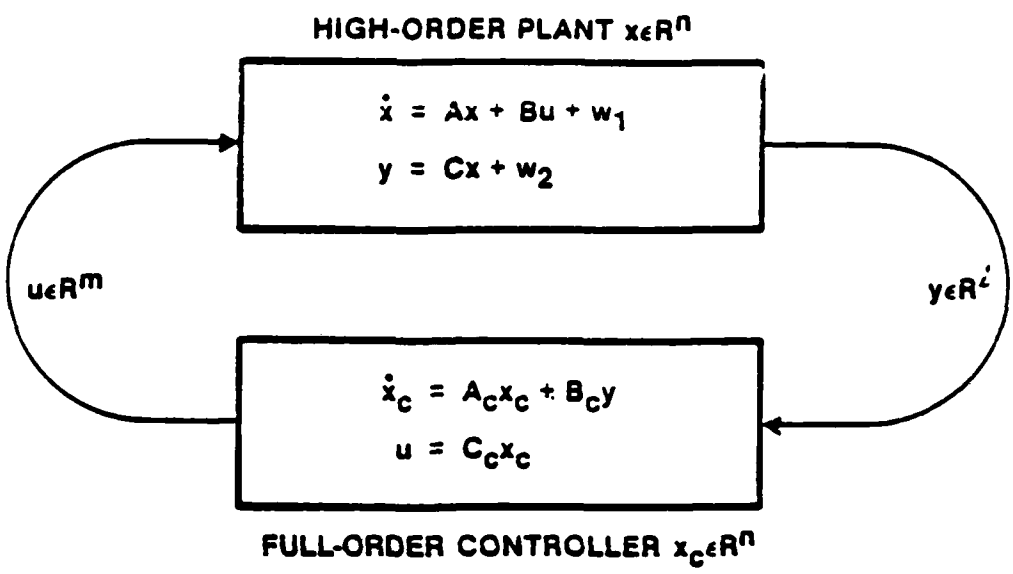

STEADY-STATE PERFORMANCE CRITERION

$$J(A_c,B_c,C_c) = \lim_{t \to \infty} E[x^T R_1 x + u^T R_2 u]$$

Figure 4. LQG Theory Addresses the Problem of Designing a Quadratically Optimal, Full-Order Dynamic Compensator

FULL-ORDER CONTROLLER GAINS

$$A_c = A - Q\bar{\Sigma} - \Sigma P$$

$$B_c = QC^T V_2^{-1}$$

$$C_c = -R_2^{-1} B^T P$$

SEPARATED RICCATI EQUATIONS

$$0 = AQ + QA^T + V_1 - Q\bar{\Sigma}Q \qquad \text{(Kalman Filter)}$$

$$0 = A^T P + PA + R_1 - P\Sigma P \qquad \text{(Regulator)}$$

$$\Sigma \equiv BR_2^{-1}B^T \qquad \bar{\Sigma} \equiv C^T V_2^{-1} C$$

Figure 5. The Optimal Full-Order (LQG) Controller Is Determined by a Pair of Separated Riccati Equations

performance requirements, robust control design must avoid conservatism with respect to modeling uncertainty which may unnecessarily degrade performance. A salient example of conservatism is illustrated in Figure 6. If uncertainty in the modal frequency is complexified in a transfer function setting, then the resulting pole location uncertainty has the form of a disk. This disk, however, intersects the right half plane in violation of energy dissipation. Hence one source of conservatism is the inability to differentiate between physically distinct parameters such as modal frequency and modal damping.

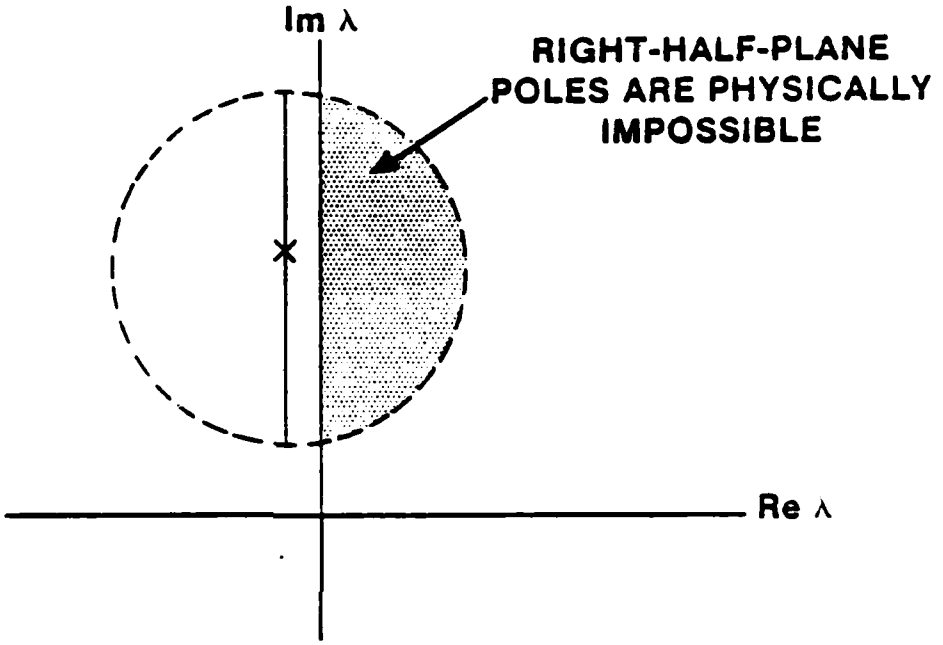

Figure 6. Complexification of Real Parameters May Lead to Robustness Conservatism

Although classical methods are inappropriate for vibration control, a wide variety of modern techniques are available. These include both multi-loop frequency-domain methods and time-domain techniques. A comprehensive review of such methods will not be attempted here. Rather, we shall merely point out aspects of several methods which motivate the philosophy of OPUS development.

As is well known, dynamic models can be transformed (at least in theory) between the frequency and time domains. Significant differences arise, however, in attempting to represent modeling errors. Specifically, model-error characterization of a particular type, which is natural and tractable in one domain, may become extremely cumbersome when transformed into the other domain. For example, consider a state space model with parameter uncertainties arising in the system matrices (A,B,C). Upon transforming to a frequency domain model $G(s) = C(sI-A)^{-1}B$ the parametric uncertainties may perturb the transfer function coefficients in a

complicated manner. A more natural measure of uncertainty for transfer functions has been developed in [2] where system uncertainty in the frequency domain is modeled by means of normed neighborhoods in the H-infinity topology. There are limitations with this approach, however, in designing controllers for vibration suppression. For example, as shown in Figure 6, complexification of real-parameter uncertainties such as modal frequencies may yield unnecessary conservatism, while norm bounds often fail to preserve the physical structure of parameter variations. A case in point is the lightly damped oscillator. As shown in [A42], norm bounds predict stability over a frequency range on the order of the damping while in fact the oscillator is unconditionally stable. Furthermore, with regard to processor throughput tradeoffs, modern frequency-domain methods typically yield high-order controllers.

Although LQG addresses performance/actuator and performance/sensor tradeoffs in a multi-loop setting, it fails to incorporate modeling uncertainty. Thus it is not surprising, as shown in [3], that LQG designs fail to possess guaranteed gain margin. Since LQG designs lack such margins, attempts have been made to apply frequency-domain techniques to improve their characteristics. One such method, known as LQG/LTR ([4,5]) seeks to recover the gain margin of full-state-feedback controllers. Specifically, full-state-feedback LQR controllers are guaranteed to remain stable in the face of perturbations of the input matrix B of the form αB where $\alpha \in [1/2, \infty)$. As shown in [6,7], however, the full-state-feedback gain margin fails to provide robustness with respect to perturbations which are not of this form. For instance, the example given in [6] with $B = [0\ 1]^T$ can be destabilized for suitable performance weightings with perturbation $B(\epsilon) = [\epsilon\ 1]^T$ for arbitrarily small ϵ in spite of the 6 dB margin. Furthermore, since LQG/LTR loop shaping is based upon singular value norm bounds, treatment of physically meaningful real parameter variations may lead to unnecessary conservatism. Several approaches have been proposed for circumventing these difficulties (see, e.g., [8]).

The importance of addressing the problem of structured uncertainty in finite element models cannot be overemphasized. Structural characteristics such as modal frequencies, damping ratios, and mode shapes appear explicitly in (A,B,C) state-space models as physically meaningful parameters. Uncertainty in mode shapes, for example, which appear as columns of the B matrix, cannot in general be expected to be of a multiplicative form in accordance with traditional gain-margin specifications. This is precisely the problem illustrated by the example of [6] discussed above. Furthermore, uncertainties in modal frequencies and damping ratios must be carefully differentiated since, roughly speaking, modal frequency uncertainties affect only the imaginary part of the pole location while damping uncertainty affects the real part. Although these and related observations

concerning uncertainty in the dynamic characteristics of lightly damped structures may be self evident, they have remained largely unexploited in standard control-design methods.

2. OPUS: New Machinery for Control-System Design

In view of the ability of LQG theory to synthesize dynamic controllers for multi-input, multi-output controllers, it is not surprising that LQG forms the basis for a variety of structural control methods. However, as discussed previously, LQG lacks the ability to address performance/processor and performance/robustness tradeoffs. This situation has thus motivated the development of numerous variants of LQG which entail additional procedures which attempt to remedy these defects. OPUS, however, is distinctly different. Rather than append additional procedures to LQG design, OPUS extends LQG theory itself by generalizing the basic underlying machinery.

As shown in Figure 5, the basic machinery of LQG consists of a pair of separated Riccati equations whose solutions serve to directly and explicitly synthesize the gains of an optimal dynamic compensator. The contribution of OPUS is to directly expand this machinery. The overall approach is illustrated in Figure 7 which portrays <u>two</u> distinct generalizations of the basic LQG machinery. As Figure 7 illustrates, these generalizations can be developed individually when either low-order or robust controllers are desired. The appealing aspect of OPUS, however, is the ability to extend LQG to address both problems <u>simultaneously</u> in a <u>unified</u> manner.

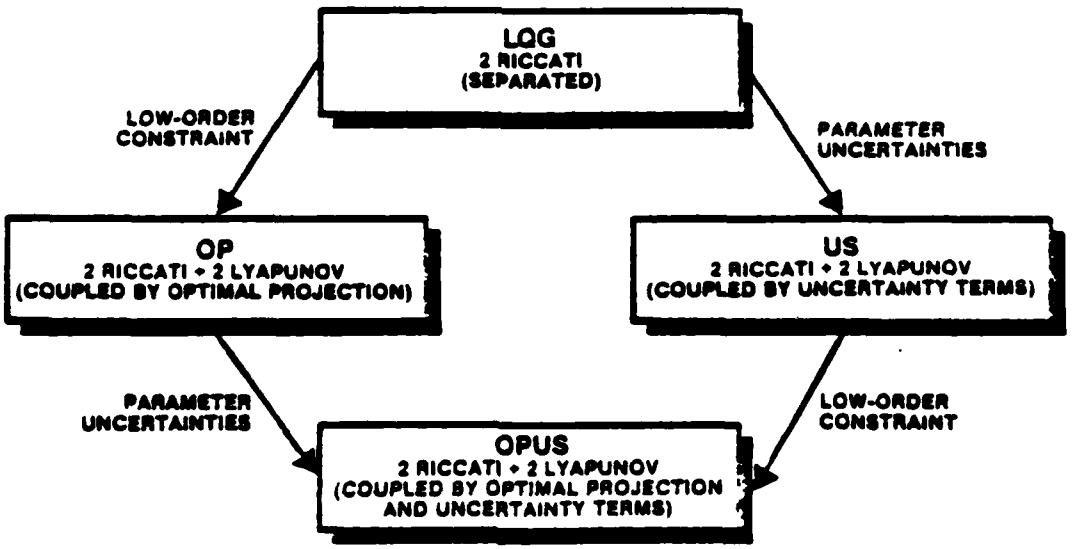

Figure 7. The Standard LQG Result Is Generalized by Both the Fixed-Order Constraint and Modeling of Parameter Uncertainties

In the following sections the generalizations depicted in Figure 7 will be reviewed following the left branch. That is, the optimal projection approach to reduced-order controller design will first be discussed in Section 3 without introducing plant uncertainties. In Section 4 the reduced-order constraint will be retained while considering, in addition, uncertainties in the system model. In each case the discussion will focus on the underlying ideas with a minimum of technical detail.

Clearly, in order for a novel design methodology to be of practical value it must be computationally tractable. Hence Section 5 will present an overview of the current state of algorithm development for solving the OPUS design equations. Finally, Section 6 will briefly summarize further OPUS generalizations of LQG theory which are relevant to structural control.

3. Extensions of LQG to Reduced-Order Dynamic Compensation

The simplest, most direct way to obtain optimal reduced-order controllers is to redevelop the standard LQG result in the presence of a constraint on controller dimension (Figure 8). The mathematical technique required to do this is remarkably straightforward. Specifically, the structure and order of the controller are fixed and the performance is optimized with respect to the controller gains. The resulting necessary conditions obtained using Lagrange multipliers thus characterize the optimal gains.

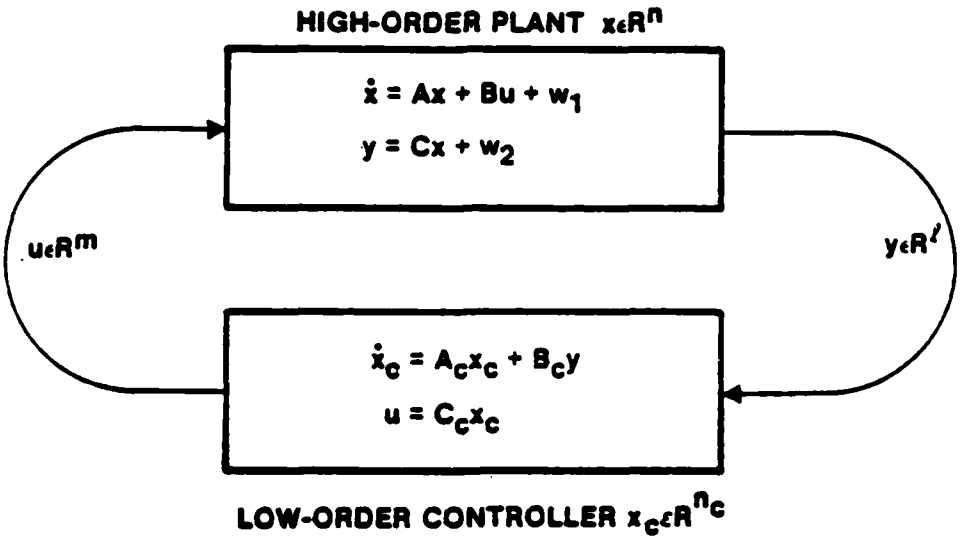

STEADY-STATE PERFORMANCE CRITERION

$$J(A_c, B_c, C_c) = \lim_{t \to \infty} E[x^T R_1 x + u^T R_2 u]$$

Figure 8. In Accordance With On-Board Processor Requirements, a Reduced-Order Constraint Is Imposed on the Dimension of the Dynamic Compensator

This parameter optimization approach as such is not new and was investigated extensively in the 1970's. Typically, however, the optimality conditions were found to be complex and unwieldy while offering little insight and requiring gradient search methods for numerical solution.

One curious aspect of the parameter optimization literature is that no attempt was made to actually use this direct method to rederive the LQG result itself. Such an exercise, it may be surmised, might reveal hidden structure within the optimality conditions which would shed light on the reduced-order case. Indeed, such an approach led to the realization that an oblique projection (idempotent matrix) is the key to unlocking the unwieldy optimality conditions ([A7,A17]). Although the result is mathematically straightforward, it is by no means obvious since in the full-order (LQG) case the projection is the identity and hence not readily apparent.

By exploiting the presence of the projection, the necessary conditions can be transformed into a coupled system of four algebraic matrix equations consisting of a pair of modified Riccati equations and a pair of modified Lyapunov equations (Figure 9). The coupling is via the oblique projection π which appears in all four equations and which is determined by the solutions $\hat{Q}$ and $\hat{P}$ of the modified Lyapunov equations. A satisfying feature of the optimality conditions is that in the full-order case the projection becomes the identity, the modified Lyapunov equations drop out, and, since $\tau_1 = 0$, the modified Riccati equations specialize to the usual separated Riccati equations of LQG theory. Since, furthermore, $G = \Gamma =$ nxn identity, the standard LQG gain expressions are recovered.

Although the modified Riccati equations specialize to the standard Riccati equations in the full-order case, the modified Lyapunov equations have no counterpart in the standard theory. The role of these equations can be understood by considering the problem of optimal model reduction alone. For this problem the optimal reduced-order model is characterized by a pair of coupled modified Lyapunov equations (see [A22]). Thus the modified Lyapunov equations arising in the reduced-order dynamic-compensation problem are directly analogous to the modified Lyapunov equations arising in model reduction alone. The modified Lyapunov equations arising in the control problem, however, are intimately coupled with the modified Riccati equations. Hence it cannot be expected that reduced-order control-design techniques based upon LQG will generally yield optimal fixed-order controllers (Figure 10). It is interesting to note that several such methods discussed in [1] are based upon balancing which was shown in [A22] to be suboptimal with respect to the quadratic (least squares) optimality criterion.

REDUCED-ORDER CONTROLLER GAINS

$$A_c = \Gamma(A - Q\bar{\Sigma} - \Sigma P)G^T$$

$$B_c = \Gamma Q C^T V_2^{-1}$$

$$C_c = -R_2^{-1}B^T P G^T$$

COUPLED RICCATI/LYAPUNOV EQUATIONS

$$0 = AQ + QA^T + V_1 - Q\bar{\Sigma}Q + \tau_1 Q\bar{\Sigma}Q\tau_1^T$$

$$0 = A^T P + PA + R_1 - P\Sigma P + \tau_1^T P\Sigma P\tau_1$$

$$0 = (A - \Sigma P)\hat{Q} + \hat{Q}(A - \Sigma P)^T + Q\bar{\Sigma}Q - \tau_1 Q\bar{\Sigma}Q\tau_1^T$$

$$0 = (A - Q\bar{\Sigma})^T\hat{P} + \hat{P}(A - Q\bar{\Sigma}) + P\Sigma P - \tau_1^T P\Sigma P\tau_1$$

$$\text{rank } \hat{Q} = \text{rank } \hat{P} = \text{rank } \hat{Q}\hat{P} = n_c$$

$$\hat{Q}\hat{P} = G^T M \Gamma \qquad \Gamma G^T = I_{n_c}$$

$$\tau = G^T\Gamma = \hat{Q}\hat{P}(\hat{Q}\hat{P})^{\#} \qquad \tau_1 = I_n - \tau$$

$$\Sigma = BR_2^{-1}B^T \qquad \bar{\Sigma} = C^T V_2^{-1} C$$

Figure 9. The Optimal Reduced-Order Compensator Is Determined by a Pair of Modified Riccati Equations and a Pair of Modified Lyapunov Equations Coupled by the Oblique Projection τ

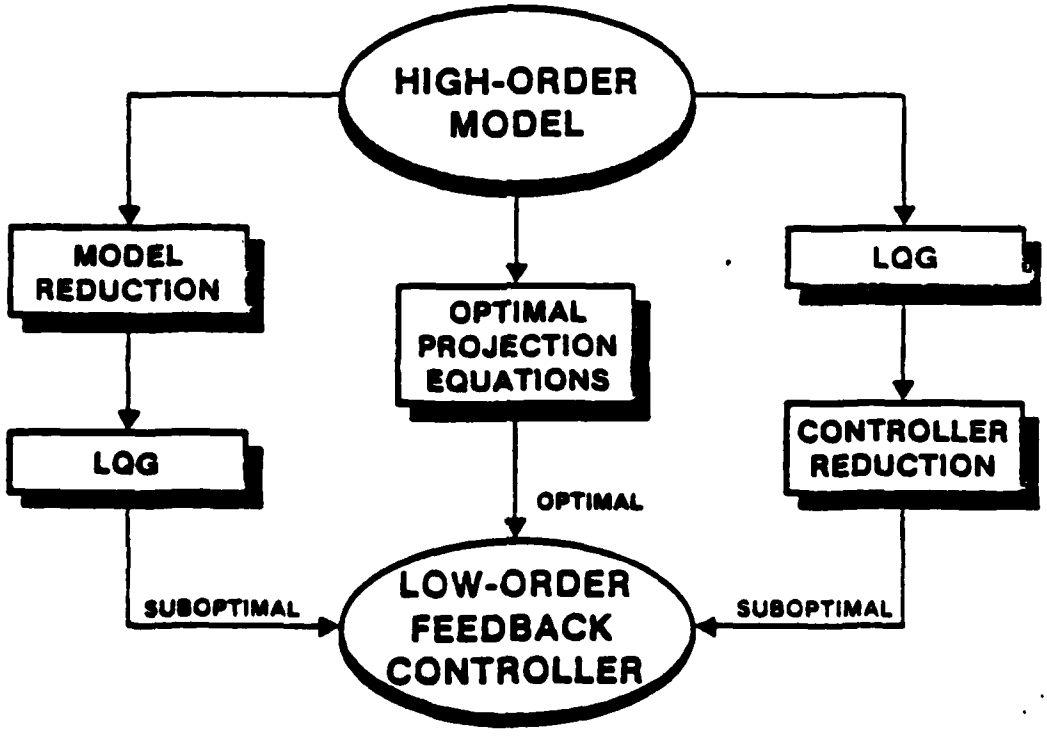

Figure 10. The Optimal Projection Equations Provide a Direct Path to Optimal Reduced-Order Dynamic Compensators

In summary, the optimal projection equations for reduced-order dynamic compensation comprise a direct extension of the basic LQG machinery to the reduced-order control problem. The design equations, which reduce to the standard LQG result in the full-order case, provide direct synthesis of optimal reduced-order controllers in accordance with implementation constraints.

4. Extensions of LQG to Uncertain Modeling

Two fundamental sources of error in modeling flexible structures are truncated modes and parameter uncertainties. Since the optimal projection approach permits the utilization of the full dynamics model, modal truncation can be largely avoided. There remains, however, a tendency to truncate poorly known modes and thus it is essential to incorporate a model of parameter uncertainty in both well-known and poorly known components of the system. Hence the problem formulation of Figure 8 is now generalized in Figure 11 to include uncertain parameters σ_i appearing in the A, B and C matrices. The parameter σ_i is assumed to lie within the interval $[-\delta_i, \delta_i]$ in accordance with identification accuracy. Clearly, when uncertainty is absent, i.e., when A_i, B_i, C_i = 0, the reduced-order design problem of Figure 8 is recovered.

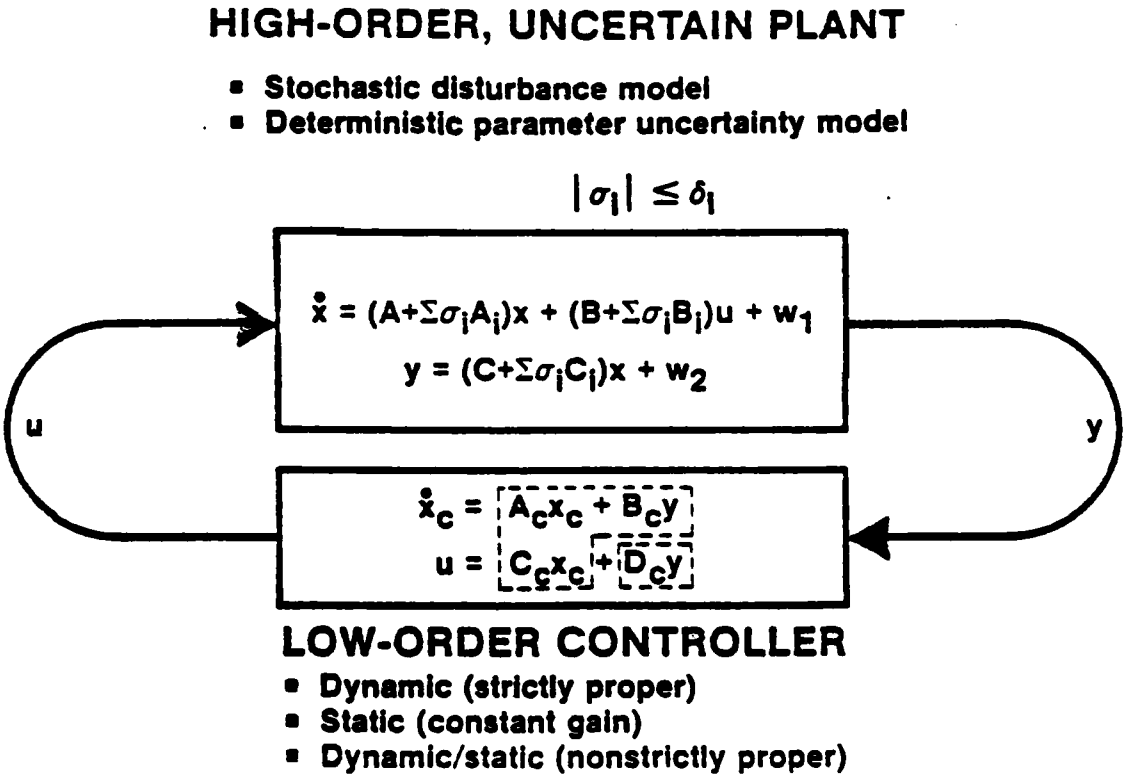

Figure 11. Robust Optimal Projection Design Is Based Upon a Hybrid Uncertainty Model Involving a Deterministic Parameter Uncertainty Model and a Stochastic Disturbance Model

A salient feature of the design model is that uncertainty is modeled in two distinctly different ways. External uncertainty appearing as additive white noise is modeled stochastically. Such a model appears appropriate for disturbances such as coolant flow for which only power spectral data are available. On the other hand, internal uncertainty appearing as parameter variations is modeled deterministically. Such a model appears appropriate for uncertainty arising from directly measurable quantities such as mass and stiffness. Thus the overall uncertainty model is hybrid in the sense that it utilizes both deterministic and stochastic characterizations of uncertainty.

A natural performance measure which accounts for both types of uncertainty characterization involves the usual LQG quadratic criterion averaged over the disturbance statistics and then maximized over the uncertain parameters (Figure 12). Hence this performance measure incorporates on the average and worst case aspects in accordance with physical considerations.

PERFORMANCE CRITERION

$$J(A_c,B_c,C_c) = \sup_{\sigma_i} \; \limsup_{t\to\infty} \; E\,[x^T R_1 x + 2x^T R_{12} u + u^T R_2 u]$$

- $\sup_{\sigma_i}$ → Worst-Case → Over Parameters
- $\limsup_{t\to\infty}$ → Steady-State
- E → Average → Over Disturbance Statistics
- Quadratic

ROBUST PERFORMANCE PROBLEM

Minimize $J(A_c,B_c,C_c)$ over the class of robustly stabilizing controllers (A_c,B_c,C_c)

Figure 12. Performance Is Defined To Be Worst Case Over the Uncertain Parameters and Average Over the Disturbance Statistics

The resulting Robust Performance Problem thus involves determining the gains (A_c,B_c,C_c) to minimize the performance J. The static gain D_c can also be included but will not be discussed here. Despite the apparent complexity of the problem, remarkably simple techniques can be used. Specifically, first note that after taking the expected value the performance J has the form

$$J(A_c,B_c,C_c) = \sup_{\sigma_i} \; \limsup_{t\to\infty} \; \mathrm{tr}\, \bar{Q}(t)\bar{R}, \qquad (4.1)$$

where "tr" denotes trace of a matrix, $\bar{Q}(t)$ is the covariance of the closed-loop system, and $\bar{R}$ is an augmented weighting matrix composed of R_1, R_{12} and R_2. The covariance $\bar{Q}(t)$ satisfies the standard Lyapunov differential equation

$$\dot{\bar{Q}} = (\bar{A}+\sum\sigma_i\bar{A}_i)\bar{Q} + \bar{Q}(\bar{A}+\sum\sigma_i\bar{A}_i)^T + \bar{V}, \tag{4.2}$$

where $\bar{A}$ is the closed-loop dynamics, $\bar{A}_i$ is composed of A_i, B_i and C_i, and $\bar{V}$ is the intensity of external disturbances for the closed-loop system including the plant and measurement noise.

Two distinct approaches to this problem will be considered. The first involves bounding the performance over the class of parameter uncertainties and then choosing the gains to minimize the bound. Since bounding precedes control design this approach is known as robust design via a priori performance bounds. The second approach involves exploiting the nondestabilizing nature of structural systems via weak subsystem interaction.

4.1 Robust Design Via A Priori Performance Bounds

The key step in bounding the performance (4.1) is to replace (4.2) by a modified Lyapunov differential equation of the form

$$\dot{\bar{Q}} = \bar{A}\bar{Q} + \bar{Q}\bar{A}^T + \Psi(\bar{Q}) + \bar{V}, \tag{4.3}$$

where the bound Ψ satisfies the inequality

$$\sum\sigma_i(\bar{A}_i\bar{Q}+\bar{Q}\bar{A}_i^T) \le \Psi(\bar{Q}) \tag{4.4}$$

over the range of uncertain parameters σ_i and for all candidate feedback gains. Note that the inequality (4.4) is defined in the sense of nonnegative-definite matrices. Now rewrite (4.3) by appropriate addition and subtraction as

$$\dot{\bar{Q}} = (\bar{A}+\sum\sigma_i\bar{A}_i)\bar{Q} + \bar{Q}(\bar{A}+\sum\sigma_i\bar{A}_i)^T + \Psi(\bar{Q}) - \sum\sigma_i(\bar{A}_i\bar{Q}+\bar{Q}\bar{A}_i^T) + \bar{V}. \tag{4.5}$$

Now subtract (4.2) from (4.5) to obtain

$$\dot{\bar{Q}} - \dot{\bar{Q}} = (\bar{A}+\sum\sigma_i\bar{A}_i)(\bar{Q}-\bar{Q}) + (\bar{Q}-\bar{Q})(\bar{A}+\sum\sigma_i\bar{A}_i)^T + \Psi(\bar{Q}) - \sum\sigma_i(\bar{A}_i\bar{Q}+\bar{Q}\bar{A}_i^T). \tag{4.6}$$

Since by (4.4) the term

$$\Psi(\bar{Q}) - \sum\sigma_i(\bar{A}_i\bar{Q}+\bar{Q}\bar{A}_i^T) \tag{4.7}$$

is nonnegative definite, it follows immediately that

$$\bar{Q} \leq \bar{Q} \tag{4.8}$$

over the class of uncertain parameters. Thus the performance (4.1) can be bounded by

$$J(A_c,B_c,C_c) \leq \underline{J}(A_c,B_c,C_c) \triangleq \lim_{t\to\infty} \mathrm{tr}\ \bar{Q}\bar{R}. \tag{4.9}$$

The auxiliary cost $\underline{J}$ is thus guaranteed to bound the <u>actual</u> cost J. This leads to the <u>Auxiliary Minimization Problem</u>: Minimize the auxiliary cost $\underline{J}$ over the controller gains. The advantage of this approach is that necessary conditions for the Auxiliary Minimization Problem effectively serve as <u>sufficient</u> conditions for robust performance in the original problem. Since the bounding step <u>precedes</u> the optimization procedure, this approach is referred to as robust design via a priori performance bounds. This procedure is philosophically similar to guaranteed cost control ([9,10]). Note that since bounding precedes optimization, the bound (4.4) must hold for all gains since the optimal gains are yet to be determined.

To obtain sufficient conditions for robust stability, the bounding function Ψ must be specified. Since the ordering of nonnegative-definite matrices appearing in (4.4) is not a total ordering, a unique lowest bound should not be expected. Furthermore, each differentiable bound leads to a fundamental extension of the optimal projection equations and thus of the basic LQG machinery. In work thus far, two bounds have been extensively investigated. Only one bound, the right shift/multiplicative white noise bound, will be discussed here. The structured stability radius bound introduced in [11,12] is discussed in [A43].

The right shift/multiplicative white noise bound investigated in [A29,A41] is given by

$$\Psi(\bar{Q}) = \sum\delta_i(\alpha_i\bar{Q}+\alpha_i^{-1}\bar{A}_i\bar{Q}\bar{A}_i^T), \tag{4.10}$$

where $\alpha_i > 0$ are arbitrary scalars. Note that this bound consists of two distinct parts which must appear in an appropriate ratio. The first term $\alpha_i\bar{Q}$ arises naturally when an exponential time weighting $e^{\alpha_i t}$ is included in the performance measure. As is well known ([13]) this leads to a prescribed uniform stability margin for the

closed-loop system (Figure 13). A uniform stability margin, no matter how large, however, does not guarantee robustness with respect to arbitrary parameter variations. The complementary second term $\alpha_i^{-1}\bar{A}_i\bar{Q}\bar{A}_i^T$ is crucial in this regard.

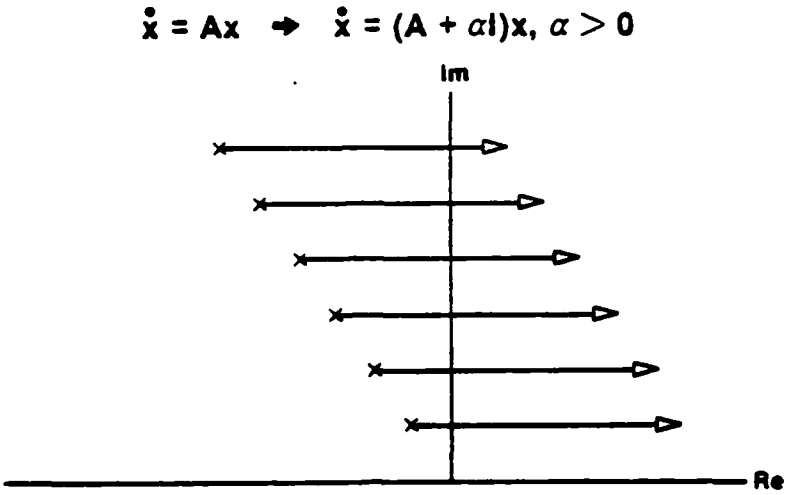

APPLY CONTROL-DESIGN TECHNIQUES TO RIGHT-SHIFTED OPEN-LOOP SYSTEM ⇨ UNIFORM STABILITY MARGIN
(Anderson and Moore, 1969)

Figure 13. Open-Loop Right-Shifted Dynamics Arising From Exponential Cost Weighting Lead to a Uniform Closed-Loop Stability Margin

Although terms of the form $\bar{A}_i\bar{Q}\bar{A}_i^T$ are unfamiliar in robust control design, they arise naturally in stochastic differential equations with <u>multiplicative</u> white noise. That is, if the uncertain parameters σ_i are <u>replaced</u> by white noise processes entering multiplicatively rather than additively, then the covariance equation for $\bar{Q}$ automatically includes terms of the form $\bar{A}_i\bar{Q}\bar{A}_i^T$. The literature on systems with multiplicative white noise is quite extensive; see [A38] for references. It should be stressed, however, that for our purposes the multiplicative white noise model is <u>not</u> interpreted literally as having physical significance. Rather, multiplicative white noise can be thought of as a useful <u>design model</u> which correctly captures the impact of uncertainty on the performance functional via the state covariance. Furthermore, just as the right shift term alone does not guarantee robustness, neither does the multiplicative white noise term. Both terms must appear simultaneously. Roughly speaking, since multiplicative white noise disturbs the plant though uncertain parameters, the closed-loop system is automatically desensitized to <u>actual</u> parameter variations.

After incorporating the right shift/multiplicative white noise bound (4.10) into (4.3) to obtain a bound $\underline{J}$ for the performance, the optimal projection equations can be rederived following exactly the same parameter optimization procedure discussed in Section 3. Again, the mathematics required is but a straightforward application of Lagrange multipliers. The additional bounding terms are carried through the derivation to yield a direct generalization of the optimal projection equations shown in Figure 14 with gains given in Figure 15.

$$0 = A_s Q + Q A_s^T + \Lambda Q \Lambda^T + V_1 + (\Lambda - B R_{2s}^{-1} P_s)\hat{Q}(\Lambda - B R_{2s}^{-1} P_s)^T - Q_s V_{2s}^{-1} Q_s^T + \tau_1 Q_s V_{2s}^{-1} Q_s^T \tau_1^T$$

$$0 = A_s^T P + P A_s + \Lambda^T P \Lambda + R_1 + (\Lambda - Q_s V_{2s}^{-1} C)^T \hat{P} (\Lambda - Q_s V_{2s}^{-1} C) - P_s^T R_{2s}^{-1} P_s + \tau_1^T P_s^T R_{2s}^{-1} P_s \tau_1$$

$$0 = (A_s - B_s R_{2s}^{-1} P_s)\hat{Q} + \hat{Q}(A_s - B_s R_{2s}^{-1} P_s)^T + Q_s V_{2s}^{-1} Q_s^T - \tau_1 Q_s V_{2s}^{-1} Q_s^T \tau_1^T$$

$$0 = (A_s - Q_s V_{2s}^{-1} C_s)^T \hat{P} + \hat{P}(A_s - Q_s V_{2s}^{-1} C_s) + P_s^T R_{2s}^{-1} P_s - \tau_1^T P_s^T R_{2s}^{-1} P_s \tau_1$$

Figure 14. The Robustified Optimal Projection Design Equations Account for Both Reduced-Order Dynamic Compensation and Parametric Uncertainty

GAINS

$$A_c = \Gamma(A_s - B_s R_{2s}^{-1} P_s - Q_s V_{2s}^{-1} C_s) G^T$$

$$B_c = \Gamma Q_s V_{2s}^{-1}$$

$$C_c = -R_{2s}^{-1} P_s G^T$$

NOTATION

$$\hat{Q}\hat{P} = G^T M \Gamma, \quad \Gamma G^T = I_{n_c} \; (\Rightarrow \tau = G^T \Gamma = \tau^2)$$

$$\Lambda Q \Lambda^T = \sum_{i=1}^{p} A_i Q A_i^T, \quad \Lambda Q B = \sum_{i=1}^{p} A_i Q B_i, \text{ etc.}$$

$$R_{2s} = R_2 + B^T(P+\hat{P})B \qquad V_{2s} = V_2 + C(Q+\hat{Q})C^T$$

$$Q_s = Q C_s^T + V_{12} + \Lambda(Q+\hat{Q})C^T \qquad P_s = B_s^T P + R_{12}^T + B^T(P+\hat{P})\Lambda$$

Figure 15. The OPUS Controller Gains Are Explicitly Characterized as a Direct Generalization of the Classical LQG Gains

The robustified optimal projection equations comprise a system of four matrix equations coupled by both the optimal projection and uncertainty terms. When the uncertainty terms are absent, the optimal projection equations of Figure 9 are immediately recovered. On the other hand, if the order of the controller is set equal to the order of the plant, then all terms involving τ_1 can be deleted. However, in this case the modified Lyapunov equations do not drop out since $\hat{Q}$ and $\hat{P}$ still appear in the modified Riccati equations. Hence the basic machinery of LQG is again extended to include a pair of Lyapunov equations coupled to a generalization of the standard LQG equations. It is interesting to note that a related result in the context of multiplicative noise also appeared in the Soviet literature ([14]). It should also be pointed out that although the modified Lyapunov equations arising in the reduced-order control-design problem have analogues in model reduction, the modified Lyapunov equations appearing in the full-order robustified equations represent new machinery not anticipated in robustness theories. Hence using straightforward mathematical techniques, the basic LQG machinery has again been extended in novel directions.

Solving the design equations shown in Figures 14 and 15 yields controllers with guaranteed levels of robustness. The actual robustness levels may, however, be larger than specified by a priori bounds. Thus, to achieve desired robustification levels for the uncertainty structure specified by the a priori bounds, the design procedure may be utilized within an iterative synthesis/analysis procedure (Figure 16).

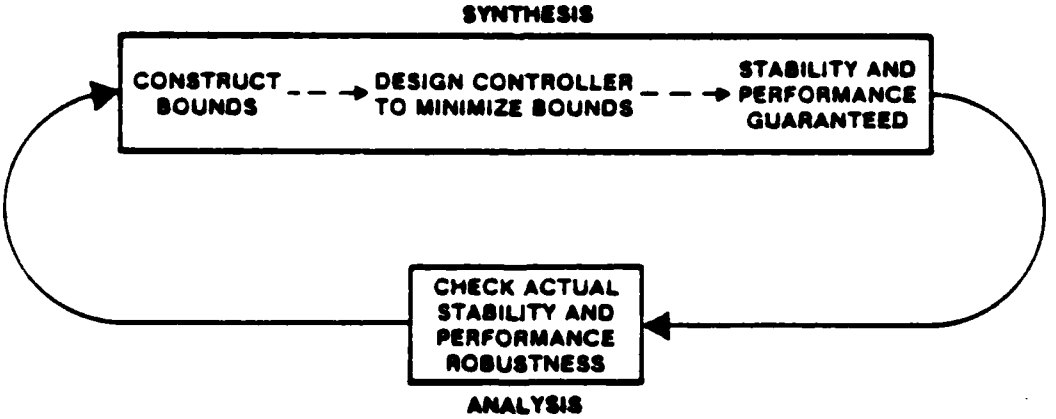

Figure 16. Optimal Projection/Guaranteed Cost Control Provides Direct Synthesis of Robust Dynamic Compensators

4.2 Robust Design Via Weak Subsystem Interaction

The mechanism by which LQG was robustified in Section 4.1 involved bounding the performance over the class of parameter uncertainties and then determining optimal controller gains for the performance bound. As discussed in Section 2,

however, flexible structures possess special properties which may, in addition, be exploited to achieve robustness. Specifically, aside from rigid-body modes, energy dissipation implies that mechanical structures are open-loop stable regardless of the level of uncertainty. That is, flexible structures possess only nondestabilizing uncertainties. Hence, in the closed loop, a given controller may or may not render a particular uncertainty destabilizing. A priori bounds on controller performance must, however, be valid for all gains since bounding precedes optimization. Hence, a priori bounding may in certain cases fail to exploit nondestabilizing uncertainties.

A familiar example of a nondestabilizing uncertainty involves uncertain modal frequencies. Such an uncertainty will not, of course, destabilize an uncontrolled (open-loop) structure. If particular modal frequencies are poorly known then it is clearly advisable to avoid applying high authority control. Hence, rather than the right-shift approach of Figure 13, it appears advantageous (although, at first, counterintuitive) to utilize just the opposite, namely, a left shift (Figure 17). Furthermore, in view of the fact that uncertainty usually increases with modal frequency (Figure 18), a variable left shift appears to be more appropriate than a uniform left shift. By left-shifting high-frequency poorly known modes, the control-system design procedure applies correspondingly reduced authority to modes "perceived" as highly damped. Hence the variable left shift can be roughly thought of as a device for achieving suitable authority rolloff. As will be seen, however, the underlying robustification mechanism, namely, weak subsystem interaction, is far more subtle than the approach of classical rolloff techniques. It is also interesting to note that the weak subsystem interaction approach to robustness is entirely distinct from classical robustness approaches which utilize high loop gain to reduce sensitivity.

$$\dot{x} = Ax \quad \Rightarrow \quad \dot{x} = (A + \frac{1}{2}\sum_{i=1}^{p} A_i^2)x$$

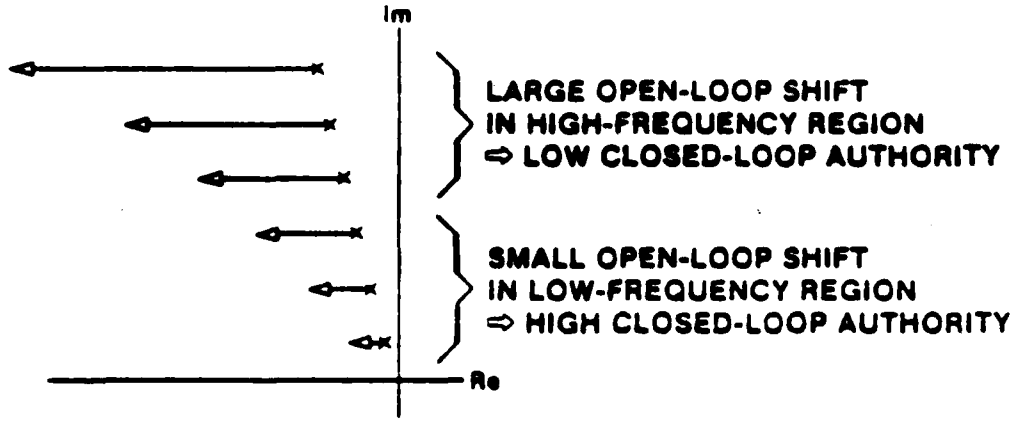

Figure 17. A Variable Left Shift Exploits Open-Loop Nondestabilizing Uncertainties

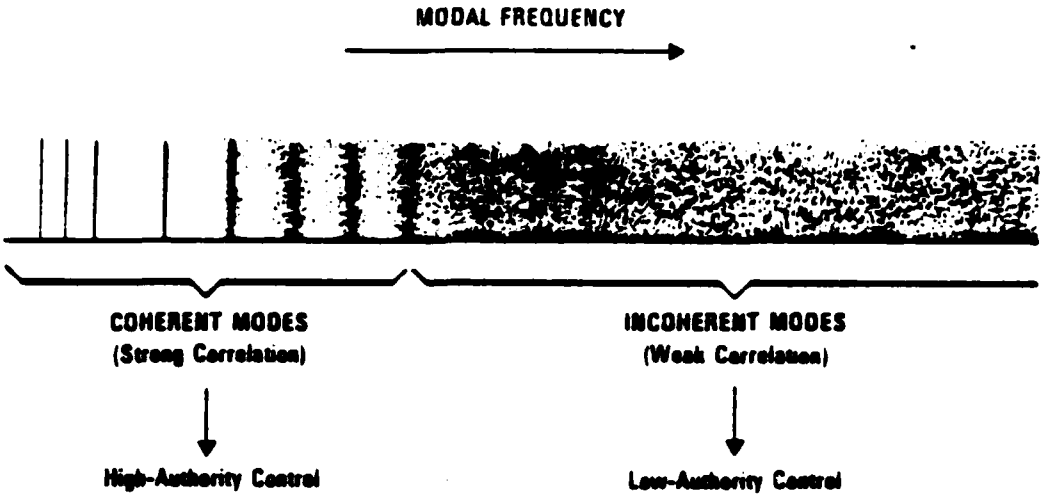

Figure 18. Modal Uncertainty Generally Increases With Frequency

A variable left shift can readily be introduced into the robustified optimal projection design equations by replacing A by

$$A_s = A + \tfrac{1}{2}\sum A_i^2, \tag{4.11}$$

where A_i denotes the structure of modal frequency uncertainty (Figure 19). Most interestingly, such a modification of the dynamics matrix arises naturally from a multiplicative white noise model defined not in the usual Ito sense but rather in the sense of Stratonovich. Thus, as in the a priori bounding approach, a stochastic

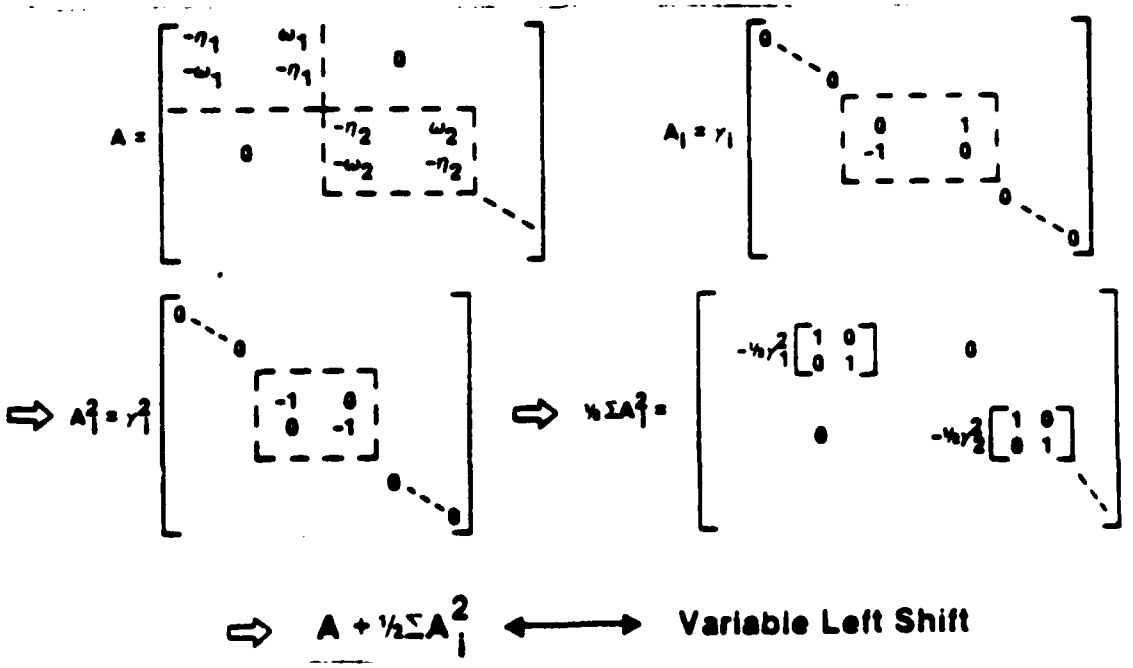

Figure 19. For Modal Systems With Frequency Uncertainty the Stratonovich Correction Corresponds to a Variable Left Shift

model serves to suggest a mechanism for robustification (Figure 20). Again it is important to stress that the multiplicative white noise model is not interpreted literally as having physical significance, but rather can be thought of as a useful design model which correctly captures the impact of uncertainty on the performance functional via the state covariance.

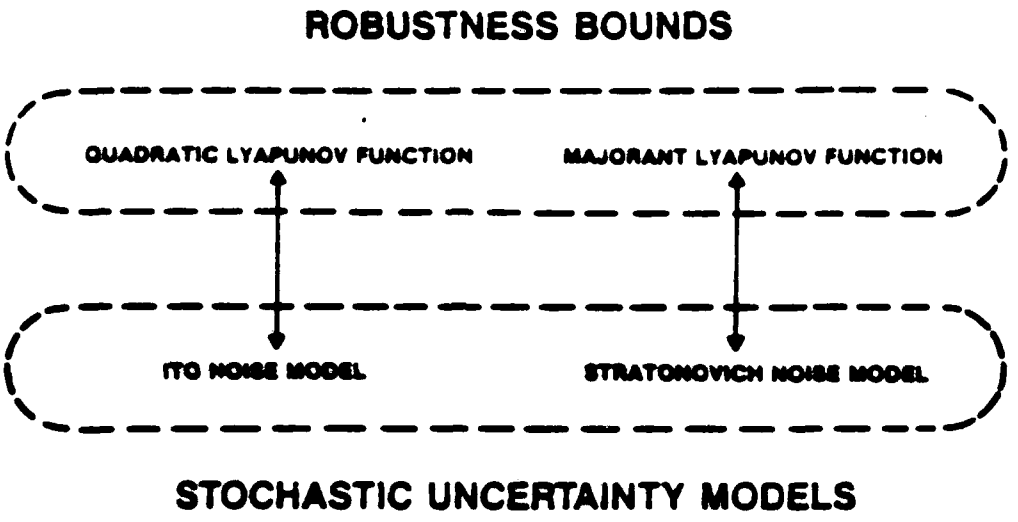

Figure 20. Stochastic Models and Robustness Bounds Are Fundamentally Related

In earlier work the Stratonovich dynamics model was justified by means of the minimum information/maximum entropy approach ([A1-A15]). A central result of the maximum entropy approach is that the high authority/low authority transition of a vibration control system from well-known low-frequency modes to poorly known high-frequency modes (Figure 18) is directly reflected in the structure of the state covariance matrix (Figure 21). A full-state feedback design applied to a simply

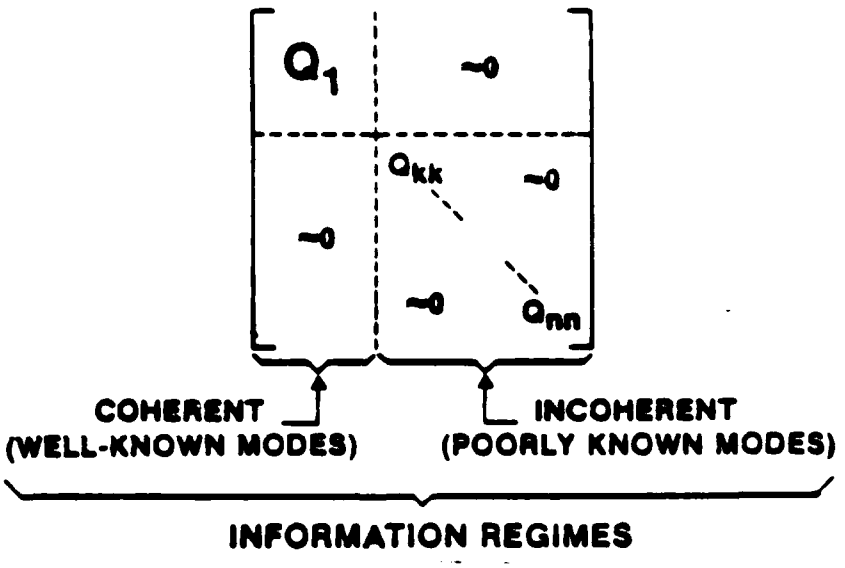

Figure 21. Frequency Uncertainties in the Stratonovich Model Lead to Suppressed Cross Correlation in the Steady-State Covariance

supported beam illustrates this point (Figure 22). By assuming that uncertainty in modal frequencies increases linearly with frequency, the structure of the covariance matrix leads directly to the control gains illustrated in Figure 23. Note that in the high-frequency region the position gains are essentially zero and thus the control law approaches positive-real energy dissipative rate feedback. This, of course, is precisely the type of structural controller expected in the presence of poor modeling information. Of course, any effective control-design theory for active vibration suppression in flexible structures should produce energy dissipative controllers when structural modeling information is highly uncertain.

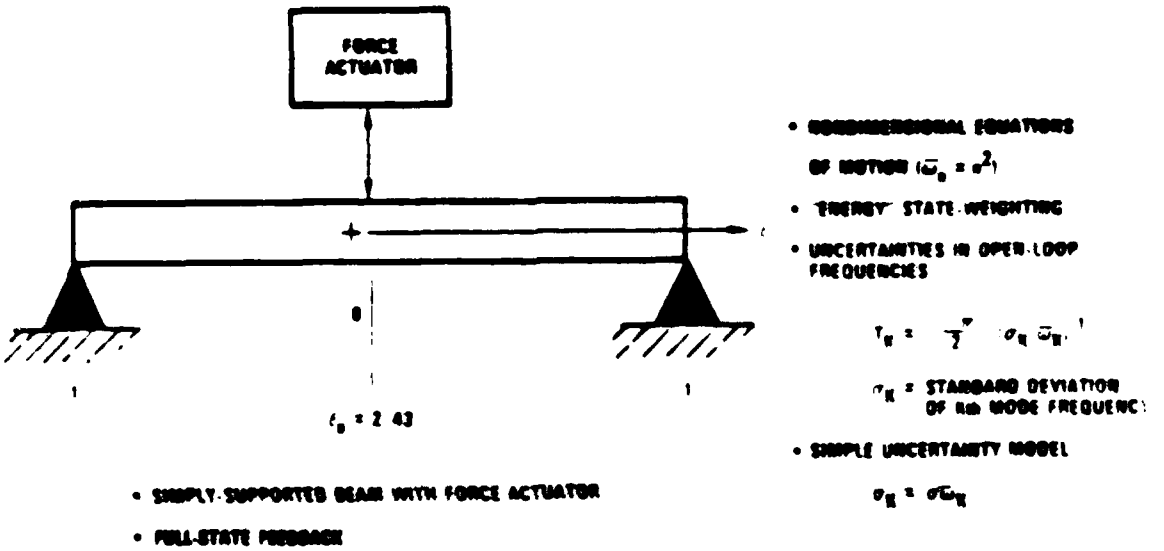

Figure 22. The Effects of Frequency Uncertainties Can Be Illustrated for a One-Dimensional Beam With Idealized Full-State Feedback

To carry out robustified optimal projection design in the presence of left-shifted open-loop dynamics, it is only necessary to utilize the left-shifted dynamics matrix (4.11) in place of the right-shifted matrix. All of the robustified optimal projection machinery, including gain expressions, can be utilized directly. It is also important to stress that the left shift must be used in conjunction with terms of the form $\bar{A}_i \bar{Q} \bar{A}_i^T$.

One explanation for the mechanism by which robustification is achieved is illustrated in Figure 24. By left shifting the open-loop dynamics within the design process, the compensator poles are similarly left-shifted. Thus the compensator poles are effectively moved further into the left half plane away from the actual plant poles. Since the interaction between compensator and plant poles is weakened, the closed-loop system is correspondingly robustified with respect to uncertainties in the plant pole locations. A sensitivity analysis of this mechanism utilizing a uniform left shift in the context of LQG design is given in [15].

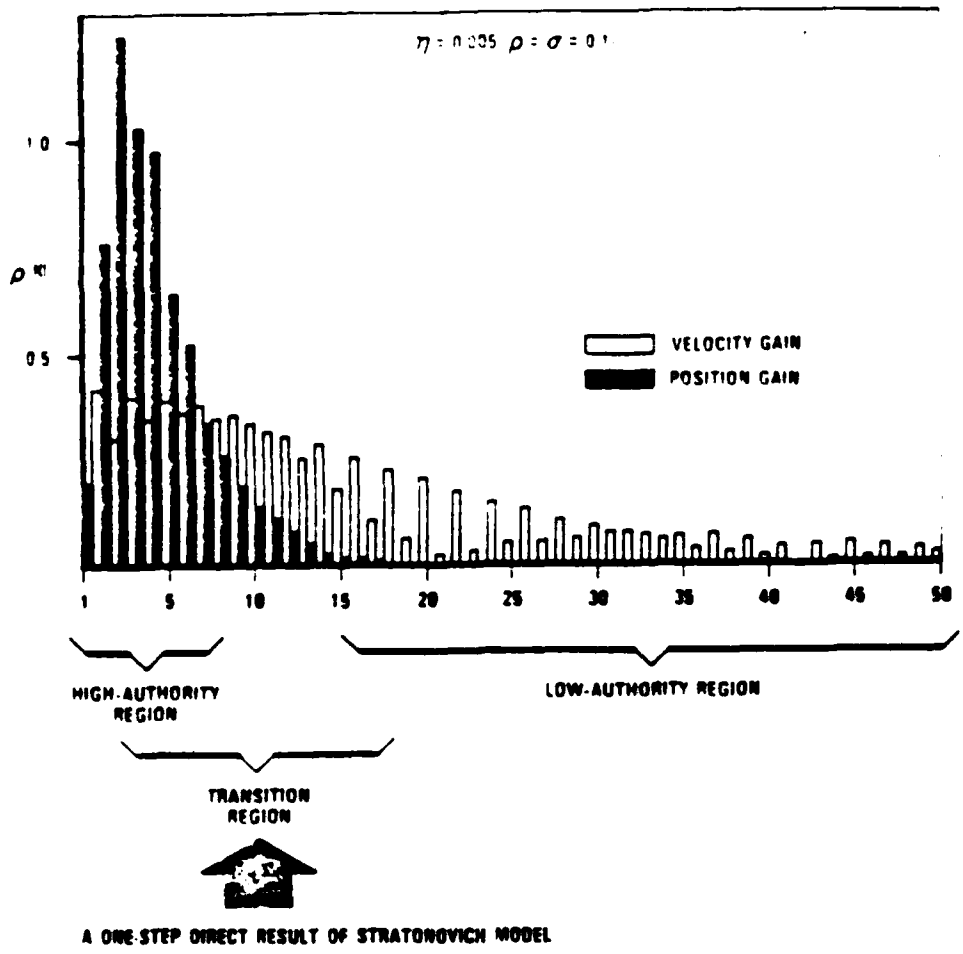

Figure 23. The Maximum Entropy Controller Approaches Rate Feedback in the Limit of Poor Modeling Information (High Uncertainty)

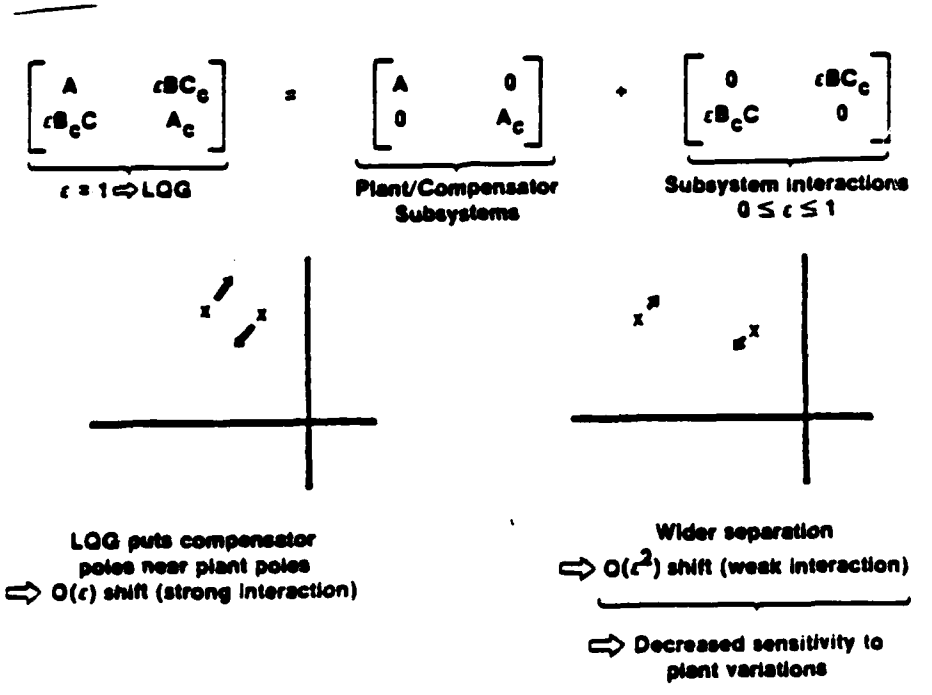

Figure 24. The Stratonovich Variable Left-Shift Model Effectively Places the Compensator Poles Further Into the Left Half Plane Where Plant/Compensator Interaction Is Weakened

As discussed above, the left-shift approach exploits open-loop nondestabilizing uncertainties and thus cannot operate through a priori bounding. Thus the actual level of robustification achieved from the robustified optimal projection equations for a given level of uncertainty modeling cannot be predicted a priori, i.e., in advance of control design. Indeed, this situation is to be expected when nondestabilizing uncertainties are exploited in a nonconservative design theory. Thus a suitable robust analysis technique is required for nonconservatively determining the robustification of the closed-loop system with respect to open-loop nondestabilizing uncertainties.

A suitable robustness analysis technique, known as majorant Lyapunov analysis, has indeed been developed ([A42]). Essentially, this technique employs a new type of Lyapunov function for assessing robustness due to weak subsystem interaction. The underlying machinery consists of the block-norm matrix which is a nonnegative matrix each of whose elements is the norm of a block of a suitably partitioned matrix (Figure 25). A matrix which bounds the block-norm matrix in the sense of nonnegative matrices, i.e., element by element, is known as a majorant. Majorants were introduced in [16] and were applied to srability analysis of integration algorithms for ODE's in [17].

(Ostrowski, 1961; Dahlquist, 1983)

$$M = \begin{bmatrix} M_1 & M_{12} & \cdots \\ M_{21} & M_2 & \ddots \\ \vdots & & \end{bmatrix}$$

$$m = \begin{bmatrix} \|M_1\| & \|M_{12}\| & \cdots \\ \|M_{21}\| & \|M_2\| & \ddots \\ \vdots & & \end{bmatrix}$$

NONNEGATIVE CONE ORDERING

$$m \leq\leq \hat{m}$$

Figure 25. The Matrix Majorant Is a Bound for the Matrix Block Norm, i.e., the Nonnegative Matrix Each of Whose Elements Is the Norm of the Corresponding Block of a Given Matrix

To apply majorants to dynamical systems, the model is written in the form shown in Figure 26. The matrix A is block diagonal and consists of subsystem dynamics. The subsystem interactions represented by the partitioned matrix G are assumed to be uncertain. By suitable manipulation, uncertainties in the diagonal blocks of A can also be captured by G. By assuming that the spectral norm (largest singular value) of the blocks of G satisfy given bounds, the covariance block-norm inequality is obtained (Figure 27). This inequality is interpreted in the sense of nonnegative matrices, i.e., element-by-element, and * denotes the Hadamard (element-by-element) product.

$$\dot{x} = (A + G)x + w \qquad \dot{Q} = (A + G)Q + Q(A + G)^T + V$$

$$A = \begin{bmatrix} A_1 & 0 & \cdots \\ 0 & A_2 & \ddots \\ \vdots & \ddots & \end{bmatrix} \qquad G = \begin{bmatrix} 0 & G_{12} & \cdots \\ G_{21} & 0 & \ddots \\ \vdots & \ddots & \end{bmatrix}$$

Known Subsystem Dynamics — Uncertain Subsystem Interactions

$$V = \begin{bmatrix} V_1 & V_{12} & \cdots \\ V_{21} & V_2 & \ddots \\ \vdots & \ddots & \end{bmatrix} \qquad Q = \begin{bmatrix} Q_1 & Q_{12} & \cdots \\ Q_{21} & Q_2 & \ddots \\ \vdots & \ddots & \end{bmatrix}$$

Noise Intensity — State Covariance

Figure 26. The Large-Scale System Model Involves Known Local Dynamics and Uncertain Interactions

$$\dot{x} = (A + G)x + w \qquad J = E[x^T R x] = \operatorname{tr} QR$$

$$0 = (A + G)Q + Q(A + G)^T + V \qquad \mathcal{A} = |\mathcal{E}(A_i \bullet A_j)|$$

$$\mathcal{V} = \begin{bmatrix} \|V_1\|_F & \|V_{12}\|_F & \cdots \\ \|V_{21}\|_F & \|V_2\|_F & \ddots \\ \vdots & \ddots & \end{bmatrix} \qquad \mathcal{Q} = \begin{bmatrix} \|Q_1\|_F & \|Q_{12}\|_F & \cdots \\ \|Q_{21}\|_F & \|Q_2\|_F & \ddots \\ \vdots & \ddots & \end{bmatrix}$$

$$\begin{bmatrix} 0 & \mathcal{E}(Q_{12}) & \cdots \\ \mathcal{E}(Q_{21}) & 0 & \ddots \\ \vdots & \ddots & \end{bmatrix} \leq \leq \mathcal{G}$$

$$\Downarrow$$

$$\mathcal{A} \bullet \mathcal{Q} \leq\leq \mathcal{G}\mathcal{Q} + \mathcal{Q}\mathcal{G}^T + \mathcal{V}$$

Figure 27. The Block-Norm Matrix of the State Covariance Satisfies a Lyapunov-Type Inequality Involving Nonnegative Matrices

To achieve robustness, the covariance block-norm inequality is replaced by the majorant Lyapunov equation (Figure 28). The solution of the majorant Lyapunov equation provides a bound (majorant) for the block norm of the covariance thereby guaranteeing both robust stability and performance.

MAJORANT LYAPUNOV EQUATION

$$\mathcal{A} * \hat{\mathcal{Q}} = \mathcal{G}\hat{\mathcal{Q}} + \hat{\mathcal{Q}}\mathcal{G}^T + \mathcal{V}$$

$$\bar{\sigma}(G_{ij}) \leq \mathcal{G}_{ij}$$

$$\Downarrow$$

$$Q \leq\leq \hat{Q}$$

$$\Downarrow$$

- **Robust Stability**
- **Robust Performance**

Figure 28. The Corresponding Nonnegative Matrix Equation Yields a Majorant for the State Covariance and Hence Robust Stability and Performance

It is interesting to note that numerical solution of the majorant Lyapunov equation requires no new techniques. Utilizing properties of M matrices, the solution can be obtained monotonically by means of a straightforward iterative technique (Figure 29).

MLE has a unique solution iff $\{\hat{\mathcal{Q}}_K, K=0, 1, \ldots, \infty\}$ **where:**

$$\hat{\mathcal{Q}}_0 = 0$$

$$\hat{\mathcal{Q}}_{K+1} = \mathcal{A}^{III} * (\mathcal{G}\hat{\mathcal{Q}}_K + \hat{\mathcal{Q}}_K\mathcal{G}^T + \mathcal{V})$$

$$(\mathcal{A}^{III}_{mn} \triangleq \mathcal{A}^{-1}_{mn})$$

converges. If so, then:

$$\hat{\mathcal{Q}} = \lim_{K\to\infty} \hat{\mathcal{Q}}_K$$

$$J - J_0 \leq 2\sum_{K=1}^{r} (\mathrm{tr}\,\hat{P}_K)(\mathcal{G}\hat{\mathcal{Q}})_{KK}$$

$$(0 = A_K^T \hat{P}_K + \hat{P}_K A_K + R_K)$$

Figure 29. By Exploiting the Properties of M-Matrices, the Majorant Lyapunov Equation Can Be Solved Monotonically by Means of a Simple Iterative Technique

An illustrative application of the majorant Lyapunov equation involves lightly damped subsystems (Figure 30). As shown in [A42] (and expected intuitively), robustness with respect to uncertain subsystem interaction is proportional to the frequency separation between the subsystems. The ability to capture this robustification mechanism is a unique feature of the majorant Lyapunov function not available from quadratic (i.e., scalar) Lyapunov functions or vector Lyapunov functions ([18,19]).

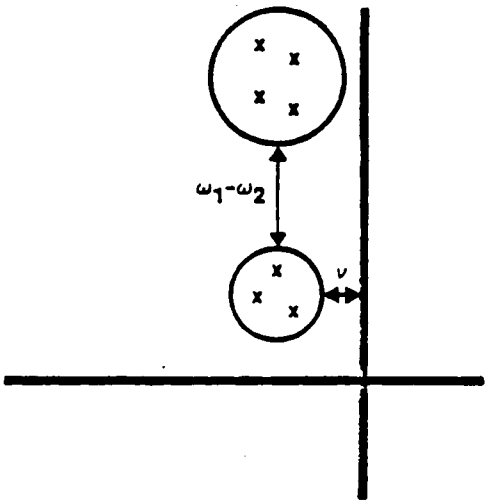

Majorant Lyapunov Equation Bound $\sim \nu \sqrt{(2\nu)^2 + (\omega_1-\omega_2)^2}$

Figure 30. Robustness Bounds for Uncertain Coupling in Modal Systems Are Proportional to the Frequency Separation Between Subsystems

The next step in the majorant development involves a hierarchy of finer and finer robustness bounds which account for higher order subsystem interactions, e.g., the interaction between the ith and jth subsystems via the kth subsystem. The second member of the hierarchy (Figure 31) provides robustness guarantees with respect to frequency uncertainties. The interesting aspect of this robustness test is the fact that the performance bound is characterized precisely by a Stratonovich model. Hence the Stratonovich model can be viewed as an approximation to a robustness bound, while exploiting the Stratonovich/majorant relationship leads to a natural synthesis/analysis scheme (Figure 32) which nonconservatively exploits open-loop destabilizing uncertainties.

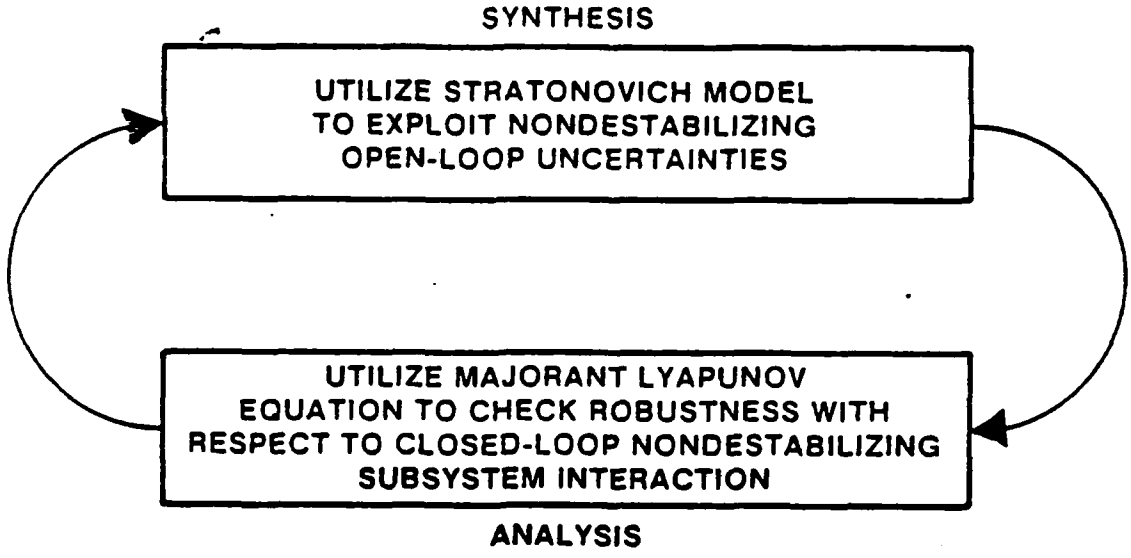

Stratonovich synthesis = approximation to majorant analysis

Figure 31. The Stratonovich Synthesis Model Provides a First Approximation to the Majorant Analysis Bounds

Second member of the hierarchy:

$$\mathcal{A} * \hat{Q} + \hat{\mathcal{H}}[\hat{Q}] = \mathcal{G}\langle\hat{Q}\rangle + \langle\hat{Q}\rangle\mathcal{G}^T + \mathcal{V}$$

$$J - \mathrm{tr}[\hat{Q}R] \leq 2\sum_{K=1}^{r} (\mathrm{tr}\,\hat{P}_K)(\mathcal{G}\langle\hat{Q}\rangle)_{KK}$$

$$0 = A\hat{Q} + \hat{Q}A^T + \mathcal{H}[\hat{Q}] + V$$
$$0 = A^T\hat{P} + \hat{P}A + \mathcal{H}^\dagger[\hat{P}] + R$$

where:

$\langle\hat{Q}\rangle \triangleq$ **off-diagonal part of** $\hat{Q}$

$\mathcal{H}[.]$ **= Stratonovich model operator**

- **Tighter bound—incorporates more information on A and G**
- **Predicts stability when** $(A + A^T)$ **stable,** $G = -G^T$
- **"Nominal" performance, tr** $[\hat{Q}R]$**, given by Stratonovich model**

Figure 32. The Refined Majorant Bound Incorporates a Stratonovich Covariance Model

5. Numerical Algorithms and Examples

Practical design of controllers is only possible when efficient, reliable algorithms are available. Indeed, the optimal projection equations are readily solvable and have been applied to a wide variety of examples. Numerical results appear in [A3-A6,A8,A11,A12,A14-A16,A18,A19,A21-A24,A26-A28,A30-A33,A39,A42,A44,A46]. Two distinctly different algorithms have been developed thus far, namely, an iterative method and a homotopy algorithm.

The iterative method, developed in [A14,A16,A44] and further studied in [20,21], is outlined in Figure 33. The nice feature of this approach is that only a standard LQG software package is required for its implementation. The basic motivation for the method is the observation that the main source of coupling is via the terms involving τ_1. The coupling is absent, of course, when τ is the identity, i.e., LQG. Note also that the terms involving τ_1 are small when R_2 and V_2 are large, i.e., when control cost is high and the measurement noise is significant. This case, which yields low-authority controllers, is approximately characterized by decoupled control-design and controller-reduction operations. Thus it is not surprising that LQG reduction techniques are most successful when controller authority is low.

Since the τ_1 terms occasion the greatest difficulty, it appears advantageous to bring them into play gradually. This can be accomplished by fixing τ after each iteration to yield updated values of Q, P, $\hat{Q}$ and $\hat{P}$. Furthermore, τ is introduced gradually by means of α to reduce its rank.

The crucial step of the algorithm concerns the construction of the projection τ from the pseudogramians $\hat{Q}$ and $\hat{P}$. Specifically, τ can be characterized (see [A22]) as the sum of eigenprojections of $\hat{Q}\hat{P}$, where each choice of eigenprojections may correspond to a local extremal. However, the necessary conditions do not specify which eigenprojections are to be selected for obtaining a particular local solution. Nevertheless, there do exist useful methods for constructing τ. For example, component-cost decomposition methods ([22]) when applied within the optimal projection framework often permit efficient identification of the global optimum.

Although the iterative method is convenient to use because it utilizes readily available software, it is suboptimal in the sense that it does not fully exploit the structure of the equations. Specifically, while the iterative method addresses a system of four nxn matrix equations, careful analysis reveals that because of the rank deficiency of the projection the problem can be recast as four $n_c$xn equations. Hence, when n_c is much smaller than n, which is clearly the most

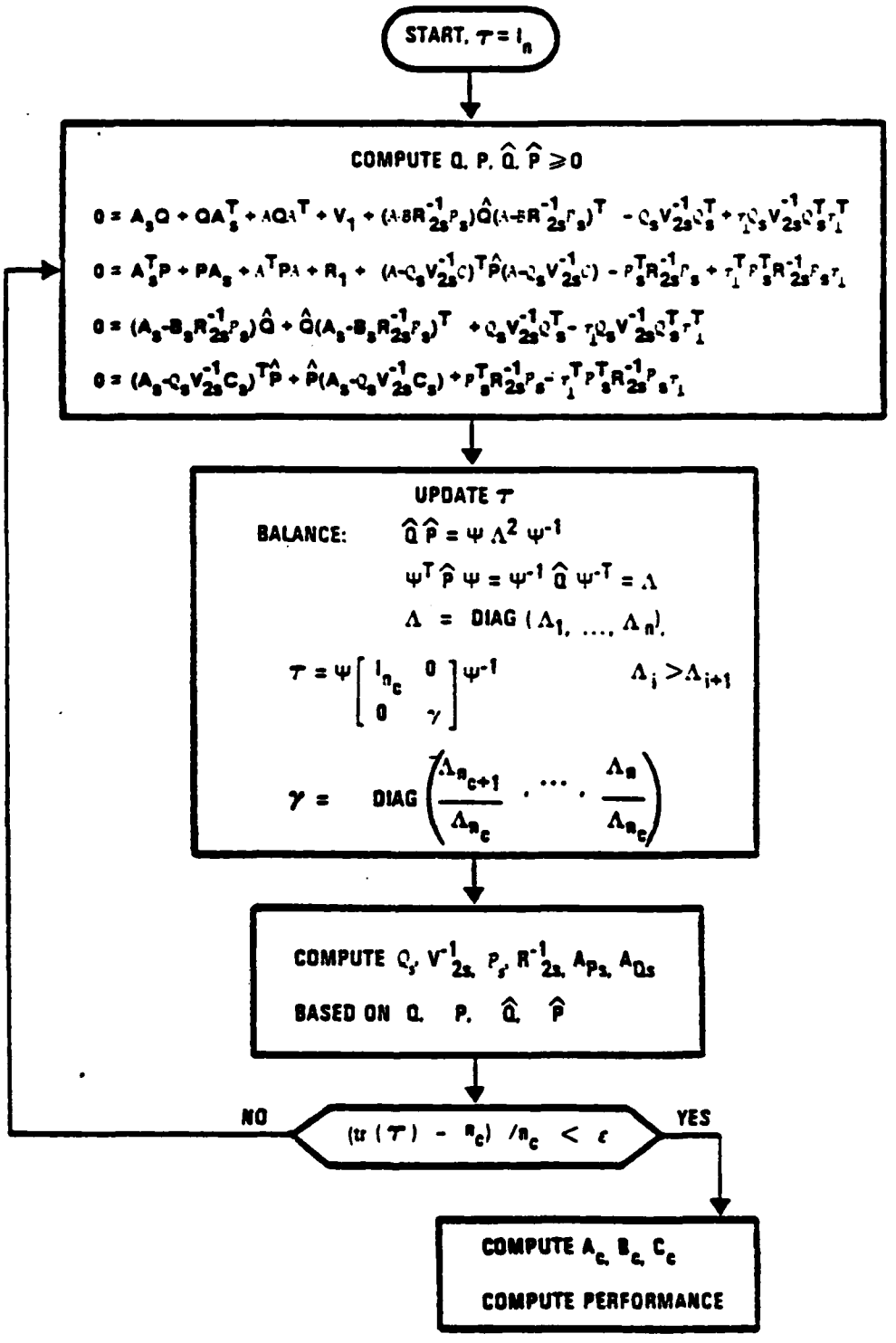

Figure 33. The Iterative Method for Solving the Robustified OPUS Design Equations Requires Only an LQG Software Package and Involves Refinement of the Optimal Projection τ

desirable case for practical implementation, there exists considerable opportunity for increased computational efficiency. Furthermore, and most satisfying, the computational complexity decreases with n_c as is intuitively expected below that required by LQG design. Hence the optimal projection approach has computational complexity less than LQG reduction methods for which LQG is but the first step.

S. Richter ([23,A46]) has developed a homotopy algorithm which fully exploits this crucial structure. Numerical experiments thus far have shown that considerable computational savings can be achieved over the iterative method. Furthermore, by applying topological degree theory to investigate the branches and character of the local extremals, it can be shown that the maximum number of possible extremals is

$$\binom{\min(n,m,\ell)}{n_c}$$

if $n_c \leq \min(n,m,\ell)$ or 1 otherwise. Hence in most practical cases the equations support a relatively small number of solutions.

Both the iterative method and the homotopy algorithm have been applied to a design problem involving an 8th-order flexible structure originally due to D. Enns and considered in [1]. Specifically, a variety of LQG reduction methods are compared in [1] for a range of controller authorities. These methods include:

1. Enns: This method is a frequency-weighted, balanced realization technique applicable to either model or controller reduction.

2. Glover: This method utilizes the theory of Hankel norm optimal approximation for controller reduction.

3. Davis and Skelton: This is a modification of compensator reduction via balancing which addresses the case of unstable controllers.

4. Yousuff and Skelton: This is a further modification of balancing for handling stable or unstable controllers.

5. Liu and Anderson: In place of using a balanced approximation of the compensator transfer function directly, this method approximates the component parts of a fractional representation of the compensator.

All of the above methods proceed by first obtaining the full-order LQG compensator design for a high-order state-space model and then reducing the dimension of the resulting LQG compensator.

Figure 34 summarizes the results reported in [1] for the above LQG reduction methods along with results obtained using the iterative method for solving the optimal projection equations. Here q_2 is a scale factor for the plant disturbance noise affecting controller authority. Clearly, LQG reduction methods experience increasing difficulty as authority increases, i.e., as the r_1 terms become increasingly more important in coupling the control and reduction operations. For the low authority cases, the optimal projection calculations, which were performed on a Harris H800 minicomputer, appeared to incur roughly the same computational burden as the LQG reduction methods. Although the optimal projection computational burden increases with authority, comparison with the LQG reduction methods is not meaningful because of the difficulty experienced by these methods in achieving closed-loop stability. See [A44] for further details and for comparisons involving transient response.

The homotopy algorithm was also applied to the example considered in [1]. One of the main goals of the development effort was to extend the range of disturbance intensity or, equivalently, observer bandwidth, out beyond $q_2 = 2000$. To this end, second-order ($n_c = 2$) controllers were obtained with relatively little computation for $q_2 = 10{,}000$, $100{,}000$ and $1{,}000{,}000$. In addition, the performance of each reduced-order controller was within 25% of LQG. These cases can surely be expected to present a nontrivial challenge to both the LQG reduction methods and the iterative optimal projection method.

Numerical solution of the robustified optimal projection equations has been carried out for several examples. For illustrative purposes a 2x2 example was considered in [A26] and the results illustrated in Figure 35 indicate performance/robustness tradeoffs possible. The variable left-shift technique was applied in [A19] to the NASA SCOLE problem with frequency uncertainties. The robustness of LQG and two robustified designs is shown in Figure 36. The plots illustrate the degradation in performance due to simultaneous perturbation of all modal frequencies. Note that LQG is rendered unstable by +5% frequency perturbation while a high-authority robustified design improves this region to +8%. The low-authority design increases this region significantly while sacrificing 6% nominal performance.

Method	q_2 / n_c	0.01	0.1	1	10	100	1000	2000
Enns	7	S	S	S	S	S	S	S
	6	S	S	S	S	S	S	S
	5	S	S	S	S	S	S	S
	4	S	S	S	S	S	S	U
	3	S	S	S	S	S	S	S
	2	S	S	S	S	U	U	U
Glover	7	S	S	S	S	S	U	S
	6	S	S	S	S	U	U	U
	5	S	S	S	S	U	U	U
	4	S	S	S	S	U	U	U
	3	S	S	U	S	U	U	U
	2	S	U	S	U	S	U	U
Davis & Skelton	7	S	U	U	S	S	S	S
	6	S	S	S	S	S	S	S
	5	S	U	S	S	S	U	U
	4	S	S	U	S	S	U	U
	3	U	U	U	U	U	U	U
	2	S	U	S	U	U	U	U
Yousuff & Skelton	7	S	S	S	S	U	U	U
	6	S	S	S	S	U	U	U
	5	S	S	S	U	U	U	U
	4	S	S	S	U	U	U	U
	3	S	U	U	U	U	U	U
	2	S	S	S	U	U	U	U
Liu & Anderson	7	S	S	S	S	S	S	U
	6	S	S	S	S	S	S	U
	5	S	S	S	S	S	S	S
	4	S	S	S	S	S	S	S
	3	S	S	S	S	S	U	U
	2	S	S	S	S	S	S	S
Optimal Projection	7	S	S	S	S	S	S	S
	6	S	S	S	S	S	S	S
	5	S	S	S	S	S	S	S
	4	S	S	S	S	S	S	S
	3	S	S	S	S	S	S	S
	2	S	S	S	S	S	S	S

S - The closed-loop system is stable
U - The closed-loop system is unstable

Figure 34. The Optimal Projection Approach Was Compared to Several LQG Reduction Techniques Over a Range of Controller Authorities for an Example of Enns

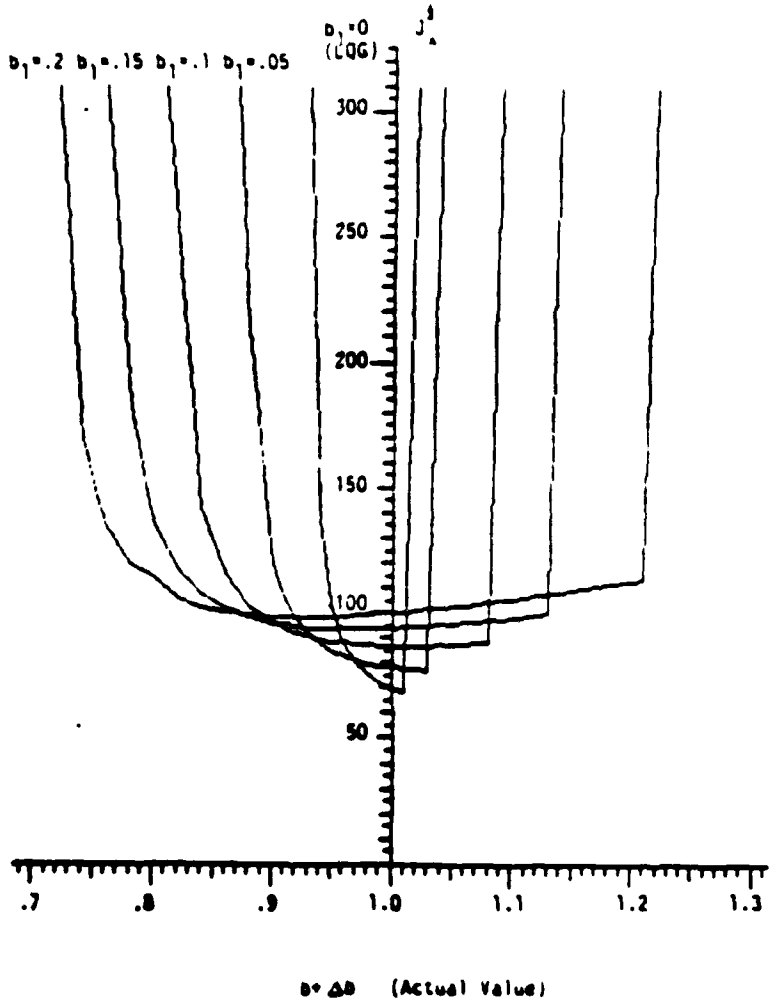

Figure 35. The Robustified Optimal Projection Equations Provide Robustness/Performance Tradeoffs for a Highly Sensitive Nominal LQG Design

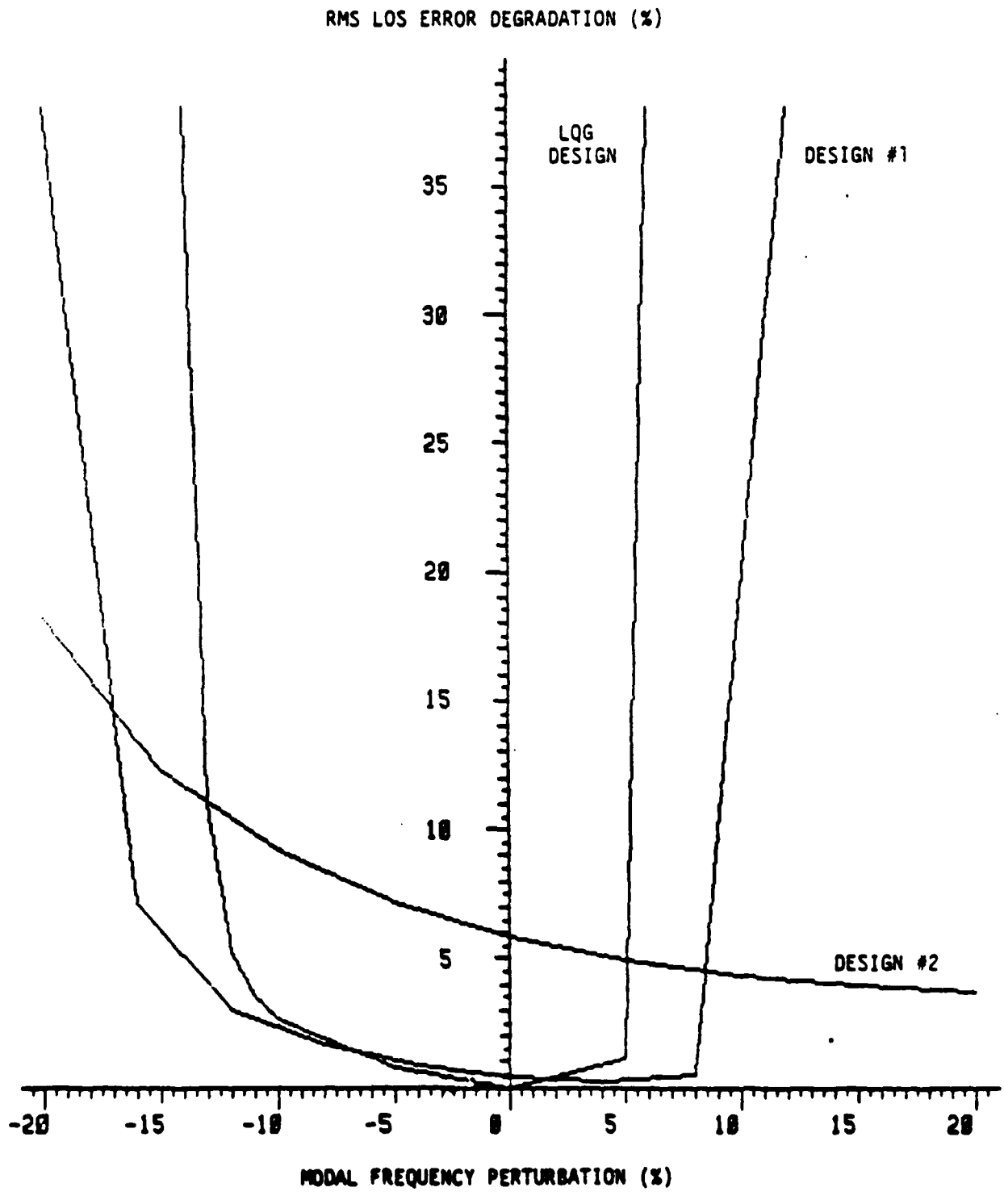

Figure 36. The Stratonovich Model Robustifies the LQG Design for the NASA SCOLE Model with Uncertain Modal Frequencies

6. Additional Extensions

The robustified optimal projection design machinery has been further extended to encompass a larger number of design cases arising in practical application. Here we merely list the extensions:

1. Discrete-time and sampled-data controllers ([A28,A30,A34,A35]).

2. Decentralized controllers ([A39]).

3. Nonstrictly proper controllers ([A37]).

4. Distributed parameter systems ([A25]).

7. Concluding Remarks

The machinery provided by OPUS for designing active controllers for flexible structures has been reviewed. The basic machinery is a system of coupled Riccati and Lyapunov equations which directly generalize the classical LQG result to include both a constraint on controller order and a model of parameter uncertainty. The overall approach thus encompasses all major design tradeoffs arising in vibration-suppression applications. Substantial numerical experience has been gained through an iterative method requiring only an LQG software package and, more recently, by means of a highly efficient homotopy algorithm developed by S. Richter. The overall approach opens the door for effective design of implementable controllers for large precision space structures.

Acknowledgment. We wish to thank Ms. Jill M. Straehla for the excellent preparation of this paper.

General References.

1. Y. Liu and B. D. O. Anderson, "Controller Reduction Via Stable Factorization and Balancing," Int. J. Contr., Vol. 44, pp. 507-531, 1986.

2. G. Zames, "Feedback and Optimal Sensitivity: Model Reference Transformations, Multiplicative Seminorms, and Approximate Inverses," IEEE Trans. Autom. Contr., Vol. AC-26, pp. 301-320, 1981.

3. J. C. Doyle, "Guaranteed Margins for LQG Regulators," IEEE Trans. Autom. Contr., Vol. AC-23, pp. 756-757, 1978.

4. J. C. Doyle and G. Stein, "Multivariable Feedback Design: Concepts for a Classical/Modern Synthesis," IEEE Trans. Autom. Contr., Vol. AC-26, pp. 4-16, 1981.

5. G. Stein and M. Athans, "The LQG/LTR Procedure for Multivariable Feedback Control Design," IEEE Trans. Autom. Contr., Vol. AC-32, pp. 105-114, 1987.

6. E. Soroka and U. Shaked, "On the Robustness of LQ Regulators," IEEE Trans. Autom. Contr., Vol. AC-29, pp. 664-665, 1984.

7. U. Shaked and E. Soroka, "On the Stability Robustness of the Continuous-Time LQG Optimal Control," IEEE Trans. Autom. Contr., Vol. AC-30, 1039-1043.

8. J. C. Doyle, "Analysis of Feedback Systems with Structured Uncertainties," IEE Proc., Vol. 129, pp. 242-250, 1982.

9. S. S. L. Chang and T. K. C. Peng, "Adaptive Guaranteed Cost Control of Systems with Uncertain Parameters," IEEE Trans. Autom. Contr., Vol. AC-17, pp. 474-483, 1972.

10. A. Vinkler and L. J. Wood, "Multistep Guaranteed Cost Control of Linear Systems with Uncertain Parameters," J. Guid. Contr., Vol. 2, pp. 449-456, 1979.

11. I. R. Petersen and C. V. Hollot, "A Riccati Equation Approach to the Stabilization of Uncertain Systems," Automatica, Vol. 22, pp. 433-448, 1986.

12. D. Hinrichsen and A. J. Pritchard, "Stability Radius for Structured Perturbations and the Algebraic Riccati Equation," Sys. Contr. Lett., Vol. 8, pp. 105-113, 1986.

13. B. D. O. Anderson and J. B. Moore, Linear Optimal Control, Prentice-Hall, Englewood Cliffs, NJ, 1970.

14. G. N. Milstein, "Design of Stabilizing Controller with Incomplete State Data for Linear Stochastic System with Multiplicative Noise," Autom. Remote Contr., Vol. 43, pp. 653-659, 1982.

15. G. A. Adamian and J. S. Gibson, "Sensitivity of Closed-Loop Eigenvalues and Robustness," preprint.

16. A. M. Ostrowski, "On Some Metrical Properties of Operator Matrices and Matrices Partitioned into Blocks," J. Math. Anal. Appl., Vol. 2, pp. 161-209, 1961.

17. G. Dahlquist, "On Matrix Majorants and Minorants, with Applications to Differential Equations," Lin. Alg. Appl., Vol. 52/53, pp. 199-216, 1983.

18. D. D. Siljak, Large-Scale Dynamic Systems, Elsevier North-Holland, 1978.

19. M. Ikeda and D. D. Siljak, "Generalized Decompositions of Dynamic Systems and Vector Lyapunov Functions," IEEE Trans. Autom. Contr., Vol. AC-26, pp. 1118-1125, 1981.

20. A. Gruzen, "Robust Reduced Order Control of Flexible Structures," C. S. Draper Laboratory Report #CSDL-T-900, April 1986.

21. A. Gruzen and W. E. Vander Velde, "Robust Reduced-Order Control of Flexible Structures Using the Optimal Projection/Maximum Entropy Design Methodology," AIAA Guid. Nav. Contr. Conf., Williamsburg, VA, August 1986.

22. A. Yousuff and R. E. Skelton, "Controller Reduction by Component Cost Analysis," IEEE Trans. Autom. Contr., Vol. AC-24, pp. 520-530, 1984.

23. S. Richter and R. DeCarlo, "Continuation Methods: Theory and Applications," IEEE Trans. Autom. Contr., Vol. 28, pp. 660-665, 1983.

OPUS References

A1. D. C. Hyland, "The Modal Coordinate/Radiative Transfer Formulation of Structural Dynamics—Implications for Vibration Suppression in Large Space Platforms," MIT Lincoln Laboratory, TR-27, 14 March 1979.

A2. D. C. Hyland, "Optimal Regulation of Structural Systems with Uncertain Parameters," MIT Lincoln Laboratory, TR-551, 2 February 1981, DDC# AD-A099111/7.

A3. D. C. Hyland, "Active Control of Large Flexible Spacecraft: A New Design Approach Based on Minimum Information Modelling of Parameter Uncertainties," Proc. Third VPI&SU/AIAA Symposium, pp. 631-646, Blacksburg, VA, June 1981.

A4. D. C. Hyland, "Optimal Regulator Design Using Minimum Information Modelling of Parameter Uncertainties: Ramifications of the New Design Approach," Proc. Third VPI&SU/AIAA Symposium, pp. 701-716, Blacksburg, VA, June 1981.

A5. D. C. Hyland and A. N. Madiwale, "Minimum Information Approach to Regulator Design: Numerical Methods and Illustrative Results," Proc. Third VPI&SU AIAA Symposium, pp. 101-118, Blacksburg, VA, June 1981.

A6. D. C. Hyland and A. N. Madiwale, "A Stochastic Design Approach for Full-Order Compensation of Structural Systems with Uncertain Parameters," Proc. AIAA Guid. Contr. Conf., pp. 332-338, Albuquerque, NM, August 1981.

A7. D. C. Hyland, "Optimality Conditions for Fixed-Order Dynamic Compensation of Flexible Spacecraft with Uncertain Parameters," AIAA 20th Aerospace Sciences Meeting, paper 82-0312, Orlando, FL, January 1982.

A8. D. C. Hyland, "Structural Modeling and Control Design Under Incomplete Parameter Information: The Maximum Entropy Approach," AFOSR/NASA Workshop in Modeling, Analysis and Optimization Issues for Large Space Structures, Williamsburg, VA, May 1982.

A9. D. C. Hyland, "Minimum Information Stochastic Modelling of Linear Systems with a Class of Parameter Uncertainties," Proc. Amer. Contr. Conf., pp. 620-627, Arlington, VA, June 1982.

[illegible] "Minimum Effort Stochastic Approach to Control Design for Uncertain Structural Systems," Proc. Amer. Contr. Conf., pp. 640-646, Arlington, VA, June 1982.

A11. D. C. Hyland, "Minimum Information Modeling of Structural Systems with Uncertain Parameters," Proceedings of the Workshop on Applications of Distributed System Theory to the Control of Large Space Structures, J. Rodriguez, ed., pp. 51-68, JPL, Pasadena, CA, July 1982.

A12. D. C. Hyland and A. K. Maldwale, "Fixed-Order Dynamic Compensation Through Optimal Projection," Proceedings of the Workshop on Applications of Distributed System Theory to the Control of Large Space Structures, J. Rodriguez, ed., pp. 409-427, JPL, Pasadena, CA, July 1982.

A13. D. C. Hyland, "Mean-Square Optimal Fixed-Order Compensation--Beyond Spillover Suppression," paper 1-03, AIAA Astrodynamics Conference, San Diego, CA, August 1982.

A14. D. C. Hyland, "The Optimal Projection Approach to Fixed-Order Compensation: Numerical Methods and Illustrative Results," AIAA 21st Aerospace Sciences Meeting, paper 83-0303, Reno, NV, January 1983.

A15. D. C. Hyland, "Mean-Square Optimal, Full-Order Compensation of Structural Systems with Uncertain Parameters," MIT Lincoln Laboratory, TR-626, 1 June 1983.

A16. D. C. Hyland, "Comparison of Various Controller-Reduction Methods: Suboptimal versus Optimal Projection," Proc. AIAA Dynamics Specialists Conf., pp. 381-389, Palm Springs, CA, May 1984.

A17. D. C. Hyland and D. S. Bernstein, "The Optimal Projection Equations for Fixed-Order Dynamic Compensation," IEEE Trans. Autom. Contr., Vol. AC-29, pp. 1034-1037, 1984.

A18. D. C. Hyland, "Application of the Maximum Entropy/Optimal Projection Control Design Approach for Large Space Structures," Proc. Large Space Antenna Systems Technology Conference, pp. 617-654, NASA Langley, December 1984.

A19. L. D. Davis, D. C. Hyland and D. S. Bernstein, "Application of the Maximum Entropy Design Approach to the Spacecraft Control Laboratory Experiment (SCOLE)," Final Report, NASA Langley, January 1985.

A20. D. S. Bernstein and D. C. Hyland, "The Optimal Projection Equations for Reduced-Order State Estimation," IEEE Trans. Autom. Contr., Vol. AC-30, pp. 583-585, 1985.

A21. D. S. Bernstein and D. C. Hyland, "Optimal Projection/Maximum Entropy Stochastic Modelling and Reduced-Order Design Synthesis," Proc. IFAC Workshop on Model Error Concepts and Compensation, Boston, MA, June 1985, pp. 47-54, R. E. Skelton and D. H. Owens, eds., Pergamon Press, Oxford, 1986.

A22. D. C. Hyland and D. S. Bernstein, "The Optimal Projection Equations for Model Reduction and the Relationships Among the Methods of Wilson, Skelton and Moore," IEEE Trans. Autom. Contr., Vol. AC-30, pp. 1201-1211, 1985.

A23. D. S. Bernstein and D. C. Hyland, "The Optimal Projection/Maximum Entropy Approach to Designing Low-Order, Robust Controllers for Flexible Structures," Proc. 24th IEEE Conf. Dec. Contr., pp. 745-752, Fort Lauderdale, FL, December 1985.

A24. D. S. Bernstein, L. D. Davis, S. W. Greeley and D. C. Hyland, "Numerical Solution of the Optimal Projection/Maximum Entropy Design Equations for Low-Order, Robust Controller Design," Proc. 24th IEEE Conf. Dec. Contr., pp. 1795-1798, Fort Lauderdale, FL, December 1985.

A25. D. S. Bernstein and D. C. Hyland, "The Optimal Projection Equations for Finite-Dimensional Fixed-Order Dynamic Compensation of Infinite-Dimensional Systems," SIAM J. Contr. Optim., Vol. 24, pp. 122-151, 1986.

A26. D. S. Bernstein and S. W. Greeley, "Robust Controller Synthesis Using the Maximum Entropy Design Equations," IEEE Trans. Autom. Contr., Vol. AC-31, pp. 362-364, 1986.

A27. D. C. Hyland, D. S. Bernstein, L. D. Davis, S. W. Greeley and S. Richter, "MEOP: Maximum Entropy/Optimal Projection Stochastic Modelling and Reduced-Order Design Synthesis," Final Report, Air Force Office of Scientific Research, Bolling AFB, Washington, DC, April 1986.

A28. D. S. Bernstein, L. D. Davis and D. C. Hyland, "The Optimal Projection Equations for Reduced-Order, Discrete-Time Modelling, Estimation and Control," J. Guid. Contr. Dyn., Vol. 9, pp. 288-293, 1986.

A29. D. S. Bernstein and S. W. Greeley, "Robust Output-Feedback Stabilization: Deterministic and Stochastic Perspectives," Proc. Amer. Contr. Conf., pp. 1818-1826, Seattle, WA, June 1986.

A30. D. S. Bernstein, L. D. Davis and S. W. Greeley, "The Optimal Projection Equations for Fixed-Order, Sampled-Data Dynamic Compensation with Computation Delay," IEEE Trans. Autom. Contr., Vol. AC-31, pp. 859-862, 1986.

A31. D. S. Bernstein, "OPUS: Optimal Projection for Uncertain Systems," Annual Report, Air Force Office of Scientific Research, Bolling AFB, Washington, DC, October 1986.

A32. B. J. Boan and D. C. Hyland, "The Role of Metal Matrix Composites in Vibration Suppression in Large Space Structures," Proc. MMC Spacecraft Survivability Tech. Conf., MMCIAC Kaman Tempo Publ., Stanford Research Institute, Palo Alto, CA, October 1986.

A33. D. C. Hyland, "An Experimental Testbed for Validation of [illegible] in Large Space Optical Structures," SPIE Optoelectronic [illegible] Applications Conference, Los Angeles, CA, January [illegible]

A34. W. M. Haddad and D. S. Bernstein, "The Optimal [illegible] Discrete-Time Reduced-Order State Estimator [illegible] Multiplicative White Noise," Sys. Contr. Lett. [illegible]

A35. D. S. Bernstein and W. M. Haddad, "The Optimal [illegible] Discrete-Time Fixed-Order Dynamic Compensator [illegible] Multiplicative White Noise," Int. J. Contr. [illegible]

A36. W. M. Haddad and D. S. Bernstein, "The Optimal [illegible] Reduced-Order State Estimator [illegible] Trans. Autom. Contr., 1987

A37. D. S. Bernstein, "The Optimal [illegible] Output Feedback: The Singular [illegible]

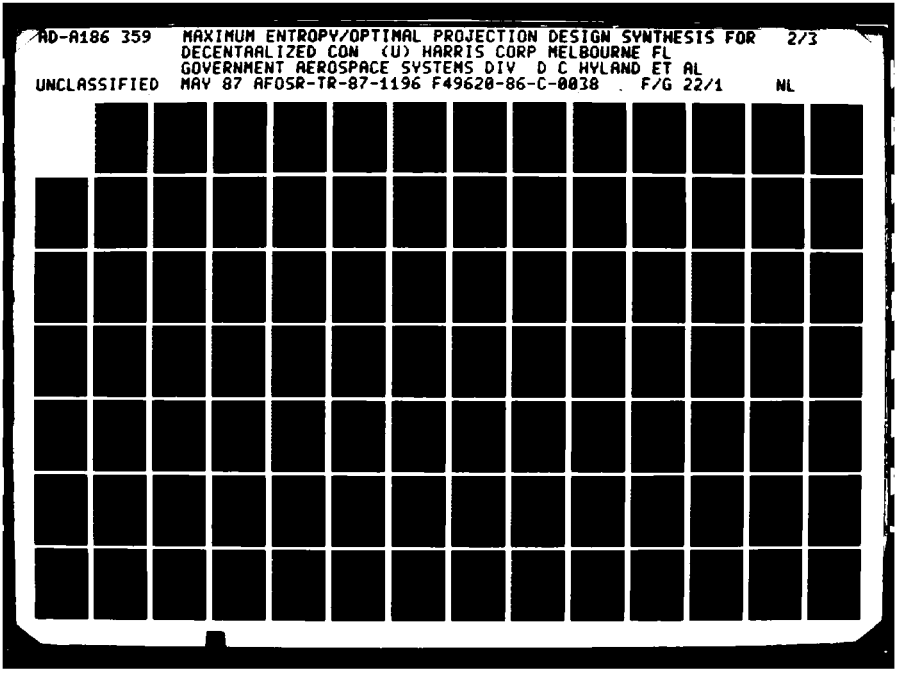
AD-A186 359 MAXIMUM ENTROPY/OPTIMAL PROJECTION DESIGN SYNTHESIS FOR 2/3
DECENTRALIZED CON (U) HARRIS CORP MELBOURNE FL
GOVERNMENT AEROSPACE SYSTEMS DIV D C HYLAND ET AL
UNCLASSIFIED MAY 87 AFOSR-TR-87-1196 F49620-86-C-0038 F/G 22/1 NL

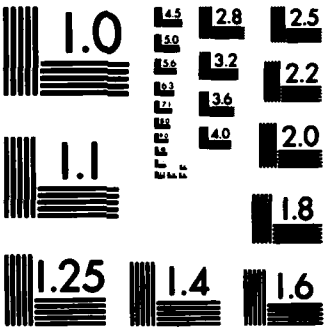

A38. D. S. Bernstein and D. C. Hyland, "The Optimal Projection Equations for Reduced-Order Modelling, Estimation and Control of Linear Systems with Multiplicative White Noise," J. Optim. Thy. Appl., 1987.

A39. D. S. Bernstein, "Sequential Design of Decentralized Dynamic Compensators Using the Optimal Projection Equations," Int. J. Contr., 1987.

A40. D. S. Bernstein and W. M. Haddad, "Optimal Output Feedback for Nonzero Set Point Regulation," Proc. Amer. Contr. Conf., Minneapolis, MN, June 1987.

A41. D. S. Bernstein, "Robust Static and Dynamic Output-Feedback Stabilization: Deterministic and Stochastic Perspectives," IEEE Trans. Autom. Contr., 1987.

A42. D. C. Hyland and D. S. Bernstein, "The Majorant Lyapunov Equation: A Nonnegative Matrix Equation for Guaranteed Robust Stability and Performance of Large Scale Systems," IEEE Trans. Autom. Contr., 1987.

A43. D. S. Bernstein and W. M. Haddad, "The Optimal Projection Equations with Petersen-Hollot Bounds: Robust Controller Synthesis with Guaranteed Structured Stability Radius," submitted.

A44. S. W. Greeley and D. C. Hyland, "Reduced-Order Compensation: LQG Reduction Versus Optimal Projection," submitted.

A45. W. M. Haddad, Robust Optimal Projection Control-System Synthesis, Ph.D. Dissertation, Department of Mechanical Engineering, Florida Institute of Technology, Melbourne, FL, March 1987.

A46. S. Richter, "A Homotopy Algorithm for Solving the Optimal Projection Equations for Fixed-Order Dynamic Compensation: Existence, Convergence and Global Optimality," Proc. Amer. Contr. Conf., Minneapolis, MN, June 1987.

APPENDIX B

REFERENCE 77

February, 1987

Robust Decentralized Optimal Output Feedback: The Static Controller Case

by

Dennis S. Bernstein*
Harris Corporation
Government Aerospace Systems Division
MS 22/4848
Melbourne, FL 32902

and

Wassim M. Haddad
Department of Mechanical Engineering
Florida Institute of Technology
Melbourne, FL 32901

Abstract

Sufficient conditions are developed for designing robust decentralized static output feedback controllers. The approach involves deriving necessary conditions for minimizing a bound on closed-loop performance over the class of uncertain parameters. The effect of plant parameter variations on the closed-loop covariance is bounded by means of a modified Lyapunov equation whose solutions are guaranteed to provide robust stability and performance.

*Supported in part by the Air Force Office of Scientific Research under contracts AFOSR F49620-86-C-0002 and F49620-86-C-0038.

Notation For Typesetting

$\mathcal{A}$, $\mathcal{S}$, etc.	Script face type
$\mathbb{R}$, $\mathbb{L}$, etc.	Open face type

1. Introduction

Because of implementation constraints, cost, and reliability considerations, a decentralized controller architecture is often required for control of large scale systems. Furthermore, such controllers must be robust to variations in plant parameters. The present paper addresses both of these concerns within the context of a robust decentralized design theory for continuous-time static controllers.

The approach to controller design considered herein involves optimizing closed-loop performance with respect to the constrained feedback gains. This approach to output feedback was studied for centralized controllers in [13,14] and for decentralized controllers in [15]. An interesting feature of [14,15] is the recognition of an oblique projection (idempotent matrix) which allows the necessary conditions to be written in terms of a modified Riccati equation. When the problem is specialized to full-state feedback, the projection becomes the identity and the modified Riccati equation coincides with the standard Riccati equation of LQR theory. It should be pointed out that the oblique projection of static output feedback is distinct from the oblique projection arising in dynamic compensation ([12]). A unified treatment of the static/dynamic (nonstrictly proper) control problem involving both projections is given in [3].

The present paper goes beyond earlier work by deriving sufficient conditions for robust stability and performance with respect to constant variations in the plant parameters. Although plant disturbances are represented in the usual manner by additive white noise, uncertainty in the plant dynamics is modeled deterministically by means of structured parameter variations within bounded sets. Thus, for example, the dynamics matrix A is replaced by $A + \sum_{k=1}^{p} \sigma_k A_k$, where σ_k is a constant uncertain parameter assumed only to lie within the interval $[-\delta_k, \delta_k]$ and A_k is a fixed matrix denoting the structure of the uncertain parameter σ_k as it appears in the nominal dynamics matrix A. The system performance is defined to be the worst-case

value over the parameter uncertainties of a quadratic criterion averaged over the disturbance statistics.

Since the closed-loop performance can be written in terms of the second-moment matrix, a performance bound over the class of uncertain parameters can be obtained by bounding the state covariance. The key to bounding the state covariance is to replace the usual Lyapunov equation for the second-moment matrix by a suitably modified Lyapunov equation. In the present paper the modified Lyapunov equation is constructed by adding two additional terms. The first term corresponds to a uniform right shift of the open-loop dynamics. As is well known ([1]), such a shift may arise from an exponential performance weighting and leads to a uniform stability margin for the closed-loop system. In order to obtain robustness with respect to specified structured parameter variations, however, an additional term of the form $A_i Q A_i^T$ is required. Such terms arise naturally in systems with multiplicative white noise; see [2] and the references therein for further details. The exponential cost weighting and multiplicative noise interpretations for the uncertainty bound have no bearing in the present paper since parameter variations are modeled deterministically as constant variations within bounded sets so that only the bound itself is required.

Having bounded the state covariance over the class of parameter uncertainties, the performance can thus be bounded in terms of the solution of the modified Lyapunov equation. The performance bound can be viewed as an auxiliary cost and thus leads to the Auxiliary Minimization Problem: Minimize the performance while satisfying the modified Lyapunov equation. The nice feature of the auxiliary problem is that necessary conditions for optimality of the performance bound now serve as sufficient conditions for robust performance in the original problem. Thus our approach seeks to rectify one of the principal drawbacks of necessity theory, namely, guarantees of stability and performance. Furthermore, it should be noted that if numerical solution of the optimality conditions yields a local extremal which is not the global optimum, then robust stability and performance are still guaranteed, although the performance of the extremal solution may not be as good as the performance provided by the global

minimum. Philosophically, the overall approach is related to guaranteed cost control ([10]).

A further extension of previous approaches considered in the present paper involves the types of feedback loops considered. Specifically, the usual approach to static output feedback involves nonnoisy measurements and weighted controls, while the dual problem involves feeding back noisy measurements to unweighted controls. This situation leads to an additional projection ([3]) which is dual to the projection discussed in [14,15]. The inclusion of the dual case now leads to a pair of modified Riccati equations coupled by both the uncertainty bounds and the oblique projections.

In addition to the two types of loops discussed above, one may wish to consider the two remaining cases, namely, feeding back noisy measurements to weighted controls and feeding back nonnoisy measurements to unweighted controls. It is easy to show, however, that the former case leads to an undefined (i.e., infinite) value for the performance while the latter case is highly singular and fails to yield explicit gain expressions.

Finally, the scope of the present paper is limited to a rigorous elucidation of sufficient conditions for robust decentralized output feedback. Numerical solution of these equations can be carried out by extending available algorithms for centralized output feedback. Numerical algorithms for solving a single modified Riccati equation in the absence of uncertainty bounds are discussed in [15].

2. Notation and Definitions

$\mathbb{R}$, $\mathbb{R}^{n\times m}$, $\mathbb{R}^{n}$, $\mathbb{E}$	real numbers, $n\times m$ real numbers, $\mathbb{R}^{n\times 1}$, expectation
I_n, $(\ )^{\mathrm{T}}$	$n\times n$ identity, transpose
$\oplus$, $\otimes$	Kronecker sum, Kronecker product ([9])
$\mathbb{S}^{n}$	$n\times n$ symmetric matrices
$\mathbb{S}_{+}^{n}$	$n\times n$ symmetric nonnegative-definite matrices

$\underline{\underline{P}}^r$	rxr symmetric positive-definite matrices
$Z_1 \leq Z_2$	$Z_2 - Z_1 \in \underline{\underline{N}}^r$, $Z_1, Z_2 \in \underline{\underline{S}}^r$
$Z_1 < Z_2$	$Z_2 - Z_1 \in \underline{\underline{P}}^r$, $Z_1, Z_2 \in \underline{\underline{S}}^r$
asymptotically stable matrix	matrix with eigenvalues in open left half plane
n, r, s, p	positive integers
i, j, k	indices, i=1,...,r, j=1,...,s, k=1,...,p
m_i, $\hat{\ell}_i$	positive integers, i=1,...,r
$\hat{m}_j$, ℓ_j	positive integers, j=1,...,s
x	n-dimensional vector
u_i, $\hat{y}_i$	m_i, $\hat{\ell}_i$-dimensional vectors, i=1,...,r
$\hat{u}_j$, y_j	$\hat{m}_j$, ℓ_j-dimensional vectors, j=1,...,s
A, ΔA	nxn matrices
B_i, ΔB_i; $\hat{C}_i$	nxm_i matrices; $\hat{\ell}_i$xn matrices, i=1,...,r
$\hat{B}_j$; C_j, ΔC_j	$nx\hat{m}_j$ matrices; $\ell_j$xn matrices, j=1,...,s
A_k	nxn matrices, k=1,...,p
B_{ik}	nxm_i matrices, i=1,...,r, k=1,...,p
C_{jk}	$\ell_j$xn matrices, j=1,...,s, k=1,...,p
D_{ci}	$m_i x\hat{\ell}_i$ matrices, i=1,...,r
D_{cj}	$\hat{m}_j x\ell_j$ matrices, j=1,...,s
α_k	positive number, k=1,...,p
δ_k	nonnegative number, k=1,...,p
γ_k	δ_k/α_k, k=1,...,p
σ_k	real number, k=1,...,p
A_α	$A + \frac{1}{2}\sum_{k=1}^{p}\delta_k\alpha_k I_n$

$w_o(t)$, $w_j(t)$ — n-dimensional, ℓ_j-dimensional white noise, $j=1,\ldots,s$

V_o, V_j — intensities of w_o, w_j; $V_o \in \underline{\underline{N}}^n$, $V_j \in \underline{\underline{P}}^{\ell_j}$, $j=1,\ldots,s$

V_{oj} — $n \times \ell_j$ cross intensity of w_o, w_j, $j=1,\ldots,s$

R_o, R_i — state and control weightings; $R_o \in \underline{\underline{N}}^n$, $R_i \in \underline{\underline{P}}^{m_i}$, $i=1,\ldots,r$

R_{oi} — $n \times m_i$ cross weighting; $R_o - R_{oi}R_i^{-1}R_{oi}^T \geq 0$, $i=1,\ldots,r$

$$\tilde{A} \qquad A + \sum_{i=1}^{r} B_i D_{ci} \hat{C}_i + \sum_{j=1}^{s} \hat{B}_j E_{cj} C_j$$

$$\Delta\tilde{A} \qquad A + \sum_{i=1}^{r} \Delta B_i D_{ci} \hat{C}_i + \sum_{j=1}^{s} \hat{B}_j E_{cj} \Delta C_j$$

$$\tilde{w}(t) \qquad w_o(t) + \sum_{j=1}^{s} \hat{B}_j E_{cj} w_j(t)$$

$$\tilde{R} \qquad R_o + \sum_{i=1}^{r} [R_{oi} D_{ci} \hat{C}_i + \hat{C}_i^T D_{ci}^T R_{oi}^T + \hat{C}_i^T D_{ci}^T R_i D_{ci} \hat{C}_i]$$

$$\tilde{V} \qquad V_o + \sum_{j=1}^{s} [V_{oj} E_{cj}^T \hat{B}_j^T + \hat{B}_j E_{cj} V_{oj}^T + \hat{B}_j E_{cj} V_j E_{cj}^T \hat{B}_j^T]$$

For arbitrary $n \times n$ Q, P define:

$$R_{ai} \triangleq R_i + \sum_{k=1}^{P} \gamma_k B_{ik}^T P E_{ik}, \quad P_{ai} \triangleq B_i^T P + R_{oi}^T + \sum_{k=1}^{P} \gamma_k L_{ik}^T P A_k, \quad i=1,\ldots,r,$$

$$V_{aj} \triangleq V_j + \sum_{k=1}^{P} \gamma_k C_{jk} Q C_{jk}^T, \quad Q_{aj} \triangleq Q C_j^T + V_{oj} + \sum_{k=1}^{P} \gamma_k A_k Q C_{jk}^T, \quad j=1,\ldots,s.$$

3. Robust Stability and Robust Performance Problems

In this section we state the Robust Stability Problem and Robust Performance Problem along with related notation for later use. Let $\underline{U} \subset \underline{\underline{R}}^{nxn} \times \underline{\underline{R}}^{nxm_1} \times \ldots \times \underline{\underline{R}}^{nxm_r} \times \underline{\underline{R}}^{\ell_1 xn} \times \ldots \times \underline{\underline{R}}^{\ell_s xn}$ denote the set of uncertain perturbations $(\Delta A, \Delta B_1, \ldots, \Delta B_r, \Delta C_1, \ldots, \Delta C_s)$ of the nominal system matrices $A, B_1, \ldots, B_r, C_1, \ldots, C_s$.

Robust Stability Problem. Determine $(D_{c1}, \ldots, D_{cr}, E_{c1}, \ldots, E_{cs})$ such that the closed-loop system consisting of the nth-order controlled plant

$$\dot{x}(t) = (A+\Delta A)x(t) + \sum_{i=1}^{r}(B_i+\Delta B_i)u_i(t) + \sum_{j=1}^{s}\hat{B}_j\hat{u}_j(t), \quad t \in [0,\infty), \tag{3.1}$$

measurements

$$\hat{y}_i(t) = \hat{C}_i x(t), \qquad i=1,\ldots,r, \tag{3.2}$$

$$y_j(t) = (C_j+\Delta C_j)x(t), \quad j=1,\ldots,s, \tag{3.3}$$

and static output-feedback controller

$$u_i(t) = D_{ci}\hat{y}_i(t), \quad i=1,\ldots,r, \tag{3.4}$$

$$\hat{u}_j(t) = E_{cj}y_j(t), \quad j=1,\ldots,s, \tag{3.5}$$

is asymptotically stable for all variations in $\underline{U}$.

Remark 3.1. In the case $\Delta A, \Delta B, \Delta C = 0$ it is well known that stabilizability is related to the existence of fixed modes ([16]). When plant uncertainties are present the problem is, of course, far more complex. In the present paper sufficient conditions for robust stability are obtained as a direct consequence of the existence of robust performance bounds.

Robust Performance Problem. Determine $(D_{c1},\ldots,D_{cr},E_{c1},\ldots,E_{cs})$ such that the closed-loop system consisting of the nth-order controlled and disturbed plant

$$\dot{x}(t) = (A+\Delta A)x(t) + \sum_{i=1}^{r}(B_i+\Delta B_i)u_i(t) + \sum_{j=1}^{s}\hat{E}_j\hat{u}_j(t) + w_o(t), \quad t \in [0,\infty), \tag{3.6}$$

nonnoisy and noisy measurements

$$\hat{y}_i(t) = \hat{C}_i x(t), \quad i=1,\ldots,r, \tag{3.7}$$

$$y_j(t) = (C_j+\Delta C_j)x(t) + w_j(t), \quad j=1,\ldots,s, \tag{3.8}$$

and static output feedback controller (3.4), (3.5), the performance criterion

$$J(D_{c1},\ldots,D_{cr},E_{c1},\ldots,E_{cs}) \triangleq \tag{3.9}$$

$$\sup_{\underline{U}} \limsup_{t\to\infty} \underline{E}[x^T(t)R_o x(t) + 2\sum_{i=1}^{r} x^T(t)R_{oi}u_i(t) + \sum_{i=1}^{r} u_i^T(t)R_i u_i(t)]$$

is minimized.

Remark 3.2. Note that the controller architecture includes two distinctly different types of decentralized loops. The first type indexed by $i=1,\ldots,r$, involves feeding back nonnoisy measurements to weighted controls. This is the standard setting in the optimal output-feedback literature ([13-15]). In addition, we include the dual situation indexed by $j=1,\ldots,s$, which involves feeding back noisy measurements to unweighted controls. The case in which only one type of loop is present can be formally recovered from our results by ignoring B_i and $\hat{C}_i$ or $\hat{E}_j$ and C_j as required.

For each controller $(D_{c1},\ldots,D_{cr},E_{c1},\ldots,E_{cs})$ and variation in $\underline{U}$, the undisturbed closed-loop system (3.1)-(3.5) is given by

$$\dot{x}(t) = (\tilde{A}+\Delta\tilde{A})x(t), \quad t \in [0,\infty), \tag{3.10}$$

while the disturbed closed-loop system (3.4)-(3.8) can be written as

$$\dot{x}(t) = (\tilde{A}+\Delta\tilde{A})x(t) + \tilde{w}(t), \quad t \in [0,\infty), \tag{3.11}$$

where $\tilde{w}(t)$ is white noise with intensity $\tilde{V} \in \underline{\underline{P}}^n$.

For the Robust Performance Problem the cost can be expressed in terms of the second-moment matrix. The following result is immediate.

Proposition 3.1. For each decentralized controller $(D_{c1},\ldots,D_{cr},E_{c1},\ldots,E_{cs})$ and variation in $\underline{U}$, the second-moment matrix

$$Q_{\Delta A}(t) = \underline{\underline{E}}[x(t)x^T(t)], \quad t \in [0,\infty), \tag{3.12}$$

satisfies

$$\dot{Q}_{\Delta A}(t) = (\tilde{A}+\Delta\tilde{A})Q_{\Delta A}(t) + Q_{\Delta A}(t)(\tilde{A}+\Delta\tilde{A})^T + \tilde{V}, \quad t \in [0,\infty). \tag{3.13}$$

Furthermore,

$$J(D_{c1},\ldots,D_{cr},E_{c1},\ldots,E_{cs}) = \sup_{\underline{U}} \limsup_{t\to\infty} \operatorname{tr} Q_{\Delta A}(t)\tilde{R}. \tag{3.14}$$

4. Sufficient Conditions for Robust Stability and Performance

In practice, steady-state performance is only of interest when the closed-loop system (3.10) is stable over $\underline{U}$. The following result follows from Proposition 3.1.

Lemma 4.1. Suppose the system (3.10) is stable for all variations in $\underline{U}$. Then

$$J(D_{c1},\ldots,D_{cr},E_{c1},\ldots,E_{cs}) = \sup_{\underline{U}} \operatorname{tr} Q_{\Delta A}\tilde{R}, \tag{4.1}$$

where $Q_{\Delta A} \in \underline{\underline{P}}^n$ is the unique solution to

$$0 = (\tilde{A}+\tilde{\Delta A})Q_{\Delta A} + Q_{\Delta A}(\tilde{A}+\tilde{\Delta A})^T + \tilde{V}. \tag{4.2}$$

Remark 4.1. When $\underline{U}$ is compact, "sup" in (4.1) can be replaced by "max".

Since it is difficult to determine $J(D_{c1},\ldots,D_{cr},E_{c1},\ldots,E_{cs})$ explicitly, we shall seek upper bounds. Our assumptions allow us to obtain robust stability as a consequence of robust performance.

Theorem 4.1. Let Ω: $\underline{\underline{P}}^n \times \underline{\underline{R}}^{m_1\times\hat{\ell}_1} \times \ldots \times \underline{\underline{R}}^{m_r\times\hat{\ell}_r} \times \underline{\underline{R}}^{\hat{m}_r\times\ell_1} \times \ldots \times \underline{\underline{R}}^{\hat{m}_s\times\ell_s} \to \underline{\underline{S}}^n$ be such that

$$\tilde{\Delta A}Q + Q\tilde{\Delta A}^T \le \Omega(Q,D_{c1},\ldots,D_{cr},E_{c1},\ldots,E_{cs}), \tag{4.3}$$

for all variations in $\underline{U}$ and $(Q,D_{c1},\ldots,D_{cr},E_{c1},\ldots,E_{cs}) \in \underline{\underline{P}}^n \times \underline{\underline{R}}^{m_1\times\hat{\ell}_1} \times \ldots \times \underline{\underline{R}}^{m_r\times\hat{\ell}_r} \times \underline{\underline{R}}^{\hat{m}_1\times\ell_1} \times \ldots \times \underline{\underline{R}}^{\hat{m}_s\times\ell_s}$. Furthermore, for given $(D_{c1},\ldots,D_{cr},E_{c1},\ldots,E_{cs})$ suppose there exists $Q \in \underline{\underline{P}}^n$ satisfying

$$0 = \tilde{A}Q + Q\tilde{A}^T + \Omega(Q,D_{c1},\ldots,D_{cr},E_{c1},\ldots,E_{cs}) + \tilde{V}. \tag{4.4}$$

Finally, suppose the pair $(\tilde{V}^{1/2},\tilde{A}+\tilde{\Delta A})$ is detectable for all variations in $\underline{U}$. Then, for all variations in $\underline{U}$, $\tilde{A}+\tilde{\Delta A}$ is asymptotically stable,

$$Q_{\Delta A} \le Q, \tag{4.5}$$

and

$$J(D_{c1},\ldots,D_{cr},E_{c1},\ldots,E_{cs}) \leq \operatorname{tr} \tilde{Q}\tilde{R}. \tag{4.6}$$

Proof. For all variations in $\underline{U}$, (4.4) is equivalent to

$$0 = (\tilde{A}+\tilde{\Delta A})Q + Q(\tilde{A}+\tilde{\Delta A})^T + \Psi(Q,D_{c1},\ldots,D_{cr},E_{c1},\ldots,E_{cs},\tilde{\Delta A}) + \tilde{V}, \tag{4.7}$$

where

$$\Psi(Q,D_{c1},\ldots,D_{cr},E_{c1},\ldots,E_{cs},\tilde{\Delta A}) \triangleq$$

$$\Omega(Q,D_{c1},\ldots,D_{cr},E_{c1},\ldots,E_{cs}) - (\tilde{\Delta A}Q+Q\tilde{\Delta A}^T).$$

Note that by (4.3), $\Psi(\cdot) \geq 0$ for all variations in $\underline{U}$. Since $(\tilde{V}^{1/2}, \tilde{A}+\tilde{\Delta A})$ is detectable for all variations in $\underline{U}$, it follows from Theorem 3.6 of [17] that $((\tilde{V}+\Psi(Q,D_{c1},\ldots,D_{cr},E_{c1},\ldots,E_{cs},\tilde{\Delta A}))^{1/2}, \tilde{A}+\tilde{\Delta A})$ is detectable for all variations in $\underline{U}$. Hence Lemma 12.2 of [17] implies $\tilde{A}+\tilde{\Delta A}$ is asymptotically stable for all variations in $\underline{U}$.

Next, subtracting (4.2) from (4.7) yields

$$0 = (\tilde{A}+\tilde{\Delta A})(Q-Q_{\tilde{\Delta A}}) + (Q-Q_{\tilde{\Delta A}})(\tilde{A}+\tilde{\Delta A})^T + \Psi(Q,D_{c1},\ldots,D_{cr},E_{c1},\ldots,E_{cs},\tilde{\Delta A}),$$

or, equivalently, (since $\tilde{A}+\tilde{\Delta A}$ is asymptotically stable)

$$Q - Q_{\tilde{\Delta A}} = \int_0^\infty e^{(\tilde{A}+\tilde{\Delta A})t}\Psi(Q,D_{c1},\ldots,D_{cr},E_{c1},\ldots,E_{cs},\tilde{\Delta A})e^{(\tilde{A}+\tilde{\Delta A})^T t}\,dt \geq 0,$$

which implies (4.5). Finally, (4.5) and (4.1) yield (4.6).

We also note a sufficient condition for the solution Q of (4.4) to be positive definite.

Proposition 4.1. Let Ω be as in Theorem 4.1, let $(D_{c1},\ldots,D_{cr},E_{c1},\ldots,E_{cs})$ be given, and suppose there exists $Q \in \underline{L}^n$

satisfying (4.4). If $(\tilde{V}^{1/2}, \tilde{A}+\tilde{\Delta A})$ is observable for some variation in $\underline{U}$, then Q is positive definite.

Proof. If $(\tilde{V}^{1/2}, \tilde{A}+\tilde{\Delta A})$ is observable for some variation in $\underline{U}$, then by Theorem 3.6 of [17], $((\tilde{V}+\Psi(Q,D_{c1},\ldots,D_{cr},E_{c1},\ldots,E_{cs},\tilde{\Delta A})^{1/2}, \tilde{A}+\tilde{\Delta A})$ is also observable for the same variation in $\underline{U}$. It thus follows from (4.7) and Lemma 12.2 of [17] that Q is positive definite.

Remark 4.2. If $\tilde{V}$ is positive definite then the detectability and observability hypotheses of Theorem 4.1 and Proposition 4.1 are automatically satisfied.

5. Uncertainty Structure and the Right Shift/Multiplicative White Noise Bound

The uncertainty set $\underline{U}$ is assumed to be of the form

$$\underline{U} = \{(\Delta A,\Delta B_1,\ldots,\Delta B_r,\Delta C_1,\ldots,\Delta C_s):$$

$$\Delta A = \sum_{k=1}^{p}\sigma_k A_k, \quad \Delta B_i = \sum_{k=1}^{p}\sigma_k B_{ik}, \quad i=1,\ldots,r, \tag{5.1}$$

$$\Delta C_j = \sum_{k=1}^{p}\sigma_k C_{jk}, \quad j=1,\ldots,s, \quad |\sigma_k| \le \delta_k, \quad k=1,\ldots,p\},$$

where, for k=1,...,p: $(A_k,B_{1k},\ldots,B_{rk},C_{1k},\ldots,C_{sk})$ are fixed matrices denoting the structure of the parametric uncertainty; δ_k is a given uncertainty bound; and σ_k is an uncertain parameter. The closed-loop system thus has structured uncertainty of the form

$$\tilde{\Delta A} = \sum_{k=1}^{p}\sigma_k \tilde{A}_k,$$

where

$$\bar{A}_k = A_k + \sum_{i=1}^{r} D_{ik} D_{ci} \hat{C}_i + \sum_{j=1}^{s} \hat{D}_j E_{cj} C_{jk}, \quad k=1,\ldots,p. \tag{5.2}$$

To obtain explicit gain expressions for $(D_{c1},\ldots,D_{cr},E_{c1},\ldots,E_{cs})$ we require that

$$[(B_{1k},\ldots,B_{rk}) \neq 0 \Longrightarrow (C_{1k},\ldots,C_{sk}) = 0], \quad k=1,\ldots,p. \tag{5.3}$$

That is, for each uncertain parameter σ_k, either $(B_{1k},\ldots,B_{rk})$ is zero or $(C_{1k},\ldots,C_{sk})$ is zero. Of course, both $(B_{1k},\ldots,B_{rk})$ and $(C_{1k},\ldots,C_{sk})$ may be zero, and there are no restrictions on A_k.

Given the structure of $\underline{U}$ defined by (5.1), the bound Ω satisfying (4.3) can now be specified.

Proposition 5.1. Let $\alpha_1,\ldots,\alpha_p$ be arbitrary positive scalars. Then the function

$$\Omega(Q,D_{c1},\ldots,D_{cr},E_{c1},\ldots,E_{cs}) = \sum_{k=1}^{p} \delta_k^2 (\alpha_k Q + \alpha_k^{-1} \bar{A}_k Q \bar{A}_k^T) \tag{5.4}$$

satisfies (4.3) with $\underline{U}$ given by (5.1).

Proof. For $k=1,\ldots,p$,

$$0 \leq [\sigma_k (\alpha_k/\delta_k)^{1/2} I_n - (\delta_k/\alpha_k)^{1/2} \bar{A}_k] Q [\sigma_k (\alpha_k/\delta_k)^{1/2} I_n - (\delta_k/\alpha_k)^{1/2} \bar{A}_k]^T$$

$$= \sigma_k^2 (\alpha_k/\delta_k) Q + (\delta_k/\alpha_k) \bar{A}_k Q \bar{A}_k^T - \sigma_k (\bar{A}_k Q + Q \bar{A}_k^T).$$

Summing over k and using $\sigma_k^2 \leq \delta_k^2$ yields (4.3). □

Remark 5.1. Note that the bound Ω given by (5.4) consists of two distinct terms in a specific ratio. The first term $\alpha_k Q$ can be thought of as arising from an exponential time weighting of the cost, or, equivalently, from a uniform right shift of the open-loop dynamics ([1]). The second term

$\alpha_k^{-1}\bar{A}_k C \bar{A}_k^T$ arises naturally from a multiplicative white noise model ([8]). Such interpretations have no bearing on the results obtained here since only the bound Ω defined by (5.4) is required.

6. The Auxiliary Minimization Problem and Necessary Conditions for Optimality

Rather than minimizing the actual cost (3.9), we shall consider the upper bound (4.6). This leads to the following problem.

Auxiliary Minimization Problem. Determine

$$(C, D_{c1}, \ldots, D_{cr}, E_{c1}, \ldots, E_{cs}) \in \underline{P}^n \times \underline{P}^{m_1 \times \ell_1} \times \ldots \times \underline{P}^{m_r \times \ell_r} \times \underline{P}^{n_1 \times \ell_1} \times \ldots \times \underline{P}^{n_s \times \ell_s}$$

which minimizes

$$\underline{J}(C, D_{c1}, \ldots, D_{cr}, E_{c1}, \ldots, E_{cs}) \triangleq \operatorname{tr} C\bar{R} \tag{6.1}$$

subject to

$$0 = \bar{A}C + C\bar{A}^T + \sum_{k=1}^{p} [\delta_k \alpha_k C + \gamma_k \bar{A}_k C \bar{A}_k^T] + \bar{V} \tag{6.2}$$

and

$$(\bar{V}^{1/2}, \bar{A} + \bar{\Delta}) \text{ is detectable for all variations in } \underline{U}. \tag{6.3}$$

Definition 6.1. $(C, D_{c1}, \ldots, D_{cr}, E_{c1}, \ldots, E_{cs}) \in \underline{P}^n \times \underline{P}^{m_1 \times \ell_1} \times \ldots \times \underline{P}^{m_r \times \ell_r} \times \underline{P}^{n_1 \times \ell_1} \times \ldots \times \underline{P}^{n_s \times \ell_s}$ is admissible if and only if $(C, D_{c1}, \ldots, D_{cr}, E_{c1}, \ldots, E_{cs})$ satisfies (6.2) and (6.3).

Proposition 6.1. If there exists admissible $(Q,D_{c1},\ldots,D_{cr},E_{c1},\ldots,E_{cs})$ then $\bar{A}+\Delta A$ is asymptotically stable for all variations in $\underline{U}$, and

$$J(D_{c1},\ldots,D_{cr},E_{c1},\ldots,E_{cs}) \leq \underline{J}(Q,D_{c1},\ldots,D_{cr},E_{c1},\ldots,E_{cs}). \tag{6.4}$$

Proof. With Ω given by (5.4), Proposition 5.1 implies that (4.3) is satisfied. Furthermore, admissibility implies that (4.4) has a solution $Q \in \underline{P}^n$. Hence, with (6.3), the hypotheses of Theorem 4.1 are satisfied so that robust stability with performance bound (4.6) is guaranteed. Note that with definition (6.1), (6.4) is merely a restatement of (4.6). □

To avoid having to verify constraint qualifications that arise in Kuhn-Tucker theory, the derivation of the necessary conditions for the Auxiliary Minimization Problem is based upon the Fritz John form of the Lagrange multiplier theorem. Rigorous application of this technique requires that $(Q,D_{c1},\ldots,D_{cr},E_{c1},\ldots,E_{cs})$ be restricted to the open set

$$\underline{S} \triangleq \{(Q,D_{c1},\ldots,D_{cr},E_{c1},\ldots,E_{cs}) \in$$

$$\underline{P}^n \times \underline{P}^{n_1 \times \hat{n}_1} \times \ldots \times \underline{P}^{n_r \times \hat{n}_r} \times \underline{P}^{m_1 \times \hat{m}_1} \times \ldots \times \underline{P}^{m_s \times \hat{m}_s}:$$

$$\bar{A} \text{ is asymptotically stable}\},$$

where

$$\bar{\bar{A}} \triangleq (\bar{A}+\frac{1}{2}\sum_{k=1}^{P}\alpha_k\delta_k I_n) \oplus (\bar{A}+\frac{1}{2}\sum_{k=1}^{P}\alpha_k\delta_k I_n) + \sum_{k=1}^{P}\gamma_k \bar{A}_k \otimes \bar{A}_k.$$

The requirement $(Q,D_{c1},\ldots,D_{cr},E_{c1},\ldots,E_{cs}) \in \underline{S}$ implies that Q and its nonnegative-definite dual P are unique solutions of the modified Lyapunov equations (6.2) and

$$0 = \bar{A}^T P + P\bar{A} + \sum_{k=1}^{P}[\alpha_k\delta_k P + \gamma_k \bar{A}_k^T P \bar{A}_k] + \bar{R}. \tag{6.5}$$

An additional technical requirement is that $(Q,D_{c1},\ldots,D_{cr},E_{c1},\ldots,E_{cs})$ be confined to the set

$$\underline{S}^+ \triangleq \{(Q,D_{c1},\ldots,D_{cr},E_{c1},\ldots,E_{cs}) \in \underline{S}: \hat{C}_i Q \hat{C}_i^T > 0, \quad i=1,\ldots,r,$$

$$\text{and } \hat{E}_j^T P \hat{E}_j > 0, \quad j=1,\ldots,s\}.$$

The positive definiteness conditions in the definition of $\underline{S}^+$ hold when $\hat{C}_i$ and $\hat{B}_j$ have full row and column rank, respectively, and Q and P are positive definite. As can be seen from the proof of Theorem 6.1 these conditions imply the existence of the projections τ_i and $\hat{\tau}_j$ corresponding to the two distinct types of feedback loops.

Proposition 6.2. The set $\underline{S}^+$ is open.

Proof. It need only be noted that $\underline{S}^+$ is the intersection of three open sets. □

Remark 6.1. It is extremely important to emphasize that Proposition 6.1 shows that it is not necessary for guaranteed robust stability and performance that an admissible $(Q,D_{c1},\ldots,D_{cr},E_{c1},\ldots,E_{cs})$ obtained by solving the necessary conditions actually be shown to be an element of $\underline{S}$. As will be seen from the proof of Theorem 6.1, the set $\underline{S}$ constitutes sufficient conditions under which the Lagrange multiplier technique is applicable to the Auxiliary Minimization Problem.

Theorem 6.1. Suppose $(Q,D_{c1},\ldots,D_{cr},E_{c1},\ldots,E_{cs}) \in \underline{S}^+$ solves the Auxiliary Minimization Problem with $\underline{V}$ given by (5.1) and let $\alpha_1,\ldots,\alpha_p > 0$. Then there exist $Q, P \in \underline{P}^n$ such that $D_{c1},\ldots,D_{cr},E_{c1},\ldots,E_{cs}$ are given by

$$D_{ci} = -\Gamma_{ai}^{-1} B_{ai} Q \hat{C}_i^T (\hat{C}_i Q \hat{C}_i^T)^{-1}, \quad i=1,\ldots,r, \tag{6.6}$$

$$E_{cj} = -(\hat{E}_j^T P \hat{B}_j)^{-1} \hat{E}_j^T P C_{aj} V_{aj}^{-1}, \quad j=1,\ldots,s, \tag{6.7}$$

and such that Q, P satisfy

$$0 = (A_\alpha - \sum_{i=1}^{r} B_i R_{\alpha i}^{-1} P_{\alpha i} \tau_i) Q + Q(A_\alpha - \sum_{i=1}^{r} B_i R_{\alpha i}^{-1} P_{\alpha i} \tau_i)^T + V_o$$

$$+ \sum_{k=1}^{p} \gamma_k (A_k - \sum_{i=1}^{r} B_{ik} R_{\alpha i}^{-1} P_{\alpha i} \tau_i) Q (A_k - \sum_{i=1}^{r} B_{ik} R_{\alpha i}^{-1} P_{\alpha i} \tau_i)^T \qquad (6.8)$$

$$- \sum_{j=1}^{s} C_{\alpha j} V_{\alpha j}^{-1} C_{\alpha j}^T + \sum_{j=1}^{s} \hat{\tau}_{j1} C_{\alpha j} V_{\alpha j}^{-1} C_{\alpha j}^T \hat{\tau}_{j1}^T,$$

$$0 = (A_\alpha - \sum_{j=1}^{s} \hat{\tau}_j C_{\alpha j} V_{\alpha j}^{-1} C_j)^T P + P(A_\alpha - \sum_{j=1}^{s} \hat{\tau}_j C_{\alpha j} V_{\alpha j}^{-1} C_j) + F_o$$

$$+ \sum_{k=1}^{p} \gamma_k (A_k - \sum_{j=1}^{s} \hat{\tau}_j C_{\alpha j} V_{\alpha j}^{-1} C_{jk})^T P (A_k - \sum_{j=1}^{s} \hat{\tau}_j C_{\alpha j} V_{\alpha j}^{-1} C_{jk}) \qquad (6.9)$$

$$- \sum_{i=1}^{r} F_{\alpha i}^T R_{\alpha i}^{-1} P_{\alpha i} + \sum_{i=1}^{r} \tau_{i1}^T P_{\alpha i}^T R_{\alpha i}^{-1} P_{\alpha i} \tau_{i1},$$

where

$$\tau_i = Q C_i^T (C_i Q C_i^T)^{-1} C_i, \quad \tau_{i1} = \tau_i - I_n, \quad i=1,\ldots,r, \qquad (6.10)$$

$$\hat{\tau}_j = \hat{P}_j (\hat{P}_j^T P \hat{P}_j)^{-1} \hat{P}_j^T P, \quad \hat{\tau}_{j1} = \hat{\tau}_j - I_n, \quad j=1,\ldots,s. \qquad (6.11)$$

Proof. To optimize (6.1) over the open set $\hat{\Sigma}$, where

$$\hat{\Sigma} \triangleq \{(Q, P_{c1}, \ldots, P_{cr}, P_{c1}, \ldots, P_{cs}) \in \Sigma^1 : \ (6.2) \text{ is satisfied}\},$$

subject to the constraint (6.2), form the Lagrangian

$$L(Q,D_{c1},\ldots,D_{cr},E_{c1},\ldots,E_{cs}) \triangleq \operatorname{tr}[\lambda Q\bar{R} + (\bar{A}Q+Q\bar{A}^{T}+\sum_{k=1}^{r}\alpha_k\delta_k Q+\gamma_k\bar{A}_k Q\bar{A}_k^{T}+\bar{V})P],$$

where the Lagrange multipliers $\lambda \geq 0$ and $P \in \underline{P}^{n\times n}$ are not both zero. Setting $\partial L/\partial Q = 0$, $\lambda = 0$ implies $P = 0$ since $(Q,D_{c1},\ldots,D_{cr},E_{c1},\ldots,E_{cs}) \in \underline{S}$. Hence, without loss of generality set $\lambda = 1$. Thus the stationarity conditions are given by

$$\frac{\partial L}{\partial Q} = \bar{A}^{T}P + P\bar{A} + \sum_{k=1}^{p}[\delta_k\alpha_k P + \gamma_k\bar{A}_k^{T}P\bar{A}_k] + \bar{R} = 0, \tag{6.12}$$

$$\frac{\partial L}{\partial D_{ci}} = R_{ai}D_{ci}\hat{C}_i Q\hat{C}_i^{T} + P_{ai}Q\hat{C}_i^{T} = 0, \quad i=1,\ldots,r, \tag{6.13}$$

$$\frac{\partial L}{\partial E_{cj}} = \hat{B}_j^{T}P\hat{B}_j E_{cj}V_{aj} + \hat{B}_j^{T}PQ_{aj} = 0, \quad j=1,\ldots,s. \tag{6.14}$$

Since $(Q,D_{c1},\ldots,D_{cr},E_{c1},\ldots,E_{cs}) \in \underline{S}^{+}$, $\hat{C}_i Q\hat{C}_i^{T}$ and $\hat{B}_j^{T}P\hat{B}_j$ are invertible and hence (6.13) and (6.14) imply (6.6) and (6.7). Finally, (6.8) and (6.9) are equivalent to (6.2) and (6.5). □

Remark 6.2. Several special cases can be recovered formally from Theorem 6.1. For example, when the control weighting is nonsingular and the measurement noise is zero, i.e., when $\hat{u}_i$ and y_i are absent for $i=1,\ldots,r$, delete (6.7) and set $\hat{\tau}_j = 0$ in (6.8). Deleting also the uncertainty terms A_k, B_k, C_k yields the results of [15]. Furthermore, assuming a centralized structure for the static controller, i.e., $r=1$, yields the usual static output feedback result ([13,14]).

References

[1] B. D. O Anderson and J. B. Moore, Linear Optimal Control (Prentice-Hall, Englewood Cliffs, NJ, 1970).

[2] D. S. Bernstein, Sequential design of decentralized dynamic compensators using the optimal projection equations, Int. J. Contr., 1987, to appear.

[3] D. S. Bernstein, The optimal projection equations for static and dynamic output feedback: The singular case, IEEE Trans. Autom. Contr., 1987, to appear.

[4] D. S. Bernstein, Robust static and dynamic output-feedback stabilization: Deterministic and stochastic perspectives, IEEE Trans. Autom. Contr., 1987, to appear.

[5] D. S. Bernstein, L. D. Davis and S. W. Greeley, The optimal projection equations for fixed-order, sampled-data dynamic compensation with computation delay, IEEE Trans. Autom. Contr., AC-31 (1986) 859-862.

[6] D. S. Bernstein, L. D. Davis and D. C. Hyland, The optimal projection equations for reduced-order, discrete-time modelling, estimation and control, J. Guid. Contr. Dyn., 9 (1986) 288-293.

[7] D. S. Bernstein and W. M. Haddad, The optimal projection equations with Petersen-Hollot bounds: Robust controller synthesis with guaranteed structured stability radius, submitted.

[8] D. S. Bernstein and D. C. Hyland, The optimal projection equations for reduced-order modelling, estimation and control of linear systems with multiplicative white noise, J. Optim. Thy. Appl., 1987, to appear.

[9] J. W. Brewer, Kronecker products and matrix calculus in system theory, IEEE Trans. Circ. Sys., CAS-25 (1978) 772-781.

[10] S. S. L. Chang and T. K. C Peng, Adaptive guaranteed cost control of systems with uncertain parameters, IEEE Trans. Autom. Contr., AC-17 (1972) 474-483.

[11] W. M. Haddad, Robust Optimal Projection Control-System Synthesis, Ph.D. Dissertation, Department of Mechanical Engineering, Florida Institute of Technology, Melbourne, FL, (March 1987).

[12] D. C. Hyland and D. S. Bernstein, The optimal projection equations for fixed-order dynamic compensation, IEEE Trans. Autom. Contr., AC-29 (1984) 1034-1037.

[13] W. S. Levine and M. Athans, On the determination of the optimal constant output feedback gains for linear multivariable systems, IEEE Trans. Autom. Contr., AC-15 (1970) 44-48.

[14] J. Medanic, On stabilization and optimization by output feedback, Proc. Twelfth Asilomar Conf. Circ., Sys. Comp., (1978) 412-416.

[15] S. Renjen and D. P. Looze, Synthesis of decentralized output/state regulators, Proc. Amer. Contr. Conf., Arlington, VA, (1982) 758-762.

[16] S. H. Wang and E. J. Davison, On the stabilization of decentralized control systems, IEEE Trans. Autom. Contr., AC-18 (1973) 473-478.

[17] W. M. Wonham, Linear Multivariable Control: A Geometric Approach (Springer-Verlag, New York, 1979).

APPENDIX C

REFERENCE 56

SEQUENTIAL DESIGN OF DECENTRALIZED DYNAMIC COMPENSATORS USING THE OPTIMAL PROJECTION EQUATIONS: AN ILLUSTRATIVE EXAMPLE INVOLVING INTERCONNECTED FLEXIBLE BEAMS

Dennis S. Bernstein*

Harris Corporation
Government Aerospace Systems Division
MS 22/4848
Melbourne, FL 32902

Abstract

A straightforward and natural application of reduced-order control-design methods is to design decentralized controllers by viewing each subcontroller as a reduced-order controller for the augmented system comprised of the plant and all other subcontrollers. A suitable reduced-order control-design method for this purpose is the optimal projection approach because of its reliability in yielding stable controllers and because it is based upon an optimality criterion which serves as a convenient convergence indicator. The approach is illustrated on an interconnected flexible beam example.

1. Introduction

In [1,2] the following approach to designing decentralized dynamic compensators was proposed: view each subcontroller as a reduced-order controller for the augmented system consisting of the plant and all other subcontrollers. Initially, the dynamic subcontroller can be determined sequentially accounting fully for previously specified subcontrollers. After initial gains have been specified for each subcontroller, the overall design can be refined sequentially by replacing current subcontroller gains with updated gains. Such an approach appears to be a straightforward and natural application of reduced-order design methods. Candidate methods include either LQG reduction ([3]) or fixed-order optimization ([4]).

One criticism of this approach which often arises is that "no new insights or qualitatively new properties germane only to the decentralized case are obtained." Indeed, quite the contrary, the strength of this approach lies in the fact that no new properties are required. Numerous decentralized control-design schemes have been proposed which are based upon system decomposition with centralized design procedures applied to the individual subsystems. There then remains the problem of determining conditions under which the reassembled closed-loop system has acceptable behavior. An additional drawback of decomposition methods is that the decentralized controller architecture specified by implementation contraints may be completely unrelated to any subsystem decomposition arising from physical considerations. For example, implementation constraints may impose a particular decentralized architecture which does not correspond to any discernible decomposition. Furthermore, subsystem decomposition as a design tool may constrain the class of attainable designs at the expense of achievable performance.

Of course, in many cases, such as in the presence of high dimensionality, subsystem decomposition is absolutely essential for making progress in designing decentralized controllers. However, only by developing methods which avoid unnecessary constraints on the design space can the efficiency of decomposition methods be assessed. Furthermore, methods which retain the full system dynamics may provide a useful context for applying existing decomposition techniques as well as an advantageous starting point for developing new methods. Finally, subsystem decomposition techniques are also relevant to the approach suggested here by providing a near-optimal starting point for subsequent refinement.

In sequentially applying reduced-order design methods to decentralized control, a number of issues immediately arise, including the subcontroller refinement sequence, feasibility of the reduced-order design method at each step, and convergence of the overall process. Note that after initial gain determination the existence of a stabilizing design at each step is not at issue here since at least one stabilizing controller exists, namely, the present gain values supplied by the previous step. One of the chief concerns, however, is that the reduced-order design method be sufficiently reliable to permit flexibility in choosing the refinement sequence. Many reduced-order design methods do not, however, consistently yield stabilizing controllers of a given order when stabilizing controllers are clearly known to exist. For example, in [5], the LQG reduction methods reviewed in [3] were compared to the optimal projection approach to fixed-order dynamic

---

*Harris Corporation, MS 22/4848, Melbourne, FL 32902. This research was supported in part by the Air Force Office of Scientific Research under contracts F49620-86-C-0002 and F49620-86-C-0038.

compensation [(4)]. For an 8th-order example due to Enns over a range of control authorities, only the optimal projection approach consistently provided stable designs for each case considered. Thus, the optimal projection approach appears to be a promising candidate for reliable sequential subcontroller refinement.

In addition to reliably producing stable designs at each step, the optimal projection approach is based upon a quadratic performance criterion which readily permits assessment of convergence of the refinement procedure. Specifically, at each subcontroller refinement step, a given subcontroller is replaced by an improved subcontroller. Here "improved" refers to the situation in which all subcontrollers except one are "frozen," while the performance functional is optimized with respect to the remaining free gains. If this procedure is feasible at each step and if the global minimum for each subcontroller design problem is attainable, then the closed-loop performance must improve at each step. Since the performance is also bounded below by zero, then it must converge. Although such observations are immediate, they depend upon optimality considerations and hence are not valid for most reduced-order control-design procedures.

As discussed previously, stabilizability is not the issue here; after subcontroller initialization at least one stabilizing controller at each refinement step exists, namely, the gains provided by the previous step. Hence the principal remaining issue concerns the existence of and ability to compute the global optimum. Using topological degree theory and homotopic continuation methods, these issues have been addressed in [6]. These results show that the local extremals can be enumerated from the basic problem data and the global optimum can be efficiently computed. Furthermore one of the principal results of [6] states that when the compensator order is greater than either the number of inputs or outputs minus the dimension of the unstable subspace, then a unique global minimum exists.

It should also be noted that alternative optimality criteria may be utilized in place of the quadratic performance functional. For example, an H-infinity criterion may be utilized, although it appears to be more difficult to characterize globally optimal reduced-order H-infinity controllers.

The approach proposed in [1,2] involves solving the optimal projection equations developed in [4] to sequentially refine each subcontroller until convergence is reached. The structure of the optimal projection equations shows that the optimal solution is characterized by a collection of oblique projections, specifically, one for each subcontroller. Since each projection operates on the plant dynamics augmented by the other subcontrollers' dynamics, it is clear that a high degree of coupling exists among the subcontrollers. This, of course, is to be expected in general, while design methods which attempt to decouple the subcontroller design process are generally suboptimal.

2. Problem Statement

Given the controlled system

$$\dot{x}(t) = Ax(t) + \sum_{i=1}^{p} B_i u_i(t) + w_0(t), \quad (2.1)$$

$$y_i(t) = C_i x(t) + w_i(t), \quad i=1,\ldots,p, \quad (2.2)$$

design a fixed-structure decentralized dynamic compensator

$$\dot{x}_{ci}(t) = A_{ci} x_{ci}(t) + B_{ci} y_i(t), \quad i=1,\ldots,p, \quad (2.3)$$

$$u_i(t) = C_{ci} x_{ci}(t), \quad i=1,\ldots,p, \quad (2.4)$$

which minimizes the steady-state performance criterion

$$J(A_{c1},B_{c1},C_{c1},\ldots,A_{cp},B_{cp},C_{cp}) \triangleq$$

$$\lim_{t\to\infty} \underline{E}[x(t)^T R_0 x(t) + \sum_{i=1}^{p} u_i(t)^T R_i u_i(t)], \quad (2.5)$$

where, for $i=1,\ldots,p$: $x \in \underline{R}^n$, $u_i \in \underline{R}^{m_i}$, $y_i \in \underline{R}^{\ell_i}$, $x_{ci} \in \underline{R}^{n_{ci}}$, $n_c \triangleq \sum_{i=1}^{p} n_{ci}$, $n_{ci} \leq n+n_c-n_{ci}$, A, B_i, C_i, A_{ci}, B_{ci}, C_{ci}, R_0 and R_i are matrices of appropriate dimension with R_0 (symmetric) nonnegative definite and R_i (symmetric) positive definite; w_0 is white disturbance noise with nxn nonnegative-definite intensity V_0, and w_i is white observation noise with $\ell_i x \ell_i$ positive-definite intensity V_i, where $w_0, w_1, \ldots, w_p$ are mutually uncorrelated and have zero mean. $\underline{E}$ denotes expectation and superscript T indicates transpose. With this notation the optimal projection equations can be applied separately to each subcontroller with all other subcontrollers fixed (see [1,2]).

3. Proposed Algorithm

Sequential Design Algorithm.

Step 1: Choose starting point consisting of initial subcontroller designs;

Step 2: For a sequence $\{i_k\}_{k=1}^{\infty}$, where $i_k \in \{1,\ldots,p\}$, $k=1,2\ldots$, redesign subcontroller i_k as an optimal fixed-order centralized controller for the plant and remaining subcontrollers;

Step 3: Compute performance J_k of current design and check $J_k - J_{k-1}$ for convergence.

Note that the first two steps of the algorithm consist of 1) bringing suboptimal subcontrollers "on line" and 2) iteratively refining each subcontroller. As discussed in Section 1, the choice of a starting design for Step 1 can be obtained by a variety of existing methods such as subsystem decomposition. As for subcontroller refinement, note that each subcontroller redesign procedure is equivalent to replacing a suboptimal subcontroller with a subcontroller which is optimal with respect to the plant and remaining subcontrollers.

4. Application to Interconnected Flexible Beams

To demonstrate the applicability of the sequential design algorithm, we consider a pair of simply supported Euler-Bernoulli flexible beams interconnected by a spring (see Fig. 1). Each beam possesses one rate sensor and one force actuator. Retaining two vibrational modes in each beam, we obtain the 8th-order interconnected model

$$A = \begin{bmatrix} A_{11} & A_{12} \\ A_{21} & A_{22} \end{bmatrix}, \quad B_1 = \begin{bmatrix} B_{11} \\ 0_{4x1} \end{bmatrix}, \quad B_2 = \begin{bmatrix} 0_{4x1} \\ B_{22} \end{bmatrix},$$

$$C_1 = [C_{11} \quad 0_{1x4}], \quad C_2 = [0_{1x4} \quad C_{22}],$$

where

$$A_{ii} = \begin{bmatrix} 0 & \omega_{1i} & 0 & 0 \\ -\omega_{1i}-(k/\omega_{1i})(\sin \pi c_i)^2 & -2\zeta_i\omega_{1i} & -(k/\omega_{2i})(\sin \pi c_i)(\sin 2\pi c_i) & 0 \\ 0 & 0 & 0 & \omega_{2i} \\ -(k/\omega_{1i})(\sin \pi c_i)(\sin 2\pi c_i) & 0 & -\omega_{2i}-(k/\omega_{2i})(\sin 2\pi c_i)^2 & -2\zeta_i\omega_{2i} \end{bmatrix},$$

and

$$A_{ij} = \begin{bmatrix} 0 & 0 & 0 & 0 \\ (k/\omega_{1j})(\sin \pi c_i)(\sin \pi c_j) & 0 & (k/\omega_{2j})(\sin \pi c_i)(\sin 2\pi c_j) & 0 \\ 0 & 0 & 0 & 0 \\ (k/\omega_{1j})(\sin \pi c_j)(\sin 2\pi c_i) & 0 & (k/\omega_{2j})(\sin 2\pi c_i)(\sin 2\pi c_j) & 0 \end{bmatrix},$$

$i \neq j$,

$$B_{ii} = \begin{bmatrix} 0 \\ -\sin \pi a_i \\ 0 \\ -\sin 2\pi a_i \end{bmatrix}$$

$$C_{ii} = [0 \quad \sin \pi s_i \quad 0 \quad \sin 2\pi s_i]$$

$$a_i = \hat{a}_i/L_i, \quad s_i = \hat{s}_i/L_i, \quad c_i = \hat{c}_i/L_i.$$

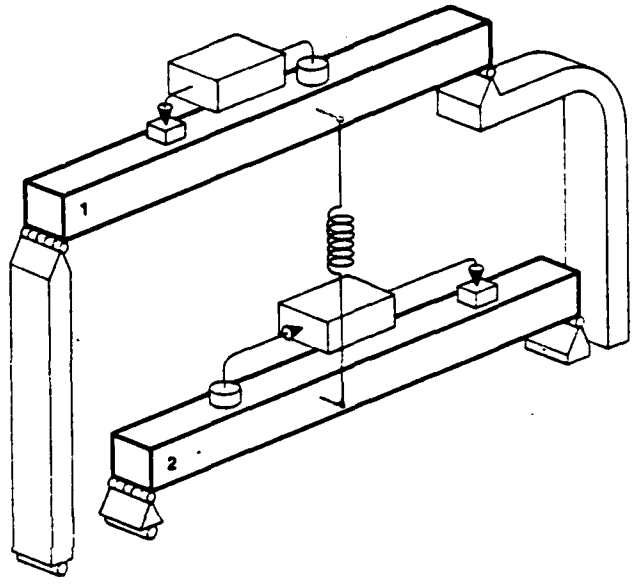

Figure 1

In the above definitions, k is the spring constant, ω_{ji} is the jth modal frequency of the ith beam, ζ_i is the damping ratio of the ith beam, L_i is the length of the ith beam, and $\hat{a}_i$, $\hat{s}_i$ and $\hat{c}_i$ are, respectively, the actuator, sensor and spring-connection coordinates as measured from the left in Fig. 1. The chosen values are

$$k = 10,$$

$$\omega_{1i} = 1, \quad \omega_{2i} = 4, \quad \zeta_i = .005, \quad L_i = 1, \quad i = 1,2,$$

$$\hat{a}_1 = .3, \qquad \hat{s}_1 = .65, \qquad \hat{c}_1 = .6,$$

$$\hat{a}_2 = .8, \qquad \hat{s}_2 = .2, \qquad \hat{c}_2 = .4.$$

In addition, weighting and intensity matrices are chosen to be

$$R_0 = \text{block-diagonal}\left(\begin{bmatrix} 1 & 0 \\ 0 & 1/\omega_{11} \end{bmatrix} \cdot \begin{bmatrix} 1 & 0 \\ 0 & 1/\omega_{21} \end{bmatrix} \cdot \begin{bmatrix} 1 & 0 \\ 0 & 1/\omega_{12} \end{bmatrix} \cdot \begin{bmatrix} 1 & 0 \\ 0 & 1/\omega_{22} \end{bmatrix}\right),$$

$$R_1 = R_2 = .1,$$

$$V_0 = \text{block-diagonal}\left(\begin{bmatrix} 0 & 0 \\ 0 & 1 \end{bmatrix} \cdot \begin{bmatrix} 0 & 0 \\ 0 & 1 \end{bmatrix} \cdot \begin{bmatrix} 0 & 0 \\ 0 & 1 \end{bmatrix} \cdot \begin{bmatrix} 0 & 0 \\ 0 & 1 \end{bmatrix}\right),$$

$$V_1 = V_2 = .1.$$

For this problem the open-loop cost was evaluated and the centralized 8th-order LQG design was obtained to provide a baseline. To provide a starting point for the sequential design algorithm, a pair of 4th-order LQG controllers were designed for each beam separately ignoring the interconnection, i.e., setting k=0. The optimal projection equations were then utilized to iteratively refine each subcontroller. The results are summarized in Table 1.

Acknowledgement. I wish to thank Scott W. Greeley for providing the beam model in Section 4 and for carrying out the design computations.

Design	Cost
Open Loop	163.5
Centralized LQG $n_c = 8$	19.99
Suboptimal Decentralized $n_{c1} = n_{c2} = 4$	59.43
Redesign Subcontroller 2	28.19
Redesign Subcontroller 1	23.29
Redesign Subcontroller 2	23.04
Redesign Subcontroller 1	22.25
Redesign Subcontroller 2	21.94
Redesign Subcontroller 1	21.86
Redesign Subcontroller 2	21.81
Redesign Subcontroller 1	21.79

Table 1

References

1. D. S. Bernstein, "The Optimal Projection Equations for Fixed-Structure Decentralized Dynamic Compensation," Proc. 24th IEEE Conf. Dec. Contr., pp. 104-107, Fort Lauderdale, FL, December 1985.

2. D. S. Bernstein, "Sequential Design of Decentralized Dynamic Compensators Using the Optimal Projection Equations," Int. J. Contr., 1987, to appear.

3. Y. Liu and B. D. O. Anderson, "Controller Reduction Via Stable Factorization and Balancing," Int. J. Contr., Vol. 44, No. 2, 507-531, 1986.

4. D. C. Hyland and D. S. Bernstein, "The Optimal Projection Equations for Fixed-Order Dynamic Compensation," IEEE Trans. Autom. Contr., Vol. AC-29, pp. 1034-1037, 1984.

5. S. W. Greeley and D. C. Hyland, "Reduced-Order Compensation: LQG Reduction Versus Optimal Projection," submitted.

6. S. Richter, "A Homotopy Algorithm for Solving the Optimal Projection Equations for Fixed-Order Dynamic Compensation: Existence, Convergence and Global Optimality," this conference.

APPENDIX D

REFERENCE 68

Revised April 1987

The Majorant Lyapunov Equation: A Nonnegative Matrix Equation for Robust Stability and Performance of Large Scale Systems

by

David C. Hyland and Dennis S. Bernstein

Harris Corporation
Government Aerospace Systems Division
MS 22/4848
Melbourne, FL 32902
(305) 729-2140

Abstract

A new robust stability and performance analysis technique is developed. The approach involves replacing the state covariance by its block-norm matrix, i.e., the nonnegative matrix whose elements are the norms of subblocks of the covariance matrix partitioned according to subsystem dynamics. A bound (i.e., majorant) for the block-norm matrix is given by the majorant Lyapunov equation, a Lyapunov-type nonnegative matrix equation. Existence, uniqueness and computational tractability of solutions to the majorant Lyapunov equation are shown to be completely characterized in terms of M matrices. Two examples are considered. For a damped simple harmonic oscillator with uncertain but constant natural frequency, the majorant Lyapunov equation predicts unconditional stability. And, for a pair of nominally uncoupled oscillators with uncertain coupling, the majorant Lyapunov equation shows that the range of nondestabilizing couplings is proportional to the frequency separation between the oscillators, a result not predictable from quadratic or vector Lyapunov functions.

This research was supported in part by the Air Force Office of Scientific Research under contracts F49620-86-C-0002 and F49620-86-C-0038.

Notation for Typesetting

$\mathcal{A}$. $\mathcal{D}$. $\mathcal{G}$. $\mathcal{Q}$. $\mathcal{V}$	Script face type
$\mathbb{A}$. $\mathbb{E}$. $\mathbb{G}$. $\mathbb{R}$	Open face type

1. Introduction

The importance of robustness in control-system analysis and design cannot be overemphasized. The past ten years' literature reflects considerable frequency-domain development ([1-10]), while recent publications indicate increasing time-domain activity ([11-19]). Wide variations in underlying assumptions, mathematical settings, and problem data render it difficult, if not impossible, to clearly delineate the relative effectiveness of different methods. Our own philosophical outlook has thus been guided by two general criteria:

1. Effectiveness for simple examples;

2. Efficiency when applied to large scale problems.

The first criterion involves applying robustness techniques to simple, perhaps trivially obvious, examples to serve as "acid tests." A given method's effectiveness on a collection of such examples can possibly reveal inherent shortcomings. As an illustration of this criterion, consider a damped harmonic oscillator with constant but uncertain natural frequency. Using the notation of [6], stability is guaranteed so long as

$$\sigma_{max}[R(j\omega)(I+G(j\omega)K(j\omega))^{-1}G(j\omega)L^{-1}(j\omega)] < 1, \quad \omega \geq 0, \qquad (1.1)$$

where, for $\nu > 0$,

$$G(s) = (s^2+2\nu s+\omega_n^2)^{-1},$$

and uncertainty in the nominal natural frequency ω_n is modelled by

$$\Delta(s) = L^{-1}(s)\theta(s)R(s) = \delta\omega_n^2,$$

$$L(s) = 1/\alpha, \ \theta(s) = \delta/\alpha, \quad R(s) = \omega_n^2, \quad K(s) = 0,$$

$$\delta \in [-\min(1,\alpha),\alpha], \quad \alpha > 0.$$

Note that

$$\sigma_{max}[\theta(j\omega)] \leq 1, \quad \omega \geq 0,$$

as required in [6]. The perturbation $\Delta(s)$ (modelled as a feedback gain) effectively replaces ω_n^2 in $G(s)$ by $(1+\delta)\omega_n^2$. Hence, for a given $\alpha > 0$ this uncertainty model permits perturbed natural frequencies in the range $[0,(1+\alpha)^{1/2}\omega_n]$. Evaluating (1.1) yields the upper bound

$$\alpha < [(\omega_n^2-\omega^2)^2 + 4\nu^2\omega^2]^{1/2}/\omega_n^2, \quad \omega \geq 0, \tag{1.2}$$

or, equivalently,

$$\alpha < 2\zeta(1-\zeta^2)^{1/2}, \tag{1.3}$$

where $\zeta \triangleq \nu/\omega_n$. The conservatism of (1.3) is obviously most pronounced when the damping ratio ζ is small. In all cases, however, the conservatism is infinite. This conservatism can be removed, however, by means of the structured singular value developed by Doyle ([5,6]).

The second criterion is obviously subjective and depends upon a variety of factors such as problem structure, designer experience, and computational resources. This criterion is, in our opinion, most important since the need for robustness techniques becomes increasingly critical as system complexity grows. Indeed, the ultimate test of a given approach is to scale it up to larger and larger problems to reveal inherent limitations. Obviously, such tests are not only difficult, but may entail a significant commitment of human and financial resources. Nevertheless, crude predictions are sometimes available, and a case in point is the "curse of dimensionality" encountered in the approach of [9]. Another example involves computational difficulties in obtaining bounds for the μ-function with more than 3 blocks ([10]).

The contribution of the present paper is a new robustness analysis method developed specifically for large scale systems. The basic idea, motivated by the work of Siljak ([30]) on connective stability, is as follows. The system is assumed to be in the form of a collection of subsystems with uncertain local dynamics and uncertain interactions.* Parameter uncertainties are modelled as either structured or unstructured constant variations contained in prescribed sets. The state covariance, partitioned conformably with the subsystem dynamics, is replaced by its block-norm matrix, i.e., the nonnegative matrix each of whose elements is the norm of the corresponding subblock of the original matrix. This nonnegative matrix satisfies a novel inequality designated the covariance block-norm inequality. The existence of a solution to the majorant Lyapunov equation, i.e., the covariance block-norm inequality interpreted as an equation, yields an element-by-element bound (i.e., majorant) for the covariance block-norm, hence assuring robust stability and performance. The relevance of this technique to large scale systems stems from the fact that replacing each subblock of the covariance by its norm can significantly reduce the dimension of the problem. Indeed, the dimension of the majorant Lyapunov equation is equal to the number of subsystems which may be significantly less than the dimension of the original system.

To illustrate the above ideas in more detail, consider the covariance equation

$$0 = (\bar{A}+G)Q + Q(\bar{A}+G)^T + V, \tag{1.4}$$

where $\bar{A}$ denotes the nominal dynamics, G denotes uncertainty in $\bar{A}$, V is the disturbance intensity, and Q is the state covariance. Assuming that $\bar{A}$ is block diagonal with r diagonal blocks and that G has only off-diagonal nonzero blocks leads to the covariance block-norm inequality (see Proposition 4.2)

$$\underline{A}^*\underline{Q} \leq\leq \underline{G}\underline{Q} + \underline{Q}\underline{G}^T + \underline{V}. \tag{1.5}$$

In (1.5), $\underline{A}$, $\underline{Q}$, $\underline{G}$ and $\underline{V}$ are rxr nonnegative matrices, i.e., each element is a nonnegative number. The matrices $\underline{Q}$ and $\underline{V}$ are formed by taking the Frobenius norm of each subblock of Q and V, while each component of $\underline{G}$ is a given constant which bounds the spectral norm (largest singular value) of the

---

*Uncertainties in a single subsystem can also be regarded as interaction uncertainties. To see this, write $\dot{x} = (A+G)x$ twice so that the uncertainty G is represented by $\begin{bmatrix} 0 & G \\ G & 0 \end{bmatrix}$.

corresponding subblock of the uncertain perturbation G. Hence $\underline{G}$ is a majorant for G in the sense of [21-23]. Each element of the matrix $\underline{A}$ is bounded above by the smallest singular value of the Kronecker sum ([24-26]) of pairs of diagonal blocks of $\bar{A}$. The operation "*" is the Hadamard product ([27,28]), and the ordering "$\underline{<<}$" denotes element-by-element comparison, i.e., the ordering induced by the cone of nonnegative matrices ([29,30]).

The majorant Lyapunov equation is obtained by replacing the inequality (1.5) by the rxr nonnegative matrix equation

$$\underline{A}^*\tilde{\underline{Q}} = \underline{G}\tilde{\underline{Q}} + \tilde{\underline{Q}}\underline{G}^T + \underline{V}. \tag{1.6}$$

A key result (Corollary 5.1) states that

$$\underline{Q} \underline{<<} \tilde{\underline{Q}} \tag{1.7}$$

for all stable $\bar{A}+G$. Consequently (see Theorem 5.1), the existence of a solution to (1.6) leads directly to a guarantee of robust stability over the range specified by $\underline{G}$ and to a performance bound involving $\underline{Q}$. Moreover, solutions of (1.6) exist if and only if the r^2xr^2 matrix

$$\underline{\underline{A}} \triangleq \text{diag}(\text{vec } \underline{A}) - \underline{G}\otimes\underline{G} \tag{1.8}$$

is an M matrix ([29,30]).

Even when the number of subsystems is large, the majorant Lyapunov equation is generally computationally tractable. Specifically, although $\underline{\underline{A}}$ is an r^2xr^2 matrix, no computations whatsoever need to be carried out with matrices of this dimension. Rather, it suffices to solve only the majorant Lyapunov equation (1.6). In this regard we show that $\tilde{\underline{Q}}$ is given by

$$\hat{\underline{Q}} = \lim_{i\to\infty} \tilde{\underline{Q}}_i, \tag{1.9}$$

where the sequence $\{\tilde{\underline{Q}}_i\}$ generated by

$$\underline{A}^*\tilde{\underline{Q}}_{i+1} = \underline{G}\tilde{\underline{Q}}_i + \tilde{\underline{Q}}_i\underline{G}^T + \underline{V}, \quad \tilde{\underline{Q}}_0 = 0, \tag{1.10}$$

is monotonically increasing. Furthermore, the convergence of this sequence is equivalent to $\underline{\underline{A}}$ being an M matrix so that is not even necessary to form $\underline{\underline{A}}$. Note that (1.6) does not require the development of new solution techniques. Indeed, since (1.10) is a straightforward iteration, (1.6) is even easier to solve than the original Lyapunov equation (1.4).

To illustrate these results we consider two examples. The first example is the damped oscillator already considered in this section. With little effort the majorant Lyapunov equation yields the (obvious) result that the oscillator is stable for <u>all</u> constant natural frequencies. The second example involves a pair of oscillators with known parameters but with uncertain coupling. The majorant Lyapunov equation yields bounds over which stability is guaranteed, and these bounds are compared to the actual stability region as a function of frequency separation. The main result shows that the robustness to uncertain coupling is proportional to the frequency separation. This weak subsystem interaction robustification mechanism is the principal contribution of the majorant theory. This example has immediate application to the problem of vibration control in flexible structures. For this class of problems the open-loop dynamics can be viewed as a collection of uncoupled oscillators which become coupled via feedback and structural uncertainties.

The majorant bound developed in the present paper is quite different from the widely used quadratic Lyapunov function (see, e.g., [11,12,17-20]). As can readily be shown using the methods of [12,17-20], the quadratic Lyapunov function yields robust stability and performance by replacing (1.4) by

$$0 = \bar{A}\hat{Q} + \hat{Q}\bar{A}^{T} + \Omega(\hat{Q}) + V, \tag{1.11}$$

where $\Omega(\cdot)$ satisfies

$$G\hat{Q} + \hat{Q}G^{T} \leq \Omega(\hat{Q}) \tag{1.12}$$

for all variations G. It can then be shown that

$$Q \leq \hat{Q}. \tag{1.13}$$

where now, in contrast (1.7), the ordering in (1.13) is defined with respect to the cone of nonnegative-definite matrices. Indeed, the majorant bound may be more closely related to vector Lyapunov functions ([30,31]) and the Lyapunov matrix function ([32,33]). It does not appear possible, however, to use these techniques to obtain the majorant results on robustness due to subsystem frequency separation.

The reader will observe that this paper exploits a wide variety of techniques including nonnegative matrices, block norms, matrix majorants, the Hadamard product, the Kronecker sum, and M matrices. Each of these techniques, except majorants, has, however, been previously applied to control problems in numerous instances. In the special case of scalar subblocks, the block-norm matrix has, moreover, been utilized by Yedavalli ([13-15]) and others for robustness analysis and design. In this case the block norm is known as the matrix modulus. The variety of algebraic structures employed in the present paper should not be surprising since the quest for increasingly refined robustness techniques can be expected to invoke correspondingly refined uncertainty bounds. Related techniques are employed in [16]. Furthermore, nonnegative matrix equations involving M matrices arise naturally in a variety of settings (see, e.g., [38,39]).

The contents of the paper are as follows. Section 2 presents notation, definitions and lemmas for use throughout the paper. In Section 3 robust stability and performance are defined for the homogeneous and nonhomogeneous systems. Detailed system structure and uncertainty characterization are given in Section 4 and the covariance block-norm inequality is derived. Section 5 analyzes the majorant Lyapunov equation to obtain a majorant for the steady-state covariance. The main result, Theorem 5.1, guarantees robust stability and provides a performance bound. Finally, the examples appear in Section 6.

2. Preliminaries

The following notation will be used throughout. All matrices are assumed to have real entries.

$\underline{\underline{E}}$	expected value
$\underline{\underline{R}}$, $\underline{\underline{R}}^{pxq}$, $\underline{\underline{R}}^{p}$	real numbers, pxq real matrices, $\underline{\underline{R}}^{px1}$
I_p, 0_{pxq}, 0_p	pxp identity matrix, pxq zero matrix, 0_{pxp}
$\bullet$, $\otimes$	Kronecker sum, Kronecker product ([24-27])
$*$	Hadamard product ([27,28])
$col_i(Z)$	ith column of matrix Z
$vec(Z)$	$\begin{bmatrix} col_1(Z) \\ \vdots \\ col_q(Z) \end{bmatrix} \in \underline{\underline{R}}^{pq}$, $Z \in \underline{\underline{R}}^{pxq}$
$Z_{(i,j)}$	(i,j) element of matrix Z
Z^T	transpose of vector or matrix Z
Z^{-T}	$(Z^T)^{-1}$ or $(Z^{-1})^T$
tr Z	trace of matrix Z
Z^{HI}	Hadamard inverse, $(Z^{HI})_{(i,j)} \triangleq [Z_{(i,j)}]^{-1}$, $Z >> 0$
$diag(Z_1,\ldots,Z_p)$	diagonal matrix with listed diagonal elements
$block\text{-}diag(Z_1,\ldots,Z_p)$	block-diagonal matrix with listed diagonal blocks
$\rho(Z)$	spectral radius of Z
asymptotically stable matrix	matrix with eigenvalues in open left half plane
nonnegative-definite matrix	symmetric matrix with nonnegative eigenvalues ($Z \geq 0$)
positive-definite matrix	symmetric matrix with positive eigenvalues ($Z > 0$)
$Z_1 \geq Z_2$	$Z_1-Z_2 \geq 0$, Z_1, Z_2 symmetric
$Z_1 > Z_2$	$Z_1-Z_2 > 0$, Z_1, Z_2 symmetric

nonnegative matrix	matrix with nonnegative elements ($Z \geq 0$) ([29,30])
positive matrix	matrix with positive elements ($Z > 0$)
$Z_1 \geq Z_2$	$Z_1 - Z_2 \geq 0$
$Z_1 > Z_2$	$Z_1 - Z_2 > 0$
block-norm matrix	nonnegative matrix each of whose elements is the norm of a corresponding subblock of a given partitioned matrix
majorant	nonnegative matrix each of whose elements bounds the corresponding element of a block-norm matrix
$\|z\|_2$	Euclidean norm of vector Z
$\sigma_i(Z)$	singular value of matrix Z
$\sigma_{min}(Z)$, $\sigma_{max}(Z)$	smallest and largest singular values of matrix Z
$\lambda_{max}(Z)$	largest eigenvalue of symmetric matrix Z
$\|Z\|_s$	$\sigma_{max}(Z)$ (spectral norm induced by $\|\cdot\|_2$)
$\|Z\|_F$	$(\text{tr } ZZ^T)^{1/2} = [\sum_{i,j=1}^{p,q} Z_{(i,j)}^2]^{1/2} = [\sum_{i=1}^{p} \sigma_i^2]^{1/2}$ (Frobenius norm [34])

In subsequent sections we shall exploit the fact that the norms $\|\cdot\|_2$, $\|\cdot\|_s$ and $\|\cdot\|_F$ coincide for vectors. Hence, if $Z \in \underline{\underline{R}}^p$ then by interpreting $\underline{\underline{R}}^p = \underline{\underline{R}}^{px1}$ it follows that

$$\|z\|_2 = \|z\|_s = \|z\|_F. \tag{2.1}$$

Furthermore, if $Z \in \underline{\underline{R}}^{pxq}$ then

$$\|z\|_s \leq \|z\|_F = \|\text{vec } z\|_F = \|\text{vec } z\|_2 = \|\text{vec } z\|_s. \tag{2.2}$$

Lemma 2.1. If $Z \in \underline{\underline{R}}^{pxp}$ and $\hat{Z} \in \underline{\underline{R}}^{pxq}$ then

$$\sigma_{min}(Z)\|\hat{Z}\|_F \leq \|Z\hat{Z}\|_F \leq \|Z\|_s\|\hat{Z}\|_F. \tag{2.3,2.4}$$

If, furthermore, $p = q$, $Z \geq 0$, and $\hat{Z}$ is symmetric, then

$$\text{tr } Z\hat{Z} \leq (\text{tr } Z)\lambda_{\max}(\hat{Z}) \leq (\text{tr } Z)\|\hat{Z}\|_s. \tag{2.5}$$

Proof. Inequality (2.4) can be found in [35], p. 263. To prove (2.3), note that when Z is singular the result is immediate. Otherwise, replace Z and $\hat{Z}$ in (2.3) by Z^{-1} and $Z\hat{Z}$, respectively. The result now follows from $[\sigma_{\max}(Z)]^{-1} = \sigma_{\min}(Z^{-1})$. Finally, (2.5) is given in [36].□

Recall ([30]) that a matrix $S \in \underline{\underline{R}}^{r\times r}$ is an N matrix if $S_{(i,j)} \leq 0$, $i,j = 1,\ldots,r$, $i \neq j$. If, in addition, all principal minors of S are positive, then S is an M matrix.

Lemma 2.2. Suppose $S \in \underline{\underline{R}}^{r\times r}$ is an N matrix. Then the following are equivalent:

(i) S is an M matrix;

(ii) $\det S \neq 0$ and $S^{-1} \geqq 0$;

(iii) for each $y \in \underline{\underline{R}}^r$, $y \geqq 0$, there exists (a unique) $x \in \underline{\underline{R}}^r$, $x \geqq 0$, such that $Sx = y$;

(iv) there exists $x \in \underline{\underline{R}}^r$, $x \geqq 0$, such that $Sx > 0$;

(v) $I_r * S > 0$ and each diagonal matrix $D \geqq I_r * S$ satisfies $\rho[D^{-1}(I_r * S - S)] < 1$.

Proof. The equivalences of statements (i), (ii), (iv) and (v) follows from [30], p. 396. The implication (ii) ==> (iii) is immediate, and (iii) ==> (iv) follows by setting $y = [1 \;\; 1 \;\; \ldots \;\; 1]^T$.□

Lemma 2.3. Suppose $S \in \underline{\underline{R}}^{r\times r}$ is an M matrix and let $\hat{S} \in \underline{\underline{R}}^{r\times r}$ be an N matrix such that $\hat{S} \geqq S$. Then $\hat{S}$ is an M matrix.

Proof. See [30], p. 400.□

3. Robust Stability and Performance Bounds

Consider the nth-order homogeneous system*

$$\dot{x}(t) = (A(\theta)+G)x(t), \quad t \in [0,\infty), \tag{3.1}$$

$$G \in \underline{\underline{G}} \subset \underline{\underline{R}}^{nxn}, \tag{3.2}$$

$$\theta \in \Theta \subset \underline{\underline{R}}^{m}, \tag{3.3}$$

where $A: \Theta \dashrightarrow \underline{\underline{R}}^{nxn}$ is continuous, $\bar{A} \triangleq A(\bar{\theta})$ denotes the known nominal dynamics for $\bar{\theta} \in \Theta$, θ denotes the unstructured parametric uncertainty in $\bar{A}$, G denotes the structured parametric uncertainty in $\bar{A}$, and $0 \in \underline{\underline{G}}$ is the nominal value of G. We first consider the stability of (3.1) over $\underline{\underline{G}}$ and Θ.

Definition 3.1. If $A(\theta)+G$ is asymptotically stable for all $G \in \underline{\underline{G}}$ and $\theta \in \Theta$, then the homogeneous system (3.1) is robustly stable over $\underline{\underline{G}}$ and Θ.

Now consider the nth-order nonhomogeneous system

$$\dot{x}(t) = (A(\theta)+G)x(t) + w(t), \quad t \in [0,\infty), \tag{3.4}$$

where $G \in \underline{\underline{G}}$, $\theta \in \Theta$, and $w(\cdot)$ is white noise with intensity $V \geq 0$. For given $G \in \underline{\underline{G}}$ and $\theta \in \Theta$, the steady-state average quadratic performance is defined by

$$J(G,\theta) \triangleq \limsup_{t \to \infty} \underline{\underline{E}}[x^{T}(t)Rx(t)]. \tag{3.5}$$

The system (3.4) may, for example, denote a control system in closed-loop configuration. There is no need in our development, however, to make such distinctions.

In practice, steady-state performance is only of interest when the system is robustly stable. The following result is immediate.

*Upon first reading the uncertainty represented by (3.3) can be ignored since the principal contribution concerns the treatment of (3.2).

Proposition 3.1. Suppose the system (3.1) is robustly stable over $\underline{\underline{G}}$ and Θ. Then for each $G \in \underline{\underline{G}}$ and $\theta \in \Theta$,

$$J(G,\theta) = \text{tr } QR, \tag{3.6}$$

where nxn nonnegative-definite Q is the unique solution to

$$0 = (A(\theta)+G)Q + Q(A(\theta)+G)^T + V. \tag{3.7}$$

We shall only be concerned with the case in which $\underline{\underline{G}}$ and Θ are compact. Since Q is a continuous function of G and θ, we can define the worst-case average steady-state quadratic performance

$$J_{\max} \triangleq \max_{G \in \underline{\underline{G}},\, \theta \in \Theta} J(G,\theta). \tag{3.8}$$

Since it is difficult to determine $J_{\max}$ explicitly, we shall seek upper bounds.

Definition 3.2. If $J_{\max} \leq \hat{\alpha}$ then $\hat{\alpha}$ is a performance bound for the nonhomogeneous system (3.4) over $\underline{\underline{G}}$ and Θ.

4. System Structure, Uncertainty Characterization and the Covariance Block-Norm Inequality

A discussed in Section 1, (3.1) and (3.4) are assumed to be in the form of a large scale system with uncoupled local dynamics and uncertain interactions. Hence, with the subsystem partitioning

$$n = \sum_{i=1}^{r} n_i, \tag{4.1}$$

the local system dynamics $A(\theta)$ can be decomposed into subsystem dynamics according to

$$A(\theta) = \underset{i=1,\ldots,r}{\text{block-diag}}\{A_i(\theta)\}, \tag{4.2}$$

where $A_i(\theta) \in \underline{\underline{R}}^{n_i x n_i}$, $\theta \in \Theta$. For convenience, denote

$$\bar{A} \triangleq \underset{i=1,\ldots,r}{\text{block-diag}}\{\bar{A}_i\}.$$

Accordingly, R is assumed to be of the form

$$R = \underset{i=1,\ldots,r}{\text{block-diag}}\{R_i\}, \tag{4.3}$$

where $R_i \in \underline{\underline{R}}^{n_i x n_i}$, $R_i \geq 0$, $i=1,\ldots,r$. The intensity V and steady-state covariance Q satisfying (3.7) are assumed to be conformably partitioned, i.e.,

$$V = \{V_{ij}\}_{i,j=1}^{r}, \qquad V_{ij} \in \underline{\underline{R}}^{n_i x n_j}, \tag{4.4}$$

$$Q = \{Q_{ij}\}_{i,j=1}^{r}, \qquad Q_{ij} \in \underline{\underline{R}}^{n_i x n_j}. \tag{4.5}$$

For notational simplicity define

$$V_i \triangleq V_{ii}, \quad Q_i \triangleq Q_{ii}, \quad i=1,\ldots,r. \tag{4.6}$$

Taking the Frobenius norm of each subblock of V and Q leads to the rxr symmetric nonnegative matrices $\underline{V}$ and $\underline{Q}$ defined by

$$\underline{V} \triangleq \{\|V_{ij}\|_F\}_{i,j=1}^{r}, \qquad \underline{Q} \triangleq \{\|Q_{ij}\|_F\}_{i,j=1}^{r}. \tag{4.7}$$

Note that

$$\|\underline{Q}\|_F = \|Q\|_F, \quad \|\underline{V}\|_F = \|V\|_F. \tag{4.8}$$

A few observations concerning the nominal system, i.e., with $G = 0$ and $\theta = \bar{\theta}$, are worth noting. If $\bar{A}$ is stable then so is $\bar{A}_i$, $i=1,\ldots,r$, and there exist unique, nonnegative-definite $\hat{Q}_i$, $\hat{P}_i \in \underline{\underline{R}}^{n_i \times n_i}$, $i=1,\ldots,r$, satisfying

$$0 = \bar{A}_i \hat{Q}_i + \hat{Q}_i \bar{A}_i^T + V_i, \tag{4.9}$$

$$0 = \bar{A}_i^T \hat{P}_i + \hat{P}_i \bar{A}_i + R_i. \tag{4.10}$$

Proposition 4.1. Suppose $\bar{A}$ is asymptotically stable. Then the nominal performance J_{nom} is given by

$$J_{nom} \triangleq J(0,\bar{\theta}) = \sum_{i=1}^{r} \operatorname{tr} \hat{Q}_i R_i = \sum_{i=1}^{r} \operatorname{tr} \hat{P}_i V_i. \tag{4.11}$$

Proof. First note that with $G = 0$ and $\theta = \bar{\theta}$ the diagonal blocks of Q satisfying (3.7) coincide with $\hat{Q}_1,\ldots,\hat{Q}_r$. Thus

$$\begin{aligned}
J(0,\bar{\theta}) &= \sum_{i=1}^{r} \operatorname{tr} \hat{Q}_i R_i \\
&= \sum_{i=1}^{r} (\operatorname{vec} \hat{Q}_i)^T \operatorname{vec} R_i \\
&= \sum_{i=1}^{r} [(\bar{A}_i \oplus \bar{A}_i)^{-1} \operatorname{vec} V_i]^T \operatorname{vec} R_i \\
&= \sum_{i=1}^{r} (\operatorname{vec} V_i)^T (\bar{A}_i^T \oplus \bar{A}_i^T)^{-1} \operatorname{vec} R_i \\
&= \sum_{i=1}^{r} (\operatorname{vec} V_i)^T \operatorname{vec} \hat{P}_i \\
&= \sum_{i=1}^{r} \operatorname{tr} \hat{P}_i V_i. \square
\end{aligned}$$

The matrices $G \in \underline{\underline{G}}$ are also conformably partitioned so that

$$G = \{G_{ij}\}_{i,j=1}^{r}, \quad G_{ij} \in \underline{\underline{R}}^{n_i \times n_j}, \tag{4.12}$$

and $\underline{\underline{G}}$ is characterized by

$$\underline{\underline{G}} \triangleq \{G \in \underline{\underline{R}}^{n \times n}: \ \sigma_{max}(G_{ij}) \leq \gamma_{ij}, \quad i,j=1,\ldots,r\}, \tag{4.13}$$

where $\gamma_{ij} \geq 0$, $i,j=1,\ldots,r$, are given constants. For convenience, define the $r \times r$ nonnegative matrix

$$\underline{G} \triangleq \{\gamma_{ij}\}_{i,j=1}^{r}. \tag{4.14}$$

The bound $\underline{G}$ is a <u>matrix majorant</u> for $G \in \underline{\underline{G}}$ in the sense of [21-23].

<u>Remark 4.1</u>. $\underline{\underline{G}}$ is compact and convex.

Finally, let symmetric $\underline{A} \in \underline{\underline{R}}^{r \times r}$ satisfy

$$\underline{A}_{(i,j)} \leq \min_{\theta \in \Theta}\{\sigma_{min}(A_j(\theta) \otimes A_i(\theta))\}, \quad i,j=1,\ldots,r. \tag{4.15}$$

<u>Proposition 4.2</u>. Let $G \in \underline{\underline{G}}$ and $\theta \in \Theta$ be such that $A(\theta)+G$ is asymptotically stable and let $n \times n$ $Q \geq 0$ satisfy (3.7). Then $\underline{Q}$ defined by (4.7) satisfies

$$\underline{\underline{A}}^* \underline{Q} \ll \underline{\underline{G}}\,\underline{Q} + \underline{Q}\,\underline{G}^T + \underline{V} \tag{4.16}$$

or, equivalently,

$$\underline{\underline{A}}\ \mathrm{vec}\ \underline{Q} \ll \mathrm{vec}\ \underline{V}, \tag{4.17}$$

where

$$\underline{\underline{A}} \triangleq [\mathrm{diag}(\mathrm{vec}\ \underline{A})] - \underline{\underline{G}} \otimes \underline{\underline{G}}. \tag{4.18}$$

Proof. Expanding (3.7) yields

$$-[A_i(\theta)Q_{ij}+Q_{ij}A_j^T(\theta)] = \sum_{k=1}^{r}[G_{ik}Q_{kj}+Q_{ik}G_{jk}^T] + V_{ij}, \quad i,j=1,\ldots,r. \tag{4.19}$$

Bounding the right hand side of (4.19) from above using (2.3) yields for all $G \in \underline{G}$

$$\left\|\sum_{k=1}^{r}[G_{ik}Q_{kj}+Q_{ik}G_{jk}^T] + V_{ij}\right\|_F \leq \sum_{k=1}^{r}[\underline{G}_{(i,k)}\underline{Q}_{(k,j)}+\underline{Q}_{(i,k)}\underline{G}_{(j,k)}] + \underline{V}_{(i,j)}.$$

while bounding the left hand side of (4.19) from below using (2.4) implies for all $\theta \in \Theta$

$$\begin{aligned}\|-[A_i(\theta)Q_{ij}+Q_{ij}A_j^T(\theta)]\|_F &= \|\mathrm{vec}(A_i(\theta)Q_{ij}+Q_{ij}A_j^T(\theta))\|_F \\ &= \|(A_i(\theta)\oplus A_i(\theta))\ \mathrm{vec}\ Q_{ij}\|_F \\ &\geq \sigma_{\min}(A_j(\theta)\oplus A_i(\theta))\|\mathrm{vec}\ Q_{ij}\|_F \\ &= \sigma_{\min}(A_j(\theta)\oplus A_i(\theta))\underline{Q}_{(i,j)} \\ &\geq \underline{A}_{(i,j)}\underline{Q}_{(i,j)}.\end{aligned}$$

Combining the above inequalities yields (4.16). □

Remark 4.2. Since $\underline{G} \gg 0$, the $r^2 x r^2$ matrix $\underline{A}$ is an N matrix ([30]).

5. The Majorant Lyapunov Equation

In this section we interpret (4.16) as an equality rather than an inequality and consider the Lyapunov-type nonnegative matrix equation

$$\underline{A}^{*}\tilde{\underline{Q}} = \underline{G}\tilde{\underline{Q}} + \tilde{\underline{Q}}\underline{G}^{T} + \underline{V} \tag{5.1}$$

or, equivalently,

$$\underline{\underline{A}}\ \mathrm{vec}\ \tilde{\underline{Q}} = \mathrm{vec}\ \underline{V}. \tag{5.2}$$

Note that since $\underline{A}$ and $\underline{V}$ are symmetric a unique solution of (5.1) is necessarily symmetric.

Proposition 5.1. The following are equivalent:

(i) $\underline{A}$ is an M matrix;

(ii) $\det \underline{\underline{A}} \neq 0$ and $\underline{\underline{A}}^{-1} \geq\!\!\geq 0$;

(iii) for each rxr symmetric $\underline{V} \geq\!\!\geq 0$ there exists (a unique) rxr $\tilde{\underline{Q}} \geq\!\!\geq 0$ satisfying (5.1);

(iv) there exist rxr symmetric $\underline{V} >> 0$ and rxr symmetric $\tilde{\underline{Q}} \geq\!\!\geq 0$ satisfying (5.1);

(v) $\mathrm{diag}(\mathrm{vec}\ \underline{A}) - (I_r * \underline{G}) \circledast (I_r * \underline{G}) >> 0$ and each diagonal matrix $\underline{D} \geq\!\!\geq \mathrm{diag}(\mathrm{vec}\ \underline{A}) - (I_r * \underline{G}) \circledast (I_r * \underline{G})$ satisfies

$$\rho(\underline{D}^{-1}[\underline{G} \circledast \underline{G} - (I_r * \underline{G}) \circledast (I_r * \underline{G})]) < 1; \tag{5.3}$$

(vi) for each rxr symmetric $\tilde{Q}_0 \geq\geq 0$ and rxr symmetric $V \geq\geq 0$, the sequence $\{\tilde{Q}_i\}_{i=1}^{\infty}$ generated by

$$A^*\tilde{Q}_{i+1} - (I_r^*G)\tilde{Q}_{i+1} - \tilde{Q}_{i+1}(I_r^*G)$$

$$= (G-I_r^*G)\tilde{Q}_i + \tilde{Q}_i(G-I_r^*G)^T + V, \quad i=0,1,\ldots, \qquad (5.4)$$

converges.

(vii) for each rxr symmetric $\tilde{Q}_0 \geq\geq 0$ there exists rxr symmetric $V >> 0$ such that the sequence $\{\tilde{Q}_i\}_{i=1}^{\infty}$ generated by (5.4) converges.

Proof. Statements (i)-(v) are equivalent to (i)-(v) of Lemma 2.2. Clearly, (vi) implies (iii), and (vii) implies (iv). To show (v) implies (vi) and (vii) note that $I_{r^2}^*(G\bullet G) = (I_r^*G)\bullet(I_r^*G)$ and

$$\text{vec}(A^*\tilde{Q}_{i+1}) = [\text{diag}(\text{vec } A)]\text{vec } \tilde{Q}_{i+1}.$$

Thus (5.4) is equivalent to

$$\text{vec } \tilde{Q}_{i+1} = [\text{diag}(\text{vec } A) - (I_r^*G)\bullet(I_r^*G)]^{-1}[G\bullet G - I_{r^2}^*(G\bullet G)]\text{vec } \tilde{Q}_i$$

$$+ [\text{diag}(\text{vec } A)]^{-1}\text{vec } V.$$

Thus (vi) and (vii) follow from (v) with $D = \text{diag}(\text{vec } A) - (I_r^*G)\bullet(I_r^*G)$. □

Since statements (i)-(vii) depend only upon A and G we have the following definition inspired by (v)-(vii).

Definition 5.1. (A,G) is stable if A is an M matrix.

Remark 5.1. When $I_r^*G = 0$, i.e., when the local dynamics have no structured uncertainty, (5.4) simplifies to

$$A^*\tilde{Q}_{i+1} = G\tilde{Q}_i + \tilde{Q}_iG^T + V, \quad i=0,1,\ldots, \qquad (5.5)$$

or, equivalently,

$$\tilde{Q}_{i+1} = A^{HI}*(G\tilde{Q}_i + \tilde{Q}_i G^T + V), \quad i=0,1,\ldots . \tag{5.5a}$$

The following result shows that for zero initial condition, the iterative sequence is monotonic.

Proposition 5.2. Suppose $\mathrm{diag}(\mathrm{vec}\, A) - I_{r^2}*(G \otimes G) \gg 0$. Then the sequence $\{\tilde{Q}_i\}_{i=1}^{\infty}$ generated by (5.4) with $\tilde{Q}_0 = 0$ and $V \gg 0$ is monotonically increasing.

Proof. To simplify notation we consider the case mentioned in Remark 5.1. Hence assume $A \gg 0$. Clearly, if $\tilde{Q}_0 = 0$ then (5.5a) implies that $\tilde{Q}_1 = A^{HI}*V \gg 0$. Hence $\tilde{Q}_1 \gg \tilde{Q}_0$. Defining $\Delta\tilde{Q}_{i+1} \triangleq \tilde{Q}_{i+1} - \tilde{Q}_i$, (5.5a) yields

$$\Delta\tilde{Q}_{i+1} = A^{HI}*(G\Delta\tilde{Q}_i + \Delta\tilde{Q}_i G^T).$$

Since $\Delta\tilde{Q}_1 \gg 0$, the result follows from induction.□

Remark 5.2. Proposition 5.2 is a particularly useful result in applications and can be utilized as follows. Setting $\tilde{Q}_0 = 0$, the sequence $\{\tilde{Q}_i\}$ can be evaluated by a simple numerical procedure. As will be shown in Theorem 5.1 below, each $\tilde{Q}_i$ corresponds to a robust performance measure $\hat{\alpha}_i$. For practical purposes the increasing sequence $\{\hat{\alpha}_i\}$ can be generated until either convergence is attained (in which case $\hat{\alpha} = \lim_{i\to\infty} \hat{\alpha}_i$ is a robust performance bound) or a maximum permissible performance level is exceeded. In the latter case the question of convergence is irrelevant since the closed-loop system is known to either be unstable for some $G \in \underline{G}$ (i.e., $\hat{\alpha} = \infty$) or exceed acceptable performance specifications, thereby necessitating system redesign.

We now prove a comparison result for solutions of (5.1).

Lemma 5.1. Assume $(\underline{A},\underline{G})$ is stable, let $\hat{\underline{A}}$, $\hat{\underline{G}}$ be rxr nonnegative matrices where $\hat{\underline{A}}$ is symmetric, and assume that

$$\underline{A} \ll \hat{\underline{A}}, \qquad \hat{\underline{G}} \ll \underline{G}. \tag{5.6}$$

Then $(\hat{\underline{A}},\hat{\underline{G}})$ is stable. Furthermore, let rxr symmetric $\hat{\underline{V}}$ satisfy

$$\hat{\underline{V}} \ll \underline{V}, \tag{5.7}$$

let $\tilde{\underline{Q}}$ be the unique, nonnegative solution to (5.1), and let $\hat{\underline{Q}}$ be the unique solution to

$$\hat{\underline{A}}^{*}\hat{\underline{Q}} = \hat{\underline{G}}\hat{\underline{Q}} + \hat{\underline{Q}}\hat{\underline{G}}^{T} + \hat{\underline{V}}. \tag{5.8}$$

Then

$$\hat{\underline{Q}} \ll \tilde{\underline{Q}}. \tag{5.9}$$

Proof. Since

$$\hat{\underline{\underline{A}}} \triangleq \operatorname{diag}(\operatorname{vec} \hat{\underline{A}}) - \hat{\underline{G}} \oplus \hat{\underline{G}}$$

is an N matrix, $\underline{\underline{A}}$ is an M matrix, and

$$\hat{\underline{\underline{A}}} - \underline{\underline{A}} = \operatorname{diag}(\operatorname{vec}(\hat{\underline{A}}-\underline{A})) + (\underline{G}-\hat{\underline{G}}) \oplus (\underline{G}-\hat{\underline{G}}) \gg 0,$$

it follows from Lemma 2.3 that $\hat{\underline{\underline{A}}}$ is an M matrix and thus $(\hat{\underline{A}},\hat{\underline{G}})$ is stable. Next note that (5.1) and (5.8) imply

$$\operatorname{vec}(\tilde{\underline{Q}}-\hat{\underline{Q}}) = \underline{\underline{A}}^{-1}(\hat{\underline{\underline{A}}}-\underline{\underline{A}})\operatorname{vec} \hat{\underline{Q}} + \underline{\underline{A}}^{-1}\operatorname{vec}(\underline{V}-\hat{\underline{V}}).$$

Since $\hat{\underline{\underline{A}}}-\underline{\underline{A}} \gg 0$, $\underline{\underline{A}}^{-1} \gg 0$ (see Lemma 2.2), and $\underline{V}-\hat{\underline{V}} \gg 0$, it follows that (5.9) is satisfied.□

Corollary 5.1. Suppose $(\underline{A},\underline{G})$ is stable and let $\bar{\underline{Q}}$ be the unique, nonnegative solution to (5.1). Furthermore, let $G \in \underline{\underline{G}}$ and $\theta \in \Theta$ be such that $A(\theta)+G$ is asymptotically stable and define $\underline{Q}$ by (4.7) for mxn $Q \geq 0$ satisfying (3.7). Then

$$\underline{Q} \ll \bar{\underline{Q}}. \tag{5.10}$$

Proof. By Proposition 4.2, $\underline{Q}$ satisfies the covariance block-norm inequality (4.18). In the notation of Lemma 5.1 define

$$\hat{\underline{A}} = \underline{A}, \quad \hat{\underline{G}} = \underline{G}, \quad \hat{\underline{V}} = \underline{A}*\underline{Q} - (\underline{G}\underline{Q}+\underline{Q}\underline{G}^{T}) \tag{5.11}$$

so that (5.6) is satisfied and (4.18) implies (5.7). Note that with the notation (5.11), equation (5.8) has the unique solution $\hat{\underline{Q}} = \underline{Q}$. Hence (5.9) implies (5.10).□

Theorem 5.1. Assume $\bar{A}$ is asymptotically stable, Θ is continuously arcwise connected, and $(\underline{A},\underline{G})$ is stable. Then the homogeneous system (3.1) is robustly stable over $\underline{\underline{G}}$ and Θ, and the nonhomogeneous system (3.4) has the performance bound

$$\hat{\sigma} = \max_{\theta \in \Theta}\{\sum_{i=1}^{r} [\mathrm{tr}(\hat{Q}_i(\theta)R_i) + 2(\mathrm{tr}\ \hat{P}_i(\theta))(\underline{\underline{\tilde{Q}}})_{(i,i)}]\}, \tag{5.12}$$

where $n_i$xn$_i$ nonnegative-definite $\hat{Q}_i(\theta)$ and $\hat{P}_i(\theta)$ satisfy

$$0 = A_i(\theta)\hat{Q}_i(\theta) + \hat{Q}_i(\theta)A_i^{T}(\theta) + V_i, \tag{5.13}$$

$$0 = A_i^{T}(\theta)\hat{P}_i(\theta) + \hat{P}_i(\theta)A_i(\theta) + R_i, \tag{5.14}$$

and rxr $\tilde{\underline{Q}}$ is the unique, nonnegative solution to (5.1).

Proof. First note that since robust stability is independent of the disturbances, we can set $V = I_n$ for convenience in proving the first result.

Hence, suppose (3.1) is not robustly stable. Since $\underline{\underline{G}}$ is convex (see Remark 4.1), A is asymptotically stable, and Θ is continuously arcwise connected, there exist $G_0 \in \underline{\underline{G}}$ and $\hat{\theta}$: [0,1] --> Θ such that $\hat{A}(\mu) \triangleq A(\hat{\theta}(\mu))+\mu G_0$ is asymptotically stable for all $\mu \in [0,1)$, and $\hat{A}(1)$ is not asymptotically stable. Define

$$Q(\mu,t) \triangleq \int_0^t e^{\hat{A}(\mu)s} e^{\hat{A}^T(\mu)s} ds, \quad t \geq 0, \quad \mu \in [0,1],$$

which is monotonically increasing in the nonnegative-definite cone with respect to t. Clearly, the limit

$$Q(\mu) \triangleq \lim_{t \to \infty} Q(\mu,t), \quad \mu \in [0,1),$$

exists and satisfies

$$0 = \hat{A}(\mu)Q(\mu) + Q(\mu)\hat{A}^T(\mu) + I_n, \quad \mu \in [0,1).$$

Now define rxr nonnegative symmetric $\underline{Q}(\mu)$ by

$$\underline{Q}(\mu) = \{ \| Q_{ij}(\mu) \|_F \}_{i,j=1}^{r},$$

where $Q_{ij}(\mu) \in \underline{\underline{R}}^{n_i x n_j}$ and $Q(\mu)$ is partitioned as in (4.5). By Corollary 5.1 with $\theta = \hat{\theta}(\mu)$ $G = \mu G_0$, $\underline{Q} \triangleq \underline{Q}(\mu)$, $\mu \in [0,1)$, and $V = I_n$, it follows from (5.10) that

$$\underline{Q}(\mu) \ll \bar{\underline{Q}}, \ \mu \in [0,1). \tag{5.15}$$

Hence, by (4.8), (5.15) implies

$$\|Q(\mu)\|_F = \|\underline{Q}(\mu)\|_F \leq \|\bar{\underline{Q}}\|_F, \ \mu \in [0,1). \tag{5.16}$$

On the other hand, for $\mu \in [0,1)$ it follows that

$$Q(\mu) = Q(\mu) - Q(\mu,t) + Q(\mu,t) - Q(1,t) + Q(1,t)$$

$$\geq Q(\mu,t) - Q(1,t) + Q(1,t),$$

which implies, for arbitrary $x \in \underline{\underline{R}}^n$,

$$x^T Q(\mu) x \geq x^T [Q(\mu,t) - Q(1,t)] x + x^T Q(1,t) x.$$

Thus, by continuity of $Q(\mu,t)$ in μ,

$$\lim_{\mu \to 1} x^T Q(\mu) x \geq x^T Q(1,t) x, \quad x \in \underline{\underline{R}}^n. \tag{5.17}$$

Now, since $\hat{A}(1)$ is not asymptotically stable and $(\hat{A}(1), I_n)$ is stabilizable, it follows from Proposition 3.2 of [37], p. 67, that for some $\bar{x} \in \underline{\underline{R}}^n$,

$$\lim_{t \to \infty} \bar{x}^T Q(1,t) \bar{x} = \infty.$$

Thus by (5.17)

$$\lim_{\mu \to 1} \bar{x}^T Q(\mu) \bar{x} = \infty,$$

and thus

$$\lim_{\mu \to 1} \|Q(\mu)\|_F = \infty. \tag{5.18}$$

However, (5.18) contradicts (5.16). Hence (3.1) is robustly stable over $\underline{\underline{G}}$ and Θ.

To derive (5.12) note that since R is block diagonal,

$$J(G,\theta) = \sum_{i=1}^{r} \operatorname{tr} Q_i R_i = \sum_{i=1}^{r} (\operatorname{vec} Q_i)^T \operatorname{vec} R_i,$$

where Q satisfies (3.7). Furthermore, (4.9) and (4.21) imply

$$\text{vec } Q_i = -[A_i(\theta) \oplus A_i(\theta)]^{-1}[\text{vec } V_i + \sum_{k=1}^{r} \text{vec}(G_{ik}Q_{ki} + Q_{ik}G_{ik}^T)].$$

Hence, using Lemma 2.1,

$$\begin{aligned}
J(G,\theta) &= \sum_{i=1}^{r} [\text{tr}(\hat{Q}_i(\theta)R_i) + \sum_{k=1}^{r} (\text{vec}[G_{ik}Q_{ki} + Q_{ik}G_{ik}^T])^T \text{vec } \hat{P}_i(\theta)] \\
&= \sum_{i=1}^{r} [\text{tr}(\hat{Q}_i(\theta)R_i) + \sum_{k=1}^{r} \text{tr } \hat{P}_i(\theta)(G_{ik}Q_{ki} + Q_{ik}G_{ik}^T)] \\
&\leq \sum_{i=1}^{r} [\text{tr}(\hat{Q}_i(\theta)R_i) + \sum_{k=1}^{r} (\text{tr } \hat{P}_i(\theta))\sigma_{\max}(G_{ik}Q_{ki} + Q_{ik}G_{ik}^T)] \\
&\leq \sum_{i=1}^{r} [\text{tr}(\hat{Q}_i(\theta)R_i) + 2(\text{tr } \hat{P}_i(\theta)) \sum_{k=1}^{r} \sigma_{\max}(G_{ik})\sigma_{\max}(Q_{ki})] \\
&\leq \sum_{i=1}^{r} [\text{tr}(\hat{Q}_i(\theta)R_i) + 2(\text{tr } \hat{P}_i(\theta)) \sum_{k=1}^{r} \sigma_{\max}(G_{ik})\|Q_{ki}\|_F \\
&\leq \sum_{i=1}^{r} [\text{tr}(\hat{Q}_i(\theta)R_i) + 2(\text{tr } \hat{P}_i(\theta)) \sum_{k=1}^{r} \underline{G}_{(i,k)}\tilde{\underline{Q}}_{(k,i)}] \\
&= \sum_{i=1}^{r} [\text{tr}(\hat{Q}_i(\theta)R_i) + 2(\text{tr } \hat{P}_i(\theta))(\tilde{\underline{G}\underline{Q}})_{(i,i)}].
\end{aligned}$$

which yields (5.12).□

6. Examples

We first confirm that the damped harmonic oscillator is asymptotically stable for all constant frequency perturbations. Hence, let

$$r = 1, \quad n = n_1 = 2,$$

and

$$\bar{A} = \bar{A}_1 = \begin{bmatrix} -\nu & \omega \\ -\omega & -\nu \end{bmatrix},$$

where $\nu > 0$ and $\omega \in \underline{\underline{R}}$. To represent frequency uncertainty let $\underline{\underline{G}} = \{0\}$, $\Theta = \underline{\underline{R}}$, $\bar{\theta} = 0$ and

$$A(\theta) = \bar{A} + \theta \begin{bmatrix} 0 & 1 \\ -1 & 0 \end{bmatrix}.$$

Note that $A(\theta)$ is stable for all $\theta \in \underline{\underline{R}}$ with poles $-\nu \pm j(\omega+\theta)$. Note that $A(\theta)$ can be diagonalized by means of the unitary transformation

$$\phi = \frac{1}{\sqrt{2}} \begin{bmatrix} 1 & 1 \\ j & -j \end{bmatrix}, \qquad \phi^{-1} = \frac{1}{\sqrt{2}} \begin{bmatrix} 1 & -j \\ 1 & j \end{bmatrix},$$

so that

$$\hat{A}(\theta) \triangleq \phi^{-1} A(\theta) \phi = \begin{bmatrix} -\nu+j(\omega+\theta) & 0 \\ 0 & -\nu-j(\omega+\theta) \end{bmatrix}.$$

Hence, using

$$A(\theta) \oplus A(\theta) = (\phi^{-1} \otimes \phi^{-1})(\hat{A}(\theta) \oplus \hat{A}(\theta))(\phi \otimes \phi),$$

it follows that

$$\sigma_{\min}(A(\theta) \oplus A(\theta)) = 2\nu, \quad \theta \in \underline{\underline{R}}.$$

Defining (see (4.15))

$$\underline{\underline{A}} = \underline{\underline{A}}_{(1,1)} = 2\nu,$$

and $\underline{\underline{G}} = 0$, the scalar majorant Lyapunov equation (5.1) has the solution

$$\underline{\tilde{Q}} = \underline{V}/2\nu,$$

where $\underline{V} = \|V\|_F$. Choosing $V = I_2$ and noting that $\underline{\underline{A}} = \underline{A} = 2\nu > 0$ is an M matrix, Theorem 5.1 guarantees robust stability for all frequency variations $\theta \in \underline{\underline{R}}$.

The next example has been chosen to demonstrate the robustness of a pair of nominally uncoupled oscillators with respect to uncertain coupling. Hence let

$$n = 4, \quad r = 2, \quad n_1 = n_2 = 2,$$

and

$$\bar{A}_i = \begin{bmatrix} -\nu & \omega_i \\ -\omega_i & -\nu \end{bmatrix}, \quad i = 1,2,$$

where $\nu, \omega_1, \omega_2 \geq 0$. Futhermore, let $\Theta = \{\bar{\theta}\}$ and

$$\underline{G} = \begin{bmatrix} 0 & \gamma_{12} \\ \gamma_{21} & 0 \end{bmatrix},$$

which denotes the fact that the local subsystem (oscillator) dynamics are assumed to be known. Since

$$\sigma_{\min}(\bar{A}_j \oplus \bar{A}_i) = [4\nu^2 + (\omega_j - \omega_i)^2]^{1/2},$$

define

$$\underline{\underline{A}} = \begin{bmatrix} 2\nu & [4\nu^2 + (\omega_1 - \omega_2)^2]^{1/2} \\ [4\nu^2 + (\omega_1 - \omega_2)^2]^{1/2} & 2\nu \end{bmatrix}.$$

Letting $V = I_4$ yields $\underline{V} = 2I_2$. Solving (5.1) yields

$$\tilde{Q}_{(1,1)} = (2\nu^2\hat{\delta} - \gamma_{12}\gamma_{21}+\sigma_{12}^2)/2\sqrt{2}\nu(\nu^2\hat{\delta}-\gamma_{12}\gamma_{21}).$$

$$\tilde{Q}_{(1,2)} = (\gamma_{12}+\gamma_{21})/2\sqrt{2}(\nu^2\hat{\delta}-\gamma_{12}\gamma_{21}).$$

$$\tilde{Q}_{(2,2)} = (2\nu^2\hat{\delta}-\gamma_{12}\gamma_{21}+\sigma_{21}^2)/2\sqrt{2}\nu(\nu^2\hat{\delta}-\gamma_{12}\gamma_{21}).$$

where

$$\hat{\delta} \triangleq [1+\delta^2]^{1/2}, \qquad \delta \triangleq (\omega_1-\omega_2)/2\nu.$$

Clearly, $\tilde{Q}$ is nonnegative if and only if

$$\gamma_{12}\gamma_{21} < \nu^2\hat{\delta}. \tag{6.1}$$

The bound (6.1) characterizes the magnitude of coupling uncertainty for which stability is guaranteed. Note that the parameter δ is a measure of the frequency separation of the oscillators relative to the damping. When $\delta >> 1$, (6.1) becomes asymptotically

$$\gamma_{12}\gamma_{21} < \tfrac{\nu}{2}|\omega_1-\omega_2|, \tag{6.2}$$

which confirms the intuitive expectation that robust stability is proportional to damping and subsystem frequency separation. This result does not appear to be predictable from quadratic or vector Lyapunov functions.

To evaluate the conservatism inherent in the bound (6.1) we solve for the actual stability region. To render the calculation tractable we assume that G_{12} and G_{21} have the structured form

$$G_{ij} = \begin{bmatrix} \alpha_{ij} & \beta_{ij} \\ -\beta_{ij} & \alpha_{ij} \end{bmatrix}. \tag{6.3}$$

By constraining (6.3) the set of coupling variations is reduced, which may or may not lead to a larger stability region. Thus our estimate of conservatism may itself be conservative, i.e., the <u>actual</u> conservatism may

indeed be less than the following analysis indicates. However, without (6.3) the development becomes intractable. This calculation will thus be called semi-exact.

By considering the characteristic equation for $\bar{A}+G$, lengthy manipulation shows that $\bar{A}+G$ is stable if and only if

$$\gamma_{12}\gamma_{21} < 2\nu^2(-\varepsilon + [1 + \delta^2(1-\varepsilon^2)]^{1/2}/(1-\varepsilon^2), \tag{6.4}$$

where $\varepsilon \in (0,1]$ is the smallest positive real root of

$$\varepsilon = (1+\varepsilon^2)[1 + \delta^2(1-\varepsilon^2)]/[2 + \delta^2(1-\varepsilon^2)]. \tag{6.5}$$

The majorant bound (6.1) and semi-exact bound (6.4) are illustrated in unified form in Figure 1. For $\delta >> 1$ note that $\varepsilon = O(\delta^{-1})$ and thus (6.4) becomes asymptotically

$$\gamma_{12}\gamma_{21} < \nu|\omega_1-\omega_2|. \tag{6.6}$$

Hence for large δ the majorant bound (6.2) is, at worst, conservative by a factor of 2 compared to the semi-exact bound.

To determine the performance bound (5.12) set $R = I_4$. Hence it can be shown that

$$J_{nom} = 2/\nu$$

and the system has the performance bound

$$\hat{\alpha} = J_{nom} + \sqrt{2}(\rho_{12}+\rho_{21})^2/\nu(1-2\rho_{12}\rho_{21}), \tag{6.7}$$

where

$$\rho_{12} = \gamma_{12}/\sqrt{2}\nu\hat{\delta}^{1/2}, \qquad \rho_{21} = \gamma_{21}/\sqrt{2}\nu\hat{\delta}^{1/2}.$$

On the other hand, the semi-exact calculation yields

$$J_{max} = \max_{\lambda\in[0,1)} \{[\rho_{12}^2 + \rho_{21}^2 + 2\rho_{12}\rho_{21}\lambda + 2\hat{\delta}(\rho_{12}\rho_{21})^2(1-\lambda^2)]/ \\ [2\hat{\delta} - 4\rho_{12}\rho_{21}\lambda - 2\hat{\delta}(\rho_{12}\rho_{21})^2(1-\lambda^2)]\}. \tag{6.8}$$

Figure 2 compares the semi-exact worst-case performance (6.8) to the majorant Lyapunov equation bound (6.7). To efficiently illustrate the results the data is specialized to the case $\rho_{12} = \rho_{21}$. Note that the semi-exact performance is plotted for several values of δ because of the explicit dependence of (6.8) on δ via $\hat{\delta}$.

Acknowledgements. We wish to thank Jill Straehla for excellent typing of the original manuscript and Bruce Bland for executing the numerical calculations.

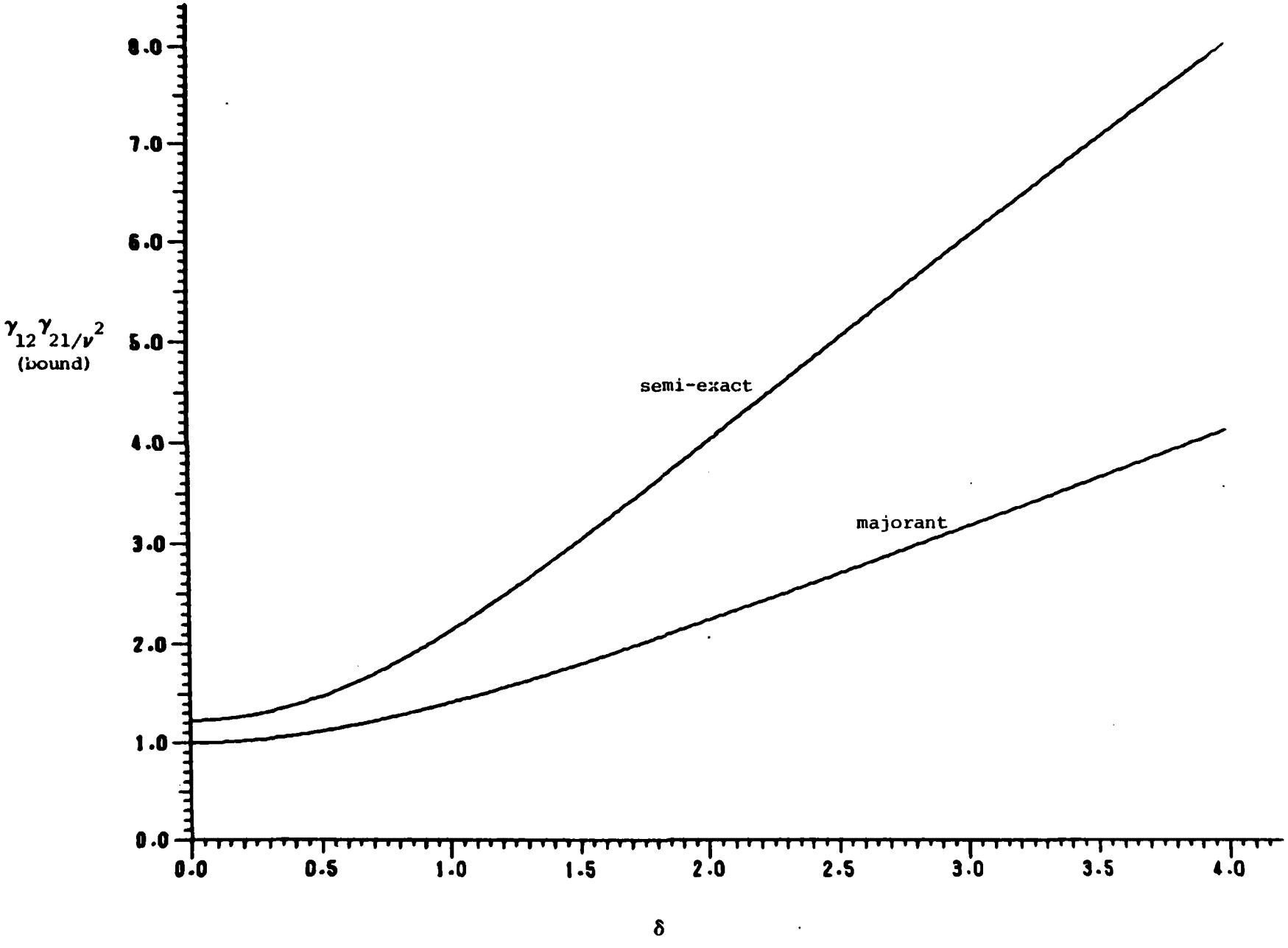
8.0
7.0
6.0
5.0
4.0
3.0
2.0
1.0
0.0
$\gamma_{12}\gamma_{21}/\nu^2$
(bound)
semi-exact
majorant
0.0
0.5
1.0
1.5
2.0
2.5
3.0
3.5
4.0
δ

Figure 1

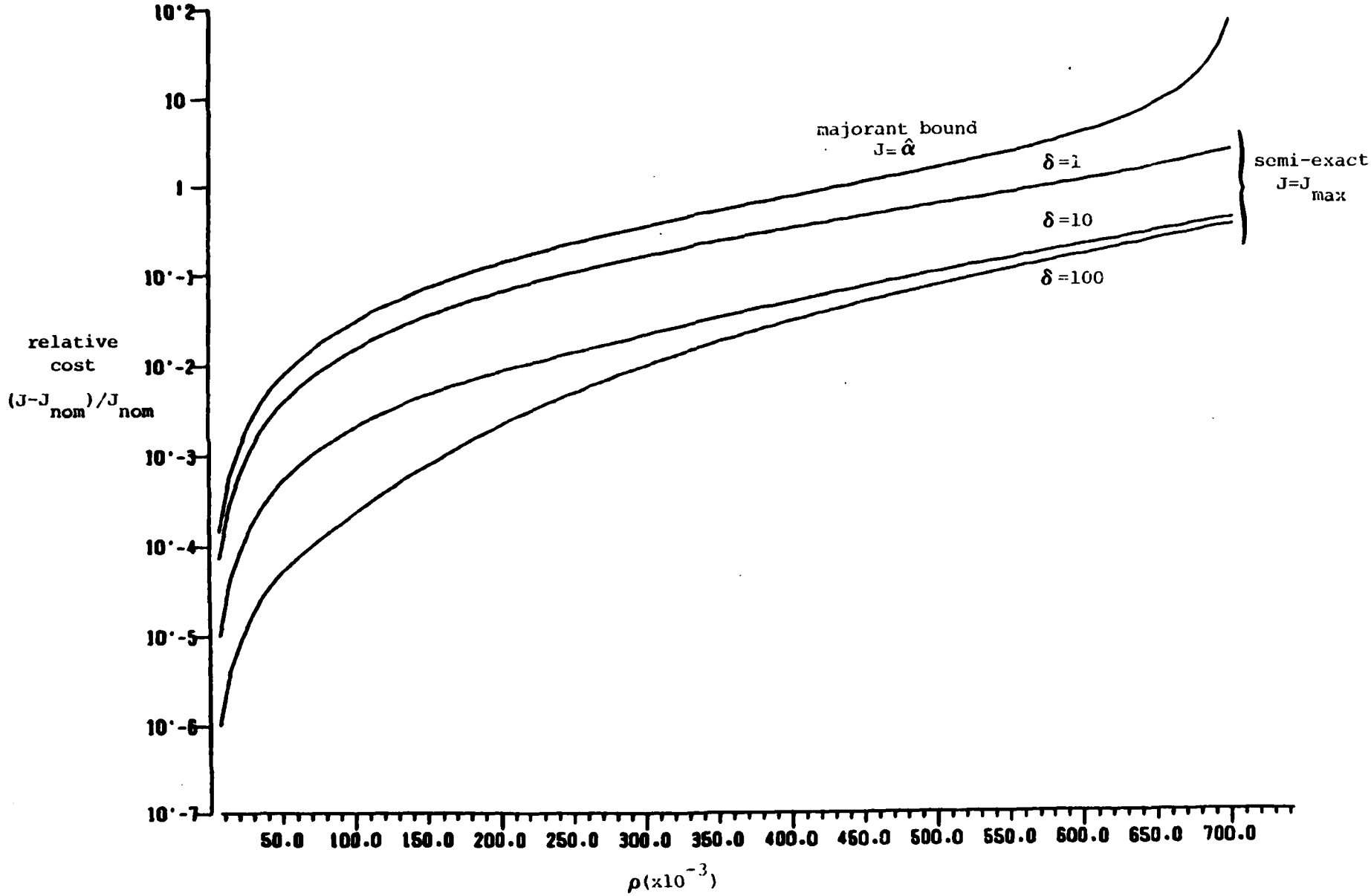
10·2
10
1
10·-1
10·-2
10·-3
10·-4
10·-5
10·-6
10·-7
relative cost
(J-J_nom)/J_nom
majorant bound
J=α̂
δ=1
δ=10
δ=100
semi-exact
J=J_max
50.0 100.0 150.0 200.0 250.0 300.0 350.0 400.0 450.0 500.0 550.0 600.0 650.0 700.0
ρ(x10^-3)

Figure 2

References

1. M. G. Safonov and M. Athans, "Gain and Phase Margin for Multiloop LQG Regulators," IEEE Trans. Autom. Contr., Vol. AC-22, pp. 173-179, 1977.

2. M. G. Safonov, Stability and Robustness of Multivariable Feedback Systems, MIT Press, Cambridge, MA, 1980.

3. N. A. Lehtomaki, N. R. Sandell, Jr., and M. Athans, "Robustness Results in Linear-Quadratic Gaussian Based Multivariable Control Designs," IEEE Trans. Autom. Contr., Vol. AC-26, pp. 75-92, 1981.

4. J. C. Doyle and G. Stein, "Multivariable Feedback Design: Concepts for a Classical/Modern Synthesis," IEEE Trans. Autom. Contr., Vol. AC-26, pp. 4-16, 1981.

5. J. C. Doyle, "Analysis of Feedback Systems with Structured Uncertainties," IEE Proc., Vol. 129, pp. 242-250, 1982.

6. J. C. Doyle, J. E. Wall and G. Stein, "Performance and Robustness Analysis for Structured Uncertainty," Proc. 21st IEEE Conf. Dec. Contr., pp. 629-636, Orlando, FL, December 1982.

7. G. Zames, "Feedback and Optimal Sensitivity: Model Reference Transformations, Multiplicative Seminorms, and Approximate Inverses," IEEE Trans. Autom. Contr., Vol. AC-26, pp. 301-320, 1981.

8. G. Zames and B. A. Francis, "Feedback, Minimax Sensitivity, and Optimal Robustness," IEEE Trans. Autom. Contr., Vol. AC-28, pp. 585-601, 1983.

9. R. R. E. de Gaston and M. G. Safonov, "A Homotopy Method for Nonconservative Stability Robustness Analysis," Proc. 24th IEEE Conf. Dec. Contr., pp. 1294-1301, Fort Lauderdale, FL, December 1985.

10. M. K. H. Fan and A. L. Tits, "Characterization and Efficient Computation of the Structured Singular Value," IEEE Trans. Autom. Contr., Vol. AC-31, pp. 734-743, 1986.

11. A. R. Galimidi and B. R. Barmish, "The Constrained Lyapunov Problem and its Application to Robust Output Feedback Stabilization," IEEE Trans. Autom. Contr., Vol. AC-31, pp. 410-419, 1986.

12. I. R. Petersen and C. V. Hollot, "A Riccati Equation Approach to the Stabilization of Uncertain Systems," Automatica, Vol. 22, pp. 397-411, 1986.

13. R. K. Yedavalli, S. S. Banda and D. B. Ridgely, "Time-Domain Stability Robustness Measures for Linear Regulators," J. Guid. Contr. Dyn., Vol. 8, pp. 520-524, 1985.

14. R. K. Yedavalli, "Perturbation Bounds for Robust Stability in Linear State Space Models," Int. J. Contr., Vol. 42, pp. 1507-1517, 1985.

15. R. K. Yedavalli, "Improved Measures of Stability Robustness for Linear State Space Models," IEEE Trans. Autom. Contr., Vol. AC-30, pp. 577-579, 1985.

16. O. D. I. Nwokah, "The Quantitative Design of Robust Multivariable Control Systems," Proc. IEEE Conf. Dec. Contr., pp. 16-24, Athens, Greece, December 1986.

17. D. S. Bernstein and S. W. Greeley, "Robust Output-Feedback Stabilization: Deterministic and Stochastic Perspectives," Proc. Amer. Contr. Conf., pp. 1818-1826, Seattle, WA, June 1986.

18. D. S. Bernstein, "Robust Static and Dynamic Output-Feedback Stabilization: Deterministic and Stochastic Perspectives," IEEE Trans. Autom. Contr., 1987, to appear.

19. D. S. Bernstein and D. C. Hyland, "Optimal Projection for Uncertain Systems (OPUS): A Unified Theory of Reduced-Order, Robust Control Design," in Large Space Structures: Dynamics and Control, S. N. Atluri and A. K. Amos, eds., Springer-Verlag, New York, 1987.

20. W. M. Haddad, Robust Optimal Projection Control-System Synthesis, Ph.D. Dissertation, Department of Mechanical Engineering, Florida Institute of Technology, Melbourne, FL, March 1987.

21. A. M. Ostrowski, "On Some Metrical Properties of Operator Matrices and Matrices Partitioned into Blocks," J. Math. Anal. Appl., Vol. 2, pp. 161-209, 1961.

22. T. Strom, "On the Practical Application of Majorants for Nonlinear Matrix Iterations," J. Math. Anal. Appl., Vol. 41, pp. 137-147, 1973.

23. G. Dahlquist, "On Matrix Majorants and Minorants, with Applications to Differential Equations," Lin. Alg. Appl., Vol. 52/53, pp. 199-216, 1983.

24. S. Barnett and C. Storey, Matrix Methods in Stability Theory, Barnes and Noble, New York, 1976.

25. J. W. Brewer, "Kronecker Products and Matrix Calculus in System Theory," IEEE Trans. Circ. Sys., Vol. CAS-25, pp. 772-781, 1978.

26. A. Graham, Kronecker Products and Matrix Calculus, Ellis Horwood, Chichester, 1981.

27. C. R. Rao and S. K. Mitra, Generalized Inverse of Matrices and Its Applications, Wiley and Sons, New York, 1971.

28. G. P. H. Styan, "Hadamard Products and Multivariate Statistical Analysis," Lin. Alg. Appl., Vol. 6, pp. 217-240, 1973.

29. A. Berman and R. J. Plemmons, Nonnegative Matrices in the Mathematical Sciences, Academic Press, New York, 1979.

30. D. D. Siljak, Large-Scale Dynamic Systems, Elsevier/North-Holland, 1978.

31. M. Ikeda and D. D. Siljak, "Generalized Decomposition of Dynamic Systems and Vector Lyapunov Functions," IEEE Trans. Autom. Contr., Vol. AC-26, pp. 1118-1125, 1981.

32. M. Djordjevic, "Stability Analysis of Interconnected Systems with Possibly Unstable Subsystems," Sys. Contr. Lett., Vol. 3, pp. 165-169, 1983.

33. A. A. Martynyuk, "The Lyapunov Matrix-Function," Nonlinear Analysis, Theory, Methods, and Applications, Vol. 8, pp. 1223-1226, 1984.

34. G. H. Golub and C. F. Van Loan, Matrix Computations, Johns Hopkins Press, Baltimore, MD, 1983.

35. T. Kato, Perturbation Theory for Linear Operators, Springer-Verlag, New York, 1980.

36. R. K. Mehra, "Optimization of Measurement Schedules and Sensor Designs for Linear Dynamic Systems," IEEE Trans. Autom. Contr., Vol. AC-21, pp. 55-64, 1976.

37. W. M. Wonham, Linear Multivariable Control: A Geometric Approach, Springer-Verlag, New York, 1974.

38. G. J. Butler, C. R. Johnson and H. Wolkowicz, "Nonnegative Solutions of a Quadra tic Matrix Equation Arising from Comparison Theorems in Ordinary Differential Equations," SIAM J. Alg. Disc. Meth., Vol. 6, pp. 47-53, 1985.

39. H. D. Victory, Jr., "On Nonnegative Solutions of Matrix Equations," SIAM J. Alg. Disc. Meth., Vol. 6, pp. 406-412, 1985.

APPENDIX E

REFERENCE 74

Reduced-Order Compensation:

LQG Reduction Versus Optimal Projection*

by

S. W. Greeley** and D. C. Hyland†

Government Aerospace Systems Division
MS 22/2406
Harris Corporation
Melbourne, Florida 32902

Abstract

Six methods for design of reduced-order compensation are compared using an example problem given by Enns. The methods considered comprise five LQG reduction techniques, reviewed in a recent paper by Liu and Anderson, and the Optimal Projection theory as implemented via a simple homotopy solution algorithm. Design results obtained by the different methods for forty-two different design cases are compared with respect to closed-loop stability and transient response characteristics. Of the LQG-reduction procedure s two are found to offer distinctly superior performance. However, only the Optimal Projection method provided stable designs in all cases. Further details are given on the performance of the numerical algorithm for solving the optimal projection equations and the corresponding design results.

---

*This research was supported in part by the Air Force Office Of Scientific Research, contract AFOSR F49620-84-C-003d. The U.S. Government assumes no responsibility for the Information presented.

**Technical Staff, Control Systems Engineering Group

†Leader, Control Systems Engineering Group

1. Introduction

The design of reduced-order dynamic controllers for high-order systems is of considerable importance for applications involving large spacecraft and flexible flight systems. Hence it is not surprising that extensive research has been devoted to this area. A recent paper by Liu and Anderson [1] subjected five reduced-order controller design methods to both theoretical and numerical comparison. The computational comparison was based upon an example problem considered by Enns [2]. The five methods compared in [1] are:

1. Method of Enns [2]: This method is a frequency-weighted, balanced realization technique applicable to either model or controller reduction

2. Method of Glover [3]: This method utilizes the theory of Hankel norm optional approximation for controller reduction

3. Davis and Skelton [4]: This is a modification of compensator reduction via balancing which covers the case of unstable controllers

4. Yousuff and Skelton [5]: This is a further modification of balancing for handling stable or unstable controllers

5. Liu and Anderson [1]: In place of using a balanced approximation of the compensator transfer function directly, this method approximates the component parts of a fractional representation of the compensator.

All of the above methods proceed by first obtaining the full-order LQG compensator design for a high-order state-space model and then reducing the dimension of this LQG compensator.

The present paper complements the results of Liu and Anderson by giving a numerical comparison (again using Enns' example) of methods 1-5 with a sixth method:

6. Optimal Projection (OP) equations [6]: Reduced-order compensator design by direct solution of the necessary conditions for quadratically optimal fixed-order dynamic compensation.

Method (6), like methods (1-5), has been shown to have intimate connections with balancing ideas [7]. Moreover, the first step in one iterative method for solution of the OP equations is almost identical to method (4). Method (6) differs from the other methods, however in that it does not reduce the order of a previously obtained LQG design but rather directly characterizes the quadratically optimal compensator of a given fixed-order. The OP equations constitute four coupled modified Riccati and Lyapunov equations wherein the steps of regulator design, observer design and order reduction are completely and inseparably intermingled.

The organization of this paper is as follows. In section 2, we state the problem considered and review the OP design equations. Section 3 gives the computational algorithm used herein for OP design synthesis. Finally, section 4 sets forth the example problem of Enns and compares the results of all six methods obtained for this example.

2. Problem Statement and Review of OP Design Equations

Here we consider the linear, finite-dimensional, time-invariant system:

$$\begin{aligned} \dot{x} &= Ax + Bu + w_1; \qquad x \in R^N, \\ y &= Cx + w_2; \qquad y \in R^P \end{aligned} \tag{1}$$

where x is the plant state, A is the plant dynamics matrix and B and C are control input and sensor output matrices, respectively. w_1 is a white disturbance noise with intensity matrix $V_1 \geq 0$ and w_2 is observation noise with nonsingular intensity $V_2 > 0$.

The reduced-order compensation problem consists in designing a constant gain dynamic compensator of order $N_c < N$:

$$\begin{aligned} u &= -Kq, \qquad u \in R^{\ell} \\ \dot{q} &= A_c q + Fy; \qquad q \in R^{N_c} \end{aligned} \tag{2}$$

Obviously, the heart of the design problem is the selection of the constant matrices K, F and A_c.

Methods 1-6 all associate with the closed-loop system (1,2) a steady-state quadratic performance index, J:

$$\begin{aligned} J &\triangleq \lim_{t_1 - t_0 \to \infty} \tilde{J} / |t_1 - t_0| \\ \tilde{J} &\triangleq \int_{t_o}^{t_1} dt \; E[x^T R_1 x + u^T R_2 u] \\ R_1 &\geq 0, \qquad R_2 > 0 \end{aligned} \tag{3}$$

Methods 1-5 first design an LQG compensator (select K, F, A_c to minimize J_s) and then reduce the order of the resulting N state compensator. Thus, in methods 1-5, the quadratic performance (3) is brought into play in the initial LQG design step, but a variety of balancing and Hankel norm approximation ideas are utilized for the subsequent compensator-order reduction step. In contrast, method 6 selects, K, F, A_c by addressing the <u>quadratically optimal, fixed-order compensation problem</u> i.e., for N_c fixed (and < N), choose K, F, A_c to minimize J . The OP design methodology

proceeds by solving the first-order necessary conditions for this optimization problem using the new forms for the necessary conditions given in [6]. The basic OP design equations reduce to four modified Lyapunov and Riccati equations all coupled by a projection of rank N_c. In general these design equations produce compensators that cannot be obtained by reduction of an LQG compensator [7].

Methods 1-5 have been reviewed extensively in [1-5], and will not be discussed in detail. Here we shall merely review the OP design equations to the extent needed to illustrate the solution algorithm used for this study.

To do this, a few preliminary results and notational conventions must be given. First, we have Lemma 1, [7]:

Lemma 1. Suppose $\hat{Q} \in R^{N \times N}$ and $\hat{P} \in R^{N \times N}$ are nonnegative definite and rank $(\hat{Q})$ = rank $(\hat{P})$ = rank $(\hat{Q}\hat{P})$. Then the product $\hat{Q}\hat{P}$ is semisimple (all Jordan blocks are of order unity) with real, non-negative eigenvalues. Moreover, there exists a nonsingular $\Psi[\hat{Q},\hat{P}]$ such that:

$$\Psi^{-1}[\hat{Q},\hat{P}]\hat{Q}\hat{P}\Psi[\hat{Q},\hat{P}] = \Lambda^2 \tag{4a}$$

$$\Psi^{T}[\hat{Q},\hat{P}]\hat{P}\Psi[\hat{Q},\hat{P}] = \Lambda \tag{4b}$$

$$\Psi^{-1}[\hat{Q},\hat{P}]\hat{Q}\Psi^{-T}[\hat{Q},\hat{P}] = \Lambda \tag{4c}$$

where

$$\Lambda = \underset{k=1\ldots N}{\text{diag}} \{\Lambda_k\} \tag{5}$$

is the positive diagonal matrix of the square roots of the eigenvalues of $\hat{Q}\hat{P}$.

When for a given pair $\hat{Q}$ and $\hat{P}$, a $\Psi[\hat{Q},\hat{P}]$ exists such that (4) hold, $\hat{Q}$ and $\hat{P}$ are said to be <u>contragrediently diagonalizable</u> and <u>balanced</u> [9] and $\Psi[\hat{Q},\hat{P}]$ constitutes a <u>simultaneous contragradient transformation</u>. Determination of such a transformation is the fundamental mathematical operation of balancing.

Furthermore, it is clear that the quantities:

$$\Pi_k[\hat{Q},\hat{P}] \triangleq \Psi[\hat{Q},\hat{P}]E^{(k)}\Psi^{-1}[\hat{Q},\hat{P}] \tag{6}$$

$$E^{(k)}_{mn} = \begin{cases} 1; & m=n=k \\ 0; & \text{otherwise} \end{cases}$$

form a set of mutually disjoint unit rank projections i.e.:

$$\Pi_k[\hat{Q},\hat{P}]\Pi_j[\hat{Q},\hat{P}] = \Pi_k[\hat{Q},\hat{P}]\delta_{kj}; \tag{7}$$

Thus the sum of r distinct Π_k's is itself a projection of rank r. Also $\hat{\hat{Q}}\hat{\hat{P}}$ can be alternatively expressed as:

$$\hat{\hat{Q}}\hat{\hat{P}} = \sum_{k=1}^{n} \Pi_k[\hat{\hat{Q}}\hat{\hat{P}}]\Lambda_k^2 \tag{8}$$

By virtue of (8) and the usage in [10], we term $\Pi_k[\hat{\hat{Q}}\hat{\hat{P}}]$ the <u>eigen-projection</u> of $\hat{\hat{Q}}\hat{\hat{P}}$ associated with the k^{th} eigenvalue.

The above results and conventions, together with the notations:

$$\sum \triangleq BR_2^{-1}B^T \tag{9a}$$

$$\overline{\sum} \triangleq C^T V_2^{-1} C \tag{9b}$$

$$\tau_1 \triangleq I_n - \tau \tag{9c}$$

allow us to state the main result [6-8] upon which the OP reduced-order compensator design method is based:

Theorem 1. Consider the quadratically optimal, fixed-order compensation problem with $N_c \leq N$ fixed.

Let nonnegative definite $Q,\ P,\ \hat{Q},\ \hat{P} \in R^{NxN}$ be determined as solutions to the following equations:

$$0 = AQ + QA^T + V_1 - Q\overline{\sum}Q + \tau_\perp Q\overline{\sum}Q\tau_\perp^T \tag{10a}$$

$$0 = A^TP + PA + R_1 - P\sum P + \tau_\perp^T P\sum P\tau_\perp \tag{10b}$$

$$0 = (A-\sum P)\hat{Q} + \hat{Q}(A-\sum P)^T + Q\overline{\sum}Q - \tau_\perp Q\overline{\sum}Q\tau_\perp^T \tag{10c}$$

$$0 = (A-Q\overline{\sum})^T\hat{P} + \hat{P}(A-Q\overline{\sum}) + P\sum P - \tau_\perp^T P\sum P\tau_\perp \tag{10d}$$

$$\tau = \sum_{K=1}^{N_c} \Pi_K[\hat{Q}\hat{P}] \tag{10e}$$

Then with $\Gamma,\ G \in R^{N_c xN}$ given by:

$$\begin{aligned} \Gamma &= [I_{N_c}, 0]\Psi^{-1}[\hat{Q}, \hat{P}] \\ G &= [I_{N_c}, 0]\Psi^T[\hat{Q}, \hat{P}] \end{aligned} \tag{11}$$

the gains:

$$\begin{aligned} K &= R_2^{-1}B^TPG^T \\ F &= \Gamma QC^TV_2^{-1} \end{aligned} \tag{12}$$

$$A_c = \Gamma(A - Q\overline{\sum} - \sum P)G^T$$

determine an extremal of the performance index J.

A has been remarked in [8], the value of the performance index is unchanged by any transformation of the compensator state basis - in other words, for any nonsingular $S \in R^{N \times N}$:

$$J(K,F,A_c) = J(KS, S^{-1}F, S^{-1}A_cS) \tag{13}$$

Furthermore, when $N_c = N$, τ is a rank N projection on R^N by virtue of (10e). Hence $\tau = I_N$ and $\tau_\perp = 0$ and equations (10a),(10b) become uncoupled Riccati equations for determination of Q and P. Also Γ and G become $\Psi^{-1}[\hat{Q},\hat{P}]$ and $\Psi^T[\hat{Q},\hat{P}]$. Finally, setting $S = \Psi^{-1}$ and using (13) and (12), extremalizing gains are given by:

$$\begin{aligned} K &= R_2^{-1}B^TP \\ F &= QC^TV_2^{-1} \\ A_c &= A - Q\overline{\sum} - \sum P \end{aligned} \tag{14}$$

with Q and P given as solutions to the independent Riccati equations, (10a,10b), with $\tau_\perp = 0$. Hence when $N_c = N$, the design equations (10), (11) and (12) immediately reduce to the LQG design for a full-order compensator.

However for $N_c < N$, equations (10) are first-order necessary conditions and generally possess multiple solutions corresponding to multiple extremals that can exist. This matter was explored in [11] relative to the related quadratically optimal model reduction problem. Basically, equation (10e) tells us that the rank N_c projection, τ, which defines the geometry of the fixed-order compensator, is the sum of N_c out of N eigenprojections of $\hat{Q}\hat{P}$. However, the necessary conditions do not tell us <u>which</u> N_c out of N eigenprojections are to be selected to secure a global

minimum of J. Indeed for any possible selection of N_c eigenprojections out of N, equations (10) may possess a solution corresponding to a local extremal. By virtue of (10e) and the notational conventions of (4) and (8), the selection of N_c eigenprojections is defined (generically) by the manner in which the eigenvalues, Λ_k, are ordered. Recently, Richter [12] has applied topological degree theory to investigate the possible solution branches and the character of the associated extrema and has devised a homotopy solution algorithm which selects the Λ-ordering which homotopically converges to the global minimum.

For the example considered in this paper, we adopt the ordering convention:

$$\Lambda_1 \geq \Lambda_2 \geq \cdots \geq \Lambda_N \tag{15}$$

in constructing $\Psi[\hat{Q},\hat{P}]$. (15) together with (10e) imply that τ is taken to be the sum of the N_c eigenprojections corresponding to the N_c largest eigenvalues of $\hat{Q}\hat{P}$. Generically, this choice leads to an unequivocal choice of one solution branch of (10) corresponding to a particular extremal.

Thus, the OP design method investigated here consists in solving (10) with convention (15) and then evaluating the gains according to (12). We apply a simple homotopy solution algorithm, described in the next section, to the example problem of Enn s specified in Section 4 and compare results with methods 1-5. A more advanced and efficient homotopy algorithm is given in [12].

3. An Algorithm for Solution of the OP Design Equations

As stated, the OP design method is to solve (10) (with stipulation (15)) for P, Q, $\hat{P}$, $\hat{Q}$, and then evaluate the gains using (11), (12). A logically distinct issue is precisely how equations (10) are to be solved. Here we present an algorithm that has been used for some time and requires

only a standard LQG software package for its implementation. For convenience this same algorithm was employed to obtain the numerical results for method 6 presented in the next section.

The basic motivation of this algorithm is the observation that the four main equations (10a)-(10d) are coupled only via the terms involving $\tau_\perp$ on the right hand sides. If these $\tau_\perp$ terms were deleted, then all five equations can be solved sequentially - moreover (10a),(10b) reduce to ordinary Riccati equations and (10a),(10b) are Lyapunov equations. Likewise under conditions in which $Q\overline{\sum}Q$ and $P\sum P$ are "small" relative to the remaining terms (e.g., sufficiently small state-weighting and disturbance noise intensity and/or sufficiently large control weighting and observation noise intensity) the $\tau_\perp$ terms are typically found to have little effect. In this situation the artifact of fixing an initial $\tau_\perp$, and then solving (10) as ordinary Riccati and Lyapunov equations is likely to give a reasonable approximation to the true solution.

Since only the $\tau_\perp$ terms on the right of (10a-10d) occasion most of the difficulties, it is necessary to somehow bring these terms into play gradually. There are two principal ways to do this. The first is an iterative relaxation approach, i.e., fix $\tau_\perp$, solve (10a)-(10d) sequentially, then update τ using (10e) and repeat until convergence, in some sense, is achieved. The second method is a homotopy approach, i.e., multiply the $\tau_\perp$ terms by a scalar parameter, $\alpha \in [0,1]$, then starting with $\alpha = 0$ and gradually incrementing α, solve (10) repeatedly until $\alpha = 1$.

The algorithm used here consists of two iterative loops. The inner loop uses the relaxation approach and is embedded within an outer loop which implements the simple homotopy approach.

The inner loop follows the earlier computational scheme discussed in [7] and is illustrated in Figure 1. Note that the parameter $\alpha \in [0,1]$ multiplies the $\tau_\perp$ terms but is held fixed within the inner loop and is only incremented on the outer loop. As Figure 1 shows, one first fixes τ equal

Figure 1: Inner Loop of OP Solution Algorithm

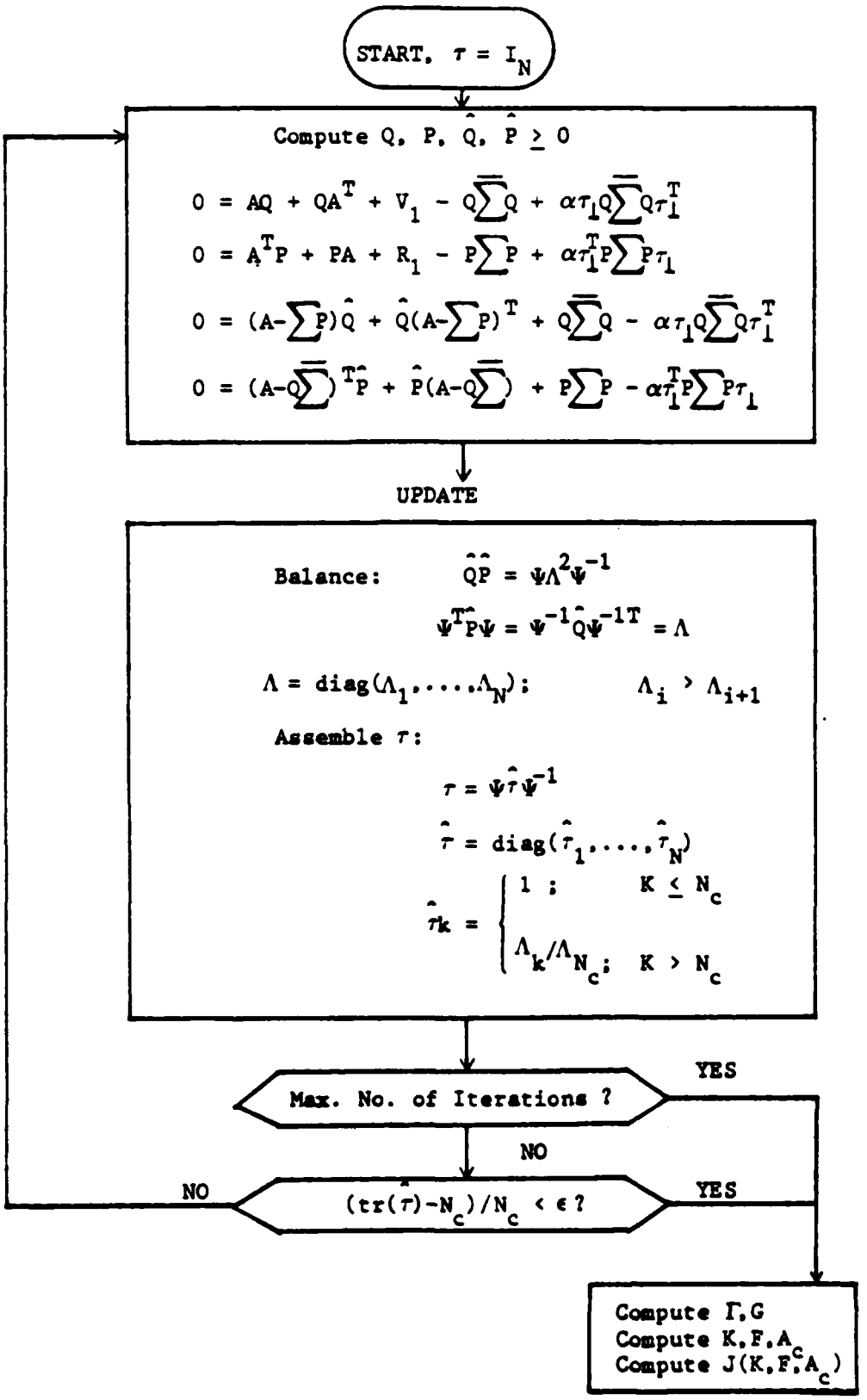

to the previous iterate (or set $\tau = I_N$ when starting) and then solves (10a)-(10d). Once new iterates for Q, P, $\hat{Q}$, $\hat{P}$ are obtained, τ is updated by determining the balancing transformation $\Psi[\hat{Q},\hat{P}]$. To enhance convergence of the modified Riccati equations, the updated τ is taken to be the weighted sum of all N eigenprojections - the first N_c eigenprojections are given unity weight while the r^{th} ($r > N_c$) eigenprojection is weighted by $\Lambda_r/\Lambda_{N_c} < 1$. As convergence proceeds, Λ_r/Λ_{N_c} approaches zero for all $r > N_c$ and the numerical rank of τ approachs N_c. The indicated convergence check tests the relative excess of the numerical rank of τ over N_c and terminates the inner loop iterations when this "rank excess" falls below tolerance ϵ. In these studies $\epsilon = 0.1$ is used. The inner loop is terminated when either this tolerance is achieved or when the prescribed number of iterations is exceeded.

When the convergence criterion is satisfied, the gains, K, F, A_c are computed using (11) and (12) and the steady-state performance, J, is evaluated. Performance evaluation invokes no assumptions regarding the convergence and optimality of the solutions to (10). Specifically, the values of K, F, A_c resulting from application of (12) are accepted as they stand and are used to construct the system matrices of the augmented system with state vector $X^T = [x^T, q^T]$. Next the 2Nx2N Lyapunov equation for the second moment matrix of the augmented, closed-loop system is solved. Finally, J is evaluated as a linear function of various sub-blocks of the augmented system second moment matrix.

The outer loop, depicted in Figure 2, implements the homotopy approach by incrementing α and controlling the increment step size. Only at the start is the inner loop initialized by $\tau = I_N$. Otherwise, when α is incremented, the inner loop is initialized using P, Q, $\hat{P}$, $\hat{Q}$, and τ as obtained with the previous value of α. α is taken to be 0 at the start and is subsequently incremented by Δ. The default value of Δ is 0.1 although other desired values may be input. However, whenever the inner loop is terminated without achieving the convergence tolerance ϵ, the homotopy parameter increment, Δ, is halved. This provides simple control over the

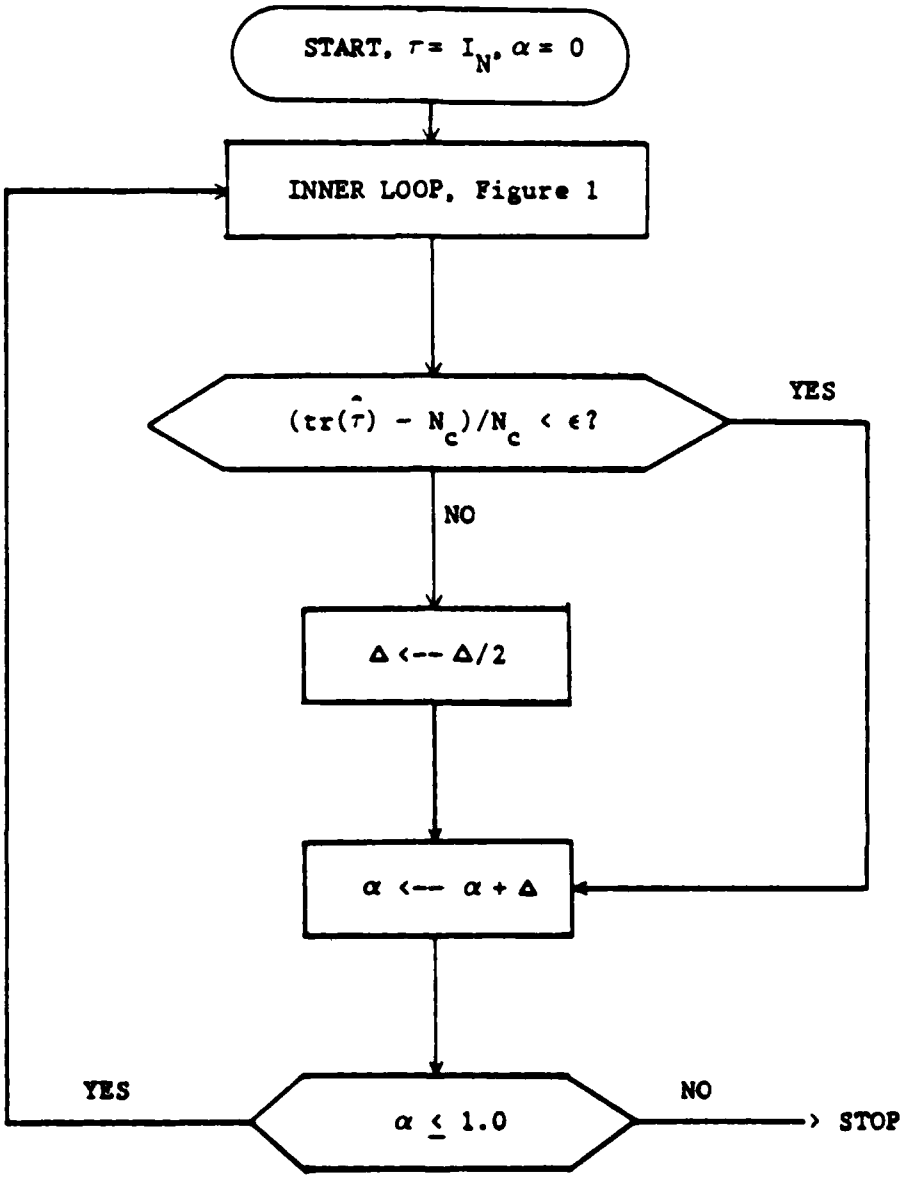

Figure 2: Outer (Homotopy) Loop of OP Solution Algorithm

homotopy step size. The entire algorithm terminates when $\alpha = 1.0$. Alternatively, at the user's option, the algorithm can be terminated when the change of the performance index, J, over two successive outer loop iterations is sufficiently small - thus indicating acceptable convergence with respect to quadratic performance.

4. A Design Example and Comparison of Results

We use the example problem given by Enns [2] to compare methods 1-6. Results on this example obtained by use of methods 1-5 are discussed in [1]. Here, we augment these results by considering method 6 and undertake an overall comparison.

The plant to be controlled in this example is a four-disk system and is linear, time-invariant, SISO, neutrally stable (with a double pole at the origin) and non-minimum phase and of eighth order. Numerical values of the matrices A, B, C, R_1, R_2, V_1, V_2 defining this problem are given in Table 1.

For each of the methods 1-6, controllers of different reduced orders (from seventh to second order) were obtained for seven different values of the disturbance noise intensity parameter, q_2:

$$q_2 = 0.01,\ 0.1,\ 1.0,\ 10,\ 100,\ 1000,\ 2000$$

Thus each method was used to obtain results on 42 different design cases.

Each of the six methods was originally devised according to a wide variety of different criterion for adequate performance of a reduced-order compensator design. Despite this wide disparity among the different aims and motivations of the several methods there are at least three criteria that may be reasonably applied to judge the success of a reduced-order design:

$$A = \begin{bmatrix} -0.161 & 1 & 0 & 0 & 0 & 0 & 0 & 0 \\ -6.004 & 0 & 1 & 0 & 0 & 0 & 0 & 0 \\ -0.5822 & 0 & 0 & 1 & 0 & 0 & 0 & 0 \\ -9.9835 & 0 & 0 & 0 & 1 & 0 & 0 & 0 \\ -0.4073 & 0 & 0 & 0 & 0 & 1 & 0 & 0 \\ -3.982 & 0 & 0 & 0 & 0 & 0 & 1 & 0 \\ 0 & 0 & 0 & 0 & 0 & 0 & 0 & 1 \\ 0 & 0 & 0 & 0 & 0 & 0 & 0 & 0 \end{bmatrix}$$

$B^T = [0,\ 0,\ 0.0064,\ .00235,\ 0.0713,\ 1.0002,\ 0.1045,\ 0.9955]$

$C = [1,\ 0,\ 0,\ 0,\ 0,\ 0,\ 0,\ 0]$

$R_1 = (1.0 \times 10^{-6})H^T H; \quad H = [0,\ 0,\ 0,\ 0,\ 0.55,\ 11,\ 1.32,\ 18.0]$

$R_2 = 1$

$V_1 = q_2 BB^T \quad (q_2 \quad [0.01,\ 2000.0])$

$V_2 = 1$

Table 1: Data Matrices for the Example Problem of Enns [2]

1. Closed-loop stability

2. Extent to which the reduced-order compensator impulse and step response match the full-order, LQG, compensator response

3. The closed-loop quadratic cost

However, item 3 will not be considered since costs for methods 1-5 were not provided [1]. The comparison in item 2 examines the output y(t) in response to an input v(t) injected in the loop as indicated in Figure 3.

First, Table 2 summarizes the closed-loop stability properties of all design methods in all 42 cases. Generally, it is seen that all methods achieve a high rate of success in achieving closed-loop stability for the larger N_c values and small q_2. On the other hand, methods 1-5 experience greater difficulties for low values of N_c and, particularly, for large q_2. With respect to stability, the only qualitative distinction among the methods is that method 6 (optimal projection) produces stable design in all 42 design cases.

The trend toward increasing difficulty of the design with increasing disturbance noise intensity is highlighted by Table 3 which shows the percentage of closed-loop stable designs given by the different methods for the different values of q_2 and in total. That the fraction of stable designs declines with increasing q_2 is to be expected since larger disturbance noise intensity increases Q, thereby increasing observer gains to produce faster observers that are more sensitive to order reduction.

Overall, for this example problem, method 4 exhibits the smallest fraction of stable designs (with 24 unstable designs) and does not achieve any order reduction for q_2 = 100, 1000, 2000. Of the LQG reduction methods (1-5), methods 1 and 5 fare best - with only 4 unstable designs out of 42. As noted, optimal projection (method 6) yields stable designs in all cases.

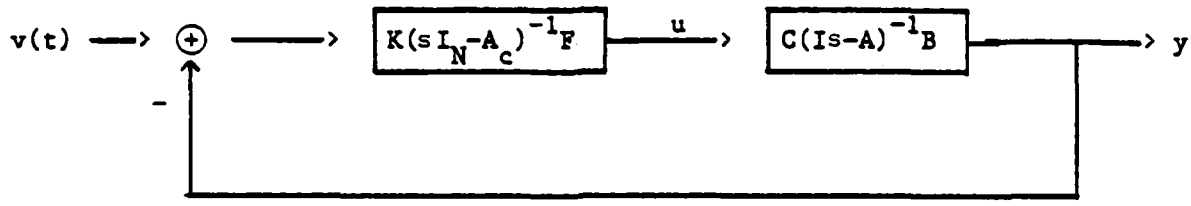

v(t) = Unit step or impulse

(K,F,A_c) = full-order LQG or reduced-order compensator gains

Figure 3. Comparison of unit step or impulse responses

Table 2. Stability of the Reduced-Order Controller by Different Methods

Method	N_c \ q_2 =	0.01	0.1	1	10	100	1000	2000
Enns (1)	7	S	S	S	S	S	S	S
	6	S	S	S	S	S	S	S
	5	S	S	S	S	S	S	S
	4	S	S	S	S	S	S	U
	3	S	S	S	S	S	S	S
	2	S	S	S	S	U	U	U
Glover (2)	7	S	S	S	S	S	U	S
	6	S	S	S	S	U	U	U
	5	S	S	S	S	U	U	U
	4	S	S	S	S	U	U	U
	3	S	S	U	S	U	U	U
	2	S	U	S	U	S	U	U
Davis & Skelton (3)	7	S	U	U	S	S	S	S
	6	S	S	S	S	S	S	S
	5	S	U	S	S	S	U	U
	4	S	S	U	S	S	U	U
	3	U	U	U	U	U	U	U
	2	S	U	S	U	U	U	U
Yousuff & Skelton (4)	7	S	S	S	S	U	U	U
	6	S	S	S	S	U	U	U
	5	S	S	S	U	U	U	U
	4	S	S	S	U	U	U	U
	3	S	U	U	U	U	U	U
	2	S	S	S	U	U	U	U
Liu & Anderson (5)	7	S	S	S	S	S	S	U
	6	S	S	S	S	S	S	U
	5	S	S	S	S	S	S	S
	4	S	S	S	S	S	S	S
	3	S	S	S	S	S	U	U
	2	S	S	S	S	S	S	S
Optimal Projection (6)	7	S	S	S	S	S	S	S
	6	S	S	S	S	S	S	S
	5	S	S	S	S	S	S	S
	4	S	S	S	S	S	S	S
	3	S	S	S	S	S	S	S
	2	S	S	S	S	S	S	S

S - The closed-loop system is stable
U - Unstable

Table 3. Percentage of Stable Designs Given By the Different Methods

Method \ q_2 =	0.01	0.1	1	10	100	1000	2000	Total % for All Cases
Enns (1)	100	100	100	100	83.3	83.3	66.7	90.5
Glover (2)	100	83.3	83.3	83.3	33.3	0	16.7	57.1
Davis & Skelton (3)	83.3	33.3	50.0	66.7	66.7	33.3	33.3	52.4
Yousuff & Skelton (4)	100	83.3	83.3	33.3	0	0	0	42.9
Liu & Anderson (5)	100	100	100	100	100	83.3	50.0	90.5
Optimal Projection (6)	100	100	100	100	100	100	100	100.0

To permit independent corroboration by interested readers of the OP design capabilities we give numerical values of the compensator gains obtained by method 6 for a selection of the more difficult cases* - namely:

$q_2 = 2000, \quad N_c = 2, 3, 4, 5, 6, 7$

$N_c = 2, \quad q_2 = 0.01, 0.1, 1.0, 10, 100, 1000, 2000$

Next, consider the accuracy with the step and impulse responses (see Figure 3) of the various reduced-order compensator designs track the corresponding response of the full-order LQG design. These characteristics exhibit similar trends as noted with respect to closed-loop stability. For example, Figure 4 shows a comparison of unit step responses for second-order compensator designs with a small value of q_2 (= 1.0). In this case, all methods exhibit stability and reasonable agreement with full order design. However, as the comparison of methods 1-5 in Figure 4.a shows, methods 1 and 5 show distinctly superior tracking accuracy. For clarity, methods 1 and 5 are compared with method 6 in Figure 4.b. Here it is clear that method 5 is somewhat closer to the LQG response than method 1 while method 6 is closest of all.

Similar trends are seen in the comparisons of the impulse responses (for the same design case) in Figure 5. Once again, of the LQG reduction methods (compared in Figure 5.a), methods 1 and 5 display significantly better agreement with the LQG response. This agreement is slightly exceeded by method 6 (Figure 5.b), but on the whole, methods 1, 5 and 6 show excellent performance.

On the other hand, for a fairly large value of q_2, both stability and agreement with LQG response is degraded somewhat for several methods. Figures 6 and 7 show comparisons of unit step and impulse responses for the case $N_c = 5$, $q_2 = 100$. In this case, only methods 1, 3, 5 and 6 yield

* See Reference [13] for a complete listing of all 42 cases

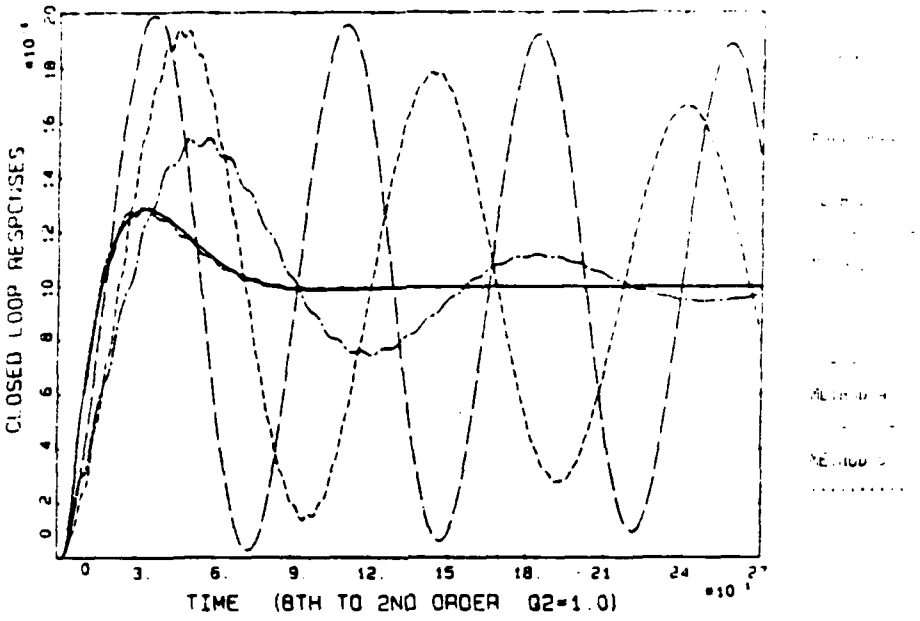

Figure 4.a – Comparison of unit step responses of second-order compensators given by methods 1-5 with full-order design (small q_2)

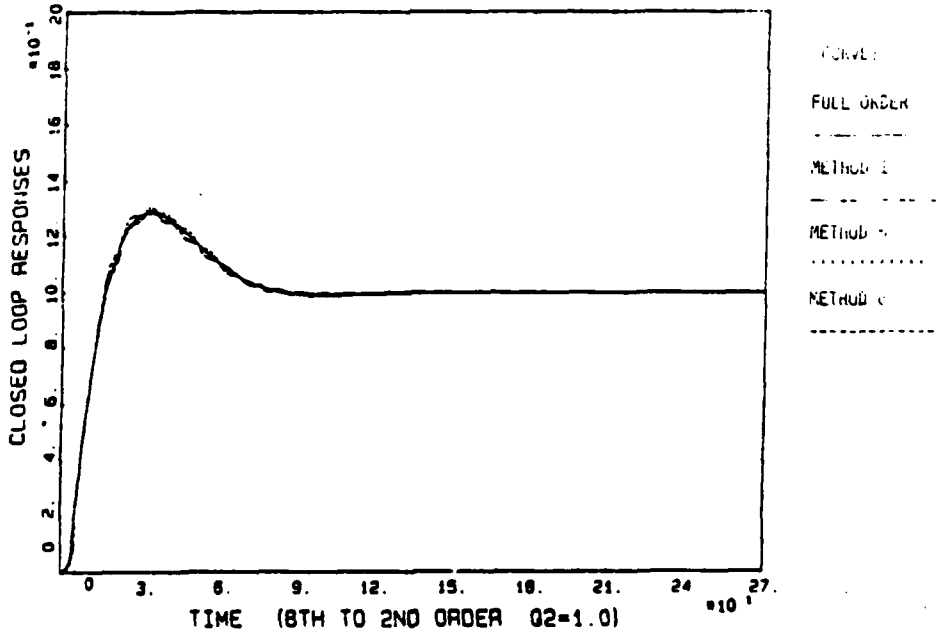

Figure 4.b – Comparison of unit step responses of second-order compensators given by methods 1, 5, and 6 with full-order design (small q_2)

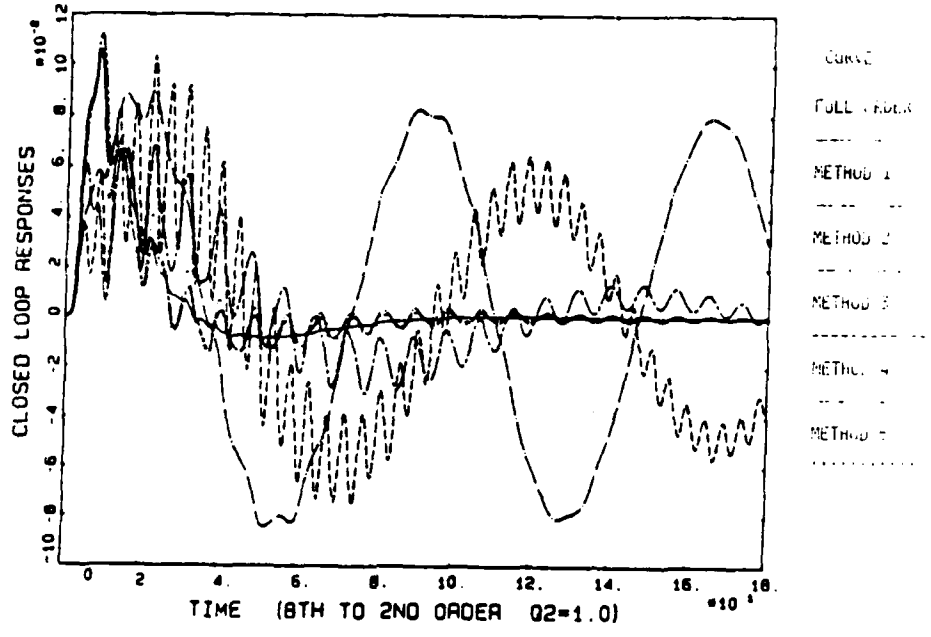

Figure 5.a - Comparison of impulse responses of second-order compensators given by methods 1-5 with full-order design (small q_2)

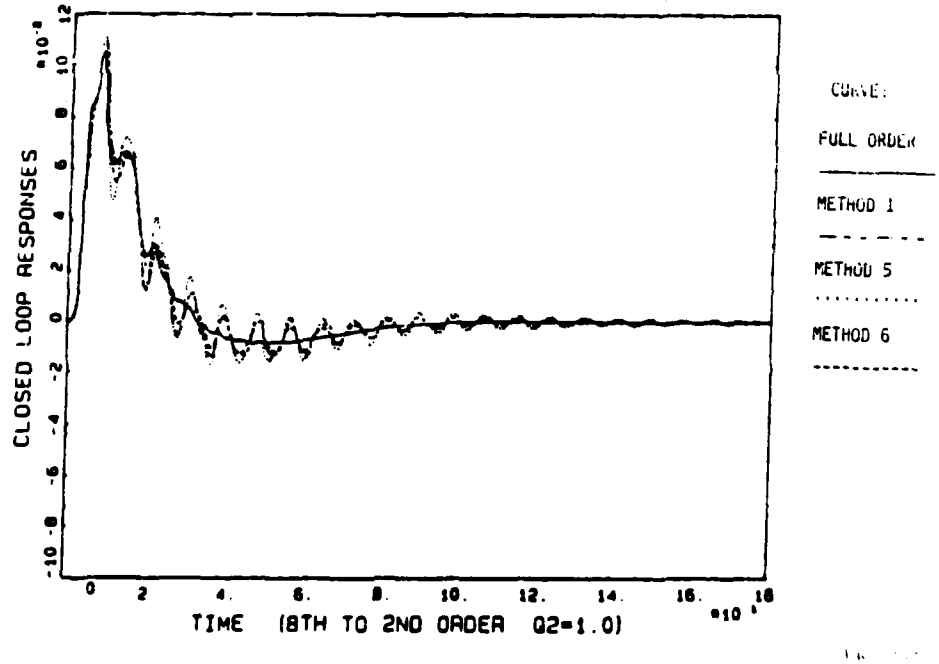

Figure 5.b - Comparison of impulse responses of second-order compensators given by methods 1, 5, and 6 with full-order design (small q_2)

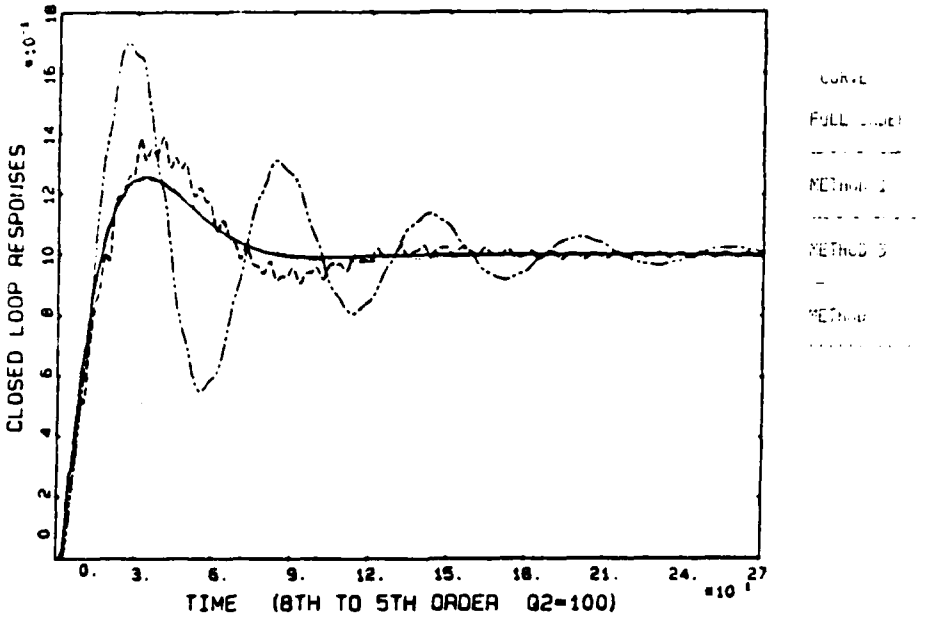

Figure 6.a - Comparison of unit step responses of fifth-order compensators given by methods 1, 3 and 5 with full-order design (large q_2)

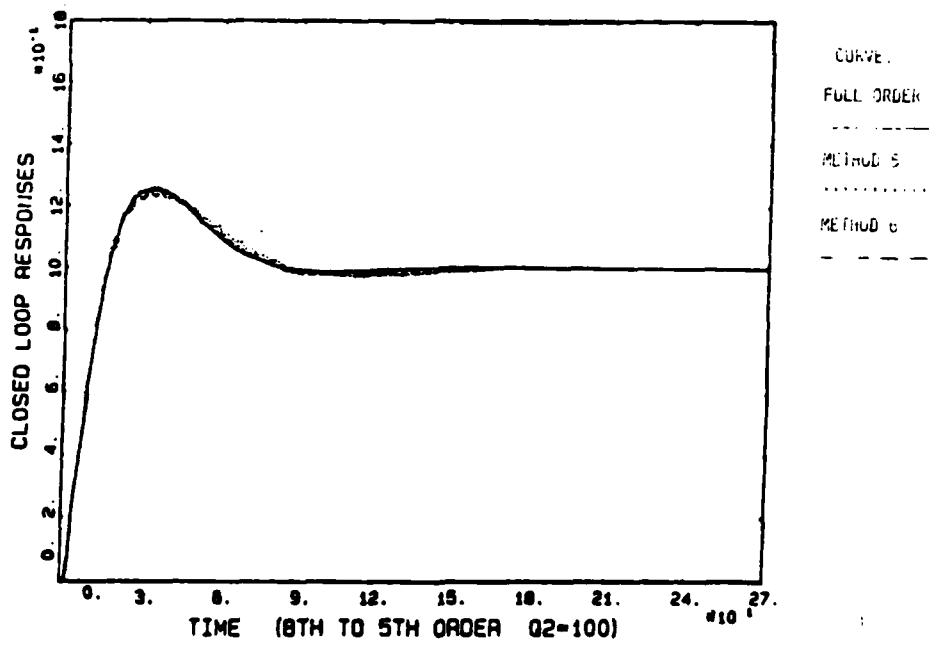

Figure 6.b - Comparison of unit step responses of fifth-order compensators given by methods 5 and 6 with full-order design (large q_2)

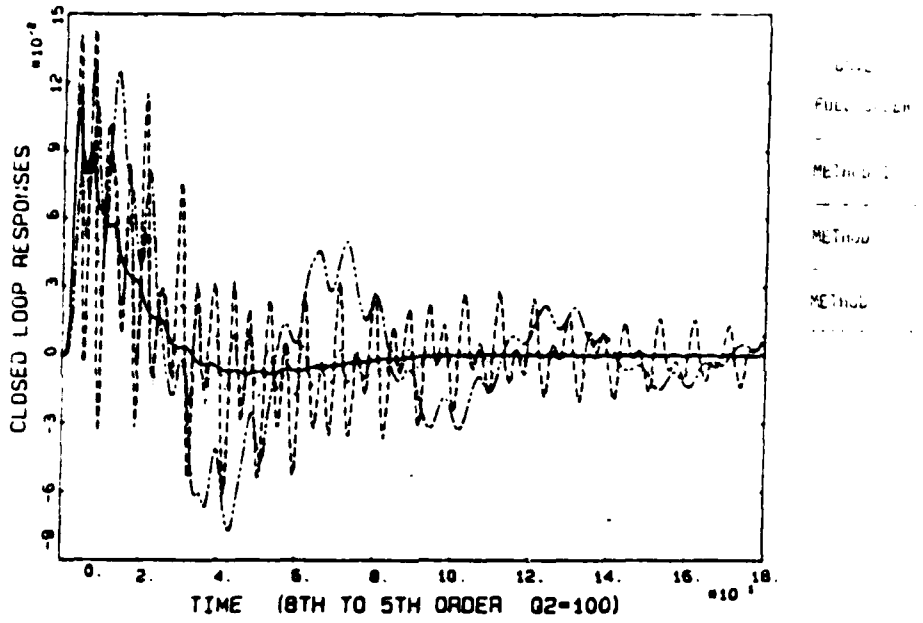

Figure 7.a - Comparison of impulse responses of fifth-order compensators given by methods 1, 3 and 5 with full-order design (large q_2)

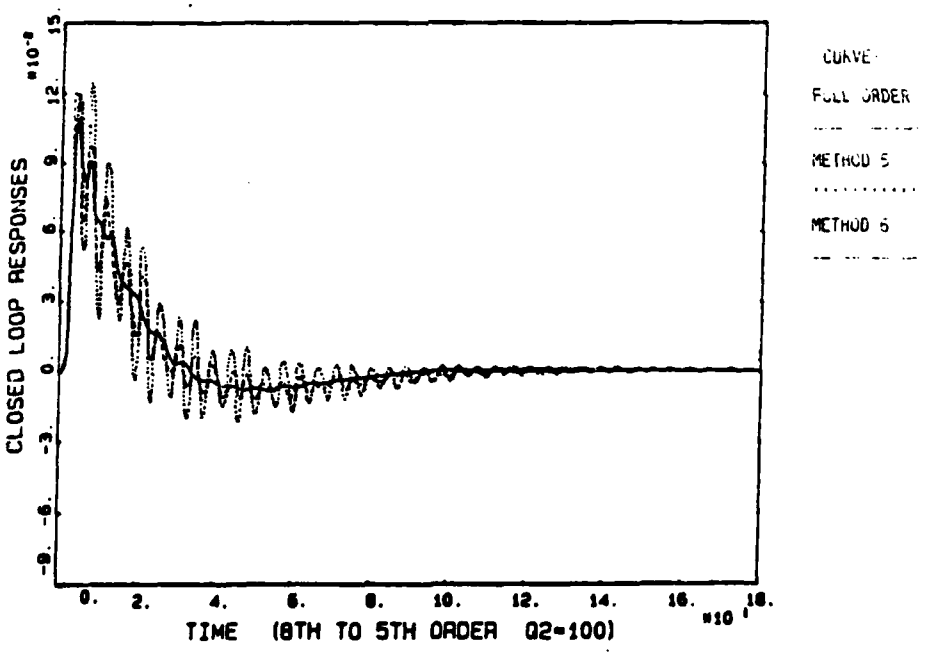

Figure 7.b - Comparison of unit step responses of fifth-order compensators given by methods 5 and 6 with full-order design (large q_2)

stable designs and are thus compared. Of the LQG reduction methods, method 5 exhibits distinctly better agreement with the LQG responses. Once again, it is found (Figures 6.b and 7.b) that method 6 somewhat excels in the accuracy with which it's transient responses track the full-order design.

Thus, for the 42 design cases studied in this example problem, methods 1 and 5 demonstrate good success in achieving stable closed-loop designs while method 6 achieves stable designs in all cases.

Also, in the cases examined, methods 1 and 5 offer good transient response characteristics while method 6 tracks the full-order compensator responses the closest.

In view of the good performance exhibited by method 6, we present, in the remainder of this section, additional details on the OP design results and the performance of the solution algorithm described in Section 3.

First, as noted, the OP design philosophy focuses on the steady state quadratic performance index, J, (defined in (3)) as the "figure of merit" for a reduced-order compensator design. Thus, we appropriately display, in Figure 8, several plots of the performance index J (normalized by q_2) versus compensator order for all 7 values of q_2. Note that apart from minor variations that are likely due to the benign convergence tolerance used in the solution algorithm, J generally decreases monotonically with increasing N_c. These graphs thus illustrate the basic tradeoff between performance and controller complexity.

Note that for small q_2 (Figure 8.a), performance is not much affected by order reduction. This is to be expected since small disturbance noise intensity, in this problem, leads to low observer gains and to small values for the terms involving τ_1 in equations (10). Since the τ_1 terms in equations (10) have little effect, the OP designs are approximated by

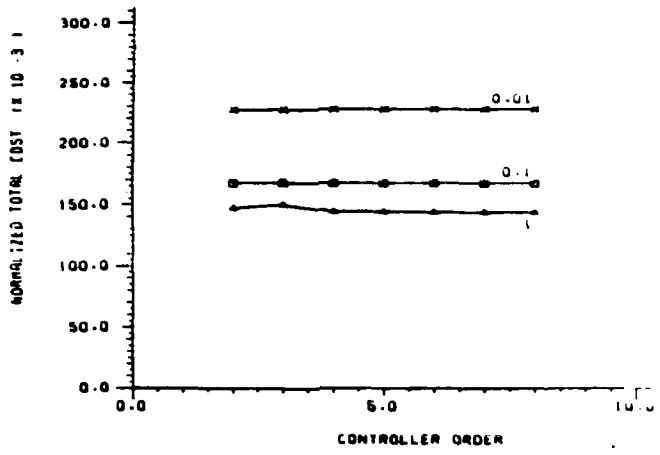

(a)

TOTAL COSTS Q2=.01..1.1

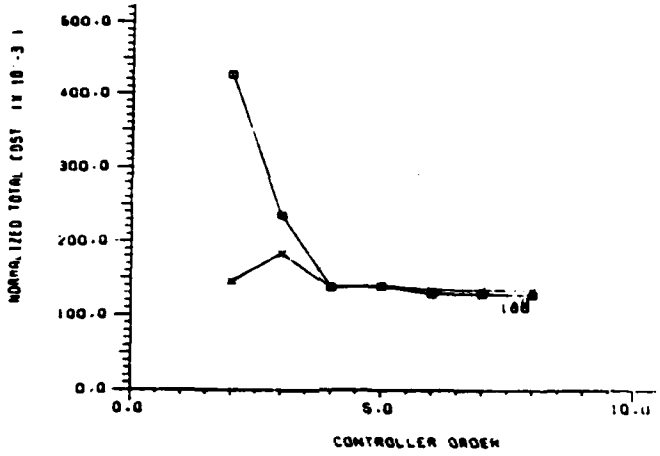

(b)

TOTAL COSTS Q2=10.100

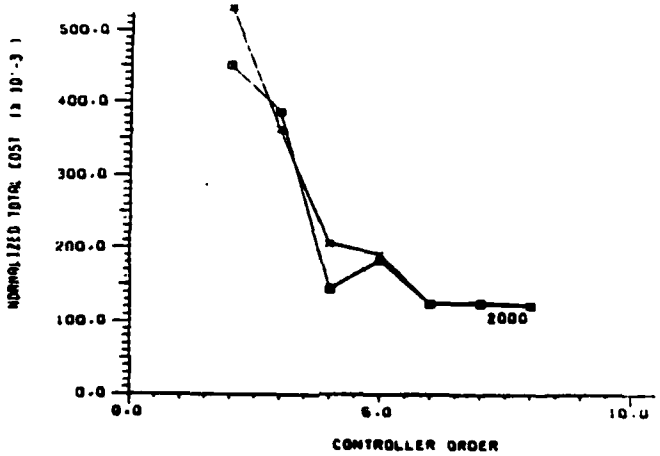

(c)

TOTAL COSTS Q2=1000.2000

Figure 8 - Steady-state quadratic performance of OP designs versus compensator order for all values of q_2.

balanced projections of the LQG design. This might also help to explain the relatively successful performance of all methods for small q_2.

For large (Figure 8.b) and for very large (Figure 8.c) values of q_2, however, the degradation of performance with reduction in order is increasingly steep. For example, while for $q_2 = 1.0$, the 2nd order performance is only 2.5% above the LQG performance, for $q_2 = 2000$, the second-order performance is 270% above the LQG value. Thus, order reduction under large disturbance noise does appear to be a more delicate matter.

While increasing difficulties with q_2 are not clearly manifested in the stability or transient response properties of the OP designs, these are reflected in the computation required to arrive at the final designs.

To explain this we now describe the specific design steps taken and the performance of the solution algorithm. Each design case was treated using the OP solution algorithm shown in Figures 1 and 2 and a maximum homotopy step size of 1.0 was input. Furthermore, for each design case, the algorithm was started "cold" - i.e., without being initialized with gain values obtained in previous cases. On initial application of the algorithm, the OP design results presented here were obtained after using the numbers of inner loop iterations given for each case in Table 4.

Note that with $\Delta = 1.0$, the logic of the outer loop (Figure 2) implies a minimum of two inner-loop iterations. Inspection of the results obtained in some of the benign cases suggested the possibility that only one inner loop iteration was needed. Consequently we re-examined the cases comprising $q_2 = 0.01, 0.1, 1.0$ and $N_c = 5, 6, 7$, by revising the outer loop logic to output gain values after only one pass through the inner loop. It was found that this produced acceptable accuracy in the cases $q_2 = 0.01$; $N_c = 5, 6, 7$, $q_2 = 0.1$, $N_c = 6, 7$ and $q_2 = 1.0$, $N_c = 7$. Thus, the revised results are as given in Table 4'. Since the gains are essentially

Table 4. Number of Inner-Loop Iterations Used in OP Solution Algorithm - Initial Design Computations

q_2 / Order, N_c	0.01	0.1	1	10	100	1000	2000
7	2	2	2	4	5	8	10
6	2	2	2	6	4	8	10
5	2	2	2	6	5	5	7
4	2	2	2	8	9	6	10
3	4	4	4	8	9	7	8
2	4	4	4	8	9	9	10

unchanged, the design results obtained on the first application are the ones presented here.

As Table 4' shows, relatively few iterations were required in the benign, small q_2, cases. In particular, only one inner loop iteration was needed in most of the cases comprising $q_2 = 0.01, 0.1, 1.0$ and $N_c = 5, 6, 7$. However, for large q_2, up to 10 iterations were required. Thus it is clear that all methods run up against a fundamental source of difficulty when disturbance noise is large.

At the time of writing, full compilation of the computation times required for all methods on the same machine is not available. All OP calculations were performed on a Harris H800 minicomputer. However, as a rough estimate, it is fair to say that in the benign cases, the OP computation is comparable to the burden incurred by methods 1-5. For the difficult, large q_2 cases the OP computational burden is clearly in excess of methods 1-5 (although certainly not excessive from a practical point of view). However, it is precisely in these cases that the LQG reduction methods experience the greatest difficulties in producing closed-loop stable designs. Thus a meaningful comparison of relative computational burden in these cases cannot be performed.

Finally it should be noted that the computational burden associated with OP for the designs presented here is also an artifact of the solution algorithm depicted in Figures 1 and 2 and is not solely the result of the design equations themselves. This algorithm was convenient to use, and was the first implemented since it requires only standard LQG software. On the other hand, the algorithm discussed in section 3 takes no particular advantage of the special structure of the fundamental design equations, (10). Its principal draw-back is that it involves the iterative solution of four NxN, nonlinear matrix equations. To remedy this, Richter [12] has developed a step-wise homotopy algorithm which requires, at each homotopy step, the solution of four N_c xN linear equations. Clearly, for small N_c, this offers the potential for computing an OP design with less computational

Table 4'. Number of Inner-Loop Iterations Used
In OP Solution Algorithm
- Revised after reconsideration of cases
$q_2 = 0.01, 0.1, 1.0$; $N_c = 5,6,7$

q_2 / Order, N_c	0.01	0.1	1	10	100	1000	2000
7	1	1	1	4	5	8	10
6	1	1	2	6	4	8	10
5	1	2	2	6	5	5	7
4	2	2	2	8	9	6	10
3	4	4	4	8	9	7	8
2	4	4	4	8	9	9	10

burden than is required for a full-order LQG design. It is anticipated that the future utilization of Richter's algorithm will permit a more accurate and definitive comparison between the computational cost of the LQG-reduction techniques and the Optimal Projection formulation.

5. Concluding Remarks

In this paper, we have used the example problem of Enns [2] to perform a computational comparison of six methods for reduced-order dynamic compensator design. Methods 1-5 are based upon LQG-reduction procedures while method 6 is based upon the Optimal Projection (OP) formulation.

Of the LQG-reduction methods, the methods of Enns [2] and of Liu and Anderson [1] exhibited particularly good stability and transient response properties. However, in the cases examined, the OP method gave somewhat better transient response characteristics and, unlike the LQG-reduction procedures, produced closed-loop stable designs for all the 42 design cases.

A precise comparison of the computational burdens incurred by the various methods is not possible at present. However, as a rough comparison, it is fair to say that the OP method entailed comparable computation in the relatively benign design cases and more computation in the difficult cases. However in this case LQG reduction methods often produce unstable designs. Thus the OP method exhibits a tradeoff between computational burden and corresponding design reliability. Present developments are directed toward implementation of advanced homotopy techniques which take particular advantage of the structure of the basic OP design equations to markedly improve design computation speed.

AD-A186 339 MAXIMUM ENTROPY/OPTIMAL PROJECTION DESIGN SYNTHESIS FOR 1/3
DECENTAALIZED CON (U) HARRIS CORP MELBOURNE FL
GOVERNMENT AEROSPACE SYSTEMS DIV D C HYLAND ET AL
UNCLASSIFIED MAY 87 AFOSR-TR-87-1196 F49620-86-C-0038 F/G 22/1 NL

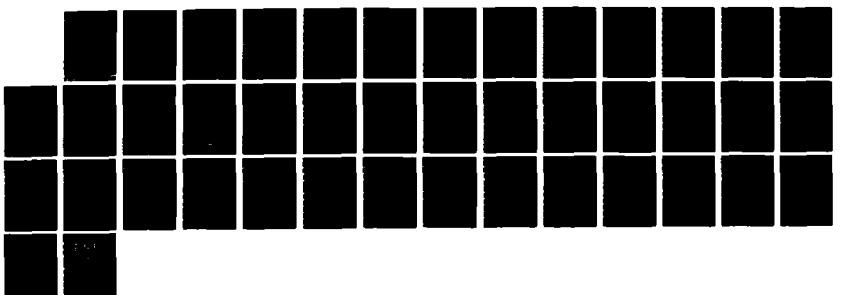

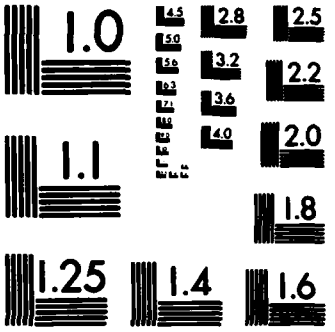

MICROCOPY RESOLUTION TEST CHART
NATIONAL BUREAU OF STANDARDS-1963-A

Appendix 1

In the following, numerical values of the reduced-order compensator gains, K, F and A_c obtained via the OP solution algorithm discussed in section 3 are given for the design cases:

$q_2 = 2000$, $N_c = 2, 3, 4, 5, 6, 7$

and

$N_c = 2$ $q_2 = 0.01, 0.1, 1.0, 10, 100, 1000, 2000$

CASE: $q_2 = 2000.$ $N_c = 7$

$$A_c = \begin{bmatrix} 0.8683E\text{-}03 & -0.3085 & -0.1180E\text{-}02 & 0.6098E\text{-}01 & -0.2844 & -0.2619 & -0.9244E\text{-}03 \\ 2.329 & -0.2821E\text{-}02 & 0.4921 & -0.1784E\text{-}01 & 0.4468E\text{-}02 & -0.4780E\text{-}01 & -0.1950E\text{-}02 \\ 0.1041E\text{-}01 & -0.6794 & -0.2057E\text{-}02 & -0.2171 & 0.6977 & 0.6175 & 0.4106E\text{-}02 \\ -1.169 & 0.1132 & 0.3505 & -0.1381 & -1.303 & -0.1929E\text{-}01 & 0.2136E\text{-}01 \\ 7.940 & -0.1091E\text{-}01 & -1.846 & 1.851 & 0.9687E\text{-}03 & 0.1872 & 0.7926E\text{-}02 \\ 19.90 & -0.4695E\text{-}01 & -4.056 & 2.398 & -0.4123 & -2.407 & -0.7051E\text{-}01 \\ 0.1906 & -0.4634E\text{-}02 & -0.3824E\text{-}01 & 0.2680E\text{-}01 & -0.5793E\text{-}01 & -0.3975 & -0.1242E\text{-}01 \end{bmatrix}$$

$$F^T = [\, 0.2832E\text{-}04 \quad 0.7462E\text{-}01 \quad 0.3362E\text{-}03 \quad -0.3801E\text{-}01 \quad 0.2586 \quad 0.6490 \quad 0.6217E\text{-}02 \,]$$

$$K = [\, -0.4387 \quad 0.5134 \quad -0.1642 \quad -1.591 \quad 0.7063E\text{-}01 \quad 3.924 \quad 0.1567 \,]$$

CASE: $q_2 = 2000$, $N_c = 6$

$$A_c = \begin{bmatrix} 0.8190E-03 & 0.3031 & 0.8960E-03 & 0.7075E-01 & 0.3110 & 0.2265 \\ -2.356 & -0.2845E-02 & 0.5058 & 0.1198E-01 & 0.3847E-02 & -0.4306E-01 \\ -0.7592E-02 & -0.6887 & -0.1431E-02 & 0.2356 & 0.7586 & 0.5132 \\ -1.358 & -0.9398E-01 & -0.3875 & -0.1281 & 1.265 & -0.8882E-01 \\ -8.168 & -0.1105E-01 & -1.861 & -1.709 & 0.1190E-02 & 0.1426 \\ -16.17 & -0.4290E-01 & -3.152 & -1.545 & -0.3782 & -1.799 \end{bmatrix}$$

$$F^T = [\ 0.2713E-04 \quad -0.7675E-01 \quad -0.2492E-03 \quad -0.4487E-01 \quad -0.2702 \quad -0.5356]$$

$$K = [-0.4324 \quad -0.5140 \quad 0.1322 \quad -1.545 \quad -0.1364 \quad -3.524]$$

CASE: $q_2 = 2000$, $N_c = 5$

$$A_c = \begin{bmatrix} 0.1335E-02 & -0.3220 & 0.5482E-02 & 0.4440E-01 & -0.1963 \\ 2.226 & -0.3920E-02 & -0.4659 & -0.3941E-01 & 0.4951E-02 \\ -0.5418E-01 & 0.6432 & -0.1099E-01 & 0.2117 & -0.4355 \\ -0.8042 & 0.2011 & -0.2791 & -0.1891 & -1.488 \\ 6.046 & -0.1203E-01 & 1.376 & 2.351 & -0.6778E-03 \end{bmatrix}$$

$$F^T = [\ 0.4018E-04 \quad 0.6557E-01 \quad -0.1614E-02 \quad -0.2413E-01 \quad 0.1817]$$

$$K = [-0.4697 \quad 0.5101 \quad 0.4346 \quad -1.795 \quad -0.4017E-01]$$

CASE: $q_2 = 2000$, $N_c = 4$

$$A_c = \begin{bmatrix} 0.3225E-02 & -0.3717 & 0.1238E-01 & -0.5735E-01 \\ 2.170 & -0.3860E-02 & -0.3623 & -0.1829E-01 \\ -0.1140 & 0.5365 & -0.2564E-01 & -0.2749 \\ 1.176 & -0.1297 & 0.3488 & -0.4452 \end{bmatrix}$$

$$F^T = [\ 0.9245E-04 \quad 0.6044E-01 \quad -0.3234E-02 \quad 0.3370E-01]$$

$$K = [-0.4871 \quad 0.5626 \quad 0.6852 \quad 2.540]$$

CASE: $q_2 = 2000$, $N_c = 3$

$$A_c = \begin{bmatrix} 0.2351E-02 & 0.1516 & 0.1492 \\ -1.447 & -0.9385E-01 & 0.6597 \\ -1.592 & -0.7041 & -0.1027E-02 \end{bmatrix}$$

$$F^T = [\ 0.5944E-04 \quad -0.3619E-01 \quad -0.3990E-01]$$

$$K = [-0.5372 \quad -1.410 \quad 0.1033]$$

CASE: $q_2 = 2000$, $N_c = 2$

$$A_c = \begin{bmatrix} -0.8378E-03 & -0.4671 \\ 2.047 & -0.1095E-01 \end{bmatrix}$$

$$F^T = [\ 0.3272E-04 \quad -0.7625E-01]$$

$$K = [\ 0.3807 \quad -0.6411]$$

CASE: $q_2 = 1000$, $N_c = 2$

$$A_c = \begin{matrix} 0.1745E\text{-}02 & 0.4039 \\ -2.129 & -0.7569E\text{-}02 \end{matrix}$$

$$F^T = [-0.6242E\text{-}04 \quad 0.7341E\text{-}01]$$

$$K = [\ 0.3753 \quad 0.5049]$$

CASE: $q_2 = 100$, $N_c = 2$

$$A_c = \begin{matrix} 0.2742E\text{-}02 & 0.4216 \\ -2.396 & -0.2274E\text{-}01 \end{matrix}$$

$$F^T = [-0.1538E\text{-}03 \quad 0.1303]$$

$$K = [\ 0.2351 \quad 0.4178]$$

CASE: $q_2 = 10$, $N_c = 2$

$$A_c = \begin{matrix} 0.7474E\text{-}02 & 0.1970 \\ -1.699 & -0.8276 \end{matrix}$$

$$F^T = [\ 0.4814E\text{-}03 \ -0.1081]$$

$$K = [-0.1740 \quad -0.9190$$

CASE: $q_2 = 1.$ $N_c = 2$

$$A_c = \begin{matrix} 0.7832E\text{-}02 & -0.1812 \\ 1.269 & -0.7143 \end{matrix}$$

$$F^T = [\ 0.8516E\text{-}03 \quad 0.1356]$$

$$K = [-0.1003 \quad 0.5206$$

CASE: $q_2 = 0.1,$ $N_c = 2$

$$A_c = \begin{matrix} 0.9915E\text{-}02 & -0.1578 \\ 0.7650 & -0.5093 \end{matrix}$$

$$F^T = [\ 0.1695E\text{-}02 \quad 0.1264]$$

$$K = [-0.5729E\text{-}01 \quad 0.2733]$$

CASE: $q_2 = 0.01,$ $N_c = 2$

$$A_c = \begin{matrix} 0.1357E\text{-}01 & -0.1398 \\ 0.3985 & -0.3430 \end{matrix}$$

$$F^T = [\ 0.3451E\text{-}02 \quad 0.9371E\text{-}01]$$

$$K = [-0.3045E\text{-}01 \quad 0.1421]$$

References

1. Y. Liu and B. D. O. Anderson, "Controller Reduction Via Stable Factorization and Balancing," Int. J. Contr., Vol. 44, No. 2, 507-531, 1986.

2. D. Enns, "Model Reduction for Control System Design," Ph.D. Thesis, Dept. of Electrical Engineering, Stanford University, 1984.

3. H. Glover, "All Optimal Hankel-Norm Approximations of Linear Multivariable Systems and Their L^{∞}-Error Bounds," Int. J. Contr., Vol. 39, 1115, 1984.

4. J. A. Davis and R. E. Skelton, System Control Lett., Vol. 4, 79, 1984.

5. A. Yousuff and R. E. Skelton, IEEE Trans. Autom. Contr., Vol. 29, 254, 1984.

6. D. C. Hyland and D. S. Bernstein, "The Optimal Projection Equations for Fixed-Order Dynamic Compensation," IEEE Trans. Autom. Contr., Vol. AC-29, pp. 1034-1037, 1984.

7. D. C. Hyland, "Comparison of Various Controller-Reduction Methods: Suboptimal Versus Optimal Projection," Proc. AIAA Dynamics Specialists Conf., pp. 381-389, Palm Springs, CA, May 1984.

8. D. S. Bernstein and D. C. Hyland, "The Optimal Projection Equations for Finite-Dimensional Fixed-Order Dynamic Compensation of Infinite-Dimensional Systems," SIAM J. Contr. Optim., Vol. 24, pp. 122-151, 1986.

9. C. R. Rao and S. K. Mitra, Generalized Inverse of Matrices and Its Applicatons, John Wiley and Sons, New York, 1971.

10. T. Kato, Perturbation Theory for Linear Operators, Springer-Verlag, New York, 1966.

11. D. C. Hyland and D. S. Bernstein, "The Optimal Projection Equations for Model Reduction and the Relationships Among the Methods of Wilson, Skelton and Moore," IEEE Trans. Autom. Contr., Vol. AC-30, pp. 1201-1211, 1985.

12. S. Richter, "A Homotopy Algorithm for Solving the Optimal Projection Equations for Fixed-Order Dynamic Compensation: Existence, Convergence and Global Optimality," in preparation.

13. S. Greeley and D. Hyland, "Optimal Projection Controller Gains for an Example of Enns," Harris GASD TR-87-1, January, 1987.

APPENDIX F

REFERENCE 58

A HOMOTOPY ALGORITHM FOR SOLVING THE OPTIMAL PROJECTION EQUATIONS FOR FIXED-ORDER DYNAMIC COMPENSATION: EXISTENCE, CONVERGENCE AND GLOBAL OPTIMALITY

Stephen Richter

Harris Corporation
Government Aerospace Systems Division
MS 22/4848
Melbourne, FL 32902

ABSTRACT

The purpose of this paper is to present a homotopy algorithm for solving the Optimal Projection Equations. Questions of existence and the number of solutions will also be examined. It will be shown that the number of stabilizing solutions to the given Optimal Projection Equations can be determined and that all solutions can be computed via a homotopic continuation from a simple problem. For an important special case, where the number of inputs or the number of outputs to the system is less than or equal to the dimension of the compensator, there is only one solution to the OPE, thus guaranteeing that globally optimum reduced order controller can be computed.

1. Introduction

Despite significant advances in the cost and performance of digital computers over the last decade, there remains a need in several technological areas for low-order, high-performance controllers. In particular, this paper is motivated by the problem of vibration suppression in large flexible space structures. Such systems are infinite-dimensional (distributed parameter) in nature and hence any finite-dimensional controller is necessarily of reduced order. The need for low-order controllers is further driven by severe constraints on cost, weight and power in space systems, not to mention the restriction to space-qualified computational hardware.

A wide variety of approaches have been proposed to obtaining reduced-order controllers. A comparison of several approaches to controller reduction is given in [1]. These methods operate by first designing a high-order LQG controller and then obtaining a suitable low-order controller by means of controller reduction.

A more direct approach to designing reduced-order controllers involves optimizing the quadratic performance functional over the class of controllers of fixed order. The controller order may be determined by implementation constraints or can be varied for performance/throughput tradeoff studies.

An interesting reformulation of the parameter optimization approach was given recently in [2]. By setting the gradients to zero, the authors showed that the first order necessary conditions can be transformed to yield explicit gain expressions for extremal fixed-order controllers. An appealing aspect of this formulation is the recasting of the necessary conditions in a form which generalizes the classical (full-order) LQG solution. Specifically, instead of a pair of separated Riccati equations, the necessary conditions for fixed-order dynamic compensation comprise a system of two modified Riccati equations and two modified Lyapunov equations coupled by an oblique projection whose rank is precisely equal to the order of the compensator. When specialized to the full-order case, the projection becomes the identity, the modified Lyapunov equations drop out, and the modified Riccati equations simplify to the classical Riccati equations. Hence this approach appears to be a natural and fundamental generalization of LQG.

Regardless of how appealing the optimal projection formulation may appear to be and in spite of the empirical advantages claimed in [2-10], its contribution is vacuous unless certain serious questions can be resolved. These include:

1. Under what conditions on the problem data can the optimal projection equations be guaranteed a priori to possess a solution?
2. Given problem data, exactly how many solutions do the equations possess?
3. Of the possible solutions, what are their stability properties, what is their performance, and which is the global optimum?
4. How can numerical algorithms be constructed which can be guaranteed to converge to any desired solution especially the global minimum?

Supported in part by the Air Force Office of Scientific Research under contract F49620-86-C-0038.

It seems clear that any attempt to address the above issues must utilize mathematical methods which are global in nature. To this end we have applied degree theory and associated homotopic continuation methods ([13-24]) to analyze the solutions to the optimal projection equations and to construct convergent, implementable algorithms for their computation. The purpose of this paper is to report significant results in this regard.

2. Homotopic Continuation and Degree Theory

2.1 Homotopic Continuation. A homotopic continuation method for solving a problem is to first solve an easy "similar" problem, and then to continuously deform the easy problem into the original problem and to follow the path of solutions as the easy problem is deformed into the original problem. This is shown conceptually in Figure 1.

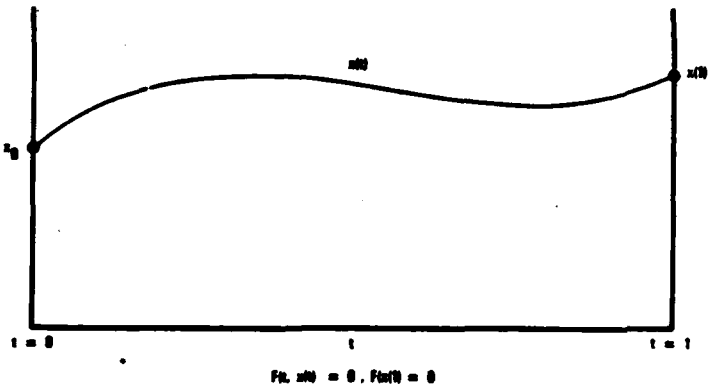

Figure 1

Example 1. Consider calculating the roots of a polynomial

$$F(Z) = Z^n + a_1 Z^{n-1} + a_2 Z^{n-2} \ldots + a_n = 0.$$

Let the easy problem be $F_0(Z) = Z^n - 1 = 0$ and deform F_0 to F

$$F(Z,t) = Z^n + t(a_1 Z^{n-1} + a_2 Z_n^{n-2} \ldots a_n) - 1 + t.$$

At $t = 0$, $F(Z,0) = F_0(Z)$ and $F(Z,1) = F(Z)$.

The solutions $Z_k(t)$ which satisfy $F(Z_k,t) = 0$ are found by differentiating $F(Z_k(t),t) = 0$ to obtain

$$\frac{dZ_k}{dt} = - \frac{a_1 Z_k^{n-1} + a_2 Z_k^{-2} \ldots a_n - 1}{n Z_k^{n-1} + t(a_1 (n-1) Z_k^{n-2} \ldots a_{n-1})}.$$

This differential equation can be integrated from the n initial values

$$Z_k(0) = e^{-\frac{i2\pi}{n} k}$$

to the n solutions at t=1.

2.2 Degree Theory.

Definition 1: Given a function f mapping D in R^N into V in R^K a regular value of f is an element p in V such that the NxK matrix of partial derivatives of f, $f_x(x)$, has full rank for each x in $f^{-1}(p)$. Note that if N=K then $f_x(x)$ having full rank is equivalent to $\det(f_x(x)) \neq 0$.

Definition 2: Given a function f mapping an open set D in R^N with boundary $\bar{D}$ into V in R^N and a point p in V, the degree of f for domain D and point p (written Deg(f,D,p)) is defined and is an integer if there is no x in the boundary $\bar{D}$ of D such that f(x)=p. If p is a regular point of f then the degree is the sum of the signs of the determinant of the Jacobians of f evaluated at all x such that f(x)=p, i.e.,

$$\deg(f,D,p) = \text{Sign}(\text{Det}(f_x(x_p)))$$

$$\text{where } f(x_p) = p$$

The degree has the following properties:

1) If $\deg(f,D,p) \neq 0$ then f(x)=p has at least one solution in D

2) Let $f(x,t) : R^N$ to R^N for each t in [0,1] with f continous. If for each t, f(x,t)=p has no solutions for x in $\bar{D}$, then deg(f,D,p) is constant for t in [0,1].

3) If f is as in (2) and $\deg(f,D,p) \neq 0$, then at least one solution of f(x,0)=p connects with a solution of f(x,1)=p.

Example 2. Every polynomial has at least one root (over the complex numbers)

Let $f(z) = z^n + a_1 z^{n-2} + \ldots a_n$

We wish to show that $\deg(f,D,0) \neq 0$.

Let $f(z,t) = z^n + t(a_1 z^{n-1} + a_2 z^{n-2} + \ldots + a_n) - 1 + t$

Let D = z s.t $|z| < R$, where R is some large number.

For z on $\bar{D}$ ($|z| = R$) z^n is much larger than $t a_i z^{n-1}$ so $f(z,r) \neq 0$ for z in $\bar{D}$, thus $\deg(f,D,0)$ is constant for t in $[0,1]$.

For $t=0$, $f(z,0) = z^n - 1$ and writing $f(r,\theta) = x + iy$ we have that the solutions to $f(r,\theta,0) = 0$ are $r = 1$, $\theta = k\pi/2n$ for $k = 0,1,\ldots,n$

$$f(z,0) = \begin{matrix} r^n\cos(n*\theta) + 1.0 \\ r^n\sin(n*\theta) \end{matrix}$$

The Jacobian of f is

$$f_{r,th} = \begin{matrix} nr^{n-1}\cos(n*\theta), & -nr^n\sin(n*\theta) \\ nr^{n-1}\sin(n*\theta), & nr^n\cos(n*\theta) \end{matrix},$$

$$\mathrm{Det}(f_{r,\theta}) = n^2 r^{2n-1}.$$

The sign of the Jacobian is always +1, thus $\deg(f,D,0) = n$

3. Homotopy for the Optimal Projection Equations

The object is to find P, Q, $\hat{P}$, $\hat{Q}$, which solve

$$0 = AQ + QA^T + V_1 - Q\bar{\Sigma}Q + \tau_\perp Q\bar{\Sigma}Q\tau_\perp^T,$$

$$0 = A^TP + PA + R_1 - P\Sigma P + \tau_\perp^T P\Sigma P\tau_\perp,$$

$$0 = (A-\Sigma P)\hat{Q} + \hat{Q}(A-\Sigma P)^T + Q\bar{\Sigma}Q - \tau_\perp Q\bar{\Sigma}Q\tau_\perp^T,$$

$$0 = (A-Q\bar{\Sigma})^T\hat{P} + \hat{P}(A-Q\bar{\Sigma}) + P\Sigma P - \tau_\perp^T P\Sigma P\tau_\perp$$

given Σ, $\bar{\Sigma}$, R_1, V_1, , n_c, A. To do this let

$$A(t) = \begin{bmatrix} D_1 & & \\ & D_2 & \\ & & D_n \end{bmatrix}(1-t) + tA$$

$$R_1(t) = I(1-t) = tR_1,\ V_1(t) = I(1-t) + tV_1$$

$$\Sigma(t) = \begin{bmatrix} \Sigma_0 & 0 \\ 0 & 0 \end{bmatrix}(1-t) + t\Sigma$$

$$\bar{\Sigma}(t) = \begin{bmatrix} \bar{\Sigma}_0 & 0 \\ 0 & 0 \end{bmatrix}(1-t) + t\bar{\Sigma}$$

For $t=0$ the solution is easy to find. The object is to follow the path or paths of solutions $P(t)$, $Q(t)$, $\hat{P}(t)$, $\hat{Q}(t)$ from $t=0$ to $t=1$. Note that if $n_c \geq \min\{\ell,n\} - n_u$ then there is only one solution at $t=0$. If $n_c < m_n\{\ell,p\} - n_u$ then there are $\binom{\min\{\ell,p\} - n_u}{n_c - n_u}$ solutions at $t=0$.

In following these initial solutions from $t=0$ to $t=1$ there are several situations which could occur (see figure 2).

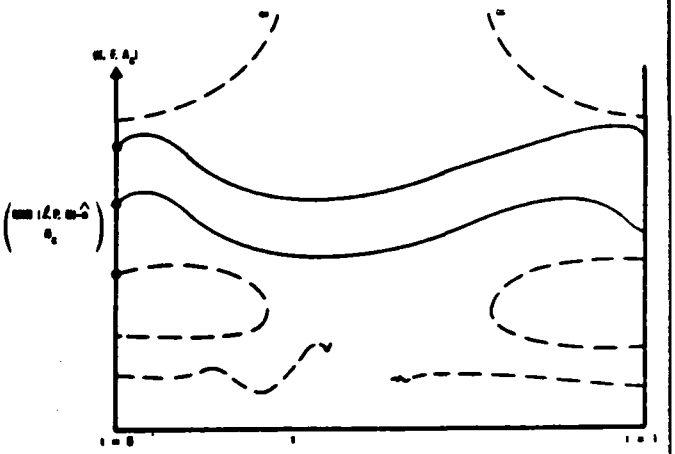

Figure 2

It can be shown using degree theory that the situations shown in dashed lines cannot occur. That is, the only solutions to the OPE at $t=1$ (or for $0 \leq t \leq 1$) are those which are continuously derived from the solutions at $t=0$.

Thus we have the following result. Let n_u denote the dimension of the unstable subspace of A.

Main Theorem. Assume that the plant is stabilizable and detectable, $V_1 > 0$, $R_1 > 0$ and $n_u \leq n_c$. Then, in the class of nonnegative-definite solutions Q, P, $\hat{Q}$, $\hat{P}$ with

$$\mathrm{rank}\,\hat{Q} = \mathrm{rank}\,\hat{P} = \mathrm{rank}\,\hat{Q}\hat{P} = n_c,$$

the optimal projection equations possess at most

$$\begin{cases} \binom{\min(n,m,\ell) - n_u}{n_c - n_u}, & n_c \leq \min(n,m,\ell), \\ 1, & \text{otherwise,} \end{cases}$$

stabilizing solutions. Each such solution is reachable via a homotopic path with starting point corresponding to diagonal initial data. Furthermore, if the plant is stabilizable by means of an n_cth-order dynamic compensator, then there exists at least one solution.

Remark 3.1. As shown in [26], stabilizing controllers of arbitrary reduced order may not always exist.

4. Algorithm Description and Numerical Results

In a homotopy path following algorithm one follows the path of solutions of $F(n(t),t)$ by integrating the initial value problem

$$\frac{dx}{dt} = F_x(x(t))\frac{dF}{dt}(x(t),t); \quad x(0) = x_0.$$

For the optimal projections equations the solution $P, \hat{P}, Q, \hat{Q}$ can be easily determined once τ is known so the $P(t) = P(\tau(t))$, $Q(t) = Q(\tau(t))$ etc. Thus the derivatives of $P, Q, \hat{P}, \hat{Q}$ can be written in terms of derivatives of G^T and Γ. Thus we obtain

$$\text{vec} \begin{bmatrix} \Gamma' \\ G^{T'} \end{bmatrix} = \begin{bmatrix} M \end{bmatrix} \text{vec } f(F, G^T).$$

which gives $2n_c n$ equation for Γ' and $G^{T'}$. P', Q', $\hat{P}'$ and $\hat{Q}'$ are then calculated from Γ' and $G^{T'}$ and finally $\Gamma(t+\Delta t)$ is updated by

$$\Gamma(t+\Delta t) = \Gamma(t) + \Gamma' \times \Delta t$$

and likewise for $G, P, Q, \hat{P}$ and $\hat{Q}$.

Figure 3 summarizes the results reported in [1] for LQG reduction methods along with results obtained using the homotopy method for solving the optimal projection equations. Here q_2 is a scale factor for the plant disturbance noise affecting controller authority. Clearly, LQG reduction methods experience increasing difficulty as authority increases, i.e., as the τ_1 terms become increasingly more important in coupling the control and reduction operations.

One of the main goals of the development effort was to extend the range of disturbance intensity or, equivalently, observer bandwidth, out beyond $q_2 = 2000$. To this end, second-order ($n_c = 2$) controllers were obtained with relatively little computation for $q_2 = 10{,}000$, $100{,}000$, $1{,}000{,}000$. The performance of these results is summarized in Figure 4.

Method	q_2 / n_c	0.01	0.1	1	10	100	1000	2000
Enns	7	S	S	S	S	S	S	S
	6	S	S	S	S	S	S	S
	5	S	S	S	S	S	S	S
	4	S	S	S	S	S	S	U
	3	S	S	S	S	S	S	S
	2	S	S	S	S	U	U	U
Glover	7	S	S	S	S	S	U	S
	6	S	S	S	S	U	U	U
	5	S	S	S	S	U	U	U
	4	S	S	S	S	U	U	U
	3	S	S	U	S	U	U	U
	2	S	U	S	U	S	U	U
Davis & Skelton	7	S	U	U	S	S	S	S
	6	S	S	S	S	S	S	S
	5	S	U	S	S	S	U	U
	4	S	S	U	S	S	U	U
	3	U	U	U	U	U	U	U
	2	S	U	S	U	U	U	U
Yousuff & Skelton	7	S	S	S	S	U	U	U
	6	S	S	S	S	U	U	U
	5	S	S	S	U	U	U	U
	4	S	S	S	U	U	U	U
	3	S	U	U	U	U	U	U
	2	S	S	S	U	U	U	U
Liu & Anderson	7	S	S	S	S	S	S	U
	6	S	S	S	S	S	S	U
	5	S	S	S	S	S	S	S
	4	S	S	S	S	S	S	S
	3	S	S	S	S	S	U	U
	2	S	S	S	S	S	S	S
Optimal Projection	7	S	S	S	S	S	S	S
	6	S	S	S	S	S	S	S
	5	S	S	S	S	S	S	S
	4	S	S	S	S	S	S	S
	3	S	S	S	S	S	S	S
	2	S	S	S	S	S	S	S

S - The closed-loop system is stable
U - The closed-loop system is unstable

Figure 3. The Optimal Projection Approach Was Compared to Several LQG Reduction Techniques Over a Range of Controller Authorities for an Example of Enns

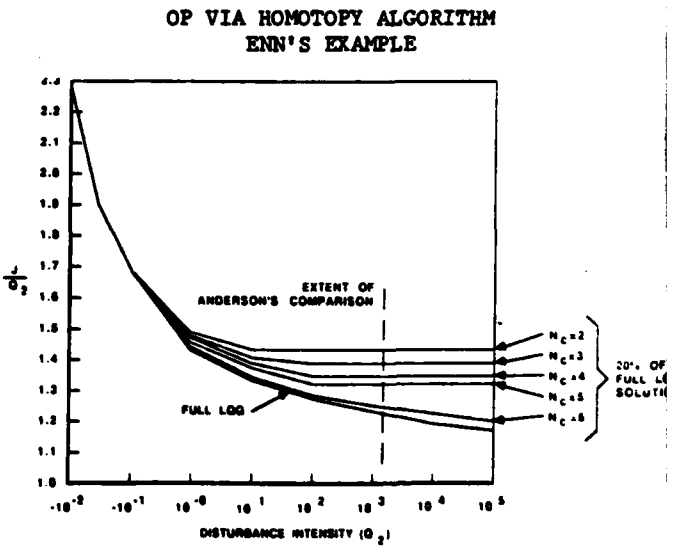

Figure 4

1. Y. Liu and B. D. O. Anderson, "Controller Reduction via Stable Factorization and Balancing," Int. J. Contr., Vol. 44, pp. 507-531, 1986.

2. D. C. Hyland and D. S. Bernstein, "The Optimal Projection Equations for Fixed-Order Dynamic Compensation," IEEE Trans. Autom. Contr., Vol. AC-29, pp. 1034-1037, 1984.

3. D. C. Hyland and D. S. Bernstein, "The Optimal Projection Equations for Model Reduction and the Relationships Among the Methods of Wilson, Skelton and Moore," IEEE Trans. Autom. Contr., Vol. AC-30, pp. 1201-1211, 1985.

4. D. C. Hyland, "The Optimal Projection Approach to Fixed-Order Compensation: Numerical Methods and Illustrative Results," AIAA 21st Aerospace Sciences Meeting, paper 83-0303, Reno, NV, January 1983.

5. D. C. Hyland, "Comparison of Various Controller-Reduction Methods: Suboptimal Versus Optimal Projection," Proc. AIAA Dynamics Specialists Conf., pp. 381-389, Palm Springs, CA, May 1984.

6. D. S. Bernstein, L. D. Davis and D. C. Hyland, "The Optimal Projection Equations for Reduced-Order, Discrete-Time Modelling, Estimation and Control," J. Guid. Contr. Dyn., Vol. 9, pp. 288-293, 1986.

7. D. S. Bernstein and D. C. Hyland, "The Optimal Projection/Maximum Entropy Approach to Designing Low-Order, Robust Controllers for Flexible Structures," Proc. 24th IEEE Conf. Dec. Contr., pp. 745-752, Fort Lauderdale, FL, December 1985.

8. D. S. Bernstein, L. D. Davis, S. W. Greeley and D. C. Hyland, "Numerical Solution of the Optimal Projection/Maximum Entropy Design Equations for Low-Order, Robust Controller Design," Proc. 24th IEEE Conf. Dec. Contr., pp. 1795-1798, Fort Lauderdale, FL, December 1985.

9. D. S. Bernstein and S. W. Greeley, "Robust Controller Synthesis Using the Maximum Entropy Design Equations," IEEE Trans. Autom. Contr., Vol. AC-31, pp. 362-364, 1986.

10. D. C. Hyland, D. S. Bernstein, L. D. Davis, S. W. Greeley and S. Richter, "MEOP: Maximum Entropy/Optimal Projection Stochastic Modelling and Reduced-Order Design Synthesis, "Final Report, Air Force of Scientific Research, Bolling AFB, Washington, DC, April 1986.

11. A. Gruzen and W. E. Vander Velde, "Robust Reduced-Order Control of Flexible Structure Using the Optimal Projection/Maximum Entropy Design Methodology," AIAA Guid. Nav. Contr. Conf., Williamsburg, VA, August 1986.

12. A. Gruzen, "Robust Reduced Order Control of Flexible Structures," C. S. Draper Laboratory Report #CSDL-T-900, April 1986.

13. E. Wasserstrom, "Numerical Solutions by the Continuation Method," SIAM Review, Vol. 15, pp. 89-119, 1973.

14. J. H. Avila, "The Feasibility of Continuation Methods for Nonlinear Equations," SIAM J. Numer. Anal., Vol. 11, pp. 102-122, 1974.

15. H. Wacker, Continuation Methods, Academic Press, New York, 1978.

16. N. G. Lloyd, Degree Theory, Cambridge University Press, London, 1978.

17. J. C. Alexander and J. A. Yorke, "The Homotopy Continuation Method: Numerically Implementable Procedures," Trans. Amer. Math. Soc., Vol. 242, pp. 271-284, 1978.

18. B. C. Eaves, F. J. Gould, H. O. Peitgen, and M. J. Todd, Homotopy Methods and Global Convergence, Plenum Press, New York, 1983.

19. M. Mariton and R. Bertrand, "A Homotopy Algorithm for Solving Coupled Riccati Equations," Optim. Contr. Appl. Meth., Vol. 6, pp. 351-357, 1985.

20. S. Richter and R. DeCarlo, "Continuation Methods: Theory and Applications," IEEE Trans. Autom. Contr., Vol. 28, pp. 660-665, 1983.

21. S. Richter and R. DeCarlo, "A Homotopy Method for Eigenvalue Assignment Using Decentralized State Feedback," IEEE Trans. Autom. Contr., Vol. AC-29, pp. 148-155, 1984.

22. S. Lefebvre, S. Richter and R. DeCarlo, "A Continuation Algorithm for Eigenvalue Assignment by Decentralized Constant-Output Feedback," Int. J. Contr., Vol. 41, pp. 1273-1292, 1985.

23. D. R. Sebok, S. Richter and R. DeCarlo, "Feedback Gain Optimization in Decentralized Eigenvalue Assignment," Automatica, Vol. 22, pp. 433-447, 1986.

24. P. T. Kabamba, R. W. Longman and S. Jian-Guo, "A Homotopy Approach to the Feedback Stabilization of Linear Systems," preprint.

25. R. de Gaston and M. Safonov, "A Homotopy Method for Nonconservative Stability Robustness Analysis," Proc. 24th IEEE Conf. Dec. Contr., pp. 1294-1301, Fort Lauderdale, FL, December, 1985.

26. Malcolm C. Smith, "On Minimal Order Stabilization of Single Loop Plants," Sys. Contr. Lett., Vol. 7, pp. 39-40, 1986.

APPENDIX G

REFERENCE 61

ACTIVE DAMPING CONTROL DESIGN FOR THE MAST FLIGHT SYSTEM

Fredric M. Ham and Scott W. Greeley

Harris Corporation
Government Aerospace Systems Division
Controls Analysis and Synthesis Group
P.O. Box 94000
Melbourne, Florida 32902

ABSTRACT

Design and development of the Mast Flight System for the COFS (Control of Flexible Structures) program for NASA is currently underway. An active damping controller is required to provide five percent damping for the first ten structural modes of a sixty meter truss beam structure. Two types of controller design methodoligies are presented to achieve the required five percent damping. The first is an LQG controller and the second is a positive-real decentralized velocity feedback type, which is the system baseline controller design. The system modelling details are also presented which includes the models for the truss beam and the collocated actuators and sensors.

1. INTRODUCTION

NASA has identified the need for large deployable space structures which will be constructed of lightweight materials and will contain a large number of joints or structural connections. These deployable space structures may have precision shape requirements and a need for active vibration suppresion during on-orbit operations. One such ongoing NASA program is COFS (Control of Flexible Structures). Harris is currently under contract to NASA Langley Research Center to design and develop the Mast Flight System[1] for the COFS program.

[1] NASA Contract Number: NAS1-18300

The basic element in the Mast Flight System is a 60.7 meter long, triangular cross section, joint-dominated truss structure referred to as the beam subsystem, see Figure 1.1. Included at the tip of the truss structure are the primary actuators, collocated sensors and a parameter modification device. A deployment/retraction subsystem is provided which also secures the stowed beam package during launch and landing.

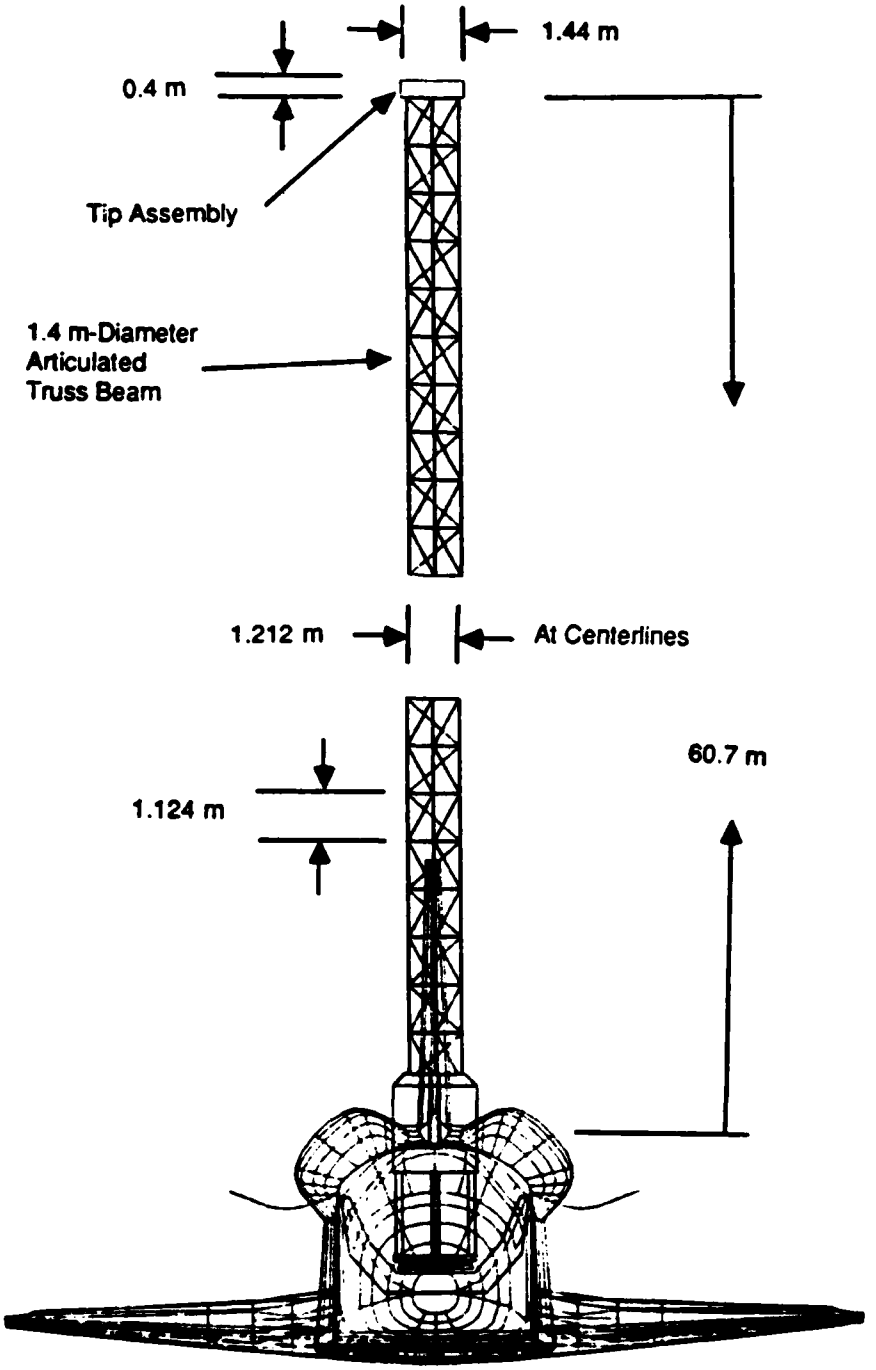

Figure 1.1. Shuttle Attached Deployed Truss Beam Configuration

The beam subsystem consists of a statically determinant, three longeron, triangular truss whose cross-section fits inside a 1.4 m diameter circle. A total of 54 bays, each 1.124 m long, make up the 60.7 m length of the beam above the deployer mechanism. Figure 1.2 illustrates more of the beam design details. Precision-machined titanium joints at each apex of the triangular cross section of each bay and a nearly over-center hinge in each diagonal allow the beam to fold into a repeatable stack with a 35:1 packing ratio. Structural members are fabricated from graphite/epoxy tubes bonded to titanium end fittings. Length ratios are determined from test data such that the overall coefficient of thermal expansion (CTE) is in the range of $\pm 0.5 \times 10^{-6} K^{-1}$.

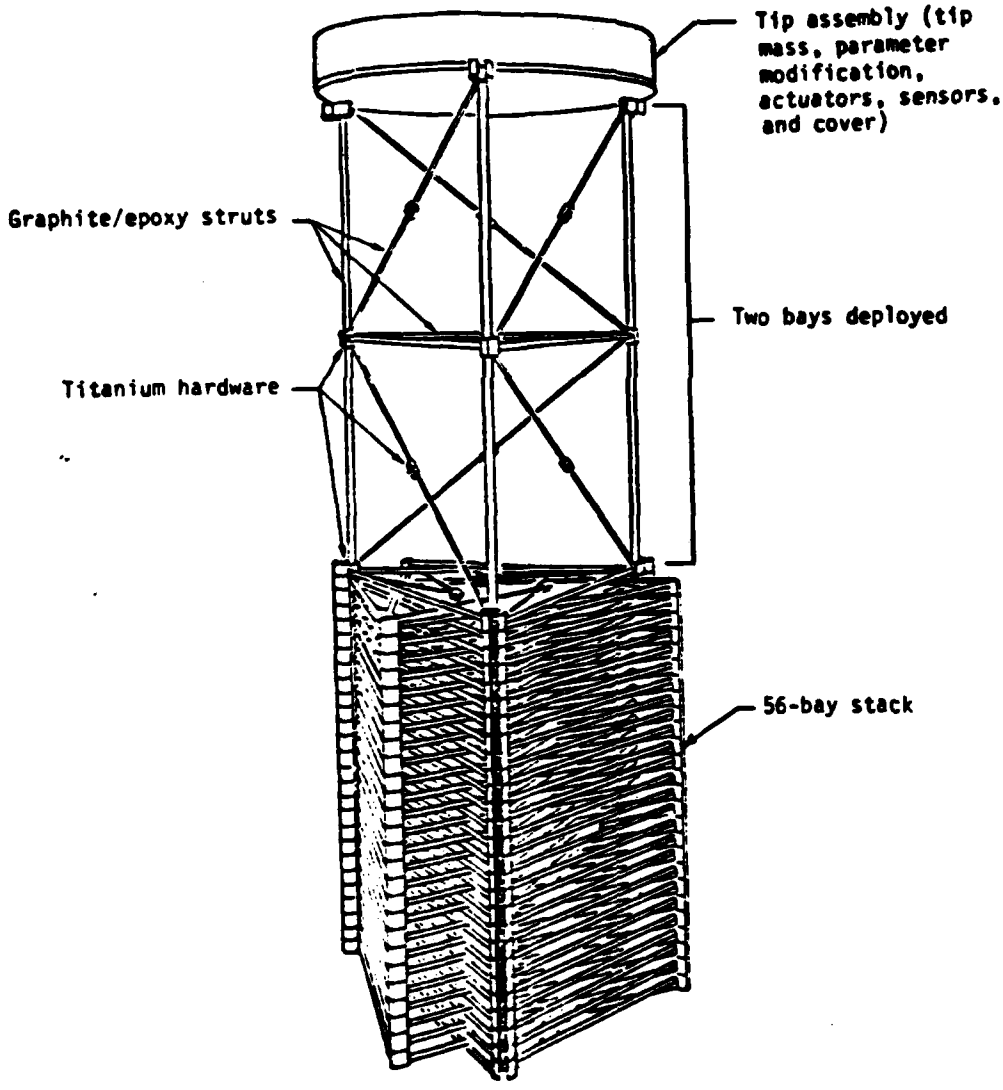

Figure 1.2. Beam Subsystem (Articulated Truss Beam With Tip Assembly)

Actuators are distributed along the beam as shown in Figure 1.3. All are proof-mass type actuators and are implemented as linear DC motors (LDCM). There are four (4) primary actuators located at the tip of the beam, two parallel to the x-axis and two parallel to the y-axis as shown in Figure 1.4. Actuators 1 and 3 may be commanded in phase to produce x-axis forces. These same two actuators can be commanded out of phase to produce torques about the beam's longitudinal or z-axis. Actuators 2 and 4 can be operated similarly, or other combinations as may be desired to achieve three degree of freedom control using only the primary tip-mounted actuators. These primary actuators are sized to sinusoidally excite the first ten (10) beam modes to a level which allows measurement of the modal characteristics to an accuracy of 1 percent via the beam-mounted sensors. These primary actuators are also sized to provide a total damping of 5 percent or 5 times the natural structural damping, whichever is greater, across the spectrum of the first 10 modes.

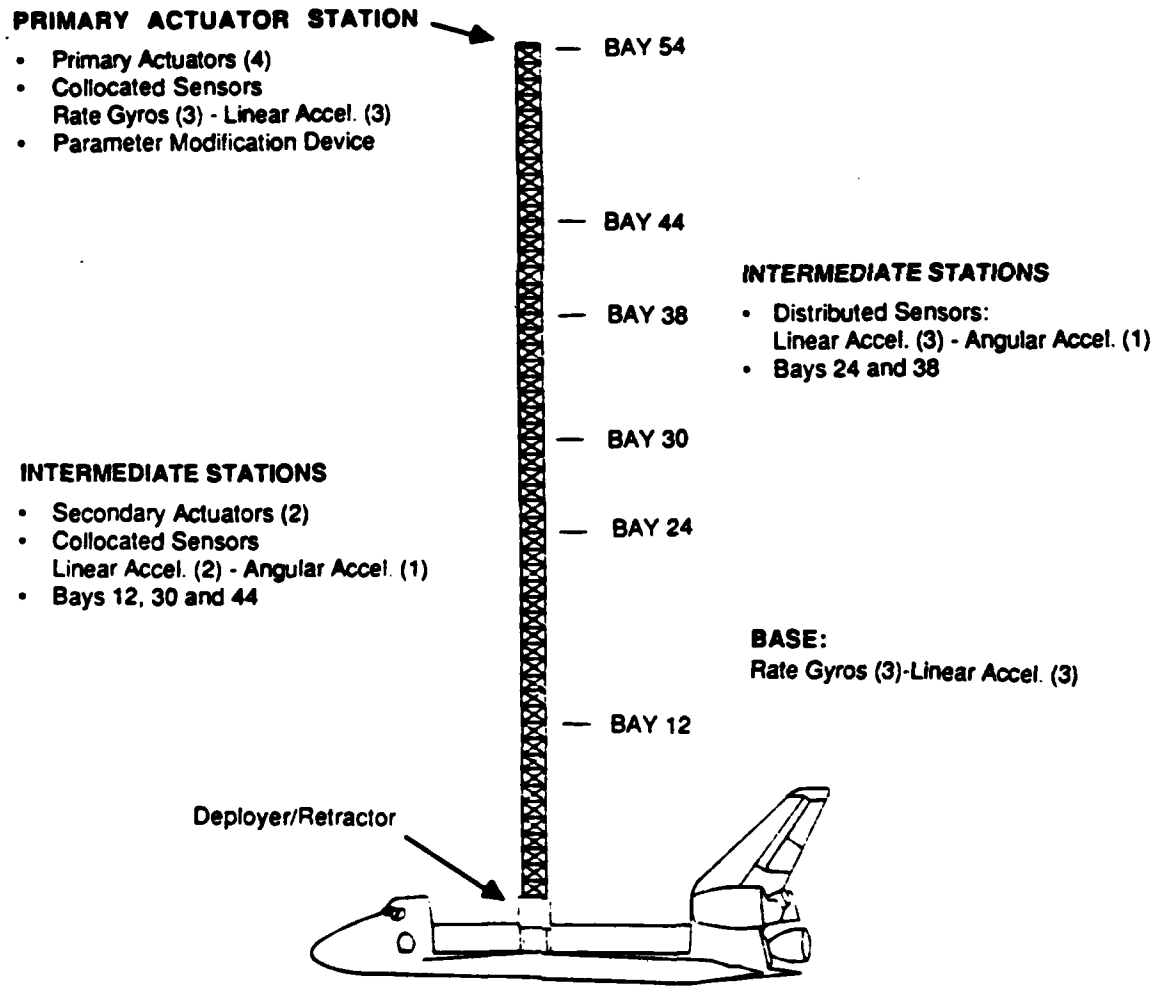

Figure 1.3. Mast Flight System Instrumentation Summary

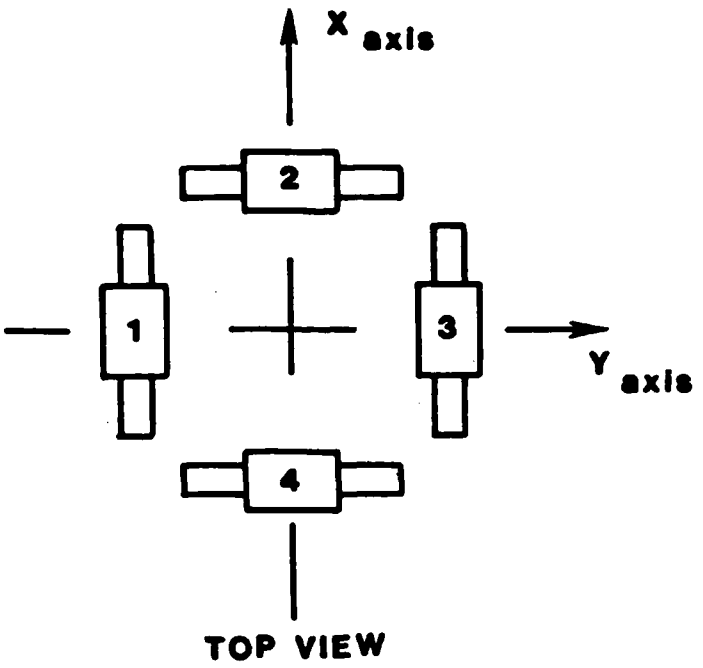

Figure 1.4. Layout of Tip-Mounted LDCM Actuators

In order to provide the required active damping, LDCMs are utilized at the intermediate stations on the truss beam as shown in Figure 1.3. The LDCMs at the intermediate stations (Bays 12,30 and 44) are smaller devices than the tip mounted ones; this is due to volume constraints. At each of the three bays are 2 LDCMs mounted in the x and y directions, thus providing excitation and damping in these directions. Table 1.1 summarizes the complement of actuators and sensors that are mounted on the truss beam. The sensing devices which are collocated with LDCMs are the only devices

Table 1.1. Actuators and Sensors Mounted on the Truss Beam*

Location	LDCMs	Rate Gyros	Angular Accelerometers	Linear Accelerometers
Tip	2-x,2-y	3-x,y,z		3-x,y,z
Bay 44	1-x,1-y		1-z	2-x,y
Bay 38			1-z	3-x,y,z
Bay 30	1-x,1-y		1-z	2-x,y
Bay 24			1-z	3-x,y,z
Bay 12	1-x,1-y		1-z	2-x,y
Base		3-x,y,z		3-x,y,z

* Note: There are additional instruments such as strain gages and thermistors mounted on the structure that will not be addressed here.

which are used for the active damping scheme. The sensors at Bays 24 and 38 are included for the purpose of completeness and will be used for other experiements.

II. MODELLING

A model of the fully deployed (60.7 m) Deployable Mast System (DMS) has been developed using a Harris proprietary finite-element code which is similar to NASTRAN. An actuator/sensor location assessment based on the modal eigenvectors of the DMS model has been conducted. Models of the actuators and sensors (i.e. LDCMs, accelerometers and rate gyros) have also been formulated from manufacturer's data.

Using Harris' Nonlinear Structural Analysis (NLSA) finite element package, a three-dimensional truss beam model of the DMS cantilevered to a model of the Shuttle Orbiter has been developed. An eigenvalue/eigenvector analysis has yielded several modal frequencies and mode shapes. Because the Shuttle Orbiter model is only accurate in terms of effective mass and inertia properties, only the pure DMS modes were considered in the modelling process (i.e. Shuttle Orbiter and DMS-Shuttle Orbiter modes are neglected). This is a good assumption for the control-system design and analysis since the mass normalized influence coefficients of the Shuttle Orbiter and the DMS-Shuttle Orbiter modes are much smaller than those of DMS modes for the practical locations and power limitations of the LDCM actuators.

A qualitative discussion of the "best" actuator/sensor locations is summarized in Table 2.1. This table shows that there are five locations that are "best" in terms of

Table 2.1 Qualitative Assessment of Actuator/Sensor Locations

DMS Mode	"Best" Actuator/Sensor Location Based on Large Influence Coefficients
1	54 (Tip)
2	54 (Tip)
3	30
4	30
5	54 (Tip)
6	12, 44
7	12, 44
8	24
9	12, 30, 44
10	12, 30, 44

controllability and observability (large influence coefficients) for the first 10 flexible modes of the DMS. Another criterion used for the placement of the instruments had to do with volume contraints, requiring that even-numbered bay locations be chosen. As stated in the introduction, four of the bays where chosen to place collocated actuators and sensors: Bays 12(x and y), 30(x and y), 44(x and y) and 54(x1,y1,x2 and y2) with each actuator at the DMS tip station placed 0.5 m from the center to allow control of the torsional modes. Control of the second torsional mode can be accomplished with the tip actuators, therefore not requiring additional actuators at Bay 24 (which would be the "best" control location) where volume constaints are more severe than at the tip of the DMS.

The weight of the LDCMs, accelerometers, rate gyros and the associated electronics were included in the finite element model. For this model the DMS modal frequencies, predicted modal damping and mode shape descriptions are summarized in Table 2.2.

Table 2.2. Description of DMS Modes

DMS Mode	Mode Frequency ω	Modal Damping η	Mode Shape Description
1	0.2	0.002	1st x-z Bending
2	0.24	0.002	1st y-z Bending
3	1.52	0.003	2nd y-z Bending
4	1.62	0.003	2nd x-z Bending
5	2.49	0.005	1st Torsion
6	4.65	0.005	3rd y-z Bending
7	4.96	0.005	3rd x-z Bending
8	8.24	0.005	2nd Torsion
9	8.55	0.005	4th y-z Bending
10	9.05	0.005	4th x-z Bending

Figures 2.1 through 2.3 show the various mode shapes for the first 10 flexble modes of the DMS. It can be seen that there are 4 pairs of x and y bending modes, each pair relatively close in frequency, and there are two torsion modes. Note that the chosen actuator/sensor locations remain the "best" locations even with the additional weight.

Based on the DMS modes and predicted damping, a state-space model of the DMS can be formulated. The following equations give the state-space representation.

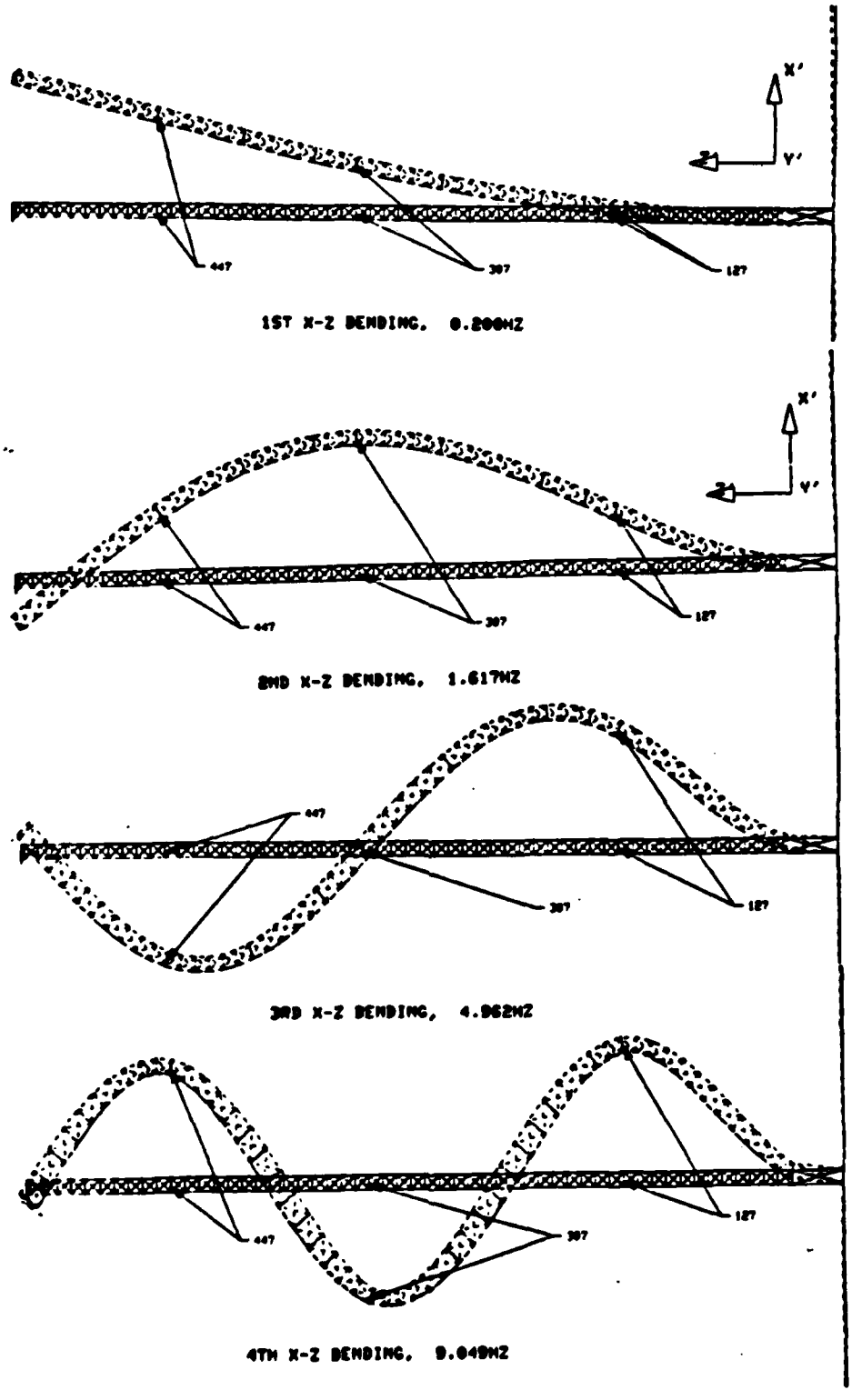

Figure 2.1. DMS x-z Mode Shapes

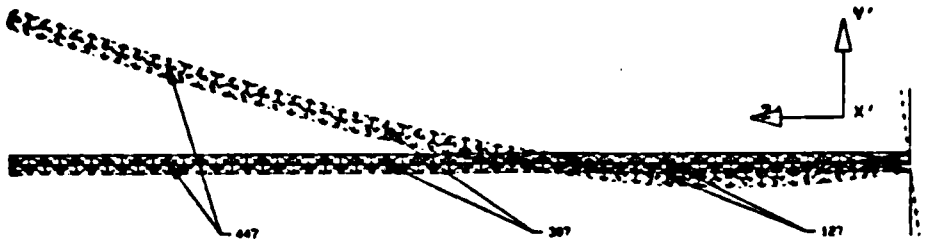

1ST Y-Z BENDING, 0.240HZ

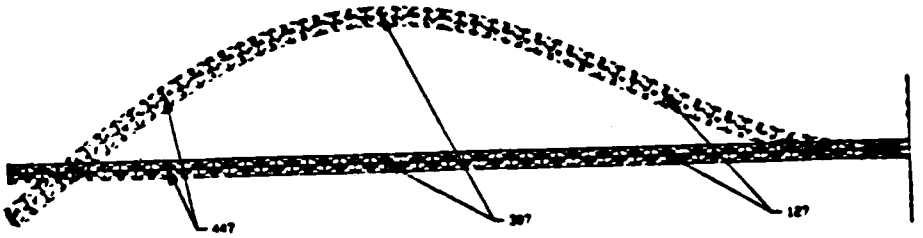

2ND Y-Z BENDING, 1.520HZ

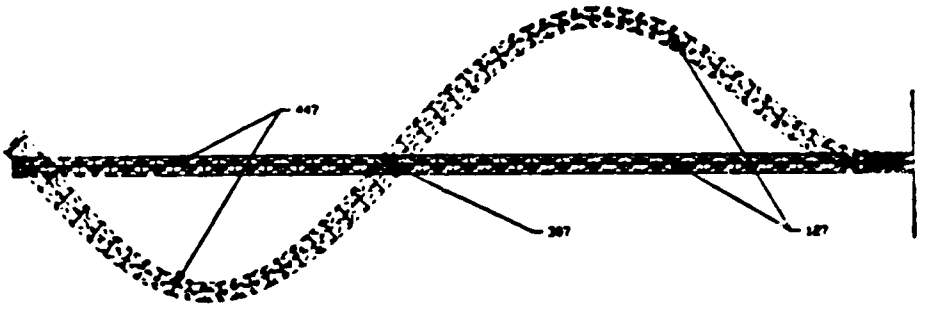

3RD Y-Z BENDING, 4.652HZ

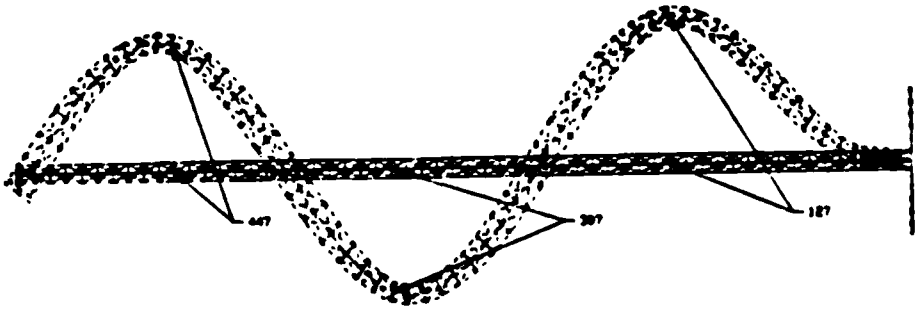

4TH Y-Z BENDING, 8.547HZ

Figure 2.2. DMS y-z Mode Shapes

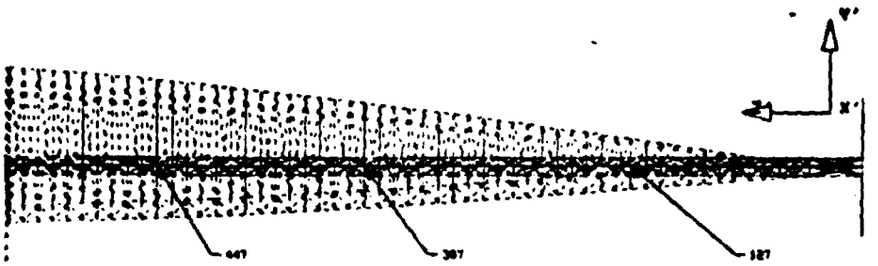

1ST TORSION, 2.490HZ

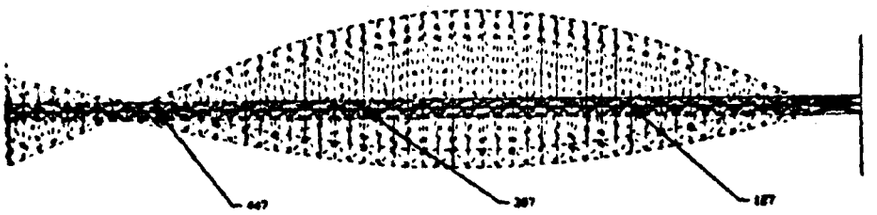

2ND TORSION, 3.237HZ

Figure 2.3. DMS Torsional Mode Shapes

$$\dot{x} = Ax + Bu + v \qquad (2.1)$$

$$y = Cx$$

where

$$A = \text{Block Diagonal} \begin{bmatrix} 0 & \omega_i \\ -\omega_i & -2\eta_i\omega_i \end{bmatrix} \qquad (2.2)$$

ω_i = ith modal frequency

η_i = ith modal damping ratio

and

$$B(k,j) = \begin{cases} 0, & k = 2i-1 \\ \phi ij, & k = 2i \end{cases}, \quad i = 1,2, \ldots, 10$$

ϕij = Mass normalized influence coefficient of the ith mode for the FEM node of jth actuator location

$$C(j,k) = \begin{cases} 0 \ , & k = 2i-1 \\ \phi ij \ , & k = 2i \end{cases} \quad , i = 1,2, \ldots, 10$$

ϕij = Mass normalized influence coefficient of the ith mode for the FEM node of jth sensor location

y = velocity output at DMS Bays 12(x and y), 30(x and y), 44(x and y) and 54 (x, y and θ_z)

u = Force input at DMS Bays 12(x and y), 30(x and y), 44(x and y) and 54(x1, y1, x2 and y2)

v = Disturbance force or torque

The acceleration at the sensor locations can be computed as

$$\dot{y} = CAx + CBu + Cv \qquad (2.3)$$

This is the system representation that is used for all control system design and analysis.

The Linear DC Motor (LDCM) is a proof-mass type actuator with a large movable mass referred to as the secondary mass. Figure 2.4 shows the basic elements of the LDCM. The secondary moves with respect to the primary or base of the LDCM which is fixed to the truss beam. The actuator is stroke limited at low frequencies (less than 1 Hz) and force limited at high frequencies (greater than 1 Hz). For a non-position compensated LDCM the position of the secondary mass is very sensitive to changes in commanded force amplitude and frequency and changes in position of its base. This due to the double integration effects of force commanded devices and unknown forces (e.g. Coulomb friction). To alleviate this problem a compensator has been developed to

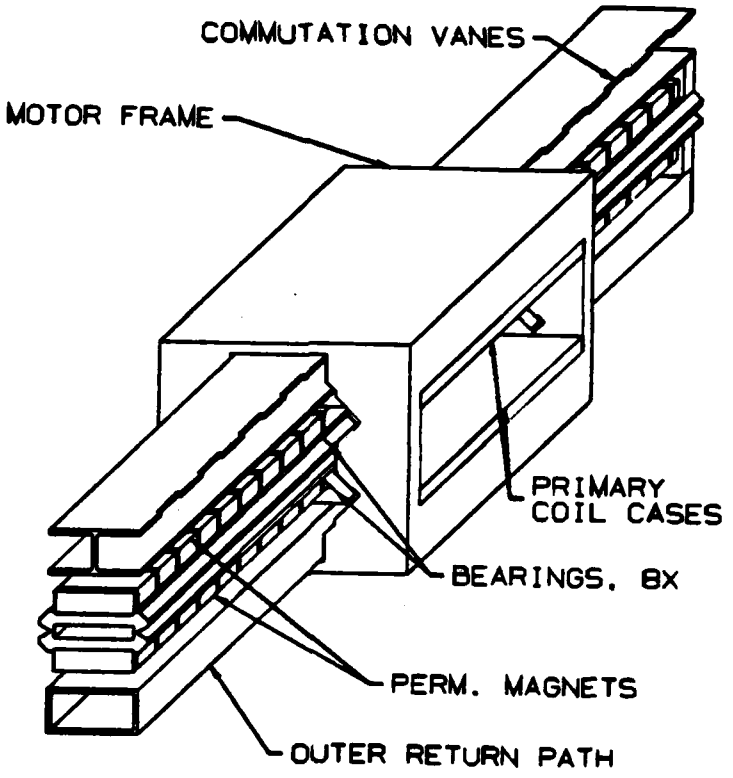

Figure 2.4. Basic Elements of a LDCM

isolate the secondary from the primary, in other words, the secondary position tracks in an inertial reference frame and is decoupled from primary motion effects over a range based on the stroke limitation.

The overall transfer function of the LDCM, taking into account pole/zero cancellation, and the isolation compensator, behaves as a second-order system of the form

$$\frac{f(s)}{v(s)} = \frac{M\sigma^2 s^2}{(s+\sigma)^2} \qquad (2.4)$$

where f - Force Output
v - Command Output

$$M = \begin{cases} 7.6 \text{ kg for LDCMs at DMS Bays 12,30 and 44} \\ 11.1 \text{ kg for LDCMs at DMS Tip (Bay 54)} \end{cases}$$

$$\sigma = 2\pi \text{ rad/sec (1 Hz)}$$

Based on manufactuer data the linear accelerometers at the DMS Bays 12, 30, 44 and 54 (all in x and y) and the rate gyro at Bay 54 (θ_z) are modelled as second order systems. These sensing devices are used in the active damping control system and are modelled as

$$\frac{y_s(s)}{y(s)} = \frac{K\omega_n^2}{s^2 + 2\eta\omega_n s + \omega_n^2} \qquad (2.5)$$

where

y_s = Output Voltage
y = Input Acceleration
K = Sensor Sensitivity

$$\omega_n = \begin{cases} 200 \text{ Hz for Linear Accelerometers} \\ 100 \text{ Hz for Rate Gyro} \end{cases}$$

$\eta = 0.707$

As shown above, the bandwidths of the sensing devices are large relative to the frequency range of interest; therefore, the sensor dynamics will have a negligible effect on the control system design and analysis.

III. CONTROL SYSTEMS DESIGN AND ANALYSIS

To achieve the design goal of 5 percent damping (i.e., modal damping ratio of 0.05) in the first ten flexible modes of the Deployable Mast System (DMS) two different controller design methodologies are compared. The first type is an LQG controller and the second is a positive-real decentralized velocity feedback (PRDVF) controller. Both of these controllers are designed using the following: 1) the design plant which includes

the first ten flexible DMS modes augmented with the dynamics of the ten LDCMs, 2) collocated sensors and actuators at Bays 12(x and y), 30(x and y), 44(x and y) and 54(x, y and θ_z), 3) velocity measurements are assumed as inputs to each of the controllers which can be obtained by integrating the accelerometer outputs. The PRDVF controller is decentralized in the sense that each sensor output is fed only to the controller of its collocated actuator as shown in Figure 3.1.

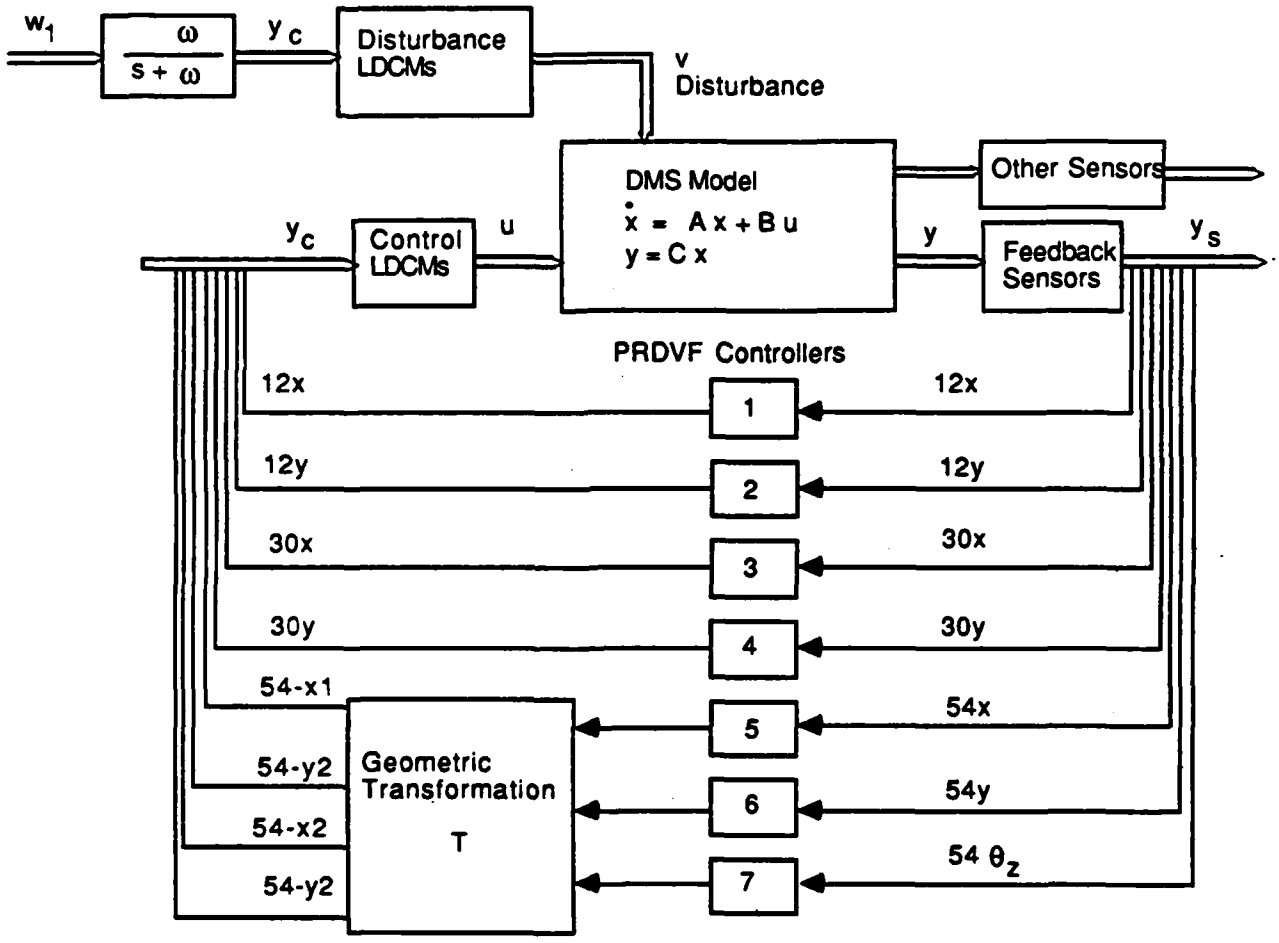

Figure 3.1. Block Diagram for Plant With PRDVF Controller for Wide-Band Disturbance Analysis

There are some interesting statements which can be made comparing the generic aspects of each controller type:

LQG:

- LQG will result in the best linear controller for a given set of quadratic design goals [1].
- In general, for large space structures, LQG designs result in high-order controllers which are often sensitive to parameter variations.
- Both of the above disadvantages can be overcome by using the Maximum Entropy/Optimal Projection (MEOP) design approach which will result in quadratically optimal low-order, robust linear controllers [2-5].

PRDVF:

- The decentralized positive-real controllers are infinitely robust to parameter variations given a positive-real plant [6,7].
- The major disadvantage of a PRDVF controller is its relative low authority.
- The PRDVF design here is very simple, with each decentralized controller being of second order or less.

An LQG controller has been designed in this study rather than a MEOP controller since a comparison of two controller types is desired in terms of a single design goal, i.e., 5 percent damping. Controller implementation limitations and robustness levels are not specified for this analysis. It also of interest to note that the PRDVF controller is only positive real over a certain frequency range. This is due to the high-frequency rolloff of the linear accelerometers and the rate gyro. However, for this analysis the PRDVF controller is positive real for the frequency range of interest.

A comparison of the controllers, as well as the open-loop case , is carried out for a scenario which includes a wide-band disturbance. New designs of the LQG controller and the PRDVF controller are made using only the collocated actuators/sensors at Bays 12(x and y), 30(x and y) and 54(x,y and θ_z) for this analysis. In this case the plant is subjected to a wide-band disturbance utilizing the LDCMs at Bay 44(x and y). These disturbance LDCMs are given independent random signals which produce a mean square force output of approximately one half of the LDCMs maximum force capability, which for the LDCMs at the intermediate stations is 15 N (the maximum force capability of the LDCMs at the tip station is 30 N).

LQG Design

A standard continous-time LQG controller is designed using the time-invariant plant consisting of the first ten flexible DMS modes augmented with the ten control LDCM dynamics. The sensor dynamics are ignored here since their natural frequencies occur well above the bandwidth of the plant. A block diagram of the plant/LQG controller is shown in Figure 3.2. Note, this block diagram is for the LQG controller used in the

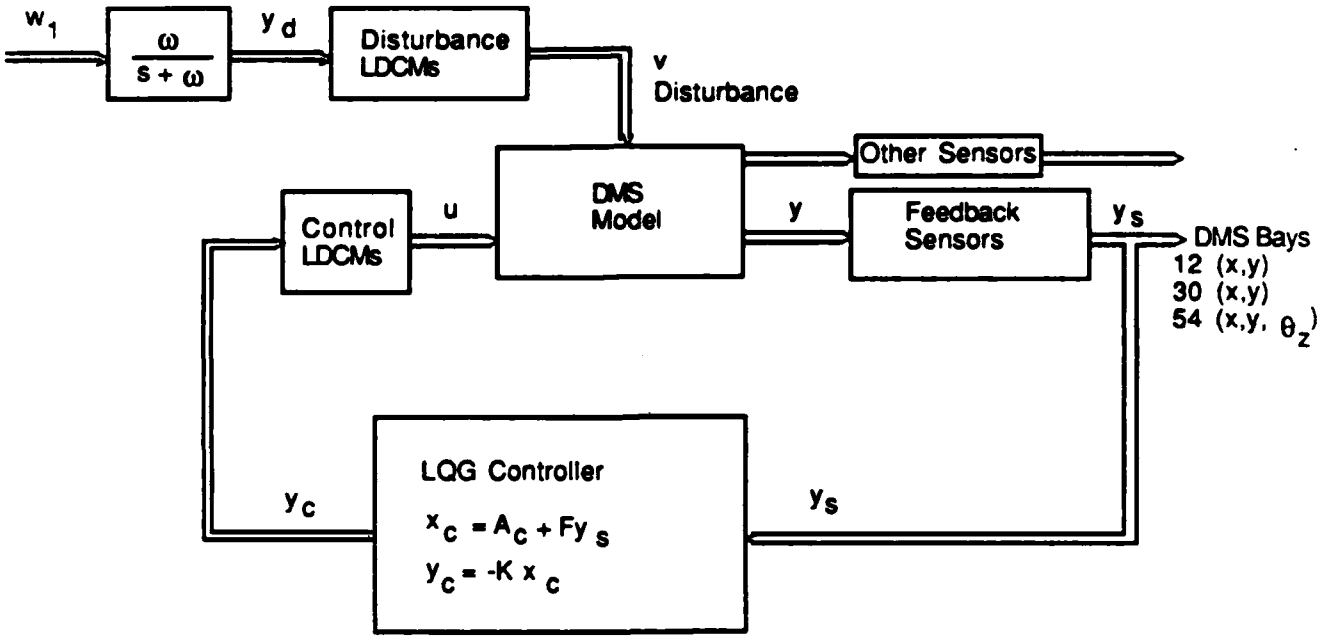

Figure 3.2. Block Diagram of Plant with LQG Controller for Wide-Band Disturbance Analysis

wide-band disturbance analysis, which uses only eight control LDCM actuators.

The LQG controller is designed to yield 5 percent damping or greater in the DMS modes. Since the design is not stated in terms of a quadratic performance criterion, and requires relatively low controller authority, the LQG controller is designed to only yield the required 5 percent modal damping.

The closed-loop modal damping ratios of the plant augmented with the LQG controller is listed in Table 3.1. As shown in the table all the values exceed the design goal.

Table 3.1. Modal Damping for Open Loop, LQG and PRDVF

DMS Model	Model Damping (%)		
	Open Loop	LQG	PRDVF
1	0.2	5.1	5.4
2	0.2	5.1	5.9
3	0.3	6.3	8.4
4	0.3	6.4	8.0
5	0.5	6.3	12.0
6	0.5	5.8	7.7
7	0.5	5.8	7.3
8	0.5	7.8	5.7
9	0.5	6.7	5.7
10	0.5	6.7	5.3

Positive-Real Decentralized Velocity Feedback Design

A PRDVF controller, which consists of 9 controller loops [DMS Bays 12(x and y), 30(x and y), 44(x and y) and 54(x, y and θ_z)], is designed to meet the 5 percent damping goal. The design procedure is to examine the actuator/sensor locations which best influence the DMS modes of interest (in an open-loop sense). For example, the accelerometers/LDCMs at the DMS tip (Bay 54) have the best influence on the first x and y bending modes and the two torsion modes; the accelerometers/LDCMs at the DMS distributed bays (Bays 12, 30 and 44) have the best influence on the 2nd, 3rd and 4th x and y bending mode pairs. Thus, the poles of the controller loop are placed to shape the gain in terms of the modes that the particular loop will be controlling, and the gains of each controller loop are tuned to obtain 5 percent damping. There will be coupling among the different loops due to interaction of the DMS. However the 5 percent damping requirement is met as shown in Table 3.1.

The generic structure of each decentralized collocated loop is of the form

$$H(s) = \frac{K(s+\sigma)^2}{s(s+\beta)} \qquad (3.1)$$

This form is chosen since it offers a simple positive-real controller that will achieve the design goal (note: sensor dynamics will cause the controller to become non-positive real beyond 200 Hz for the linear accelerometer loops and 100 Hz for the rate gyro loop). The output of the controller loops associated with Bay 54 (x, y and θ_z) are geometrically transformed such that equivalent outputs are applied to the four LDCMs at this bay location (x1, y1, x2, and y2).

Wide-Band Disturbance Analysis

For this analysis an LQG controller and a PRDVF controller are designed using only the collocated actuators/sensors at Bays 12(x and y), 30(x and y) and 54(x, y and θ_z). This is done so that the LDCMs at Bay 44(x and y) only act to provide the disturbance force. Independent wide-band random signals, each with a single-pole roll-off at 15 Hz, are applied to the disturbance LDCMs. The intensity of these disturbance signals is chosen such that the mean-square output force of the LDCMs is one half of their maximum levels.

For each of the following three cases RMS and PSDs of accelerometers and control actuators are computed.

Case: 1 - Open Loop

2 - Closed Loop with LQG Controller

3 - Closed Loop with PRDVF Controller

In each case the dynamics of the disturbance LDCMs and the single-pole filter which shapes the white noise are included in the plant model.

The RMS levels of the accelerometers at Bays 12, 30 ,44 and 54 for each of the cases are given in Table 3.2. It is shown in both closed-loop cases that the accelerometer RMS levels are greater than a factor of two below the open-loop case. Also Case 3 (PRDVF) performs better than Case 2 (LQG). Power spectral density plots for the accelerometers at Bays 12(x), 30(y) and 54(x, y and θ_z) are shown in Figures 3.3 to 3.7. These show that Case 3 (PRDVF) is more effective (suppressive) for all of the modes than Case 2 (LQG).

Control LDCM RMS levels are also given in Table 3.2. For Case 2 (LQG) the control levels are spread more evenly among the LDCMs than for Case 3 (PRDVF). It is of interest to note that the control LDCM levels are all well below their maximum capability. The power spectral density plots of the two closed-loop cases for control LDCMs at Bays 12(x), 30(y) and 54(x1 and y2) are shown in Figures 3.8 through 3.11. Case 2 (LQG) requires less power over the entire frequency range than Case 3 (PRDVF) for LDCMs at Bays 12(x) and 30(y). However, Case 3 (PRDVF) requires much less power in the higher frequency modes than Case 2 (LQG) for the LDCMs at Bay 54. This explains the lower RMS control LDCM levels for Case 3 for these LDCMs. Recall in the design of the PRDVF controller, the Bay 54 LDCMs are used primarily to control the 1st x and y bending modes of the DMS.

Table 3.2. RMS Levels for Open Loop, LQG and PRDVF

Variable Description	Units	RMS Level		
		Open Loop	LQG	PRDVF
Acceleration:				
12x	g	0.063	0.027	0.019
12y	g	0.061	0.026	0.019
30x	g	0.044	0.018	0.014
30y	g	0.042	0.018	0.013
44x	g	0.058	0.023	0.023
44y	g	0.056	0.027	0.022
54x	g	0.010	0.0043	0.0030
54y	g	0.010	0.0044	0.0034
$54\theta_z$	r/s^2	0.0027	0.0012	0.00072
Control Force:				
12x	N	-	1.2	2.2
12y	N	-	1.2	2.0
30x	N	-	0.69	0.89
30y	N	-	0.69	0.90
54 -x1	N	-	0.46	0.042
54-y1	N	-	0.45	0.060
54-x2	N	-	0.46	0.041
54-y2	N	-	0.45	0.065

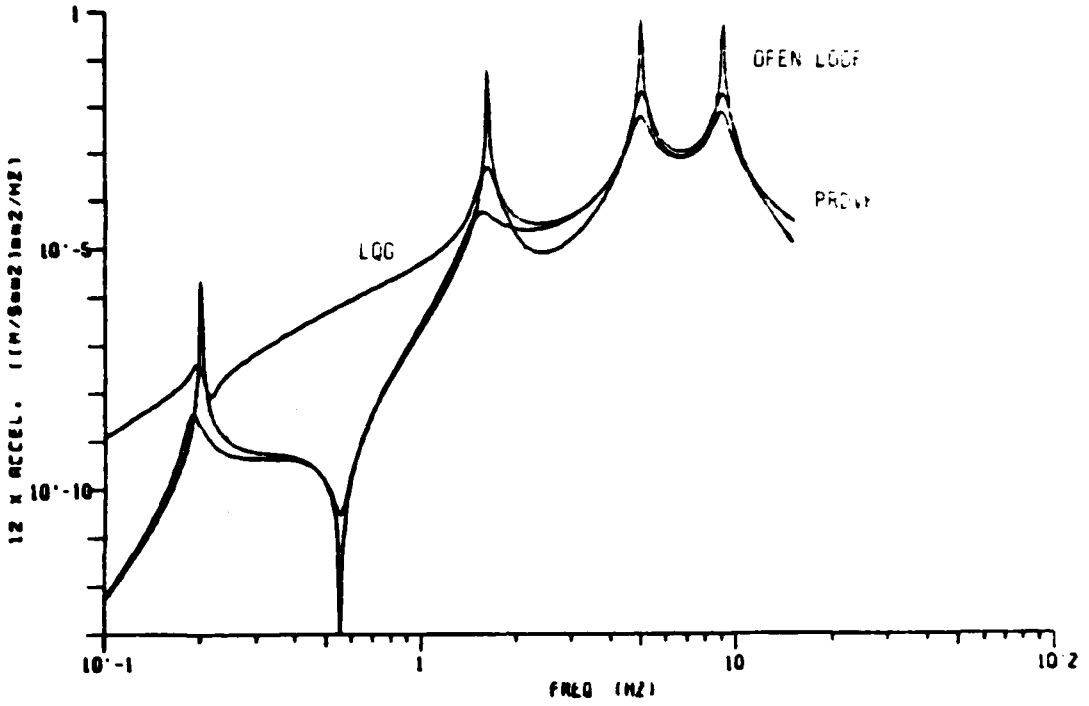

Figure 3.3. PSD for DMS Bay 12(x) Accelerometer for Cases 1,2 and 3

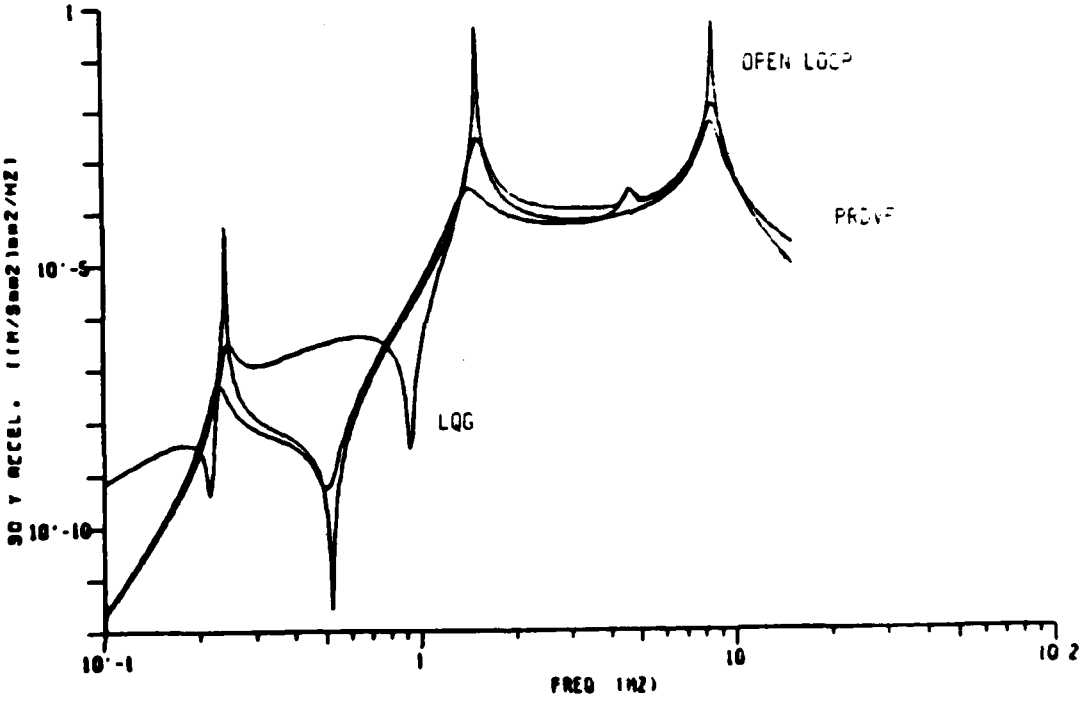

Figure 3.4. PSD for DMS Bay 30(y) Accelerometer For Cases 1,2 and 3

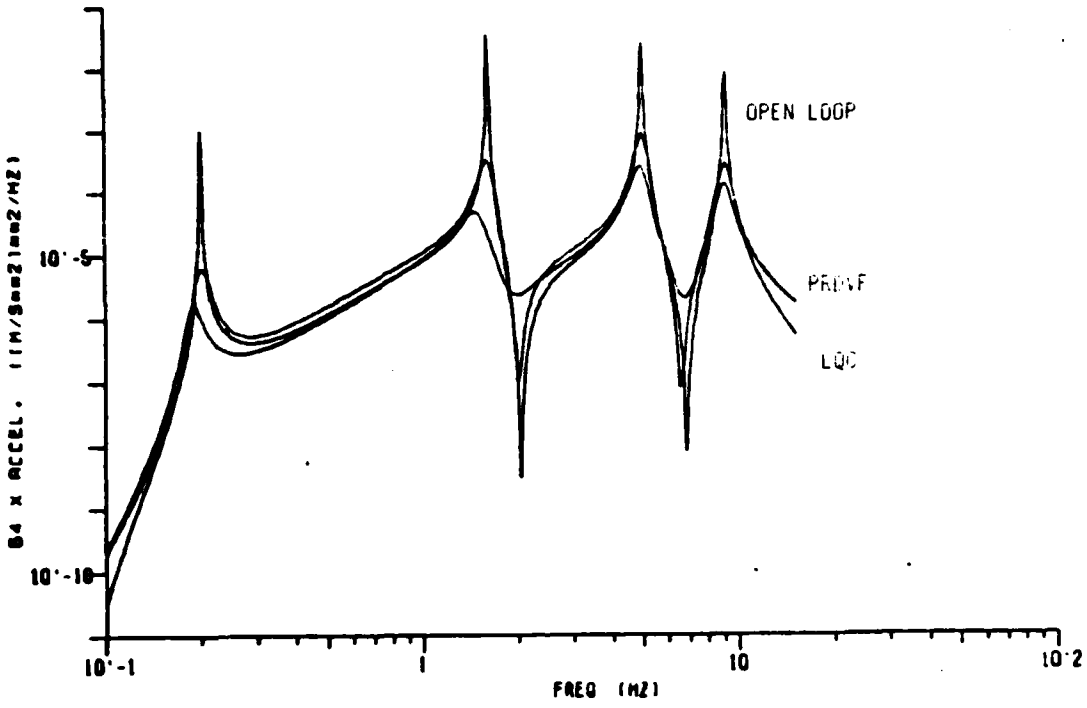

Figure 3.5. PSD for DMS Bay 54(x) Accelerometer for Cases 1,2 and 3

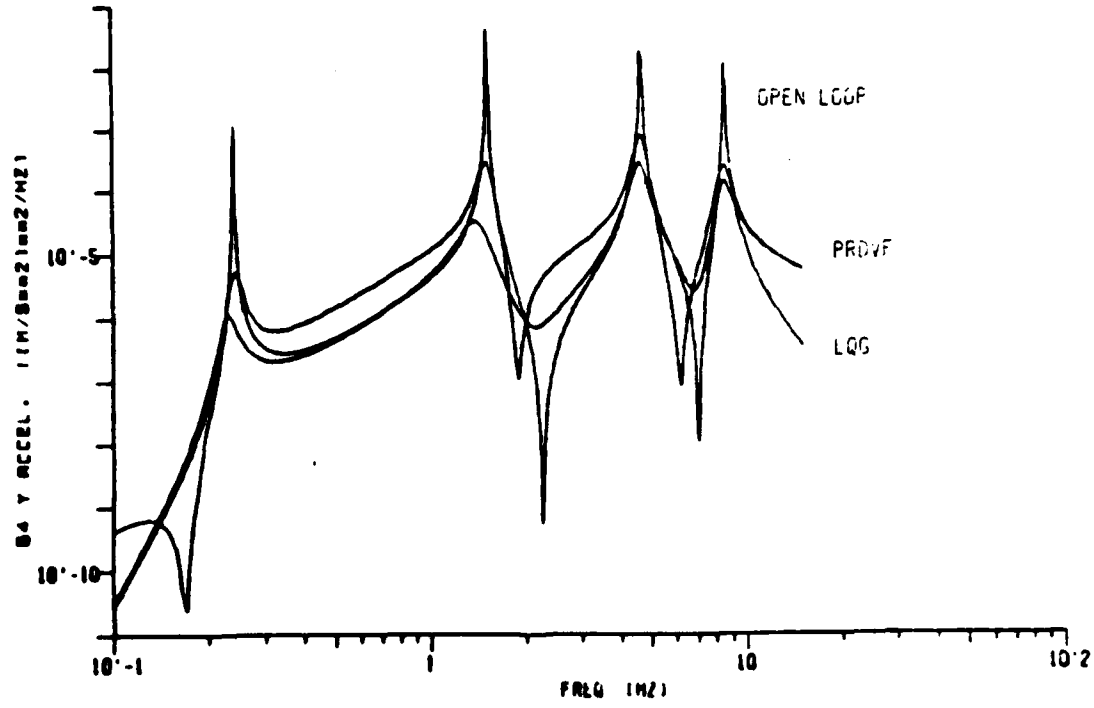

Figure 3.6. PSD for DMS Bay 54(y) Accelerometer for Cases 1,2 and 3

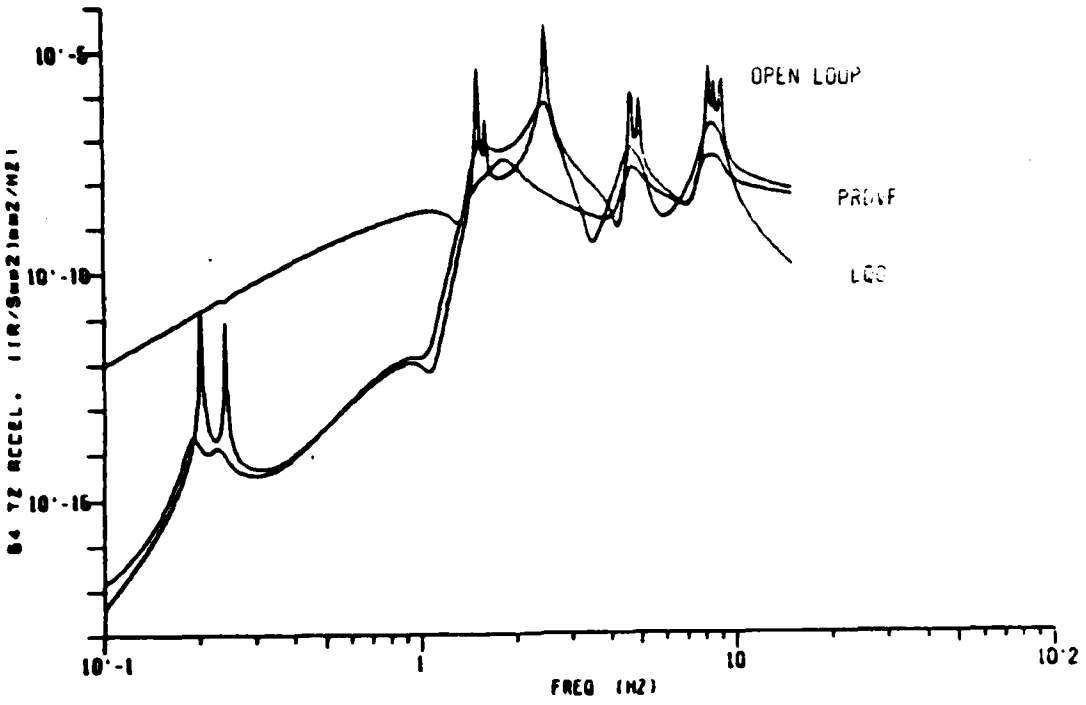

Figure 3.7. PSD for DMS Bay 54(θ_z) Accelerometer for Cases 1,2 and 3

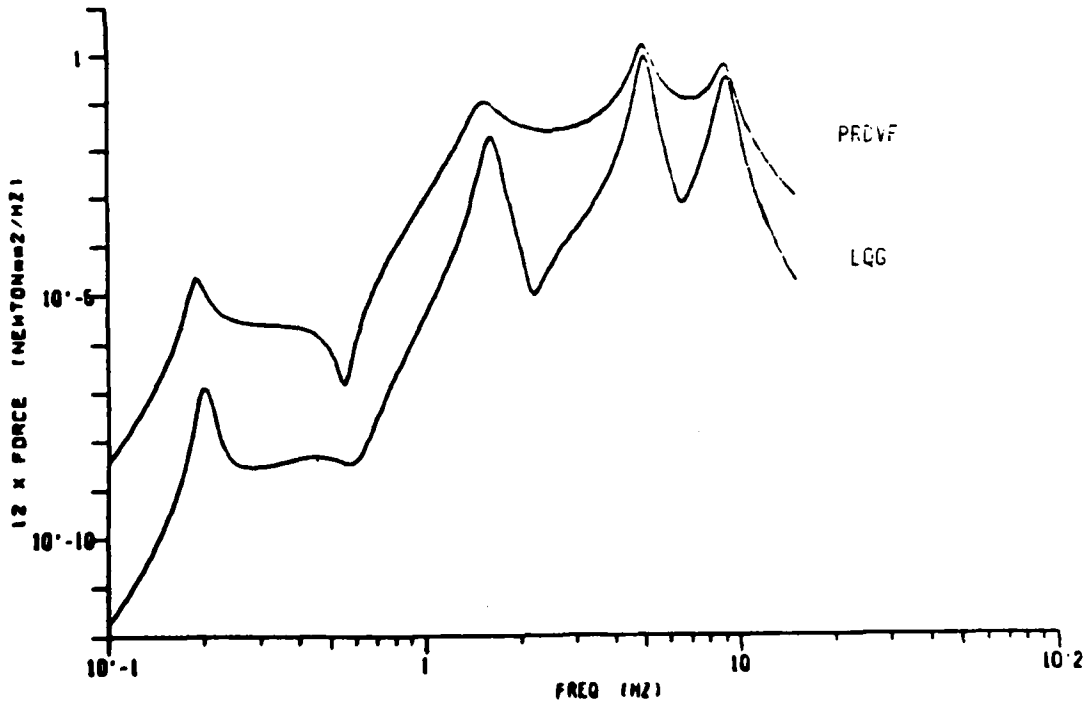

Figure 3.8. PSD for DMS Bay 12(x) LDCM for Both Closed-Loop Cases

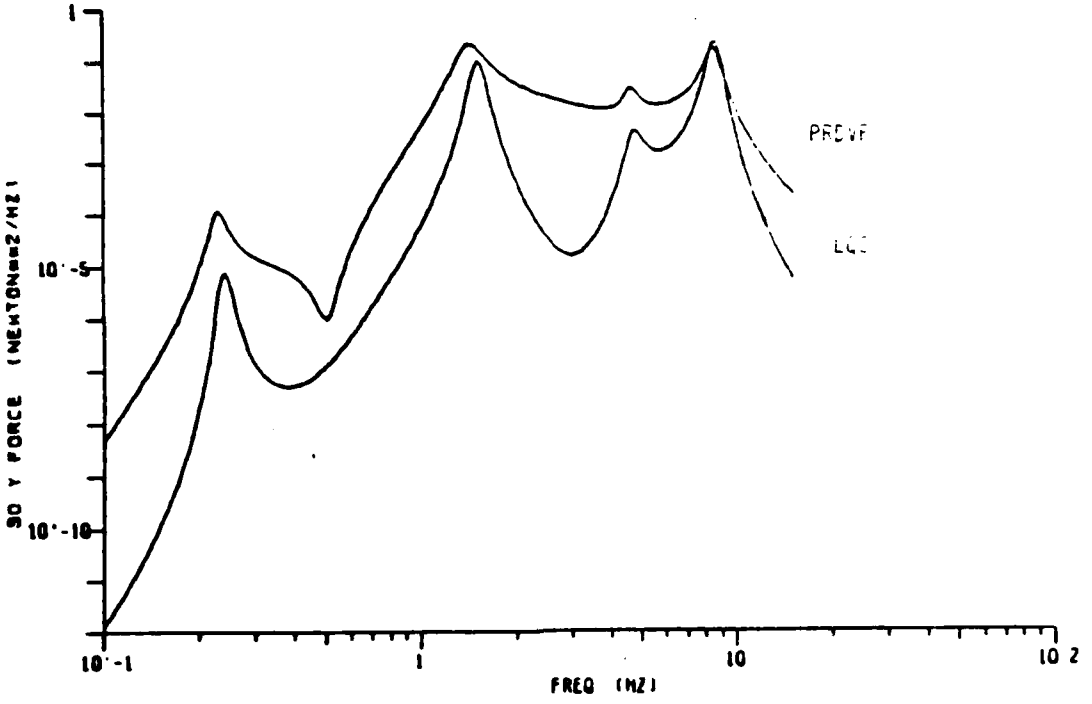

Figure 3.9. PSD for DMS Bay 30(y) LDCM for Both Closed-Loop Cases

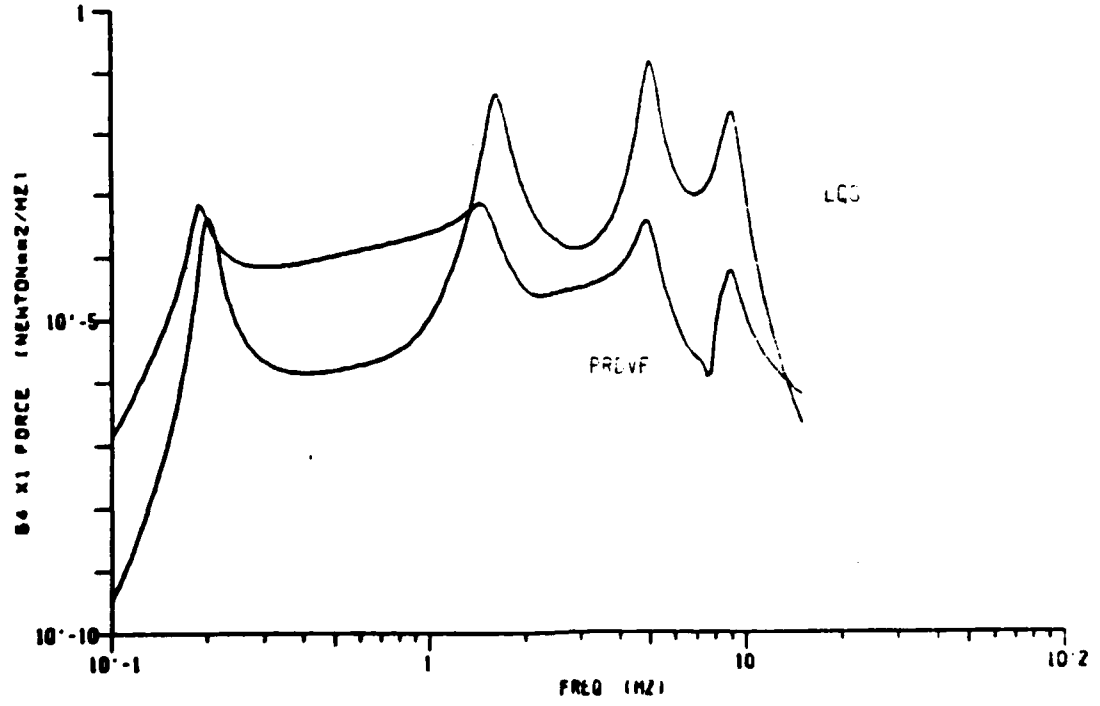

Figure 3.10. PSD for DMS Bay 54(x1) LDCM for Both Closed-Loop Cases

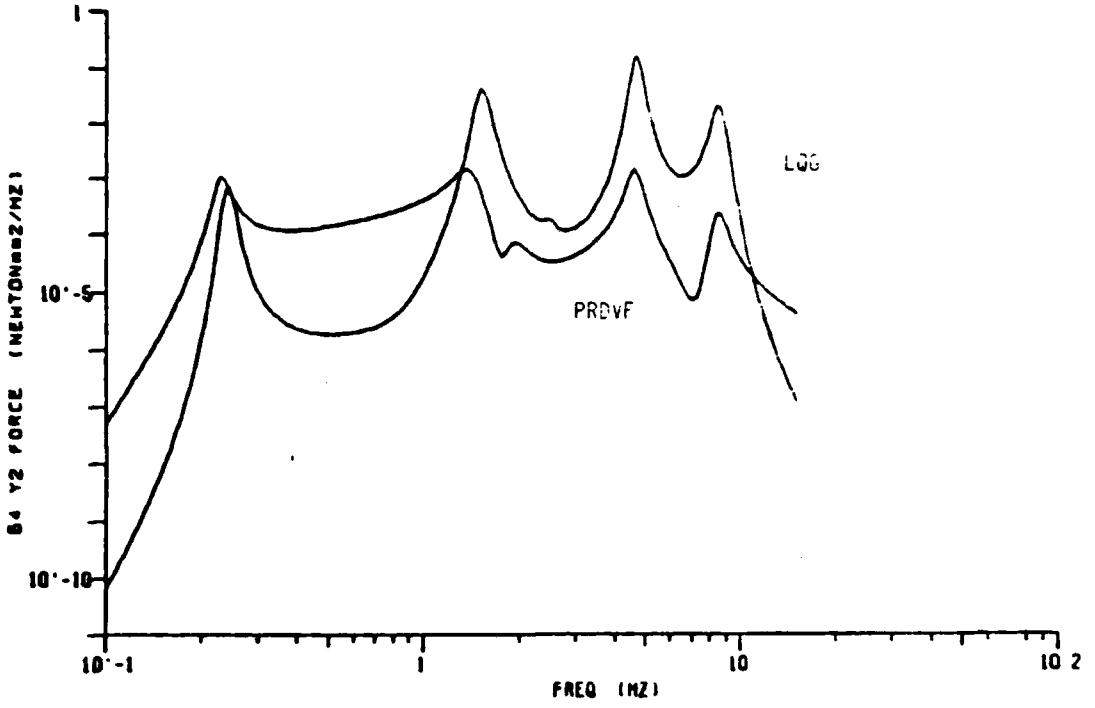

Figure 3.11. PSD for DMS Bay 54(y2) LDCM for Both Closed-Loop Cases

IV. CONCLUSIONS

An overview of the Mast Flight System for the COFS program has been presented along with some of the objectives specifically relating to the required active damping control system. The main objective of the controller for this system is to provide 5 percent structural damping for the first ten flexible structural modes. Some of the modelling issuses were discussed including: 1) the finite-element model of the Deployable Mast System (DMS) along with the state-space model which is utilized to design two different types of controllers, 2) a model for the Linear DC Motors (LDCM), 3) and a model for the collocated sensing devices.

Two different types of controllers were designed and analyzed, an LQG type controller and a Positive-Real Decentralized Velocity Feedback (PRDVF) controller. Upon comparing the two different types of controllers it is apparent that the PRDVF controller is better suited for this type of application. It offers a relatively simple approach to achieve the required 5 percent structural damping which will not burden the flight computer as much as the LQG design since the controller order is much less. The PRDVF controller is also much more robust to parameter variations than the LQG design since

LQG controllers are very sensitive to parameter perturbations. As was previously stated the PRDVF controller will always be positive real over the frequency range of interest. Finally, the PRDVF controller requires much less power for the higher frequency modes than LQG. Current activity involves applying the MEOP approach [2-5] to design low-order robust controllers. These results will be compared to the LQG and PRDVF results.

V. ACKNOWLEDGEMENTS

The authors would like to thank Mr. Larry Davis for the design of the LDCM isolation compensator. Thanks are also due to Mr. Ben Henniges for his analysis and design support.

VI. REFERENCES

1. H. Kwakernaak and R.Sivan, Linear Optimal Control Systems, Wiley-Interscience, New York, 1972.

2. D.S. Bernstein and D.C. Hyland, "The Optimal Projection/Maximum Entropy Approach to Designing Low-Order, Robust Controllers for Flexible Structures," Proceeding 24th IEEE Conf. Decision and Control, pp. 1795-1798, Fort Lauderdale, FL, December 1985.

3. D.C. Hyland, D.S. Bernstein, L.D. Davis, S.W. Greeley and S. Richter, "MEOP: Maximum Entropy/Optimal Projection Stochastic Modelling and Reduced-Order Design Synthesis, "Final Report, Air Force of Scientific Research, Bolling AFB, Washington, DC, April 1986.

4. D.S. Bernstein and S.W. Greeley, "Robust Controller Synthesis Using The Maximum Entropy Design Equations, IEEE Transactions Automatic Control, Vol. AC-31, pp 362-362, 1986.

5. L.D. Davis, D.C. Hyland and D.S. Bernstein, "Application of the Maximum Entropy Design Approach to the Spacecraft Control Laboratory Experiemnt (SCOLE), "Final Report, NASA Langley, January 1985.

6. G. Sevaston and R.W. Longman, "Optimal Positive Real Controllers for Large Space Structures," Proceedings Third VPI&SU/AIAA Symposium, pp 285-300, Blacksburg, VA, June 1981.

7. B.D.O. Anderson, "A System Theory Criterion for Positive Real Matrices," SIAM Journal on Control, Vol. 5, No. 2, pp 171-182, May 1967.

END

DATE

FILMED

DEC.

1987